博 士　論　文

Doctoral Thesis

(パーライト鋼の微視組織におけるコロニー間の相互作用に関する弾塑性変形解析)

Elasto-plastic deformation analyses of the interaction of colony structures in the microstructure of pearlite steels

2017 年 3 月

2017　March

Lidyana Binti Roslan

Empty page

要旨

パーライト鋼は強度と靭性に優れるため，橋梁のケーブルワイヤなどの構造材料として広く利用されている．その優れた性質はパーライト鋼の微視組織に由来する．パーライト鋼の微視組織は，高強度であるが脆いセメンタイトと低強度であるが延性を持つフェライトが交互に積層した構造である．セメンタイト層の配向方向が同じ領域をコロニーと言い，パーライト鋼の微視組織は多数のコロニーで構成されている．パーライト鋼の強度が積層構造に影響され，延性がコロニー構造に影響されることが実験により知られてきた．すなわち，サブミクロン寸法のフェライトが高い応力を担う一方，コロニー中のセメンタイトは塑性変形していることが観察された．しかし，このようなことが生ずる具体的なメカニズムはまだ十分に解明されていない．本研究では，積層構造を持つコロニーの弾塑性変形の詳細を検討する．

パーライト鋼の弾塑性変形は古典的な弾塑性論に基づいた有限要素法を用いて解析した．これまでの研究では，単体セメンタイトがフェライトに積層すると，セメンタイト層内に生ずるひずみ・応力の集中が抑制され，セメンタイトの塑性変形が安定化することが分かった．フェライト層の寸法がサブミクロンオーダーであることもセメンタイトの塑性変形の安定化に貢献する．コロニ

ー構造では，隣接しているコロニー内の積層の配向方向の組み合わせによって，コロニーの界面近傍やコロニー内に生ずるひずみが異なることが分かった．実験ではコロニー配向方向は表面でしか観察できないため，同じような配向方向を持つコロニーでもひずみ分布が異なる場合もある理由は十分に説明できない．近年，コロニーの三次元的な構造が観察され，奥行き方向に傾いているセメンタイト層が確認できた．

本研究では，二次元・三次元のコロニーモデルを構築し，その変形を解析した．その結果，フェライトの加工硬化能と塑性流動応力が高くなるとセメンタイトの塑性変形を安定化することが分かった．また，積層方向が引張方向に平行であると，コロニーの塑性流動応力は最も高くなり，引張方向に 45° 傾くと，塑性流動応力は最も低くなる．すなわち，積層の配向方向は単体コロニーの変形特性に大きく影響する．また積層の配向方向によって，コロニーの変形の異方性の生じ方が大きく異なる．隣接しているコロニーの塑性流動応力の差が高い場合もしくは変形の異方性の違いによってコロニー界面にひずみ・応力集中が生ずることが確認できた．つまり，コロニー構造の集合体であるパーライト鋼微視組織の弾塑性変形はコロニー間の相互作用にも影響されることが分かった．

ABSTRACT

Pearlite steels are widely used in construction structures, vehicles or other engineered productions alike because pearlite steels exhibit both high strength and toughness. The microstructure contributes to the outstanding characteristics. The microstructure is lamellar structures consist of alternately layered high-strength but brittle cementite and low-strength but ductile ferrite. A region where the cementite lamellae aligned in the same direction is called ‘colony’. Thus, a pearlite microstructure is a map of variously oriented colony structures. Experiments have proven that the strength of pearlite depends on the lamellar structures and the ductility depends on the colony structures. Specifically, sub-micron size ferrite is capable of bearing higher stress; while cementite within colonies is observed to deform plastically. However, the details of the mechanisms behind these abilities are still unclarified. For that, we study the details of the elasto-plastic deformation of colonies which are constructed from lamellar structures.

Elasto-plastic deformation of the pearlite steel is analysed by finite element method that employs the classical elasto-plastic theory. From previous studies, we learned that the increased numbers of lamellar suppress the concentration of strain and stress in cementite lamella which leads to the stability of cementite's plastic deformation. On top of that, ferrite also contributes to the stability of cementite's plastic deformation when the size is in sub-micron order. In colony structures, the difference of lamellar alignments of neighbouring colonies influences the distribution of strain around the colony boundaries and inside the colonies. Experimentally, researchers can only observe

these deformations from the surface of the specimens. Hence, detailed explanations why different distributions of strain occur between colonies with similar lamellar are yet to be elucidated. Recently, the three-dimensional structure of colonies which confirm the transversal inclination of cementite layer has been observed.

For this study, we construct two-dimensional and three-dimensional colony models and analyse the deformation. The results show that the plastic deformation of cementite stabilised when the strain-hardening rate and plastic flow of ferrite are high. Next, when the colony alignment is parallel to the tensile direction, the plastic flow stress of the colony is the highest. Meanwhile, when the colony alignment is $45°$ inclined towards the tensile direction, the plastic flow stress is the lowest. In other words, the lamellar alignment of the single-colony models significantly influences the behaviour of its deformation. Likewise, the lamellar alignment of the colony controls the anisotropy of the single-colony models. Concentrations of strain and stress around colony boundaries confirmed when the difference of plastic flow stress between two adjacent colonies is high or/and the anisotropic difference is prominent. Therefore, the elasto-plastic deformation in an assembly of colony structures such as pearlite microstructure is influenced by the interaction between colonies.

Contents

List of figures

List of table

Empty page

Chapter 1

Overview

1.1 Introduction

In 1881, Sorby [1] discovered “the *pearly* compound” which is later widely known as “Pearlite”. Pearlite is a type of eutectoid steel. It is the product of austenite decomposition [2-8] from heat treatment and subsequent cooling process. The patenting process transforms austenite into a lamellar structure consisting of high-strength yet brittle cementite and low-strength yet ductile ferrite phases [9,10]. Managing the annealing process of patenting allows manufacturers to control the strength and toughness of pearlite during the wire-making process [11-15]. Thus the applications of pearlite steels range from piano strings to steel cords found in vehicle tires and cable wires of suspension bridges [15-18]. The brittle/ductile lamellar structure allows trade-off attributes of high strength and ductility to complement each other [19-29]. To date, pearlite steel exhibits the greatest strength amongst mass-produced wire materials with the maximum tensile strength improved to more than 5 GPa [30,31].

1.2 Pearlite microstructure

Hull and Mehl [9] mentioned that Belaiew [32] initially described the pearlite colony by assuming that the cementite lamellae were arranged parallel with each other in the ferrite matrix –where they were thought to have obliged a certain crystallographic orientation. However, this orientation was considered to be different from the original austenite crystallographic orientation. Mehl and Smith [33] studied the case [32] and found that the original austenite predetermined the orientation of ferrite. Jolivet [34] observed that a pearlite nodule consisted of zones (colonies) where ferrite and cementite lamellae were alternately layered while lying parallel along a particular direction. The term “direction” [9,10,33,34] defined the orientation relationships which the recrystallized cementite/ferrite lamellar structure succeeded indirectly from the parent austenite.

Almost half a century later, Takahashi et al. [35] explained that the pearlite microstructure consisted of substructures called the "pearlite block", where the orientation of the ferritic crystallography was almost the same. A pearlite block was made up of smaller regions called the "pearlite colony" where the alignment of the cementite lamellae appeared more or less parallel to each other. Fig. 1 [36] shows the scanning electron microscope (SEM) photo of the microstructure in as-patented pearlite.

Fig. 2 is the schematic of pearlite microstructure. In pearlite, the lamellae show no particular preferred alignment. Studies showed that when pearlite deforms under uniaxial tensile deformation, for example, the cold-drawing process, the randomly aligned cementite lamellae will rotate to realign with the direction of the deformation [37-41]. Studies emphasised that cementite sustain crystal reorientation by deforming plastically. The ability for cementite to plastic-deform is crucial for the ductility of pearlite because cementite is the brittle constituent of the microstructure [22, 42, 43].

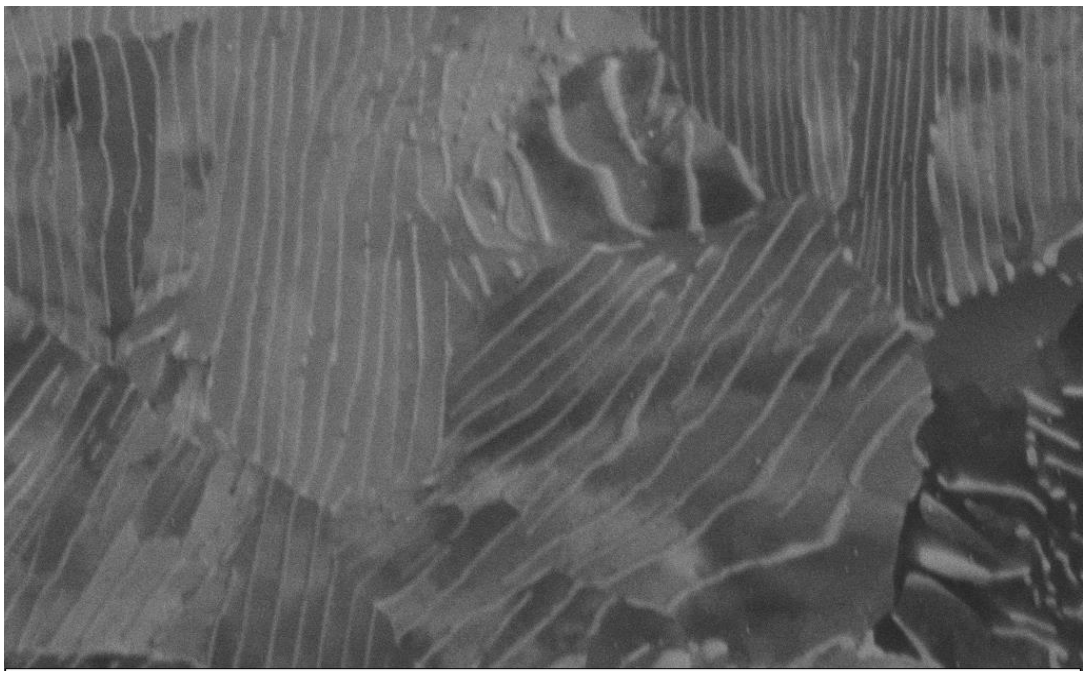

Fig. 1. SEM photo of microstructure in as-patented pearlite [36].

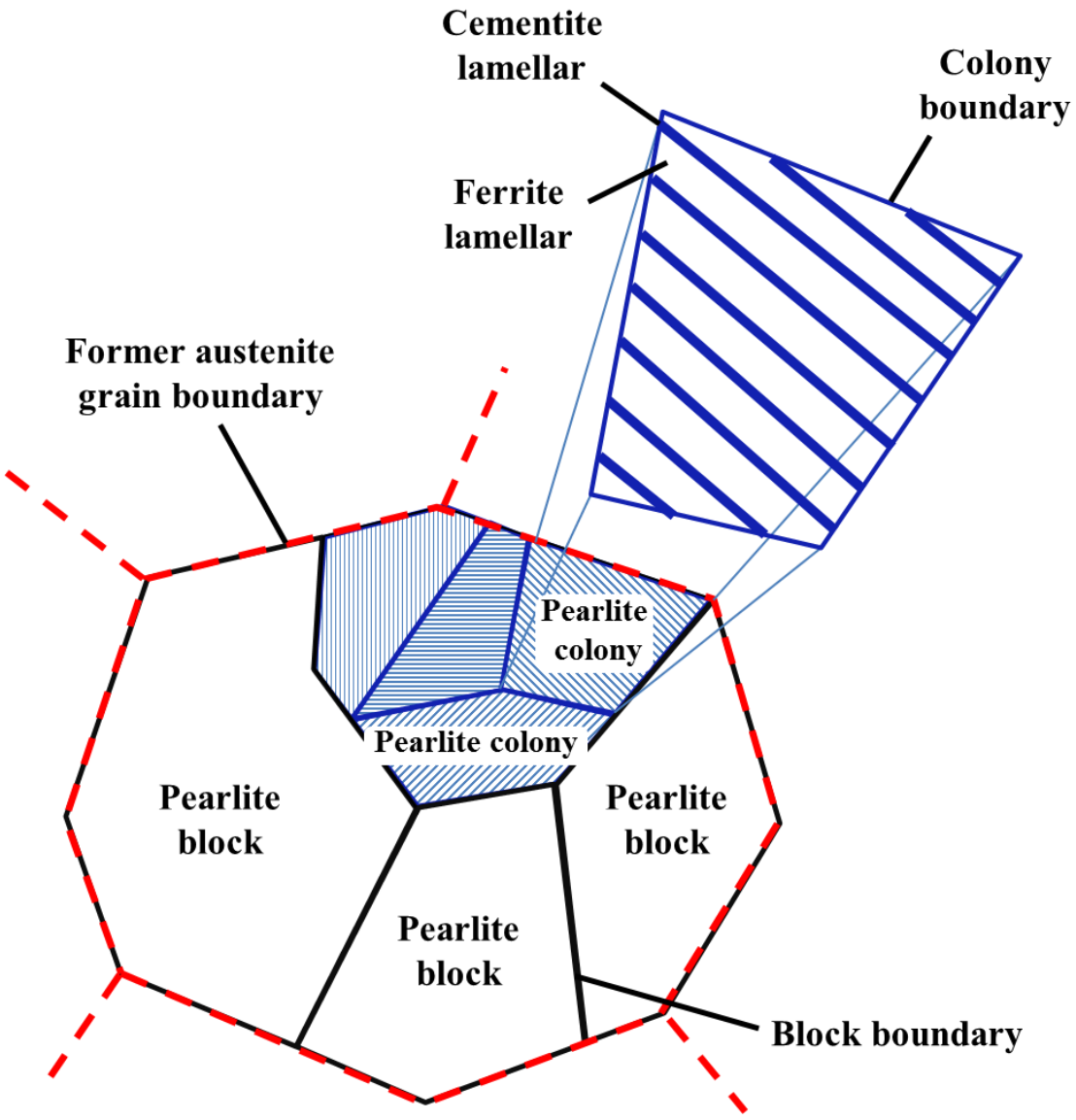

Fig. 2 Schematic diagram of the pearlite microstructure. The description explains the relative hierarchy of pearlite substructures: the pearlite block structure, the pearlite colony structure and the pearlite lamellar structure which consisted of alternate layers of cementite and ferrite lamellae [36].

1.3 Deformation of cementite in pearlite

Evidence of cementite in pearlite plastic-deforming can be picked up from researchers throughout the years [19-23]. Tanaka et al. [44] confirmed that cementite in colony structures did accommodate plastic deformation at room temperature. Puttick [19] suggested that cementite deformed plastically by slip and this was justified by Maurer and Warrington [45]. In fact, Sevillano [46] found that cementite possesses at least six slip systems, which confirmed that cementite in pearlite is potentially ductile. For multi-layered brittle/ductile composites, when the low-strength constituent yields, stress builds up and efficiently transfers to the adjacent, high strength component. These results are more or less uniform stress distribution throughout the lamellar structure [47]. Such stress partitioning between cementite/ferrite in pearlite prevents stress localisations, which improve the stability of elasto-plastic deformation in the brittle cementite. The partitioning of stress greatly enhanced by boundary-strengthening [48]. When the thickness of ferrite is reduced, the strain-hardening ability will improve especially on the scale smaller than $1\mu m$ [20]. This is known as the Hall-Petch relationship [49,50], which described that the mechanical strength of metals is inversely proportional to the square root of the mean diameter of the crystal grain. This mechanism is experimentally proven by Marder and Bramfit [51]. Our studies on

pearlite lamellar structure showed that the propagation of plastic strain in cementite phase suppressed by layering bulk cementite with ferrite lamellar [52] and the onset of plastic deformation in cementite delayed [53]. The delay stabilises the plastic deformation in cementite. These behaviours are observed in high-strength steels consisting of brittle/ductile multi-phases [54]. Our previous analyses [53] also clarified the increase of the thickness ratio of ferrite lamella to that of cementite lamella that allowed wider strain distribution in cementite lamella, which prevents strain from localising. In pearlite, the thickness, the volume fraction and the continuity nature of cementite lamellar are controlled by carbon content. Pearlite with lower carbon content shows better ductility because it can withstand greater reduction of area [24,55]. Tanaka and Matsuoka [56] used the continuum model to study the effect of lamellar alignment have on internal stress in cementite with an assumption that cementite remains elastic. They found out that the work-hardening of pearlite depends on the stress state in the ferrite matrix. However, this is applicable only when the cementite/ferrite lamellar model is an equal-stress model [57]. Equal-stress model refers to model with lamellar alignment perpendicular to the tensile direction. Ferrite as the ductile constituent will bear most of the plastic deformation because of cementite yields at higher stress. Therefore, the strain-hardening rate for the model more or less follow that of ferrite, but

at a higher stress flow because of the influence from cementite. Butler and Drucker [58] suggested the flow stress and strain-hardening of pearlite depend on the orientation of cementite because of the constraint it has upon the deformability of ferrite. Yasuda and Ohashi [59] explained it by the understanding of stress-incompatibility from the differences in the mechanical properties between cementite and ferrite.

1.4 Deformation of block/colony structures in pearlite

It is widely known that the colony influenced the ductility of pearlite [23]. When the colony size is sufficiently small, the colony boundaries would act as obstacles against brittle cracks and increase the ductility of pearlite microstructure [60]. However, for coarse pearlite, brittle fractures tend to occur between neighbouring colonies according to Miller and Smith [61].

We conducted analyses to investigate how the lamellar alignment in two adjacent colonies influences the elasto-plastic deformation of pearlite microstructure [62].

Fig. 3 shows the results of the elasto-plastic deformation in two neighbouring colonies with different lamellar alignments. The mechanical property of the matrix is the harmonic means of the mechanical properties of cementite and ferrite.

The arrangement of lamellar alignments determine the tolerance for deformation in

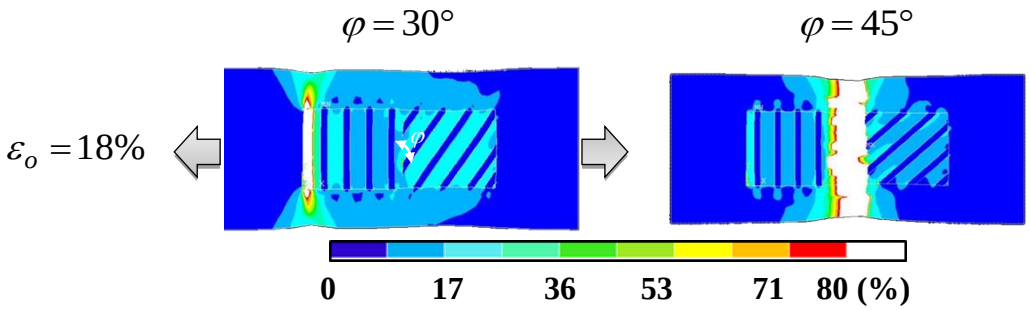

Fig. 3 Distribution of equivalent strain, ε_{eq} in two adjacent colonies at nominal strain $\varepsilon_o = 18\%$. The angle between the lamellar alignment is denoted as φ. The grey arrows indicate the tensile direction [62].

colonies [63,64]. Therefore, the interactions between the lamellar alignments in neighbouring colonies influence the elasto-plastic deformation in each colony and the concentration of strain around the colony boundaries as shown in Fig. 3.

Fig. 4 indicates the distribution of strain in specimen [36] of an as-patented pearlite. The specimen was embedded with precision markers and subjected to tensile deformation. The lamellar alignments in both regions inclined approximately at $45°$ respect to the tensile direction. Even so, the distribution of strain in Fig. 4(a) is almost the opposite of that in Fig. 4(b). Furthermore, these results are taken at a triple junction of three colonies where strain highly concentrates [60]. Adachi et al. [66] revealed that cementite lamellae were twisted and distorted while maintaining the crystal orientation

with the ferrite which suggests the irregularities of deformation shown in Fig. 4. However, the two-dimension (2-D) observations of pearlite microstructure do not provide sufficient information concerning the condition of the lamellar alignment beyond the surface.

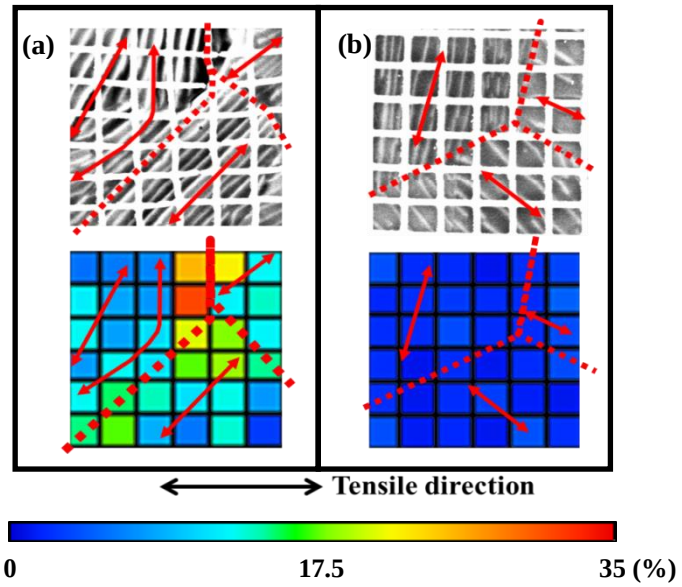

Fig. 4 Distribution of plastic strain ε^{pl} propagation at drawing strain $\varepsilon = 5\%$ around block/colony boundaries. (a) and (b) show three colonies with the similar lamellar arrangement: a triple point meet. The dotted lines and arrows represent block/colony boundaries and lamellar alignment of cementite respectfully [36].

1.5 Complications of 2-D observations

Currently, many types of research depend on the scanning electron microscope (SEM) [67,68] equipped with electron backscattered diffraction (EBSD) for image analysis to acquire reliable microstructural and crystallographic data efficiently [69-74].

Nevertheless, the existing tools and techniques only provide 2-D information from the topography of the scanned surface. In reality, the pearlite microstructure is a complex three-dimension (3-D) crystalline network of randomly aligned cementite lamellae embedded in the ferrite matrixes that have various orientations. Regardless of the arbitrary nature of the microstructure, the orientation relationships between cementite and ferrite have been established by their interfacial planes or habit planes [75-82]. With this knowledge, researchers assume the probable 3-D shape of the cementite lamellae [70,71]. To understand what might be occurring inside the pearlite microstructure, the information concerning the distribution and connectivity of cementite lamellae in 3-D space is essential. Computer-aided reconstructions by serially sectioned images revolutionise microstructure characterization from 2-D to 3-D visualisation [66,83-86]. However, most of the examinations is conducted with focused ion beam SEM (FIB-SEM). The specimen is craved by the FIB gun for interval scanning. This means, the interval sectioning eventually depletes the specimens. Hence, it physically impossible to re-examine the 3-D morphology of the same microstructure before and after mechanical testing [85,86]. Another option is the 3-D imaging by atom probe topology (ATP) [87]. ATP is indeed a powerful tool that provides atomic-scale information of a microstructure. In recent years, this method allows researchers to

observe the decomposition of cementite by counting the density of carbon atoms [88-90]. It does not provide quantitative information such as strain mapping for evaluating elasto-plastic deformation of microstructures. In the end, for mechanically tested specimen, researchers are likely given no option but to rely on 2-D based investigations.

1.6 Research outline

Chapter 1 introduces the brief history and structure of Pearlite. Pearlite colonies are randomly aligned lamellar structures consisting of high-strength but brittle cementite and low-strength but ductile ferrite. These microstructural features contribute to the remarkable strength and ductility of pearlite steel. It is important to elucidate how lamellar alignments in colonies affect the elasto-plastic deformation in colonies and around the colony boundaries to understand the mechanical responses of colony structures. For that purpose, 3-D observation of pearlite microstructure is necessary. However, researchers still depend on 2-D observations. For that reason, we propose the use of 3-D finite element analysis.

Chapter 2 explains the classical elasto-plastic theory and the established properties for cementite and ferrite. These models are isotropic and subjected to tensile

deformation. We used commercial finite element software called ANSYS©.

In Chapter 3, we explain in details the modes of modelling 3-D colony models. The normal vector determines the direction of lamellar alignment. From the perspective of the normal vector, the cementite plane has two inclinations. From the orthogonal projection, the cementite plane is inclined from the *x*-axis at the *xy*-plane. The second inclination of the normal vector is around the axis perpendicular to the *xy*-plane, the *z*-axis. In modelling the models, it is important to note that the angles used to describe the lamellar alignment in each model represent the magnitude and direction of imposed inclinations/rotations from the perspective of *x*-axis at *xy*-plane and around *z*-axis.

In modelling the 3D colony models, the direction of cementite lamella in 3-D space of (*x*,*y*,*z*) is determined by the inclination angles of the cementite plane's normal vector. Two angles of inclinations describe the direction of the normal vector, the inclination from *x*-axis at *xy*-plane and the inclination around the axis perpendicular to the *xy*-plane, *z*-axis. The basic morphology of cementite lamella is reviewed to create the simplified versions of 3-D single-colony finite element models. We investigated the effect of lamellar alignment towards the elasto-plastic deformation in single-colony models. After that, with 2-D multi-colony models, we imitated pearlite specimens to observe the interaction between colonies with various lamellar alignments.

Chapter 4, Chapter 5 and Chapter 6 unfolds the analyses of single-colony, multi-colonies, and double-colony conducted with 2-D and 3-D models.

In Chapter 4, a single-colony model is a multi-layered lamellar structure. This study is the continuity of previous analyses [52,53] on pearlite lamellar structure. We studied the mechanism behind the stability of plastic deformation in cementite phase by layering it with ferrite. Before we can study the interaction between colonies, we need to understand the influences which ferrite inflicts on cementite. In fine pearlite microstructure, ferrite hardens because of size effect. To study the effect of ferrite hardenability on the stability of cementite's plastic deformation, we modified the Swift's type equation by adding a constant. Stress vs. strain relationship expresses the mechanical response. The vertical axis and horizontal axis of the graph represents stress and strain respectively. A constant added to the graph function for the horizontal axis intercept. So, the constant controls the level of yield stress or level of flow stress. We introduced possible values for the mechanical properties of ferrite by variating the strain-hardening rate and level of flow stress. When the lamellar model subjected to tensile deformation, the effects of ferrite's strain-hardening rate and level of flow stress on the stabilisation of cementite's plastic deformation are studied. Next, we assumed four patterns for the alignment of lamellar in 3-D space to understand the effect of

lamellar direction on the elasto-plastic deformations of single-colony.

In Chapter 5, we imitate the colony structures of experimental specimens into 2-D FEM multi-colony models to compare the experimental and FEM elasto-plastic deformation of multiple colonies.

Since the interaction between colonies is complicated, In Chapter 6, we reduces the multi-colony models into double-colony models with 2-D and 3-D space lamellar configuration. Reducing the models into two adjoined single-colony models connected at the colony boundary allows us to study the fundamental interaction in colony structure.

In Chapter 7, we discussed the results obtained by dissecting the stress components of single-colony models to compare with stress partitioning in ferrite/cementite studies from the crystal plasticity analyses by Yasuda and Ohashi [59]. The discussion shows that our results agree with the plastic deformation tendencies of pearlite structure observed experimentally by Tanaka [36]. Finally, we discuss the possible configurations of dislocations [111-113].

The interesting aspect of this study is the approach of not considering the crystal plasticity of cementite and ferrite. This thesis describes the understanding of the interaction between adjacent colonies from the configuration of lamellar arrangements.

Chapter 2

Analyses condition

2.1 Introduction

Tensile deformation of pearlite single- and double-colony models will be analysed by employing the classical theory of elasto-plastic deformation in metal under uniaxial deformation. The onset of plastic deformation in metal is defined at the limit of elastic behaviour when the material yields the ability to return to its original form. A yield criterion defines this condition under any combination of stresses. For the plastic potential to be defined by such criteria constantly, certain assumptions are made. Firstly, it is assumed that the established materials will be independent of any thermal effect. Secondly, the materials are assumed to be isotropic. Finally, the Bauschinger effect is neglected.

2.2 Numerical modelling of elasto-plastic deformation

Fig. 5 shows a stress-strain curve of typical mild steel under uniaxial loading.

Initially, the stress, denoted by σ, is linearly proportional to strain, denoted by ε along $OA"$. Point $A"$ is called the proportional limit. The Young's modulus, denoted as E, is the slope of the function.

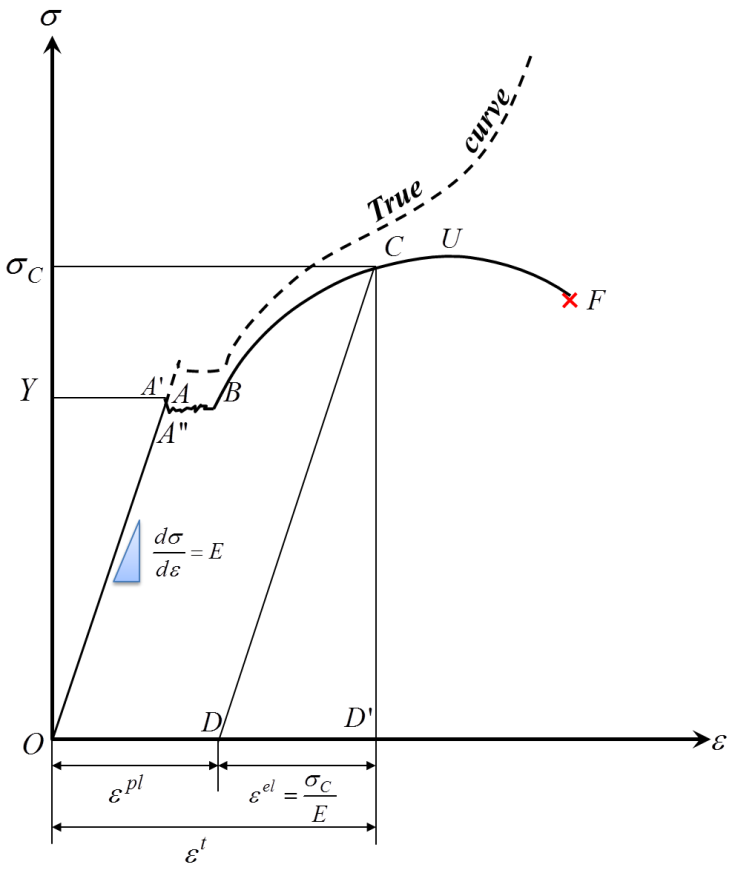

Fig. 5 Stress-strain curve of a typical mild steel under uniaxial tensile deformation.

It determines the proportionality for the increment of strain to the increment of stress. This region is known as the elastic region. It is represented by Hooke's law in (1).

$$\sigma = E\varepsilon \tag{1}$$

Chapter 2 Analyses condition

The linear deformation is true until point A', which is called the upper yield. This is followed by a local drop to the lower yield point, A, which is accepted as the elastic limit. The stress value at this point is called the yield stress, denoted as Y. The stress oscillates at a plateau to point B. The material deforms perfectly plastic through AB. At point B, the material starts to harden. From this point, stress builds up as strain increases until the ultimate tensile stress at point U. This is called strain-hardening, and the material deforms plastically. If the material is unloaded at any point between BU, for example at point C, the deformation will follow CD, which is parallel with the initial elastic deformation path, OA. The recovered strain, DD' is the elastic strain and denoted as ε^{el}. Referring to (1), the elastic strain at point DD' is tensile stress at point C which is denoted as σ_c divided by the slope, which is Young's modulus, E as mentioned. This gives the following equation:

$$\varepsilon^{el} = \frac{\sigma_C}{E} \tag{1a}$$

The remaining strain is the plastic strain, which is denoted as ε^{pl}. The total strain, ε^t is the sum of both regions, elastic and plastic, as shown in (2).

$$\begin{aligned} \varepsilon^t &= \varepsilon^{el} + \varepsilon^{pl} \\ &= \frac{\sigma}{E} + \varepsilon^{pl} \end{aligned} \tag{2}$$

After that, the material softens and become unstable because the stress decreases with

the increase of strain until it fractures at point F.

In Fig. 5, the positive slope of the true curve, which is represented by the dotted line indicates the material is becoming stronger as it is deforming plastically. This means that the true curve defines the strain-hardening of the material [90]. It is difficult to determine the true stress, which is denoted as σ_{tr}, beyond the yield point. This is because the increase of strain becomes rapid and the deformation is not uniformed throughout the material especially after necking. On the contrary, plotting the nominal curve is simpler because it is defined by the original parameters of the material, in which data are measured before mechanical testing. To apply this advantage, the nominal stress, which is denoted as σ_o, must be redefined by true stress.

The true stress, σ_{tr} is defined as load P divided by the instantaneous cross-sectional area A. The representation of true stress, σ_{tr} is given by (3).

$$\sigma_{tr} = \frac{P}{A} \tag{3}$$

Meanwhile, true strain, which is denoted as ε_{tr}, is defined as the instantaneous length increment, dL, per unit of the instantaneous length L. The rate of the instantaneous strain increment is denoted as $d\varepsilon$ and is represented as:

$$d\varepsilon = \int \frac{dL}{L} = \ln L + C \tag{4}$$

Hence, when the total length changes from the original length L_o, to a certain

instantaneous length, L, it is expressed as true strain, ε_{tr} as shown in (4a).

$$\varepsilon_{tr} = d\varepsilon = \int_{L_o}^{L} \frac{dL}{L} = \left[\ln L\right]_{L_o}^{L} = \ln L - \ln L_o = \ln \frac{L}{L_o} \tag{4a}$$

Equation (5) shows the representation of nominal stress, which is denoted by σ_o. It is defined as load, P, divided by the original cross-sectional area, A_o.

$$\sigma_o = \frac{P}{A_o} \tag{5}$$

The nominal strain is denoted as ε_o. It is defined as the increase per unit of the original length, L_o, as shown in equation (6).

$$\varepsilon_o = \frac{L - L_o}{L_o} \tag{6}$$

Equation (6) can be further rearranged as:

$$L = L_0\left(\varepsilon_o + 1\right) \tag{6a}$$

And,

$$\frac{L}{L_o} = \left(\varepsilon_o + 1\right) \tag{6b}$$

A plastic body is considered to be incompressible. This means the volume is constant throughout the deformation. The changes of volume from elastic straining are assumed to be sufficiently small and can be neglected. For that reason, the original volume, V_o is equal to the instantaneous volume, V.

$$\begin{aligned} V_o &= V \\ A_o L_o &= AL \end{aligned} \tag{7}$$

From (7), the ratio of cross-sectional areas, A_o to A is proportional with the ratio of

length, L to L_o, as shown in the following (7a).

$$\frac{A_o}{A} = \frac{L}{L_o} \tag{7a}$$

When (6a) is substituted into (7), the relationship between nominal strain, ε_o and the cross-sectional areas, A_o and A are defined as follows:

$$\begin{aligned} A_o L_o &= A L_o (\varepsilon_o + 1) \\ A_o &= A(\varepsilon_o + 1) \end{aligned} \tag{7b}$$

Hence, the ratio of cross-sectional areas is given as:

$$\frac{A_o}{A} = (\varepsilon_o + 1) \tag{7c}$$

So, the representation of nominal stress, σ_o by true stress, σ_{tr} is determined in (8) by substituting (7b) into (5).

$$\begin{aligned} \sigma_o &= \frac{P}{A_o} \\ &= \frac{P}{A(\varepsilon_o + 1)} \\ &= \frac{\sigma_{tr}}{(\varepsilon_o + 1)} \end{aligned} \tag{8}$$

The decrease of nominal stress, σ_o compared with true stress, σ can be mathematically explained by substituting equation (7c) into (8).

$$\begin{aligned} \sigma_o &= \frac{\sigma}{(\varepsilon_o + 1)} \\ &= \frac{\sigma}{\left(\frac{A_o}{A}\right)} \end{aligned} \tag{8a}$$

Equation (8a) proves that the instantaneous stress or true stress, σ_{tr} is unable to catch

up with the growing rate of cross-sectional area, $\left(\frac{A_o}{A}\right)$ when the instantaneous cross-sectional area, A of the material, rapidly decreases to compensate with the elongation as shown in (7a). Meanwhile, the nominal strain, ε_o can be represented by true strain, ε_{tr} by substituting equation (6b) into equation (4a):

$$\begin{aligned}\varepsilon_{tr} &= \ln\frac{L}{L_o} \\ &= \ln\left(\varepsilon_o + 1\right)\end{aligned} \tag{9}$$

Given that when $y = \ln x$; then $x = e^y$. So, if $\left(\varepsilon_o + 1\right)$ is ***x*** and ε_{tr} is ***y***, therefore;

$$\begin{aligned}\varepsilon_o + 1 &= e^{\varepsilon_{tr}} \\ \varepsilon_o &= e^{\varepsilon_{tr}} - 1\end{aligned} \tag{9a}$$

As shown in Fig. 5, the stress-strain curve is not straight forward. To model the stress-strain relationship of a material subjected to tensile deformation, idealisation for elasto-plastic deformation needs to be considered. For this case, two types of elasto-plastic idealisation shown in Fig. 6 are employed. Fig. 6(a) is elastic-perfect plastic material. It will be applied to establish brittle material. Fig. 6(b) is power plastic hardening material. It will be applied to establish ductile material. The non-linear work hardening will be represented by empirical equations type Swift [92]. These will be further elaborated in the next section.

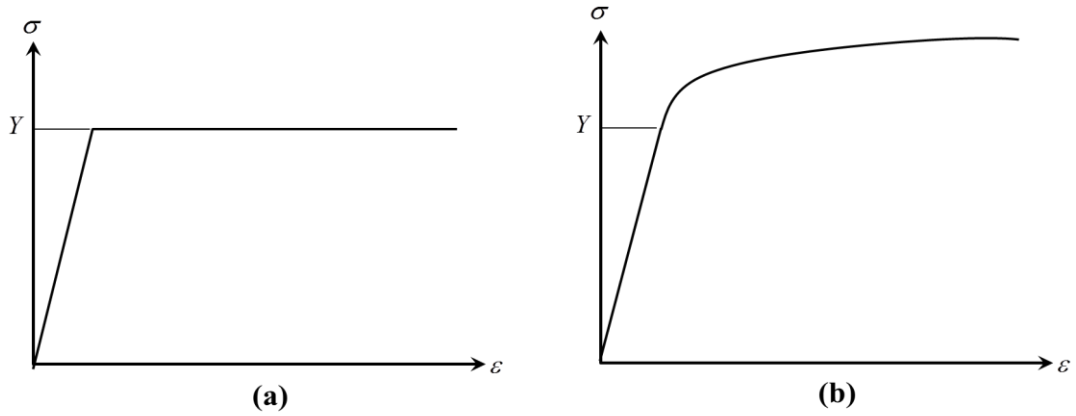

Fig. 6 Idealisation of elasto-plastic deformation. (a) Elastic-perfect plastic material, and (b) power plastic hardening material.

2.3 Material properties

Fig. 7 shows the stress-strain curves established for cementite and ferrite in this study. We used Poisson's ratio 0.3 for both materials. Young's modulus of bulk cementite ranges from 176 GPa to 186 GPa [42]. At room temperature, cementite fractures at its yield point, 2.75 GPa [42,43,89]. The Young's modulus, E, for cementite is the arithmetic mean of its Young's modulus, which is $E = 181\,\text{GPa}$. When the yield stress for cementite is denoted as Y^{θ}, then, from the Hooke's law, the elastic limit for cementite at nominal strain, ε_o is calculated in (10):

$$\varepsilon_o = \frac{Y^{\theta}}{E} = \frac{2.75GPa}{181GPa} \cong 1.593\times10^{-2}$$

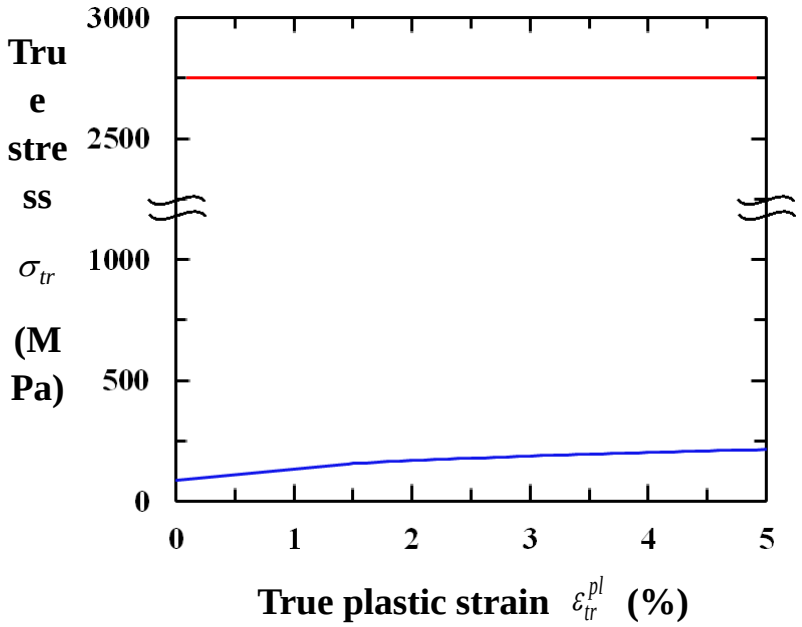

Fig. 7 Stress-strain curves for cementite and ferrite

Interestingly, Kanie et al. [94] experimentally proved the cementite can bear elastic strains, ε^{el} around 1% to 2%. However, it is tricky to simulate the brittle property of cementite numerically. Theoretically [95-97], the condition of plastic instability occurs prior to the onset of necking at the maximum load point. Load P is always proportional to the product of true stress, σ_{tr} multiplied by the cross-sectional area A. So, the condition for maximum load point is given in (11).

$$\begin{aligned} P &= \sigma_{tr} A \\ dP &= A d\sigma_{tr} + \sigma_{tr} dA = 0 \end{aligned} \tag{11}$$

During the plastic deformation, the volume of material is considered to be constant, as shown in (7). To fit (7) into the condition for maximum load point, it is differentiated on

the instantaneous area, A to obtain dA in (12):

$$AL = A_o L_o$$
$$AdL + LdA = 0$$
$$dA = -A\frac{dL}{L} \tag{12}$$

When (4a) is substituted into (12) the relationship between area and strain is derived.

$$\therefore dA = -Ad\varepsilon_{tr} \tag{12a}$$

The strain-hardening rate is obtained by substituting (12a) into the condition of maximum load point, $dP = 0$ from (11).

$$Ad\sigma_{tr} - \sigma_{tr} Ad\varepsilon_{tr} = 0$$
$$\frac{d\sigma_{tr}}{d\varepsilon_{tr}} = \sigma_{tr} \tag{12b}$$

For our analyses, cementite is modelled after the elastic-perfect plastic model. The strain-hardening rate for cementite is 0 because it is constant. The cross-section A rapidly becomes smaller to maintain the material's volume, V at yield stress. Meaning, cementite undergoes necking at the moment it yields. This condition is highly unstable because cementite is unable to harden..

The stress-strain curve for ferrite is modelled by power plastic hardening material idealisation. It is represented by the following Swift's type equation [92]:

$$\sigma_{tr} = a\left(b + \varepsilon^{pl}\right)^N \tag{13}$$

This equation is a generalised power law, where true stress, σ_{tr} is an exponential product of plastic strain, ε^{pl}. Here, a, b and N are empirical constants determined

experimentally by Umemoto [99]. Their values are $a = 493$ MPa, $b = 0.002$ and $N = 0.28$ respectively.

The input of material properties into ANSYS© is in true stress, σ_{tr} versus total strain, ε^t relationship. Since the plastic flow is determined by Swift's type equation mentioned above in (13), the values for each true stress, σ_{tr} can be determined by any given plastic strain, ε^{pl}. The elastic region is determined by Hooke's law as aforementioned in the earlier section. Therefore, the total strain, ε^t is

$$\varepsilon^t = \frac{\sigma_{tr}}{E} + \varepsilon^{pl} \tag{14}$$

For our analyses, the data input for cementite and ferrite follows the true curve. On the contrary, the models are given forced displacements, so the analysis results or simulation data are plotted nominally. Fig. 8 shows the difference between the true and nominal curve for cementite. The stress values for simulation data, which are represented by the nominal curve, will decrease around yield point because the instantaneous cross-section area A, was neglected to simplify the data harvesting.

2.4 von Mises yield condition

The onset of plastic deformation in metal occurs when the combination of stresses in the material reaches a certain critical value. The von Mises yield condition [100]

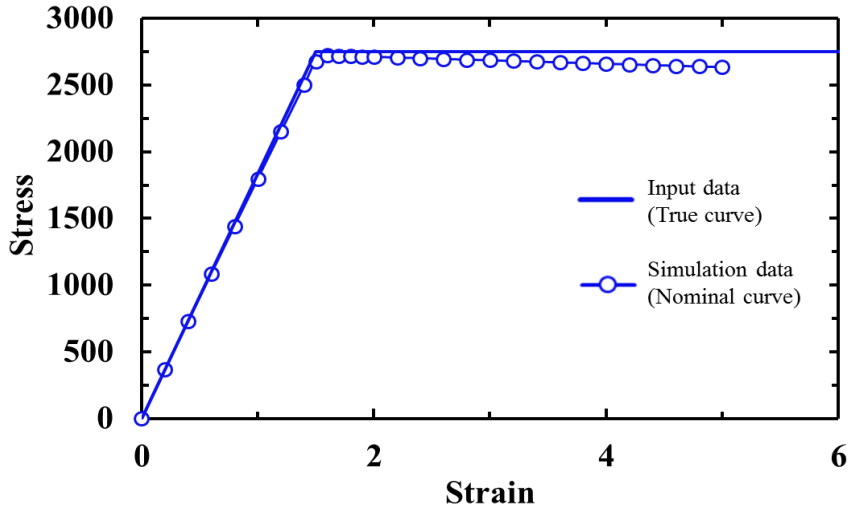

Fig. 8 Stress-strain curve for true and nominal curve for cementite. This figure shows the plastic flow stress for elastic-perfect plastic material stress established for cementite in comparison to the simulated data.

expressed in (15) defines the critical value.

$$J_2 = k^2 \tag{15}$$

The second deviatoric stress, commonly written as J_2 is related to the changes of the material shape. The yield stress in simple shear is given as k. Since there are six components of stress, J_2, (15) can be represented as follows:

$$J_2 = (\sigma_{xx} - \sigma_{yy})^2 + (\sigma_{yy} - \sigma_{zz})^2 + (\sigma_{zz} - \sigma_{xx})^2 + 6\tau_{xy}^2 + 6\tau_{yz}^2 + 6\tau_{zx}^2 \tag{15a}$$

When a material is under multiaxial loading condition, the equivalent stress denoted as σ_{eq} is defined in (16).

$$\sigma_{eq} = \sqrt{3J_2} \tag{16}$$

Square both sides of the (16) and then substitute (15a) into the equation.

$$\begin{aligned}\sigma_{eq}^2 &= 3J_2 \\ &= 3\left((\sigma_{xx}-\sigma_{yy})^2+(\sigma_{yy}-\sigma_{zz})^2+(\sigma_{zz}-\sigma_{xx})^2+6\tau_{xy}^2+6\tau_{yz}^2+6\tau_{zx}^2\right) \\ &= 3\left((\sigma_{xx}-\sigma_{yy})^2+(\sigma_{yy}-\sigma_{zz})^2+(\sigma_{zz}-\sigma_{xx})^2\right)+3\left(6\tau_{xy}^2+6\tau_{yz}^2+6\tau_{zx}^2\right) \\ &= \frac{3}{6}\left((\sigma_{xx}-\sigma_{yy})^2+(\sigma_{yy}-\sigma_{zz})^2+(\sigma_{zz}-\sigma_{xx})^2\right)+3\left(\tau_{xy}^2+\tau_{yz}^2+\tau_{zx}^2\right) \\ &= \frac{1}{2}\left((\sigma_{xx}-\sigma_{yy})^2+(\sigma_{yy}-\sigma_{zz})^2+(\sigma_{zz}-\sigma_{xx})^2\right)+3\left(\tau_{xy}^2+\tau_{yz}^2+\tau_{zx}^2\right)\end{aligned} \tag{16a}$$

Multiply both sides of (16a) with 2 to even the denominator of the equation.

$$2\sigma_{eq}^2 = (\sigma_{xx}-\sigma_{yy})^2+(\sigma_{yy}-\sigma_{zz})^2+(\sigma_{zz}-\sigma_{xx})^2+6\tau_{xy}^2+6\tau_{yz}^2+6\tau_{zx}^2 \tag{16b}$$

Thus, the equivalent stress, σ_{eq} is expressed as (15c).

$$\sigma_{eq} = \sqrt{\frac{(\sigma_{xx}-\sigma_{yy})^2+(\sigma_{yy}-\sigma_{zz})^2+(\sigma_{zz}-\sigma_{xx})^2+6\tau_{xy}^2+6\tau_{yz}^2+6\tau_{zx}^2}{2}} \tag{16c}$$

This form is also known as the von Mises stress. From (15), the relationship in (16a) can also be expressed as (17).

$$\sigma_{eq}^2 = 3J_2 = 3k^2 \tag{17}$$

In the case of uniaxial stress, the yield stress in simple shear relationship with the tensile yield stress, Y , is given in (18).

$$k = \frac{Y}{\sqrt{3}} \tag{18}$$

Square both sides of (18).

$$\begin{aligned}k^2 &= \frac{Y^2}{3} \\ 3k^2 &= Y^2\end{aligned} \tag{18a}$$

Compare (17) and (18a).

$$\sigma_{eq}^2 = 3k^2 = Y^2 \tag{18b}$$

From (18b), if $\sigma_{eq}^2 = Y^2$, therefore (16b) can be rearranged into (18c).

$$(\sigma_{xx} - \sigma_{yy})^2 + (\sigma_{yy} - \sigma_{zz})^2 + (\sigma_{zz} - \sigma_{xx})^2 + 6\tau_{xy}^2 + 6\tau_{yz}^2 + 6\tau_{zx}^2 = 2Y^2 \tag{18c}$$

This equation defines the yield surface of the von Mises circular cylinder in the principal stresses space, which is denoted by σ_1, σ_2, and σ_3, as shown in Fig. 9. The von Mises yield locus is $\sqrt{\frac{2}{3}}Y$.

In equation (18), the von Mises yield condition proposed that the onset of plastic deformation is when the equivalent stress or the von Mises stress, σ_{eq} is equal to the tensile yield stress, Y. By neglecting the Bauschinger effect, any stress points on the surface of the cylinder will correspond to a state of yielding. Whereas, any stress points inside the cylinder correspond to a state of elastic deformation. In simple tension, (18b) can be further simplified as (19).

$$\begin{aligned} \sigma_{eq}^2 &= Y^2 \\ \sigma_{eq} &= Y \\ \sigma_{eq} - Y &= 0 \end{aligned} \tag{19}$$

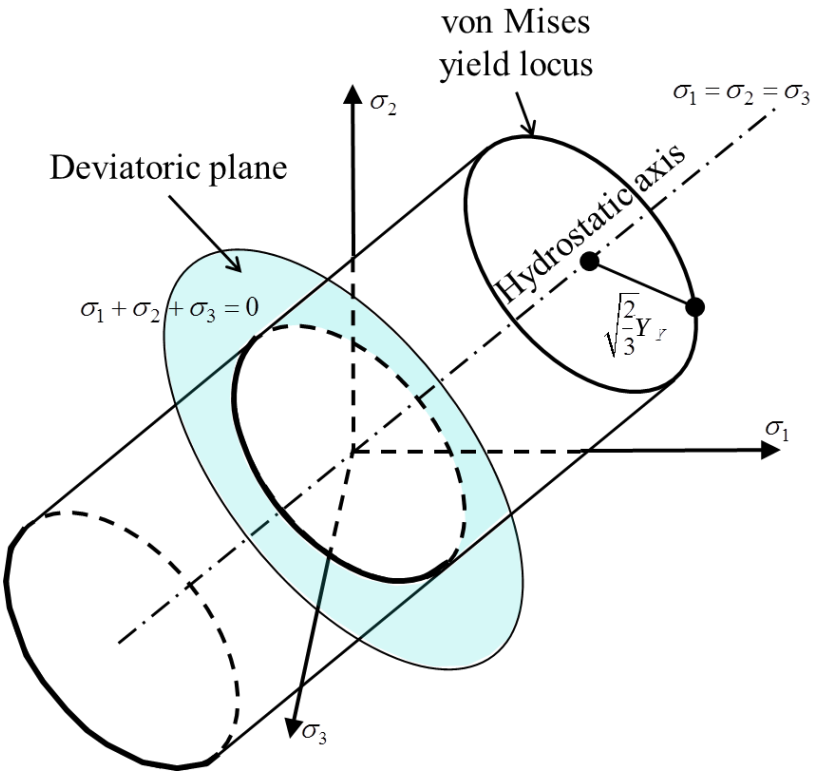

Fig. 9 Diagram of the von Mises yield condition in the principal stress space.

In Fig. 9, the cylinder is inclined so that the direction cosines of the hydrostatic axis of each of the principal stress axes are equal, $(1/\sqrt{3},1/\sqrt{3},1/\sqrt{3})$. Thus, at the hydrostatic axis, the principal stresses are equal, $\sigma_1 = \sigma_2 = \sigma_3$. On the other hand, the deviatoric plane where the sum of principle stresses are equal to zero, $\sigma_1 + \sigma_2 + \sigma_3 = 0$, is perpendicular to the hydrostatic axis. These configurations imply that the von Mises yield locus is not only parallel to the deviatoric plane, but also symmetrical at the σ_1 -, σ_2 -, σ_3 and -axes. The uniform hydrostatic stress does not affect the yield state of a

deforming body. The hydrostatic stress influences volume change, therefore, the volume of the material is constant after yielding. von Mises yield condition depends on the magnitude and direction of the deviatoric stress, as defined in (15).

2.5 The associative flow-rule

The associated flow-rule [101,102] is defined when the plastic potential of the material is the yield function. In other words, the flow rule is associated with a particular yield condition. In this study, von Mises yield condition is employed. Fig. 10 shows the axes of principal stress and principal plastic strain, which are denoted as $\sigma_1, d\varepsilon_1^{pl}$, $\sigma_2, d\varepsilon_2^{pl}$ and $\sigma_3, d\varepsilon_3^{pl}$; and their relationship with the plastic strain increment vector, which is denoted as $d\boldsymbol{\varepsilon}^{pl}$. The vector of principal stress, is denoted as $d\boldsymbol{\sigma}$. The normal to the yield surface is given as the differentiation of yield function $f\left(\sigma_{ij}\right)$

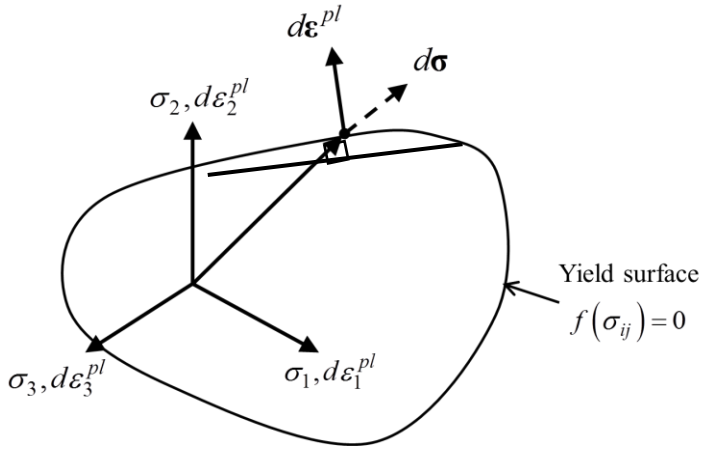

Fig. 10 The relationship between yield surface and strain increment.

towards the vector of the principal stress $d\boldsymbol{\sigma}.\sigma_{ij}$ is the multiaxial stresses. This is called the normality rule and it has been confirmed experimentally on metals. The equation of the associate flow-rule is given as:

$$d\varepsilon_{ij}^{pl} = \frac{\partial f}{\partial \sigma_{ij}} d\lambda \tag{20}$$

f is the yield function and $d\lambda$ is the principal deviatoric stresses and principal plastic strain increments. In 3-D space, which axes constitute of (*x*, *y*, *z*); the ($d\lambda$) is expressed by (20a), where the stress deviations are denoted as $s_{xx}, s_{yy}, s_{zz}, s_{xy}, s_{yz}, s_{zx}$.

$$\frac{d\varepsilon_{xx}^{pl}}{s_{xx}} = \frac{d\varepsilon_{yy}^{pl}}{s_{yy}} = \frac{d\varepsilon_{zz}^{pl}}{s_{zz}} = \frac{d\varepsilon_{xy}^{pl}}{s_{xy}} = \frac{d\varepsilon_{yz}^{pl}}{s_{yz}} = \frac{d\varepsilon_{zx}^{pl}}{s_{zx}} = d\lambda \tag{20a}$$

The stress deviations represented by s_{ij} are the subtracts of mean normal stress which is denoted as s from the normal stress tensors which are represented by σ_{ij}.

$$s_{ij} = \sigma_{ij} - s \tag{21}$$

The mean normal stress relationship with normal stress is defined in (22).

$$s = \frac{1}{3}\left(\sigma_{xx} + \sigma_{yy} + \sigma_{zz}\right) \tag{22}$$

By applying the von Mises yield condition in (19) to the example of tensile deformation in the direction of *x*, the non-vanishing stress component is σ_{xx}. The non-vanishing stress component for *y* and *z* direction are shown in (22b) together with *x*.

$$\begin{aligned} s_x &= \frac{2}{3}\sigma_{xx} \\ s_y &= -\frac{1}{3}\sigma_{yy} \\ s_z &= -\frac{1}{3}\sigma_{zz} \end{aligned} \tag{22b}$$

Regarding normal stresses, the stress-plastic strain relationships are given as:

$$\begin{aligned}
d\varepsilon_{xx}^{pl} &= \frac{2}{3}d\lambda\left[\sigma_{xx}-\frac{1}{2}\left(\sigma_{yy}+\sigma_{zz}\right)\right] \\
d\varepsilon_{yy}^{pl} &= \frac{2}{3}d\lambda\left[\sigma_{yy}-\frac{1}{2}\left(\sigma_{xx}+\sigma_{zz}\right)\right] \\
d\varepsilon_{zz}^{pl} &= \frac{2}{3}d\lambda\left[\sigma_{zz}-\frac{1}{2}\left(\sigma_{xx}+\sigma_{yy}\right)\right] \\
d\varepsilon_{xy}^{pl} &= d\lambda\tau_{xy} \\
d\varepsilon_{yz}^{pl} &= d\lambda\tau_{yz} \\
d\varepsilon_{zx}^{pl} &= d\lambda\tau_{zx}
\end{aligned} \tag{23}$$

In ANSYS©, the flow-rule for elasto-plastic deformation is calculated by the Prandtl-Reuss equations [102-104], and the equations are represented using Hooke's law as follows:

$$\begin{aligned}
d\varepsilon_{xx}^{pl} &= \frac{1}{E}\left[d\sigma_{xx}-\nu\left(d\sigma_{yy}+d\sigma_{zz}\right)\right]+\frac{2}{3}d\lambda\left[\sigma_{xx}-\frac{1}{2}\left(\sigma_{yy}+\sigma_{zz}\right)\right] \\
d\varepsilon_{yy}^{pl} &= \frac{1}{E}\left[d\sigma_{yy}-\nu\left(d\sigma_{xx}+d\sigma_{zz}\right)\right]+\frac{2}{3}d\lambda\left[\sigma_{yy}-\frac{1}{2}\left(\sigma_{xx}+\sigma_{zz}\right)\right] \\
d\varepsilon_{zz}^{pl} &= \frac{1}{E}\left[d\sigma_{zz}-\nu\left(d\sigma_{xx}+d\sigma_{yy}\right)\right]+\frac{2}{3}d\lambda\left[\sigma_{zz}-\frac{1}{2}\left(\sigma_{xx}+\sigma_{yy}\right)\right] \\
d\varepsilon_{xy}^{pl} &= \frac{1+\nu}{E}d\tau_{xy}+d\lambda\tau_{xy} \\
d\varepsilon_{yz}^{pl} &= \frac{1+\nu}{E}d\tau_{yz}+d\lambda\tau_{yz} \\
d\varepsilon_{zx}^{pl} &= \frac{1+\nu}{E}d\tau_{zx}+d\lambda\tau_{zx}
\end{aligned} \tag{23a}$$

Chapter 3

Modelling of pearlite colony

3.1 Morphology of cementite in pearlite

The morphology and evolution of pearlite microstructure is a subject of interest. Researchers are intrigued by the plastic deformability of cementite inside of pearlite because it determines the plastic deformation of pearlite [22]. The revision of literature reviews [22,37,40,41,63] disclosed that many studies agreed on categorising the morphology of cementite in pearlite during tensile deformation into three main types as shown in Fig. 11. In Fig. 11(a), the alignment of cementite is parallel to the tensile axis. In Fig. 11(b), the alignment of cementite is inclined at a certain degree of inclination angle, from the tensile axis. In Fig. 11(c), the alignment of cementite is perpendicular to the tensile axis. From the tensile axis point of view, if the lamellar alignment is parallel to the tensile axis, the angle is $0°$, whereas, if the lamellar alignment is perpendicular to the axis, the angle is $90°$. Therefore, the range for the inclination angle of a colony is considered as $0° \le \varphi \le 90°$, where φ is the inclination angle. At inclination angle

$\varphi = 45°$, the lamellar structure suffers maximum shear stress [44,56,57,99]. Therefore, this angle will be considered for the model type illustrated in **Fig. 11(b)**.

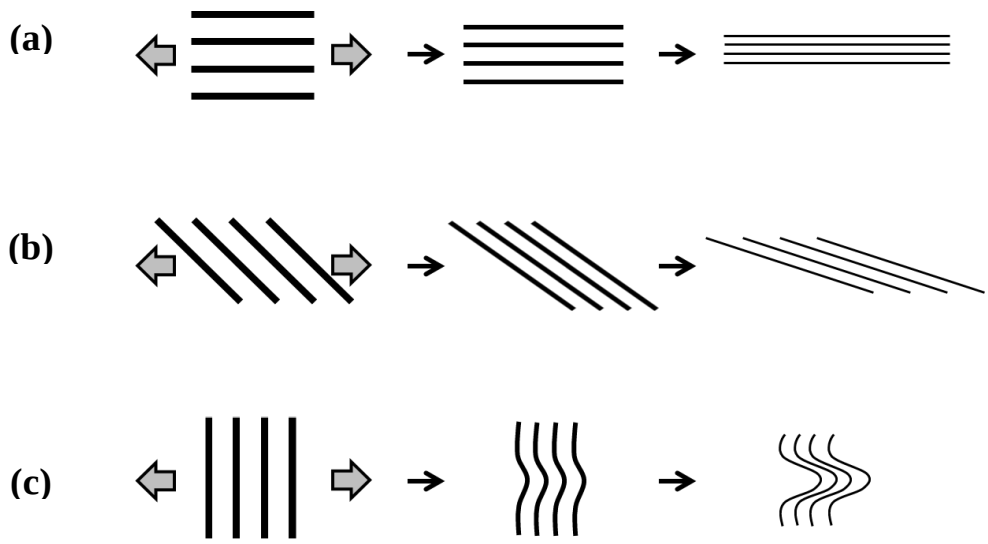

Fig. 11 Basic types of the morphology of cementite in pearlite microstructure.

3.2 Defining the alignment of cementite lamella in 3-D space

In calculating, the inclination angle of lamellar alignment in pearlite, Belaiew [32] assumed that cementite and ferrite lamellae are parallel and are closely packed inside a sphere. Inside a sphere, the coordinate of a point is determined by two angles from the orthogonal plane and the axis perpendicular to the orthogonal plane. Therefore the position of the lamella alignment in a 3-D space is explained using the idea of spherical coordinates.

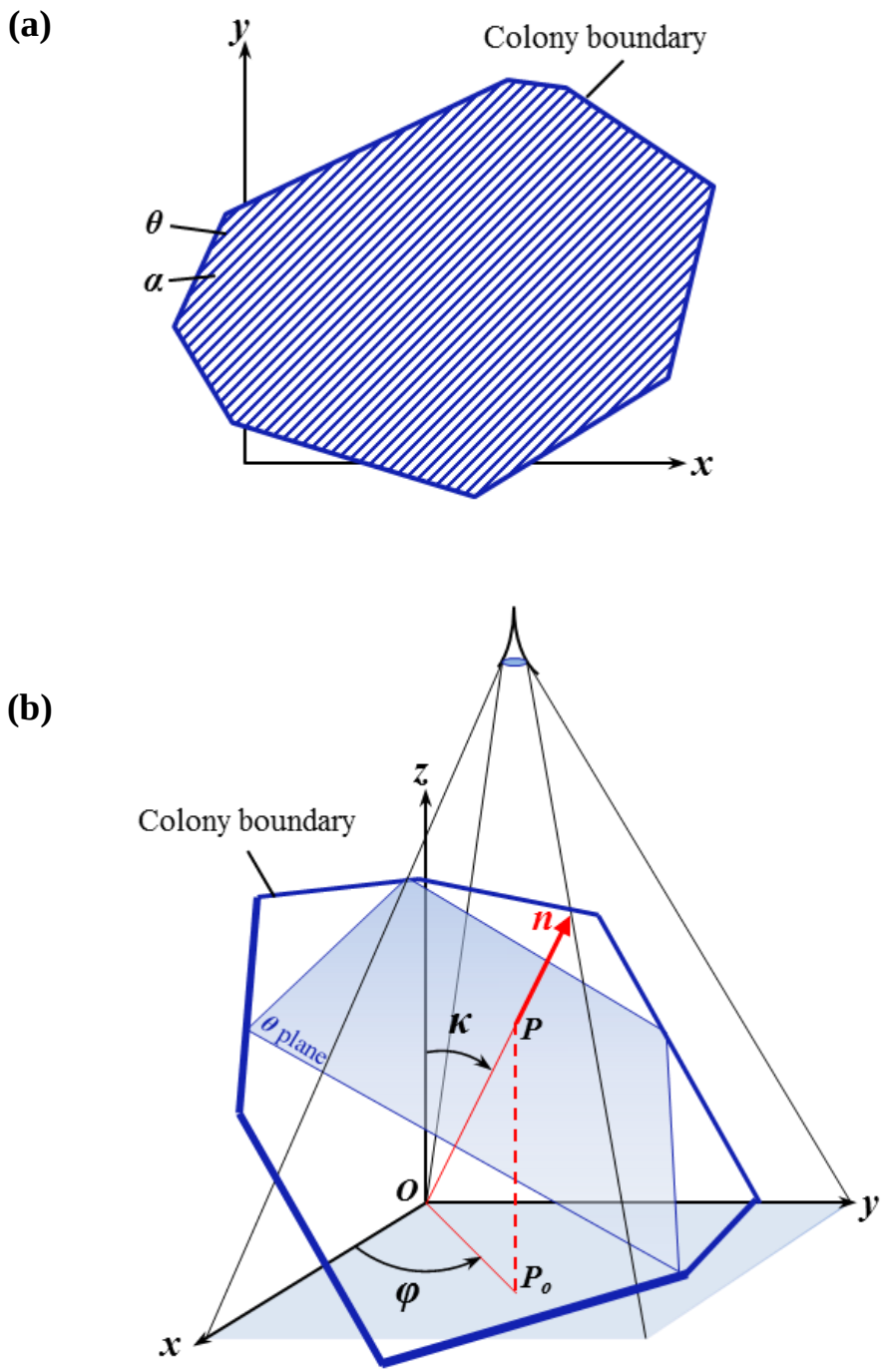

Fig. 12 Schematic of 2-D orthogonal projection and 3-D view of a pearlite colony. (a) is the orthogonal projection of cementite (θ) and ferrite (α) lamellar. (b) The direction of the θ plane is determined by the direction of normal vector, n. The direction of n is determined by the azimuthal angle at the *xy*-plane, φ and the inclination angle from *z*-axis, κ of the θ plane in 3-D space.

Fig. 12 illustrates the 2-D orthogonal projection of 3-D colony structure. Imagine the surface area of a colony lying on *xy*-plane as illustrated in Fig. 12(a). The parallel blue stripes represent cementite lamellae, which are denoted as θ. The white stripes are Ferrite lamella, iares denoted as α. From here onwards, cementite and ferrite are designated as θ and α respectively. Fig. 12(b) shows the position of a θ plane in 3-D space where the axis which is perpendicular to the *xy*-plane, is represented by the *z*-axis. The middle point of θ plane is point P where the normal vector n intersects. The direction of n will determine the alignment of θ plane in this study.

Next, point P_o is the orthogonal projection of point P on the *xy*-plane. The inclination of vector $\overline{OP_o}$ from the *x*-axis is the azimuthal angle φ. In most observations of pearlite microstructure, researches rely on the orthogonal projection of the pearlite colony. Thus, the "observed" lamellar alignment is actually the inclination of the azimuthal angle, φ. In fact, there is another angle that needs to be considered. This angle is the inclination of vector $\overline{OP}$ from the *z*-axis, angle κ.

3.3 Crystallography of cementite (θ) and ferrite (α)

The interphase plane or habit plane of θ and α in pearlite is commonly given by Bagaryatsky [75] and Pitsch-Petch [76,77] relationship. The ductile constituent α

bears the initial slip before cementite deforms [40]. Even so, the fractures in α are found to be a result of cementite shearing [67]. θ maintains the crystallography with α after severed by plastic deformation [40,66]. θ is assumed to be elastically isotropic [105], but before slip, the plastic deformation of the crystals are reported to be anisotropic [106]. Regardless, the deformation of θ is suggested to depend on the Schmid's factor [65,106]. The plastic deformation in α is influenced by θ [58]. On top of that, the deformation of θ depends on the angle of inclination of the alignment against the load axis [22,39-41,63]. Therefore, we assume α to have infinite slip systems. This assumption allows us to simplify the models and neglect the crystallography to conduct the analysis with the classical theory of elasto-plastic deformation.

Empty page

Chapter 4

Elasto-plastic deformation of single-colony models

4.1 Introduction

A single-colony is a lamellar structure. The elasto-plastic deformation in pearlite colony structure is the interaction of elasto-plastic deformation occurring between differently aligned lamellar structure. Therefore, it is crucial to understand the mechanism of a single-colony. There have been various studies dedicated to its strengthening mechanism [14-18,20-22,27,30,38,51]. The material properties for α has been established in Chapter 2.3 with Swift's type equation [92] in (13). It is well known that the strength of pearlite increases with the decrease of lamellar thickness. The lamellar thickness of α in fine pearlite steel is typically about 100*nm*. According to Hall-Petch relationship, at this size, the lamellar structure is expected to have strong scale effect, which improves the strength of pearlite altogether. The plastic deformation of bulk θ is highly unstable, but the plastic deformability of θ has improved by

layering it with α [52,53]. The plastic deformation of θ is delayed because α lamellae prevent localisation of strain by spreading the distribution of stress. Therefore, the larger the stress can be accommodated by α, the more stable the plastic deformation of θ. However, various parameters control the plastic flow stress of α. For this purpose, a hypothetical stress-strain relationship is introduced by modifying Swift's type equation. Tanaka and Matsuoka [56] studied the influence of inclination angle from the tensile axis towards stress in θ lamellar. Their studies showed that θ exhibited maximum stress because α was able to deform plastically at the highest tension stress when the alignment of lamellar was parallel to the tensile axis. This suggested the endurance of θ in pearlite depends on the plastic flow of α, which is similar with the Hall-Petch relationship of size effect. We used 2-D lamellar model to study and confirm the effect of α on the stability of plastic deformation in θ. Next, we examined the effect of lamellar alignment on the mechanical response in single-colony by studying the angular dependency of θ lamellae in colony towards the tensile axis with 3-D single-colony models.

4.2 Suppression of plastic deformation in cementite (θ) by increased strain hardenability of ferrite (α) phase.

4.2.1 Modelling of lamellar structure models

Fig. 13 is the schematic illustration of a five-layered pearlite model. To induce stress concentration in the middle layer of θ, the mid-section is indented by a cosine function in (24). θ and α are alternately layered.

$$y = d\cos\left(\frac{2\pi x}{L}\right) \tag{24}$$

The aspect ratio of the lamellar thickness and length, which are denoted as d and L, is 0.5%. The indentation is at, $x = 0$ and the thinness section is 98% of the original lamellar thickness. The model is fixed along the *x*-axis at the left lateral surface. Force-displacement is given at the right lateral surface.

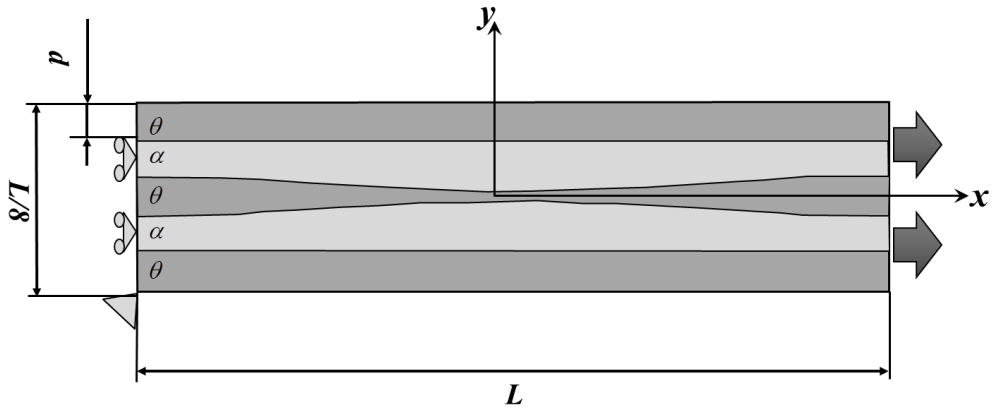

Fig. 13 Schematic of five-layered pearlite model. The indentation at the mid-section of the central cementite is a cosine function. It is fixed along the *x*-axis at the left lateral surface, while forced displacement is given at the right lateral surface. The illustration is exaggerated.

The modified Swift's type equation is shown in (25). Constant c is introduced to control the yield strength or flow stress level.

$$\sigma_{tr} = a\left(b + \varepsilon^{pl}\right)^{N} + c \tag{25}$$

The modified properties of α showed combinations of high yield stress or flow stress level and strain-hardening rate. The strain-hardening rate is the gradient of the flow stress curve derived in (12b), Chapter 2. The constant c in (24) is the interception of stress-strain curve with the true stress σ_{tr} axis (the vertical axis) at plastic strain $\varepsilon^{pl} = 0$ (on the horizontal axis). The mechanical properties of the original α are designated as Ferrite-org and the mechanical properties of the hypothetical materials, namely Ferrite5, Ferrite10 and Ferrite5n500 are listed in Table 1. The values of *a*, *b*, and *N* for Ferrite-org were taken from Umemoto [99]. The stress-strain curve is shown in Fig. 14.

Table 1 Mechanical properties of ferrite (α)

Types of Ferrite	Young's modulus [Gpa]	Poisson's ratio	Yield Stress [MPa]	a [MPa]	b	N	c [MPa]
Ferrite-org	200	0.3	86.5	493	0.002	0.28	0
Ferrite5	200	0.3	432.6	2465	0.002	0.28	0
Ferrite10	200	0.3	865.0	4930	0.002	0.28	0
Ferrite5n500	200	0.3	848.1	493	0.002	0.056	500

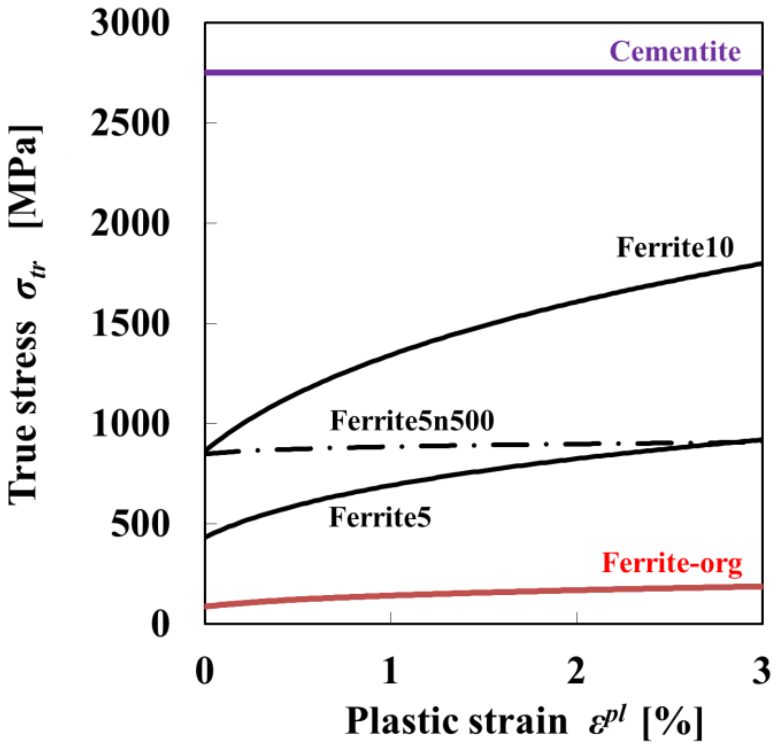

Fig. 14 True stress σ_{tr} vs. plastic strain ε^{pl} curves to compare Ferrite-org and the hypothetical Ferrite5, Ferrite 10 and Ferrite 5n500. θ is a constant.

As shown in Fig. 14, Ferrite-org displays the lowest flow stress level and the lowest strain-hardening rate. Ferrite5 shows higher flow stress level and strain-hardening rate. Ferrite 10 and Ferrite5n500 share the highest flow stress level. The strain-hardening rate of Ferrite10 is superior to all of the models while the strain-hardening rate of Ferrite5n500 is almost as low as Ferrite-org.

4.2.2 Results

Fig. 15 shows the distribution of tensile plastic component ε_{xx}^{pl} at nominal strain $\varepsilon_o = 1.529\%$ for pearlite lamellar structure with four different kinds of α. The distribution of strain is straight forward. Fig. 15(a) and Fig. 15(b) share the lowest strain-hardening rate. They exhibit bands of strain concentration originated from the central θ lamellar. If observed closely, the strain-hardening rate for Ferrite-org in Fig. 14 is slightly higher than that of Ferrite5n500. Although Ferrite5n500 have higher Flow stress level from Ferrite-org, it exhibits significant bands of strain concentration. This is why, the deformation in θ broadens around the central θ in Fig. 15(a) which indicates that higher strain-hardening help improve the plastic deformation in θ. Ferrrite5 and Ferrite10 exhibit no concentration of strain as shown in Fig. 15(c) and Fig. 15(d) respectively. Of course, the higher the level of flow stress and the strain-hardening rate, the more plastic deformation in cementite is suppressed. The strain-hardening rate influence is more significant than the level of flow stress for the stabilisation of plastic deformation in θ lamellar.

Fig. 16 shows the distribution of tensile stress component, σ_{xx} at nominal strain $\varepsilon_o = 1.529\%$ for pearlite lamellar structure with four different kinds of α. The results show that high flow stress level in α enables θ to bear stress better as shown

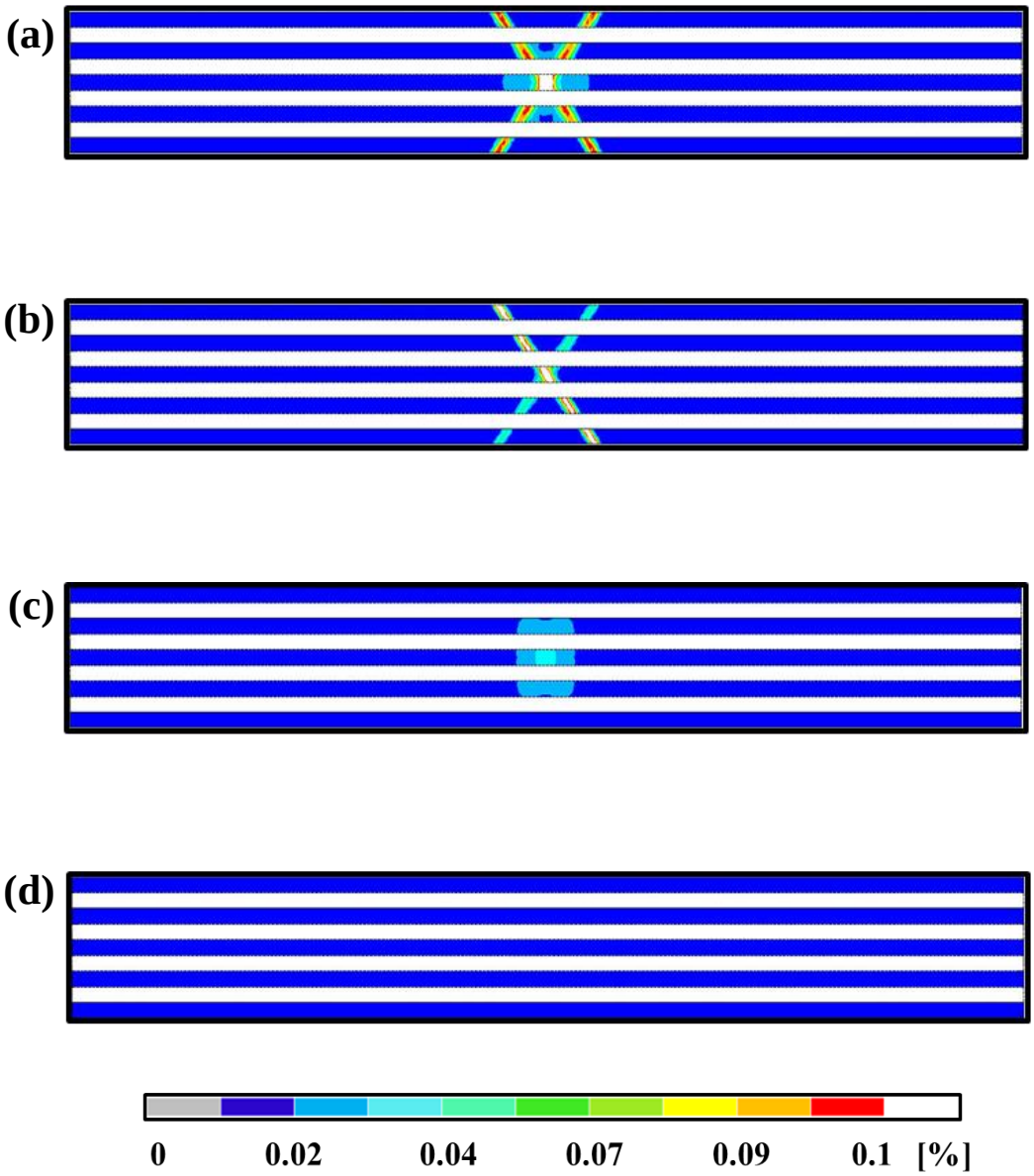

Fig. 15 Distribution of tensile plastic component ε_{xx}^{pl} at nominal strain $\varepsilon_o = 1.529\%$ in model (a) ferrite-org (low flow stress, low hardening rate), (b) Ferrite5n500 (high flow stress, low hardening rate) , (c) Ferrite5 (high flow stress, high hardening rate), and (d) Ferrite10 (high flow stress, high hardening rate).

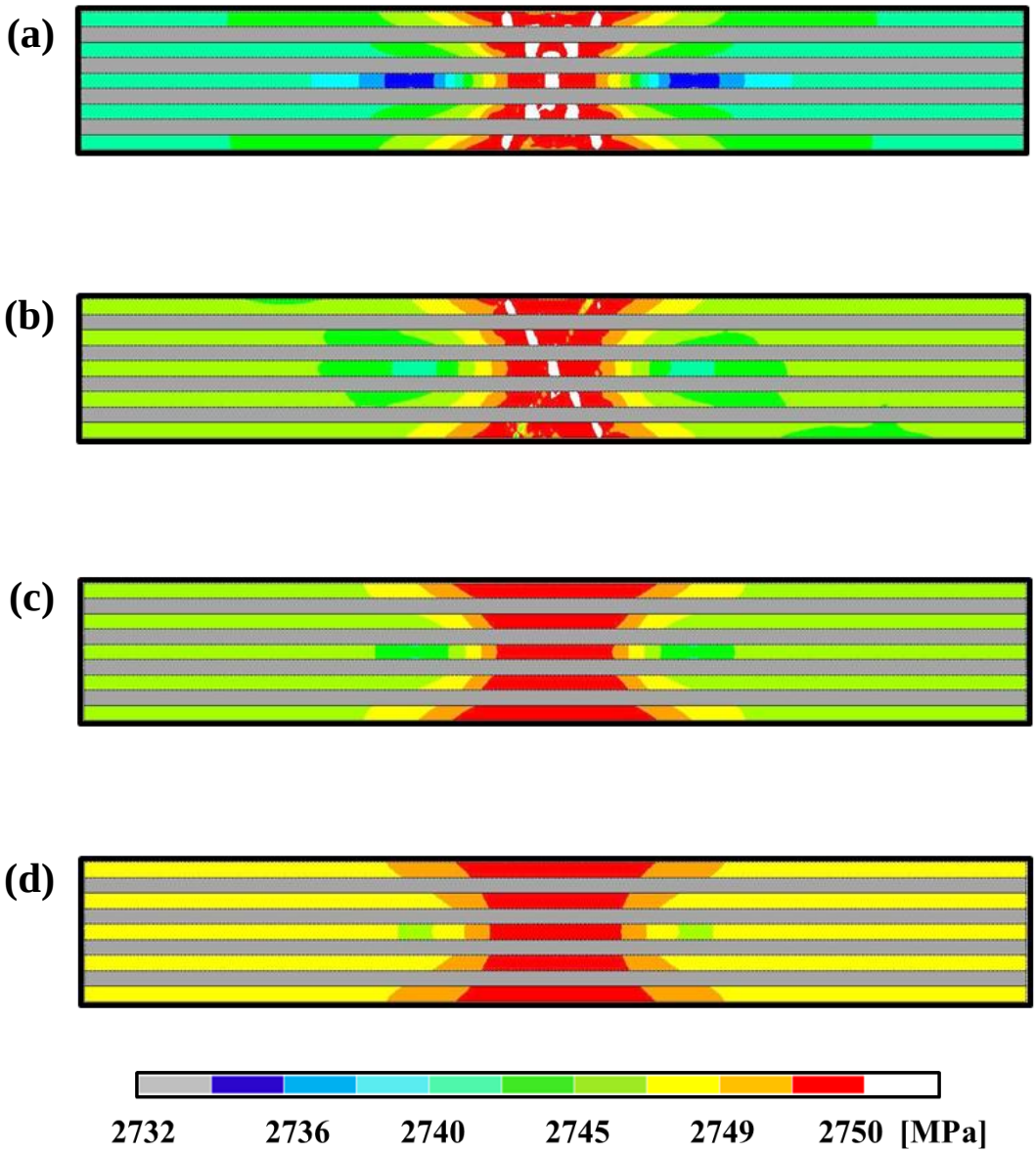

Fig. 16 Distribution of tensile stress component σ_{xx} at nominal strain $\varepsilon_o = 1.529\%$ in model (a) Ferrite-org (low flow stress, low hardening rate), (b) Ferrite5n500 (high flow stress, low hardening rate), (c) Ferrite5 (high flow stress, high hardening rate), and (d) Ferrite10 (high flow stress, high hardening rate).

in Fig. 16(b), Fig. 16(c), and Fig. 16(d).

Fig. 17 shows the nominal stress σ_o versus nominal strain ε_o curves of bulk cementite and three-layered lamellar structure models. The higher level of flow stress or yield strength of α gives higher Young's modulus to the stress-strain curves. However, models with low strain-hardening rate, Ferrite-org and Ferrite5n500, show a sudden drop of stress after θ yields, while those with higher strain-hardening rate show a slight increase before declining. This proves the strain-hardening rate of α plays a significant role in the stabilisation of plastic deformation of θ.

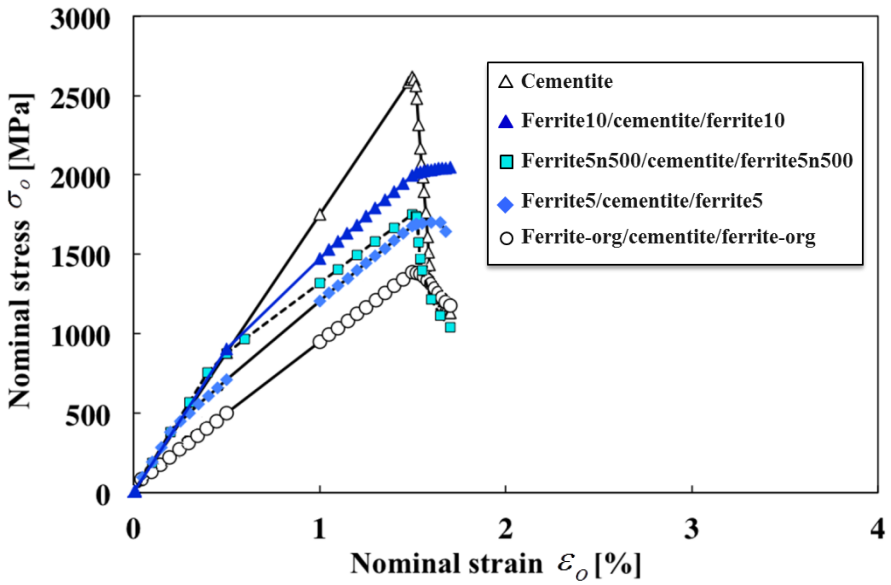

Fig. 17 The nominal stress σ_o vs. nominal strain ε_o curves of bulk cementite and three-layered lamellar structure models.

4.3 Effect of lamellar alignment of cementite (θ) towards the elasto-plastic deformation of single-colony models

4.3.1 3-D modelling of single-colony models

From the point of view of the tensile direction, which is the *x*-axis, the range that dictates the direction of n is a quadrant of the sphere if the mirror symmetry is considered. This means, the ranges of inclination are $0° \le \varphi \le 90°$ and $0° \le \kappa \le 45°$ as shown in the schematic of single-colony model in Fig. 18. The dimension of the model is $L \times L \times L$. The degrees of freedom (DOF) are fixed completely at the posterior bottom corner of the model and are fixed in the *y*-axis direction at the anterior bottom corner of the left lateral surface. The forced displacement is parallel to the *x*-axis. It is defined by the right lateral surface.

The single-colonies in Fig. 19 are alternately multi-layered cementite, denoted by θ and ferrite, denoted by α, lamellae structures. θ is dark grey and α is light grey. The orientation of each colony is determined by the normal vector *n* of the θ plane, which is the vector perpendicular towards the surface of the plane. There are four types of single-colony models, namely model-(a), model-(b), model-(c), and model-(d). The alignments of θ are arranged to be parallel, perpendicular, and inclined at $45°$ towards the tensile axis along the longitudinal axis. It must be understood that

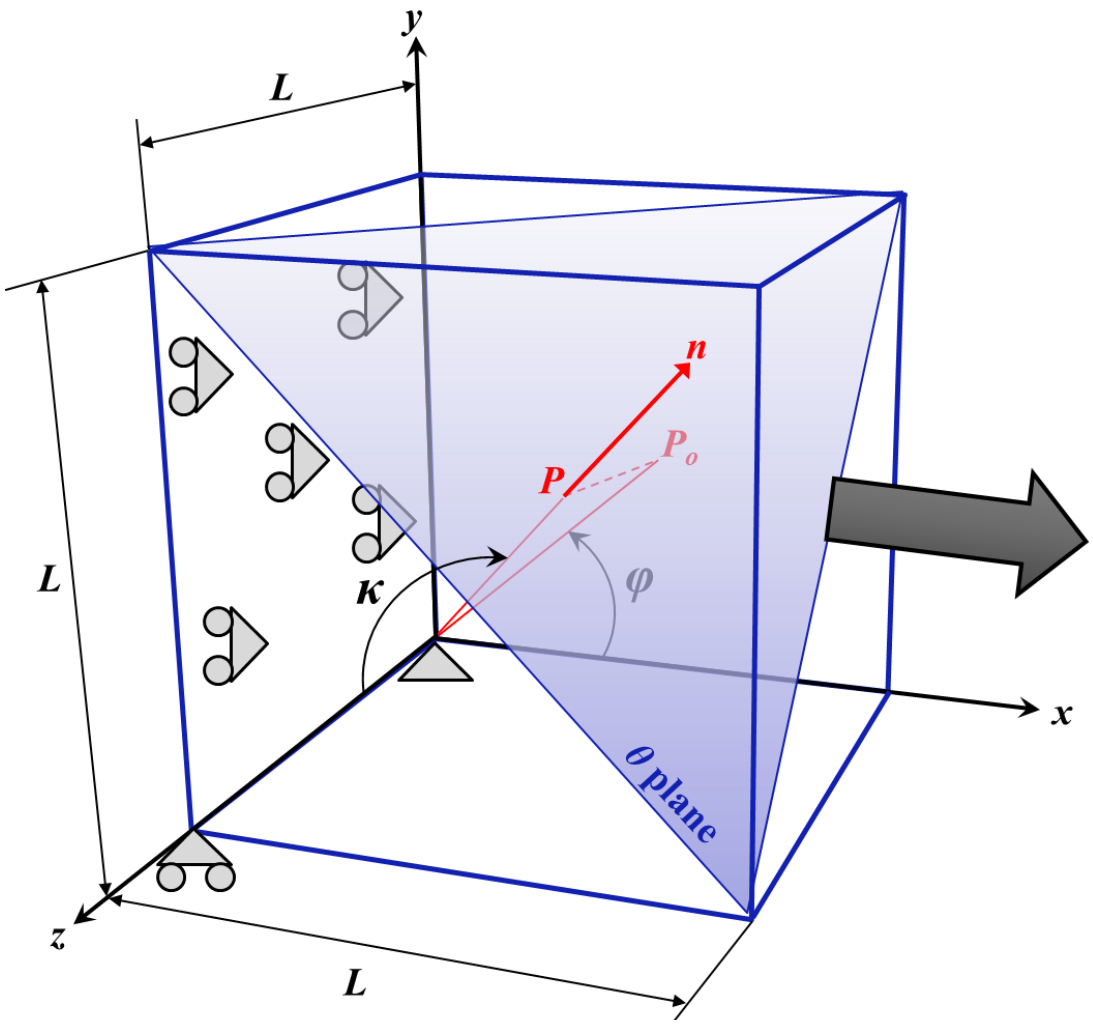

Fig. 18 Schematic of a single-colony model. Cementite lamellar is denoted as θ plane. The alignment of θ plane depends on the direction of normal vector, n which is determined by angle φ and κ. The schematic also defines the boundary conditions.

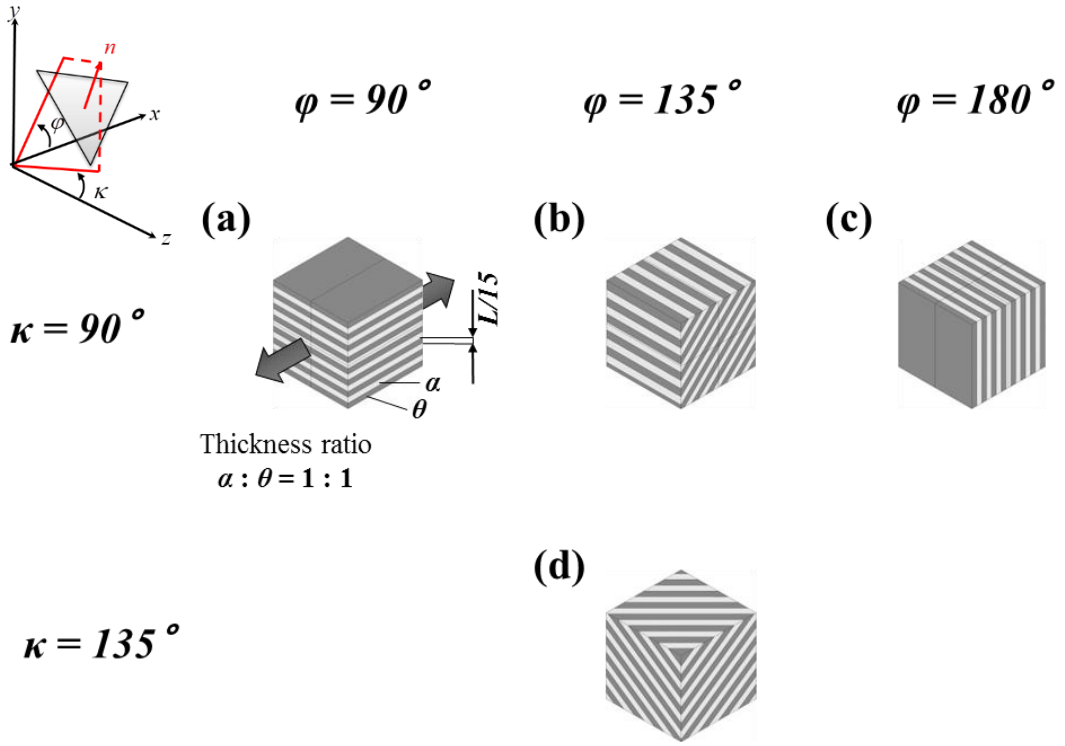

Fig. 19 Diagram of pearlite single-colony models. The dimension of the models are $L \times L \times L$. The thickness of the colony boundary, ferrite lamellae (α) and cementite lamellae (θ) are $L/15$.The alignment of θ is inclined at inclination angle φ first, then κ.

the angles φ and κ do not indicate the direction of the normal n of θ plane. Rather, they are the magnitude of the inclination angels of the lamellae in the order of: first inclination at the orthogonal plane, the *xy*-plane, which is denoted as φ and the second inclination from the normal axis of the orthogonal plane, the *z*-axis which is denoted as κ . The models are subjected to nominal strain $\varepsilon_o = 5\%$ tensile deformation by forced displacement. Ideally, the inclination angles of n are inclined at $0° \le \varphi \le 90°$ from the *x*-axis and subsequently inclined at $0° \le \kappa \le 45°$ from the *z*-axis. However, to ease the modelling process, the models are constructed at the mirror symmetry. So, the inclination angles are inclined at $90° \le \varphi \le 180°$ from the *x*-axis and subsequently inclined at $90° \le \kappa \le 135°$ from the *z*-axis.

4.3.2 Results

Fig. 20 shows the propagation of equivalent strain, ε_{eq}, in single-colonies taken at nominal strain $\varepsilon_o = 1.5\%$ and $\varepsilon_o = 3\%$. Fig. 21 shows the distribution of equivalent plastic strain ε_{eq}^{pl} and plastic tensile strain component ε_{xx}^{pl} at nominal strain $\varepsilon_o = 3\%$. From a general observation, the deformation of single-colonies generates intra-colony, and the strain expands outwardly for models that are not correctly aligned to the tensile direction as shown in Fig. 20(b), Fig. 20(c), and Fig. 20(d). By comparing Fig. 20 with

Fig. 21, it is obvious that the deformation is coherent with the tensile axis component σ_{xx} of the plastic deformation in α lamellar. Interestingly, θ phases in model-(a) and model-(c) show the tendency to deform plastically when the lamellar alignment is parallel with the tensile axis in Fig. 21(a), or perpendicular in Fig. 21(c) towards the tensile axis, rather than in model-(b) and model-(d), in which θ alignments are imposed to $45°$ of inclination as shown in Fig. 21(b) and Fig. 21(d).

Fig. 22 shows the distribution of equivalent elastic strain ε_{eq}^{el} at nominal strain $\varepsilon_o = 3\%$ in single-colonies. It seems that the small strain values of θ in model-(b) and model-(d) in Fig. 17(b) and Fig. 17(d) give an impression that these models are still at the earlier stages of elastic deformation although they are beyond the elastic limit of cementite, which is at nominal strain, $\varepsilon_o \approx 1.53\%$. When comparing the equivalent strain ε_{eq}^{pl} propagation in Fig. 20 and plastic strain components in Fig. 21 to the equivalent elastic strain ε_{eq}^{el} in Fig. 22, it seems that the plastic deformability of the α phase in single-colony models is governed by the strain incompatibility enforced by the θ phase. This idea applies to model-(a) in Fig. 20(a), Fig. 21(a), and Fig. 22(a), model-(b) in Fig. 20(b), Fig. 21(b), and Fig. 22(b) and model-(c) in Fig. 20(c), Fig. 21(c), and Fig. 22(c). The deformation of model-(d) is tricky and cannot be explained just by comparing these strain components. This also demonstrates the

necessity of 3-D finite element analyses employment in studying pearlite or any other microstructures. Unlike model-(b), θ phase in model-(d) deforms better elastically as shown in Fig. 22(d). Regardless, the α phase displays greater plastic strain value in Fig. 21(d). The configuration of θ the lamella in model-(b) and model-(d) are similar. They are both inclined at $45°$ from tensile axis, *x*-axis. However, model-(d) is further inclined at $45°$ from the *z*-axis, which is perpendicular to the *xy*-plane. The inconsistency in model-(d) provides a hint that the transversal deviation, in other words, the inclination from the *z*-axis, influences the elasto-plastic deformation of the single-colony. To understand what is occurring in model-(d), the distribution of total normal strain component ε_{yy}^{t} and total transverse strain component ε_{zz}^{t} at nominal strain $\varepsilon_o = 3\%$ shown in Fig. 23 were observed. Here, it is clear that the extra inclination angle of model-(d) in Fig. 23(d) allows the α lamellae to deform considerably in the normal and transverse axes, *y*- and *z*-axes. Although model-(b) in Fig. 23(b) shows the most value of strain for the normal c omponent; it shows little to no deformation in the transverse direction in comparison to the other models. In model-(a), Fig. 23(a) and model-(c), Fig 23(c), the distribution of strain is almost the same between the both phases. When the patterns of strain distributions in Fig. 23 were traced and compared with the equivalent plastic strain ε_{eq}^{pl} in Fig. 21, it is revealed that

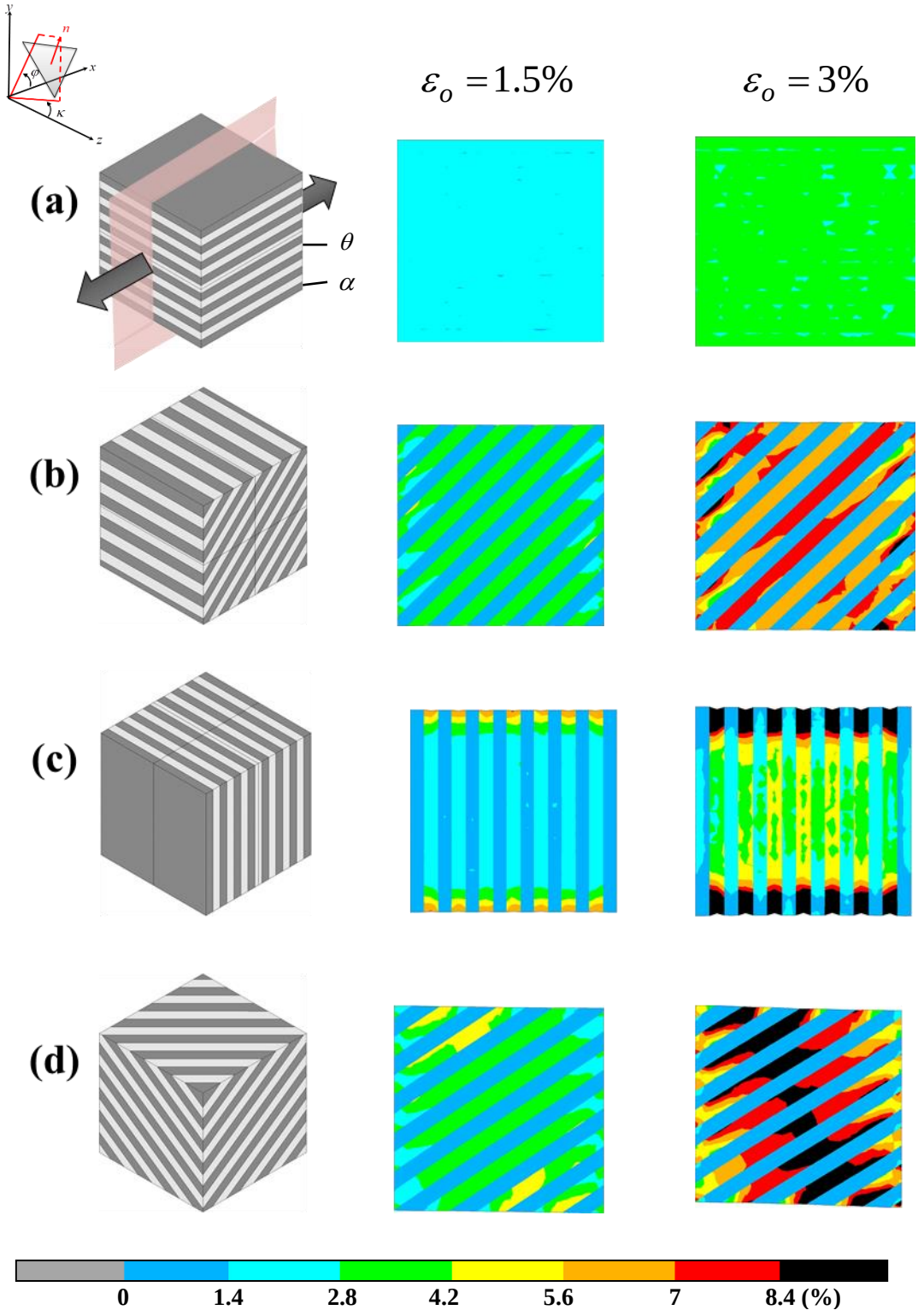

Fig. 20 Propagation of equivalent strain ε_{eq} in single-colony models at nominal strain $\varepsilon_o = 1.5\%$ and $\varepsilon_o = 3\%$.

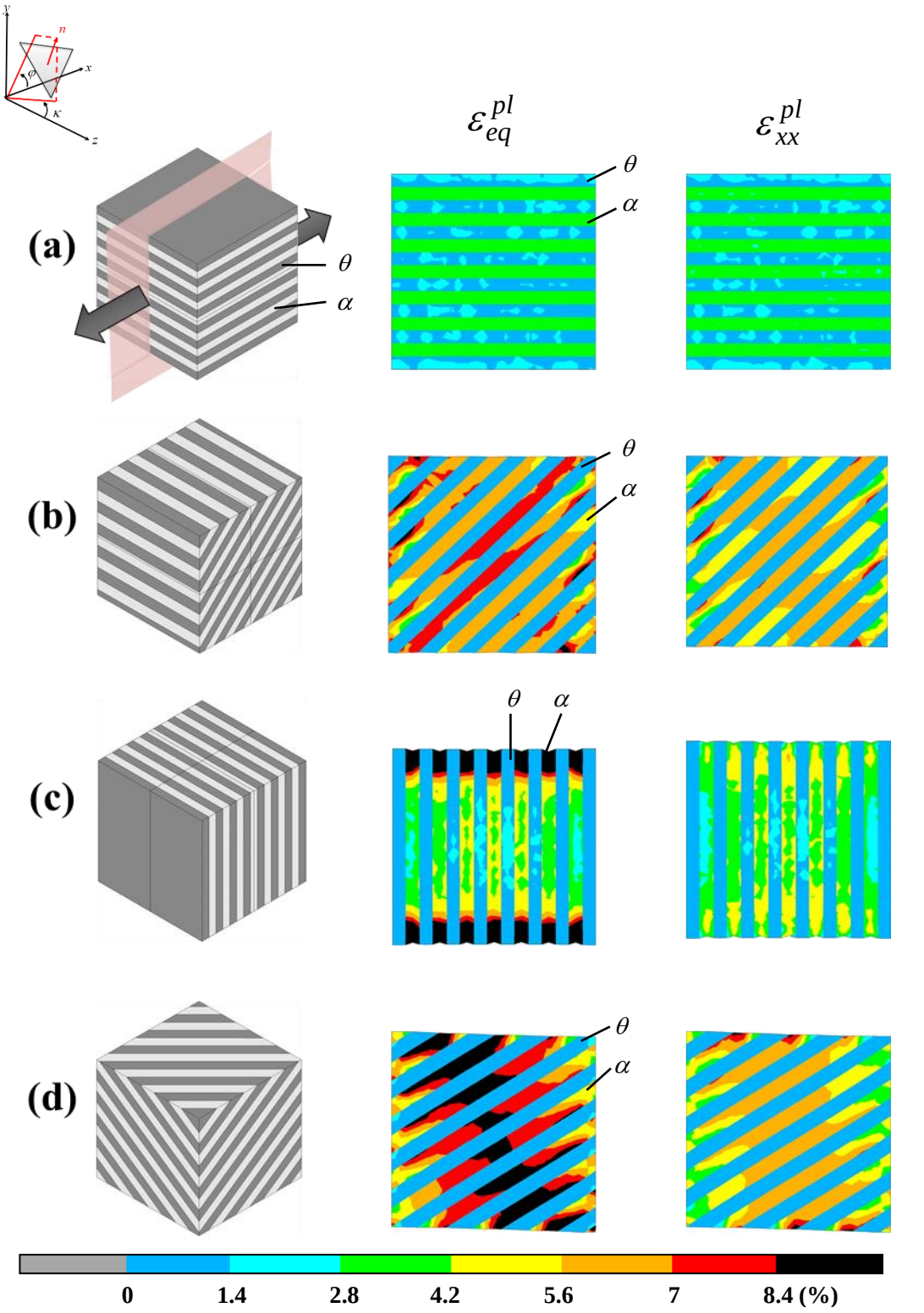

Fig. 21 Distribution of equivalent plastic strain ε_{eq}^{pl} and plastic tensile strain component ε_{xx}^{pl} in single-colony models at nominal strain $\varepsilon_o = 3\%$.

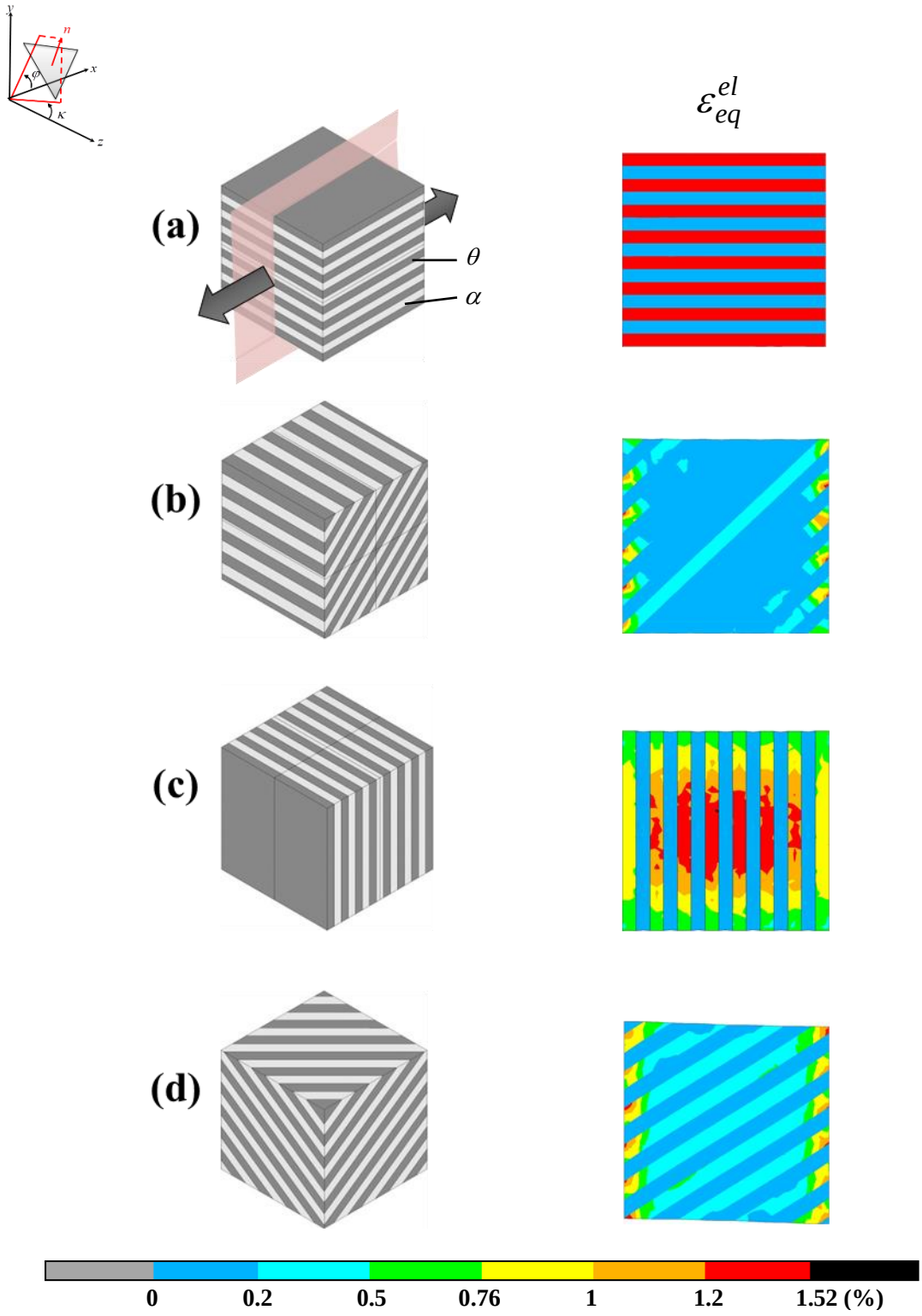

Fig. 22 Distribution of equivalent elastic strain ε_{eq}^{el} in single-colony models at nominal strain $\varepsilon_o = 3\%$.

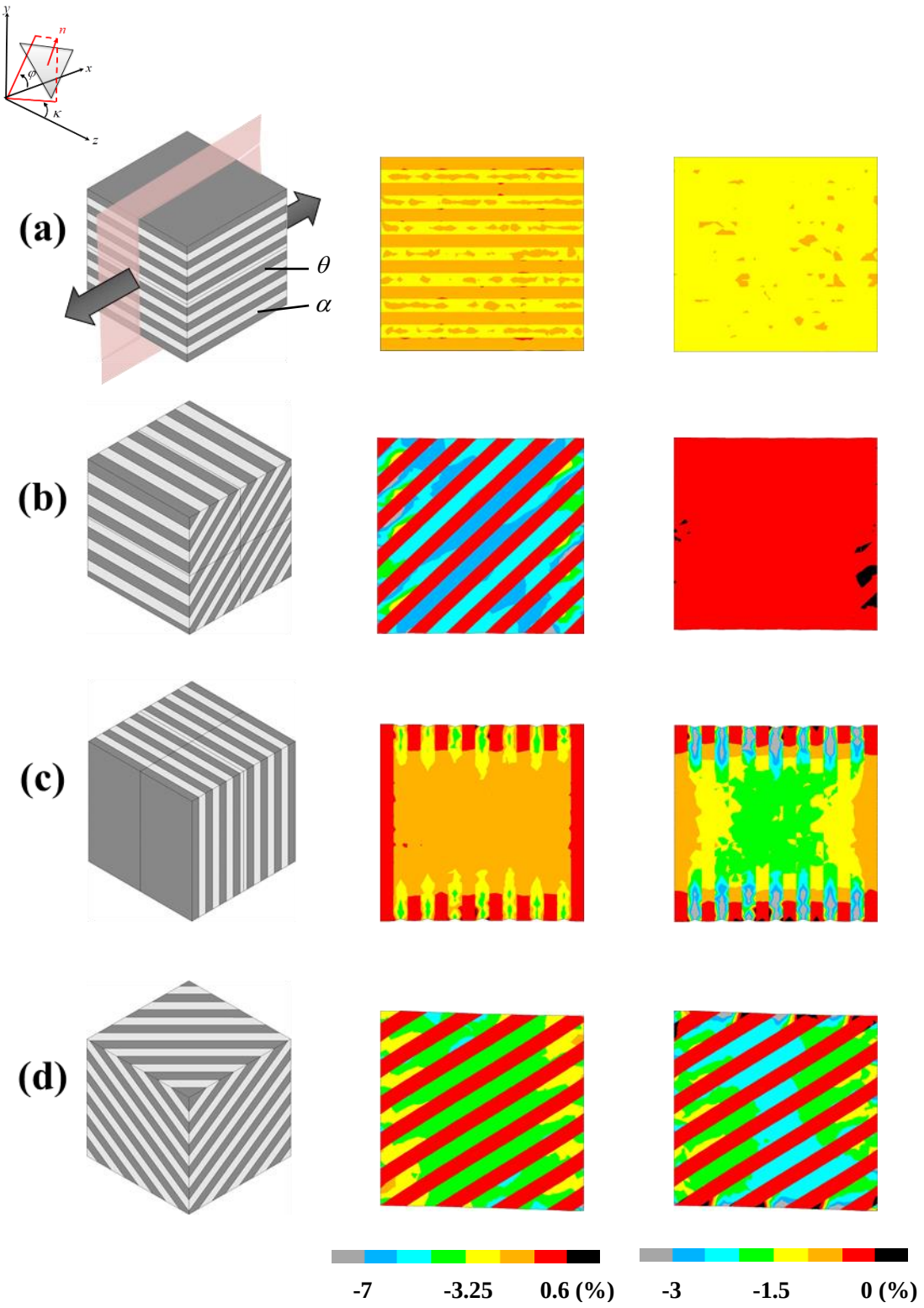

Fig. 23 Distribution of total normal strain component ε_{yy}^{t} and total transverse strain component ε_{zz}^{t} in single-colony models at nominal strain $\varepsilon_o = 3\%$.

the transversal plastic strain component ε_{zz}^{pl} accented the deformation in single-colonies especially for model-(d) in Fig. 21(d) and Fig. 23(d).

The following is Fig. 24, which shows the distribution of total shear strain of *xy*, *yz*, and *zx* components at nominal strain $\varepsilon_o = 3\%$. The surface *xy*- and *zx*-planes are parallel to the tensile direction. The *yz*-plane is the transverse surface normal to the tensile direction. The results revealed significant shear deformation at all planes occurring in model-(d) which rotates the single-colony. This is because of its multi-axial deformability. On the contrary, other models showed poor shear deformations. From these results, when the plastic deformation of α phase along the tensile direction is constrained by the deformability of θ phase, it will compensate for plastic deformation in other directions if the orientation of θ lamellae is tilted transversely. In other words, α lamellae deform along the direction of the θ lamella. Since the deformation of single-colony models is the deformation of α the lamella, therefore, the overall deformation in single-colony models is governed by the orientation of θ, whether the deformation is against the tensile direction or the transversal direction. These results also showed that the lamellar alignment needs to have more than one angular deviation from the tensile direction to shear deform.

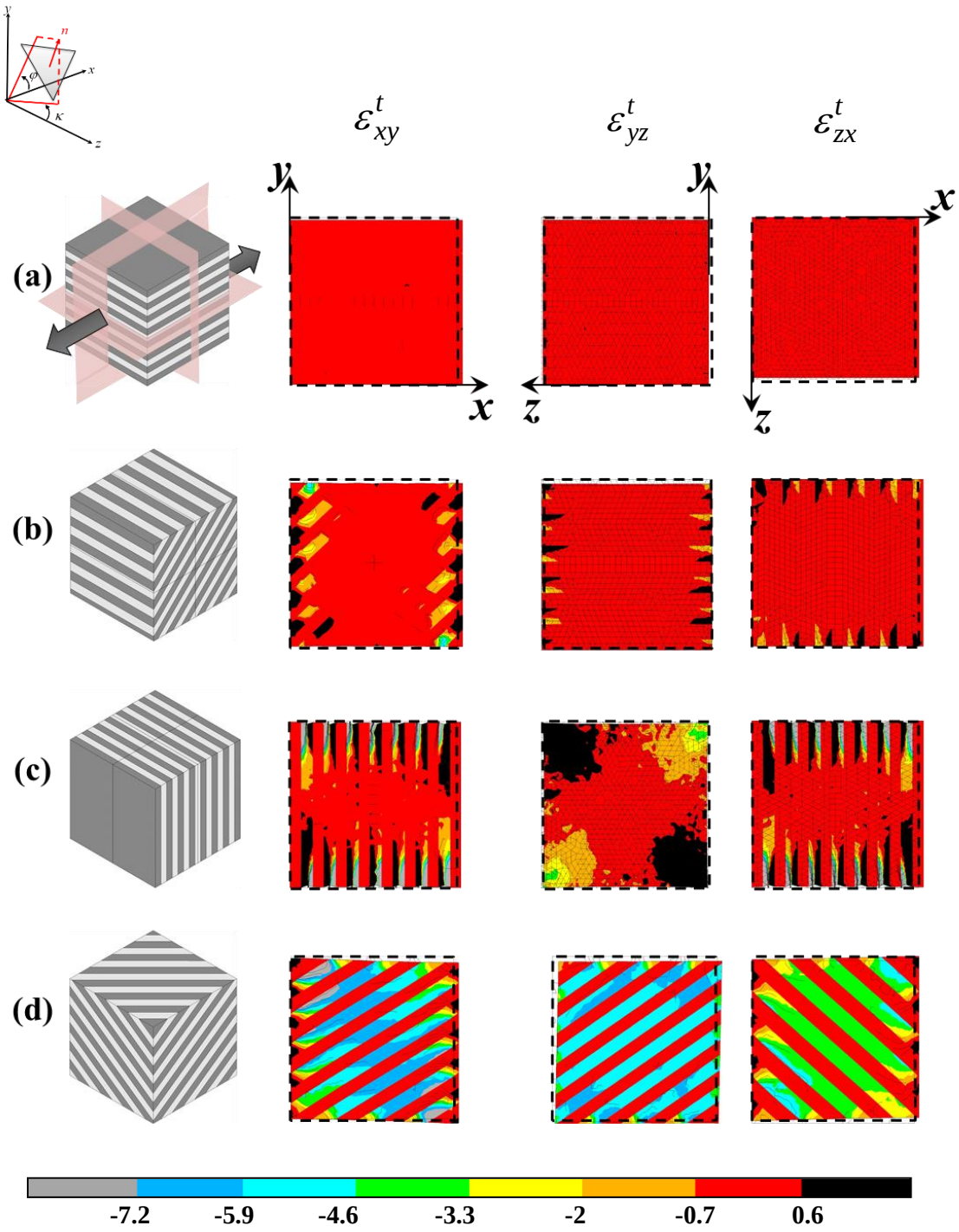

Fig. 24 Distribution of total shear strain components ε_{xy}^{t}, ε_{yz}^{t} and ε_{zx}^{t} in single-colony models at nominal strain $\varepsilon_o = 3\%$. Here *x*-, *y*-, and *z*-axes are tensile, normal and transverse axes. The surface of *xy* is the longitude surface and *zx* is the horizontal surface. They are parallel to the tensile direction. *yz* is the transverse surface normal to the tensile direction.

Fig. 25 is the distribution of equivalent stress σ_{eq} at nominal strain $\varepsilon_o = 3\%$ shown in separate stress contours to represent both θ and α phases to observe stress partitioning in single-colony models. The stresses are denoted as σ_{eq}^{θ} and σ_{eq}^{α} respectively. Model-(a) in Fig. 25(a) and model-(c) in Fig. 25(c) exhibit clear stress-partitioning because of incompatibility, where the θ lamellae bear the load at almost 2750MPa, whereas the stress value in α lamellae is about 100MPa. Fig. 25(b) shows that the stress in θ lamellae in model-(b) is approximately around 200MPa to 450MPa, which is quite small if compared with the other models. On the other hand, although it looks like that stress-partitioning occurs in Fig. 25(d), the stress in θ lamellae is about 500MPa, which is double the value of stress in α lamellae, 275MPa. The stress level is higher because the θ lamellae in model-(d) are not relaxed from elastic straining as model-(b). It may be acceptable if model-(b) and model-(d) are generalised as single-colony models with the tendency to show similar mechanical responses as α in comparison with the stress-strain curves on monolithic θ and α models.

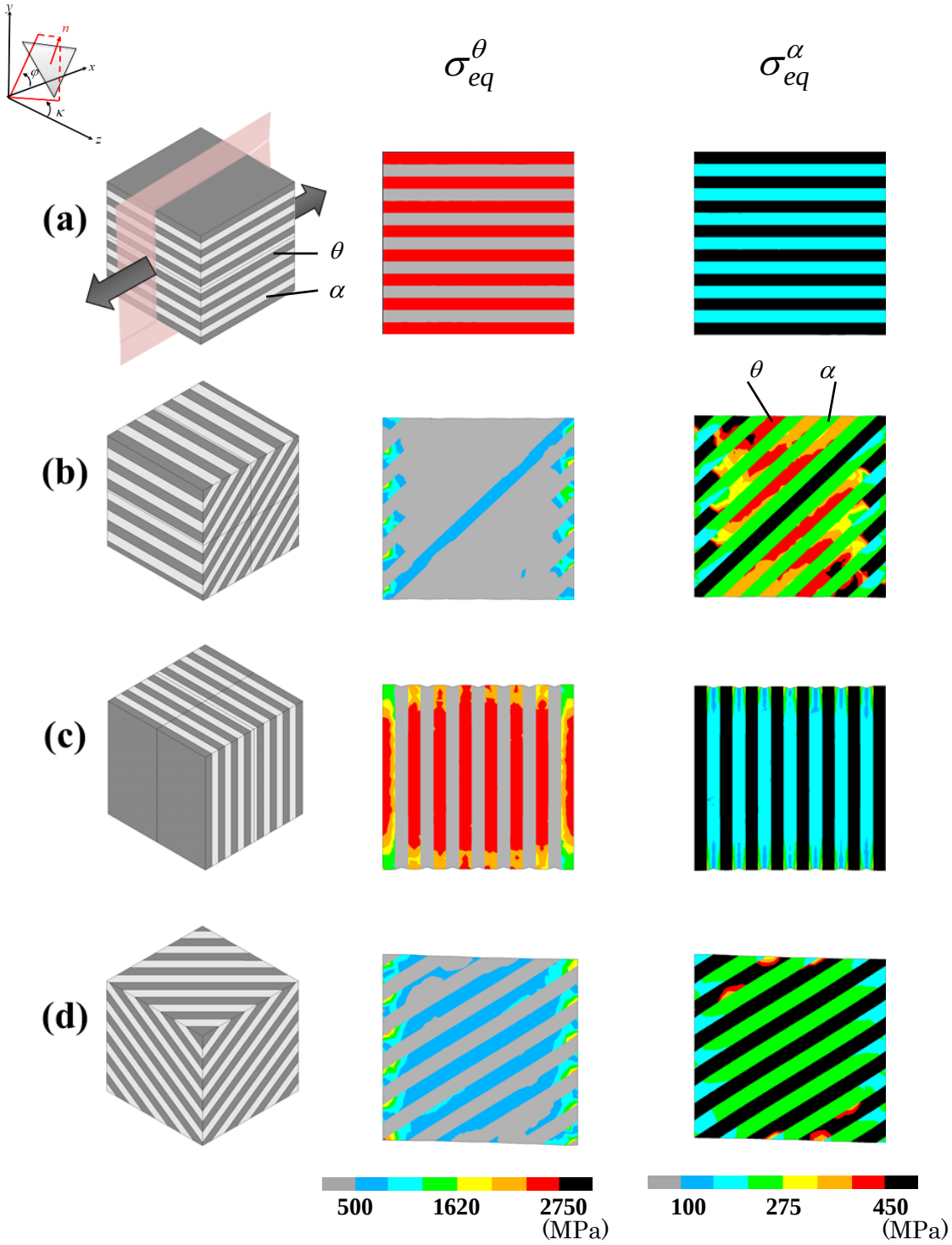

Fig. 25 Distribution of equivalent stress σ_{eq} at nominal strain $\varepsilon_o = 3\%$ shown in separate stress gauges that accommodate both stress ranges for θ and α phases. The stress is denoted as σ_{eq}^{θ} and σ_{eq}^{α} respectively.

Fig. 26 plots the nominal stress versus nominal strain of single-colony models in comparison with the monolithic θ and α. From the order of highest flow stress to the lowest is model-(a), model-(c), model-(d) and model-(b). There is a gap of almost 1000 MPa between the flow stress of model-(a) and model-(c) with model-(b) and model-(d). From Fig. 25 it is observed that maximum stress is uniformly distributed in θ phase when the lamellar alignment is parallel to the tensile axis. Whereas, when the lamellar alignment is around $45°$, the θ phase is relaxed. The lack of deformation in θ implies that the deformation is compensated α lamellae. Thus the flow stress level is similar to that of α. Although flow stress dropped to 1500 MPa after α lamellae are sandwiched alternatively with θ lamellae in model-(a) when compared with the monolithic θ model, the increase of strain-hardening rate indicates that by layering brittle phase with ductile phase, the plastic deformability in θ improves. This concludes that the mechanical responses in single-colony models are determined by the lamellar alignment of θ to the tensile direction.

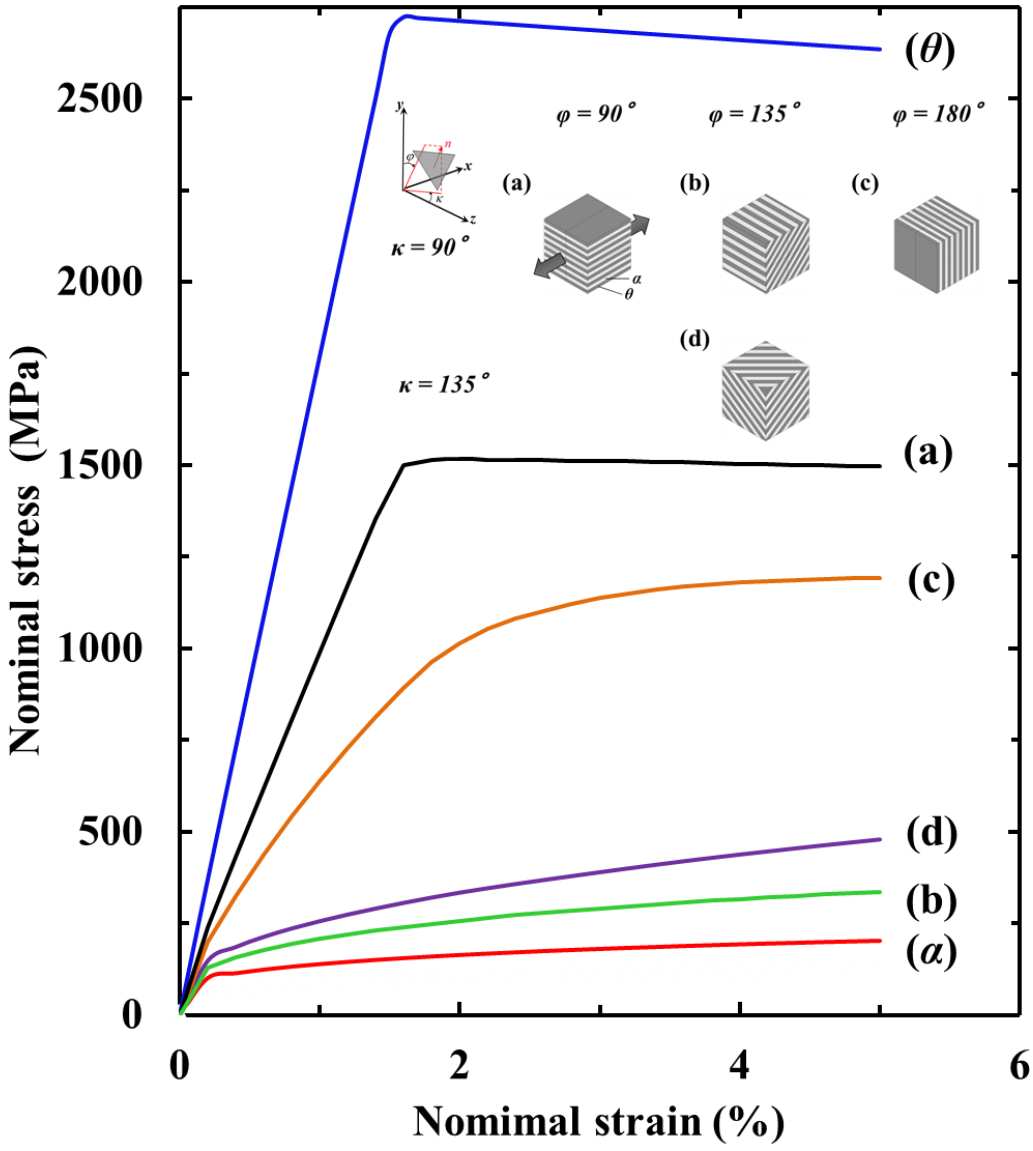

Fig. 26 The nominal stress σ_o vs. nominal strain ε_o curves of single-colony models in comparison with monolithic θ and α.

Empty page

Chapter 5

Elasto-plastic deformation of multi-colony models

5.1 Introduction

Tanaka et al. [44] measured the strain of deformation in colony structures by the displacements of lattice markers. From their investigation, they revealed that strain has higher tendencies to concentrate around the boundaries of block/colony and in regions where the cementite (θ) lamellae are inclined at the inclination angle of about $45°$. They also highlighted that plastic deformability of cementite lamellae depended on the lamellar alignment with respect to the tensile axis, and the uniformity of strain in the nearby neighbourhood is influenced by the existence of shear bands. Murakami and Adachi [65] listed three main conditions for the generation of strain which correlates with the observations by Tanaka et. al [44]. The conditions are: block/colony boundaries meet at a three-point, θ lamellar inclined at an angle of $45°$ from the tensile axis and high count of Schmidt's factor. The Schmidt's factor depends on the crystallography

of the material to achieve the critical resolved shear stress (CRSS), which initiates the plastic deformation. Since both θ and α sustain their crystallography through plastic deformation, the plastic deformation of block/colony of pearlite microstructure depends on the alignment of θ. However, the reasons behind such occurrences are still yet to be elucidated.

In Chapter 4, we studied the elasto-plastic deformation of single-colony models. The results showed that the mechanical responses of single-colony models depended on the lamellar alignment of θ and α against the tensile direction. To understand the plastic deformation in colony structure, two analyses are conducted. We imitate the real pearlite block/colony structures [36] into simplified models.

5.2 Modelling of multi-colony models

Fig. 27 shows the SEM of three types of block/colony regions taken at strain $\varepsilon = 15\%$ [36] and the simplified 2-D schematics. The models were constructed from combinations of differently aligned θ and α lamellae in a square plate with the dimension of $L \times L$.Dark and light grey regions are θ and α, respectively. To imitate possible geometrical non-uniformity in the real structure of pearlite colony especially around the colony boundary regions, the thickness of θ and α lamellar are assumed

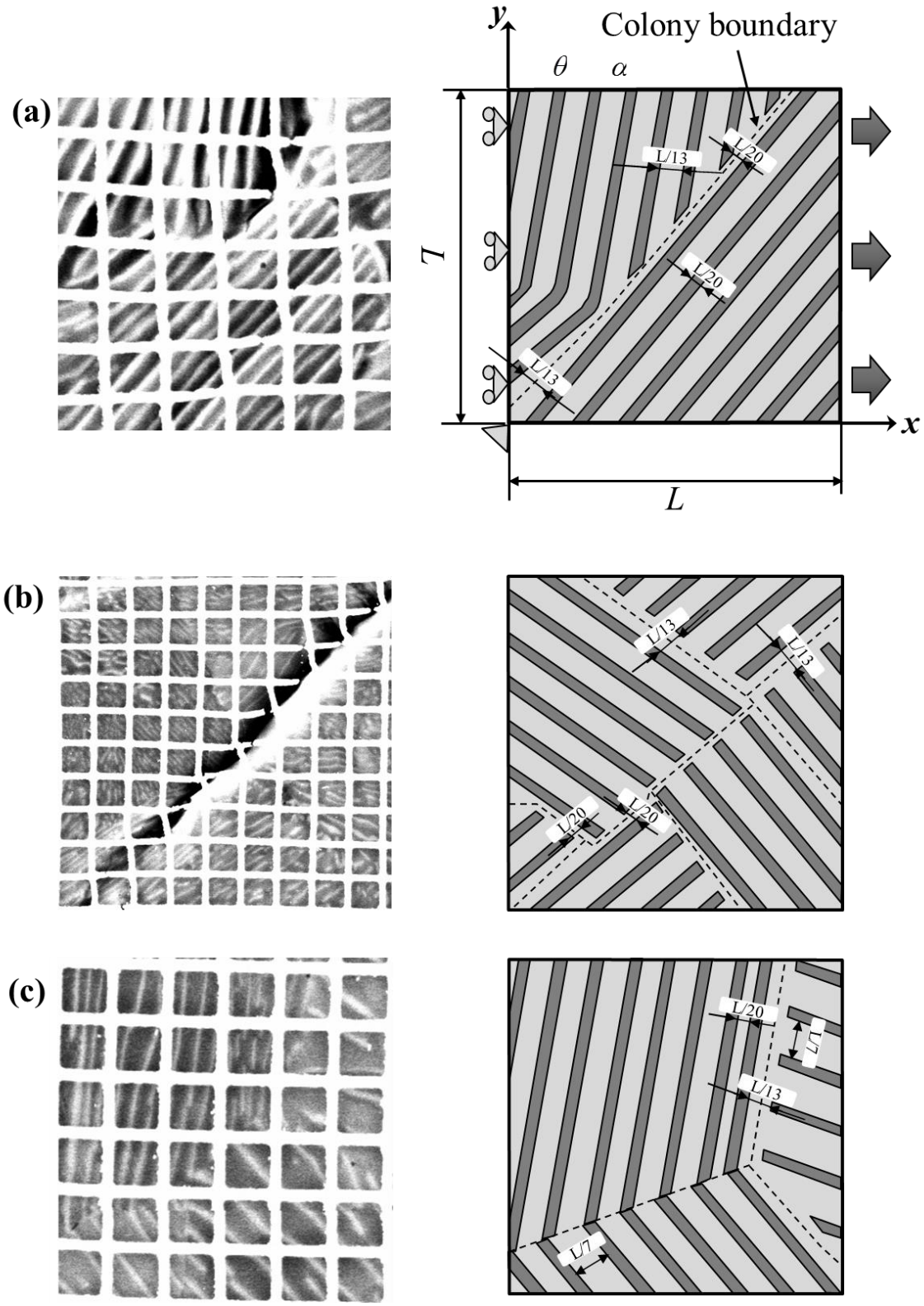

Fig. 27 SEM of three-types of block/colony regions taken at strain $\varepsilon = 5\%$ [36] and their 2-D schematics. The boundary conditions are defined at both lateral surfaces.

to be $L/20$ and $L/13$ respectively. In model-(c), the thickness of α lamellar ranges from $L/20$, $L/13$, and $L/7$. The dotted lines mark the colony boundaries which are actually α lamellae dividing the differently aligned lamellar groups. The continuous θ lamellar curve is in model-(c). The models are constrained along the tensile axis (*x*-axis) at the left lateral surface and forced displacements are given at the right lateral surface.

5.3 Results

Fig. 28 shows the distribution of plastic strain ε^{pl} in the experimental specimens at strain $\varepsilon = 5\%$ at the upper row for model-(a), -(b), and -(c). The lower row shows the distribution of plastic tensile strain component, ε_{xx}^{pl} for FEM analyses results at nominal strain ($\varepsilon_o = 5\%,10\%,13\%$ and 15%) for model -(a), -(b) and -(c). The distribution of strain in experimental and FEM results do not match. Model-(a) and model-(b) for experimental results showed three types of strain distributions.

Model-(a) shows inter- and intra-colony deformations while sharing the same strain concentration characteristic as model-(b). The strain tends to concentrates where boundaries meet at a thee-point and strain distributes along the block/colony boundaries. On the contrary, model-(c) shows almost no deformation.

Next we look into the progression of plastic strain at nominal strain $\varepsilon_o = 5\%$, $\varepsilon_o = 10\%$, $\varepsilon_o = 13\%$ and $\varepsilon_o = 15\%$ in model-(a), model-(b) and model-(c) for the analyses. Since the models are 2-D, the results are quite predictable and straight forward as explained in Section 5.1. Strain has high tendencies to localise where the boundaries of differently aligned colonies meet. Then, strain concentrates around the area before propagating selectively into the nearby α. Interestingly in model-(b), although the lamellar alignments are more or less $45°$ inclined from the tensile direction for all colonies, a colony shows almost no deformation. Although the distribution is not the same as the experimental result, it proves that strain propagation prefers the weakest link route. In this case, the deformation is influenced by boundary condition. The left colony is fixed at the lateral surface while the right colony is forced to elongate towards the tensile direction by forced displacement.

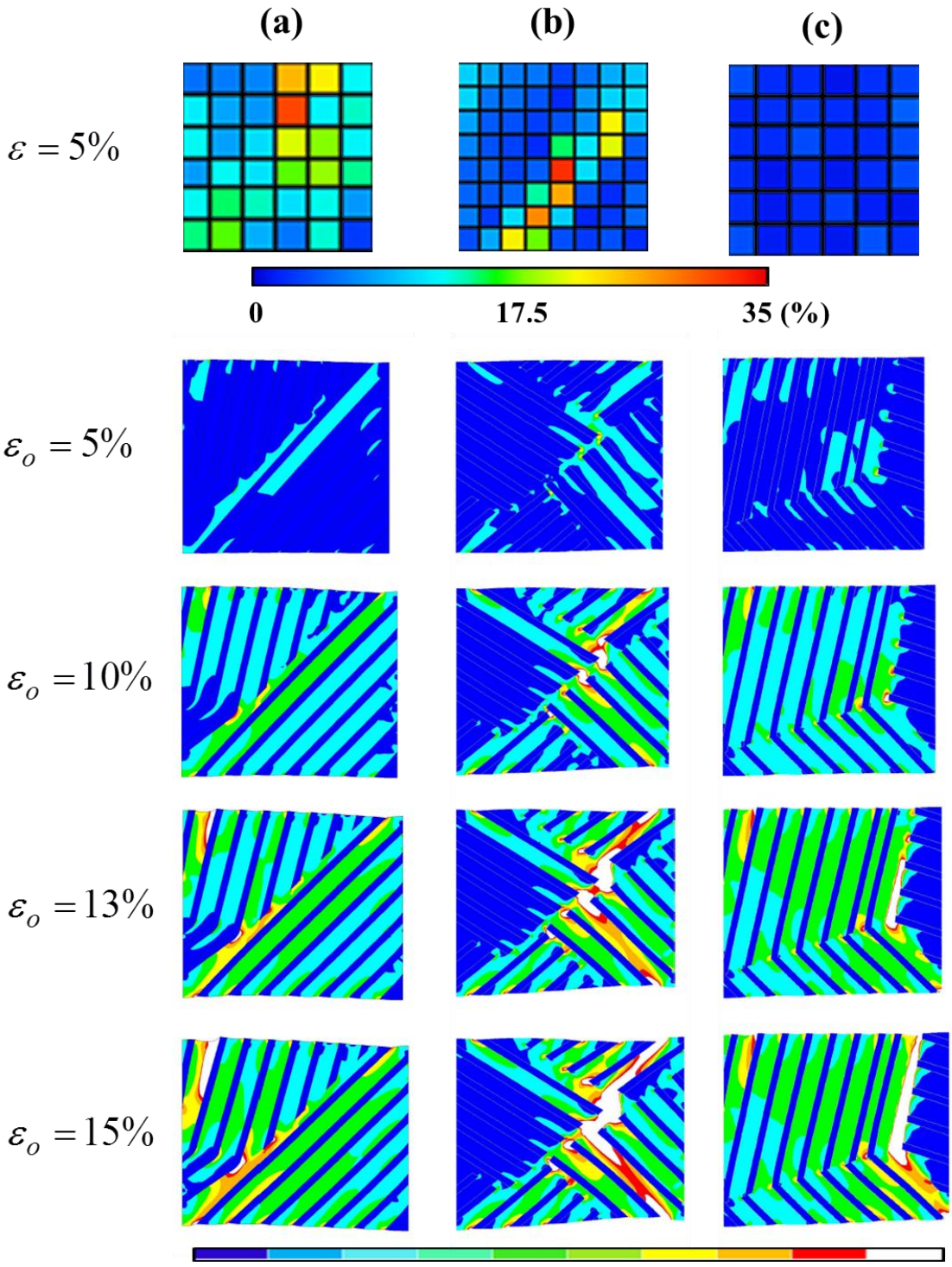

Fig. 28 The upper row shows the distribution of plastic strain ε^{pl} in experimental specimens at strain $\varepsilon = 5\%$. The lower row shows the distribution of plastic tensile strain component ε_{xx}^{pl} for FEM analyses results at nominal strain $\varepsilon_o = 5\%,10\%,13\%$ and 15% for model-(a), -(b), and -(c).

Chapter 6

Elasto-plastic deformation of double-colony models

6.1 Introduction

In Chapter 5 we studied the elasto-plastic deformation of multi-colony models. However, the multi-colony models are not straight forward because there are many parameters to put on consideration such as lamellar alignments, lamellar spacing, placing of block/colony boundaries, etc. Clausing [107] observed the existence of microcracks along the boundaries of block/colony when adjacent blocks/colonies are joined parallel with the tensile axis. At this position, the boundaries are more or less perpendicular towards the tensile direction. Henceforth, to clarify the mechanical behaviour of plastic deformation in colony structure, the multi-colony structure is reduced into the double-colony structure. The core of this thesis will be the investigation of elasto-plastic deformation between two colonies to elucidate the mechanical correspondence between two joined colonies and the affects towards the deformation of

colony boundary. For fine wires, Yamada [108] reported that the refinement of inter-lamellar spacing is inconsistent because the decomposition of θ in pearlite does not happen uniformly throughout the microstructure after severe plastic deformation. Since there is no proper elucidation available on the subject yet, Tarui et al. [109] suggested the occurrence of partial or localised strengthening in pearlite microstructure as an outcome of the ununiformed decomposition of carbon.

Consequently, the localisation of deformation is irregular throughout the microstructure resulting ununiformed distribution of strength in pearlite. Shimizu and Kawabe [110] suggested that the circumference stress in a large-sized wire can become tensile during torsion. The circumference stress is the residual stress acting normal to the fibre direction of the wire. This increases the probability of cracks along the longitudinal axis, parallel to the wire fibre. Interestingly, Sorby [1] and Belaiew [32] emphasised the importance of pearlite deformation along the longitudinal axis, which is the interaction between colonies joined to each other in the direction of the tensile axis. As mentioned above, Clausing [107] found boundaries perpendicular to the tensile axis susceptible to cracks. Thus, for double-colony models, the colonies will be arranged in such that they are aligned with the tensile direction at the *x*-axis.

6.2 Effect of the difference of lamellar alignment/orientation between two adjacent colonies on the elasto-plastic deformation of double-colony models

6.2.1 2-D modelling of double-colony models

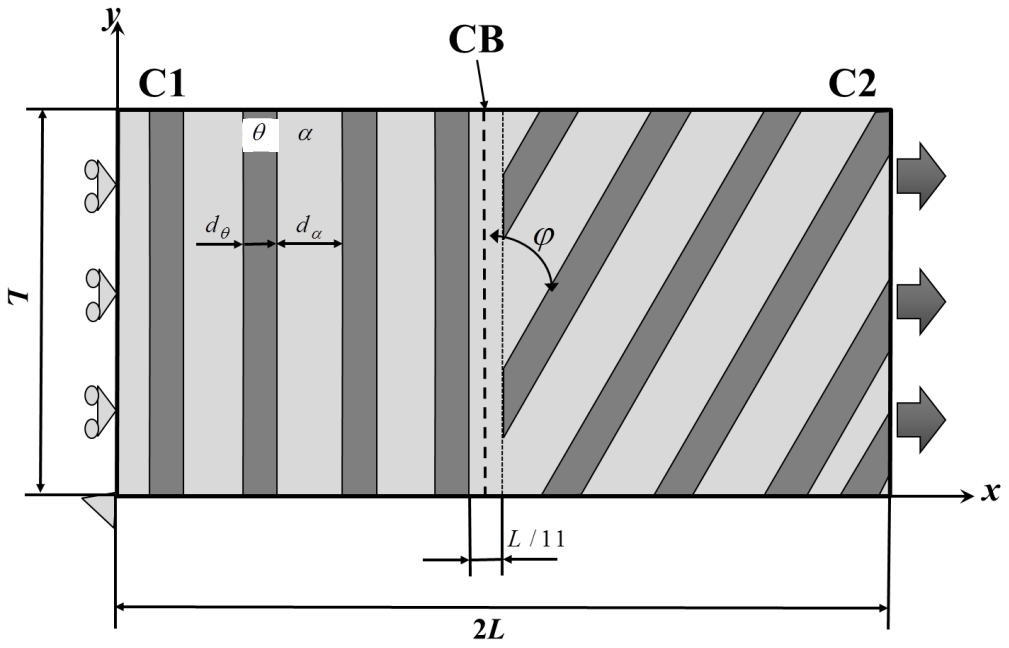

Fig. 29 Schematic of 2-D double-colony model. The model parameter is $L \times 2L$. The double-colony is divided into Colony1 (C1) and Colony2 (C2) at the colony boundary (CB). The lamellar alignment in C1 is perpendicular to the tensile axis (*x*-axis) while C2 inclines at the angle of φ from C1. The thickness ratio of α to θ is $\frac{d_\alpha}{d_\theta} = 2$; given that $d_\theta = \frac{L}{11}$. The left lateral surface is constrained, and the right lateral surface is given forced displacements.

Fig. 29 shows the schematic of 2-D double-colony model. The double-colony is divided into Colony1 (C1) and Colony2 (C2) at the colony boundary (CB). The model

parameter is $L \times 2L$. The lamellar alignment in C1 is perpendicular to the tensile axis at *x*-axis , while C2 inclines at the angle of φ from C1. The thickness ratio of α to θ is $\frac{d_\alpha}{d_\theta} = 2$; with the thickness of θ is $d_\theta = \frac{L}{11}$. The boundary conditions are defined by the lateral surfaces. The left lateral surface is constrained along the tensile axis, and the right lateral surface is given forced displacements.

6.2.2 Results

Fig. 30 shows the distributions of plastic strain component ε_{xx}^{pl} in double-colony models. The angle of difference between θ lamellar alignment in C1 and C2 are $\varphi = 30°$, $\varphi = 45°$ and $\varphi = 60°$ at nominal strain $\varepsilon_o = 5\%$, $\varepsilon_o = 10\%$, $\varepsilon_o = 13\%$ and $\varepsilon_o = 15\%$. White coloured regions indicate that plastic strain is over 80% and it is found that the high plastic strain expands in one direction with the increasing of nominal tensile strain, ε_o. The strain concentration region is different for each model. When the difference of θ lamellar alignment in C1 and C2, φ is smaller than 45°, plastic strain concentrates alongside cementite lamella. On the other hand, when the difference of lamellar orientation, φ is larger than $45°$, plastic strain concentrates around the colony boundary. Although they are joined at CB, C1 and C2 exhibit their single-colony characteristics. As the difference of lamellar alignment increases, the φ lamellar

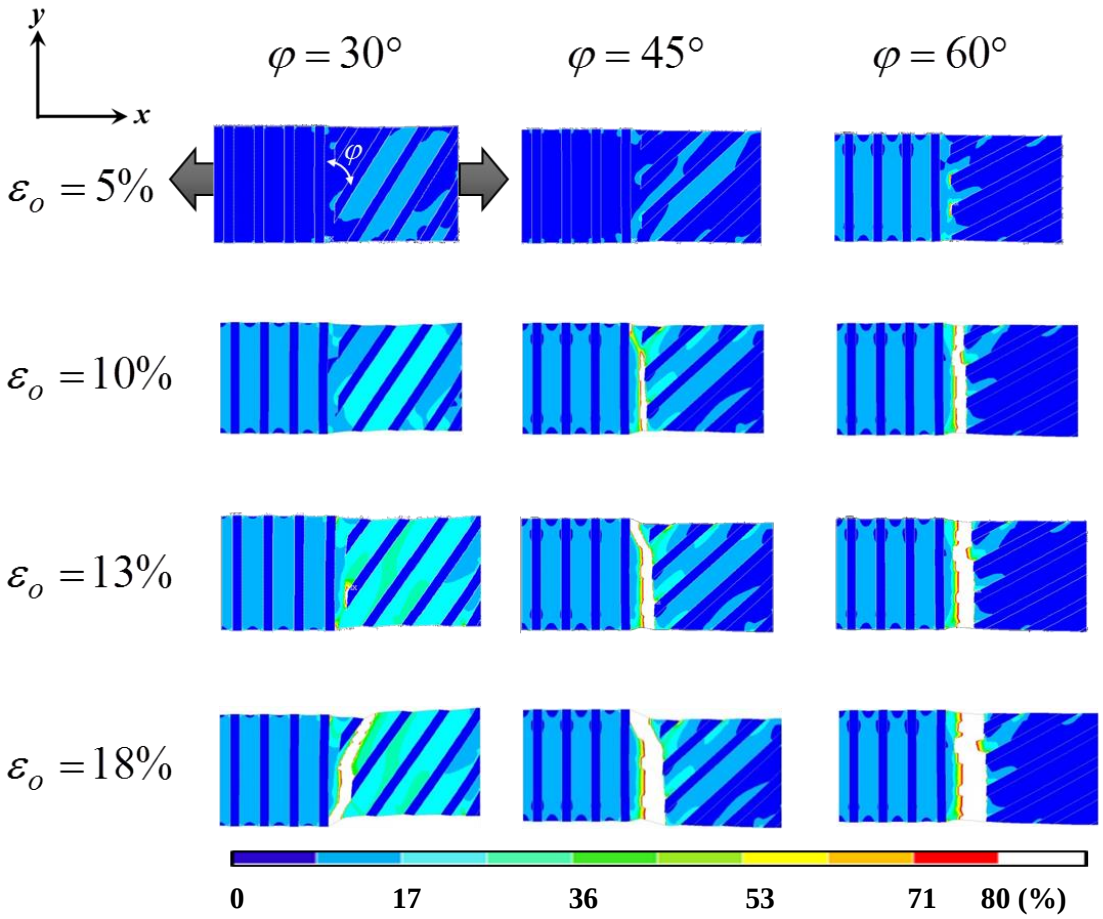

Fig. 30 Distribution of plastic tensile strain component ε_{xx}^{pl} in 2-D double-colony models at nominal strain $\varepsilon_o = 5\%, 10\%, 13\%$ and 18%. The angle of difference between θ alignments in C1 and C2 are $\varphi = 30°, 45°$ and $60°$.

alignment in C2 becomes more parallel towards the tensile axis. Therefore, the plastic deformation of α is restricted by φ hence at $\varphi = 60°$ the deformation in C2 is almost 0. As shown in Section 5.3, Fig. 28, the propagation of plastic strain is selective to the weakest link. In this case, the CB compensates for the plastic deformation of C2 and becomes the weakest part of the model.

6.3 Effect of lamellar alignment of cementite (θ) to the tensile direction of the elasto-plastic deformation of double-colony models

6.3.1 3-D modelling of double-colony models

Fig. 31 shows the schematic of 3-D double-colony model. Colony1 (C1) and Colony2 (C2) are joined at the colony boundary (CB) which is a α layer in between the two colonies and the thickness is $L/10$. The dimension of the model is $2L \times L \times L/2$. The alignment for θ plane is dictated by n, and the configuration of the inclination angles in C1 was explained in Fig. 12 of Chapter 3. For the purpose of the tensile analyses, the lamellar alignment of θ planes in C2 is fixed at $\varphi_o = 135°$. This means C2 makes an inclination of $45°$ from the tensile axis. Matsuoka and Tanaka [56] and our results in Chapter 4 showed that the stresses in θ phase depended on the angle to tensile axis. It is clear that the mechanical response of single-colonies depended on the alignment of θ in the models. The mechanical response, which is the plastic flow stress of C2 is assumed to be constant because the alignment of θ is fixed. Therefore, the deformation around colony boundary is predicted to be determined by the alignment of θ in C1 of the double-colony models from its interaction with the adjacent C2 [39, 44, 62, 65]. Furthermore, the mirror symmetry along the tensile axis

cannot be neglected because the direction of deformation in C1 and C2 will be influenced by the direction of θ, although they are inclined $45°$ from the tensile direction. Hence, the degrees of the inclination angles considered for double colonies are $0° \le \varphi \le 180°$ and $0° \le \kappa \le 90°$. The degrees of freedom (DOF) of the model is completely fixed at the posterior bottom left corner while the *y*-axis is fixed at the anterior bottom left corner. The lateral side of C1 is completely fixed at the tensile axis and force displacement is given at the lateral of C2. The lamellar thickness of θ and α are the same as the thickness of the colony boundary so that the mechanical response between two colonies are controlled by the lamellar alignments, not the thickness ratio [53].

Fig. 26 shows the diagram of pearlite double-colony models. There are nine types. C1 and C2 are joined at the CB, which is a α layer in between the two colonies. The thickness of CB, α and θ are $L/10$. C2 is the controlled variable in the analyses. The alignment of θ is fixed at $45°$ towards the tensile direction, which is indicated by the grey arrows. The alignments are arranged, so C1 will be parallel, perpendicular, and inclined around $45°$ against the tensile axis along the longitudinal axis. It must be understood that angles φ and κ do not indicate the direction of the normal n of θ. Rather, they explain the magnitude of inclinations in the modelling order of the first

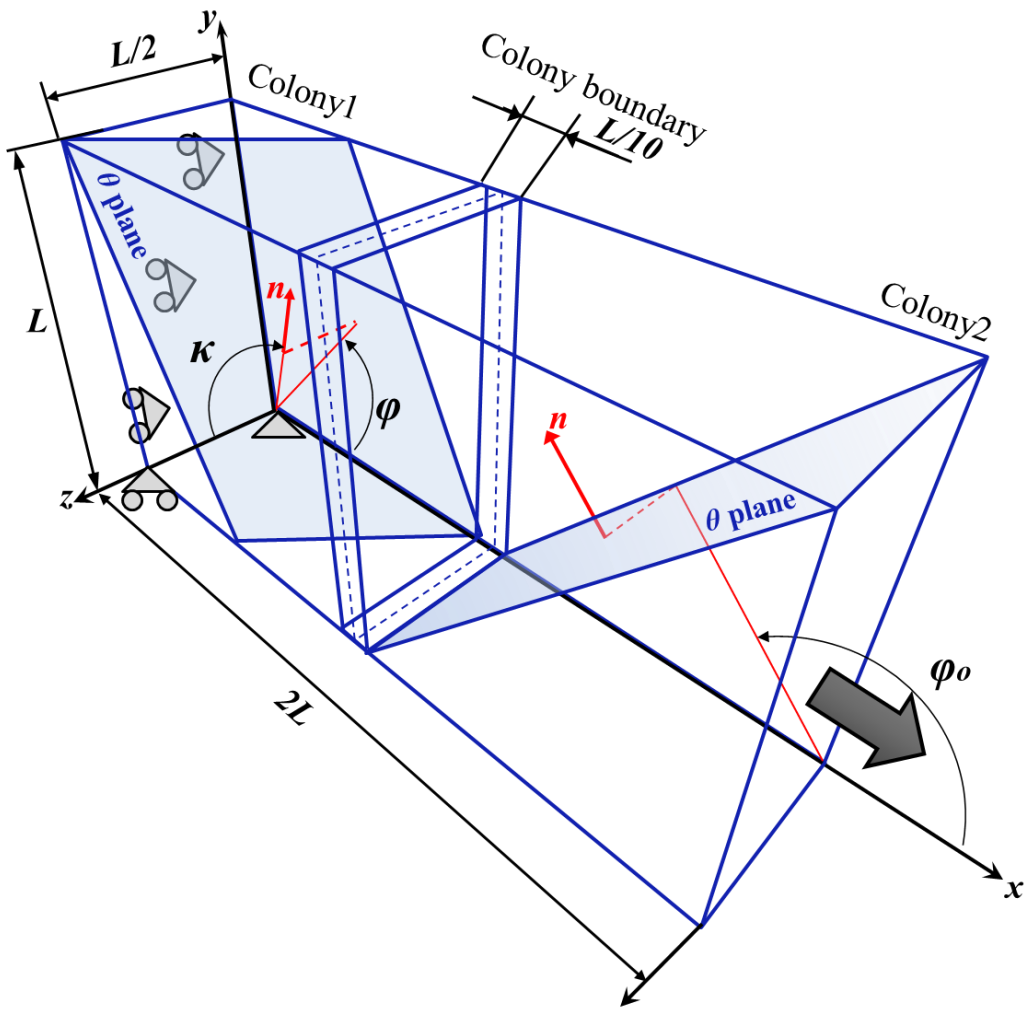

Fig. 31 Diagram of pearlite 3-D double-colony models. Colony1 (C1) and Colony2 (C2) are joined at the colony boundary (CB). The dimension of the model is $2L \times L \times L/2$. The thickness of CB, α, and θ are $L/10$. The alignment of θ in C2 is fixed. The alignment of θ in C1 is inclined at inclination angle φ first, then κ.

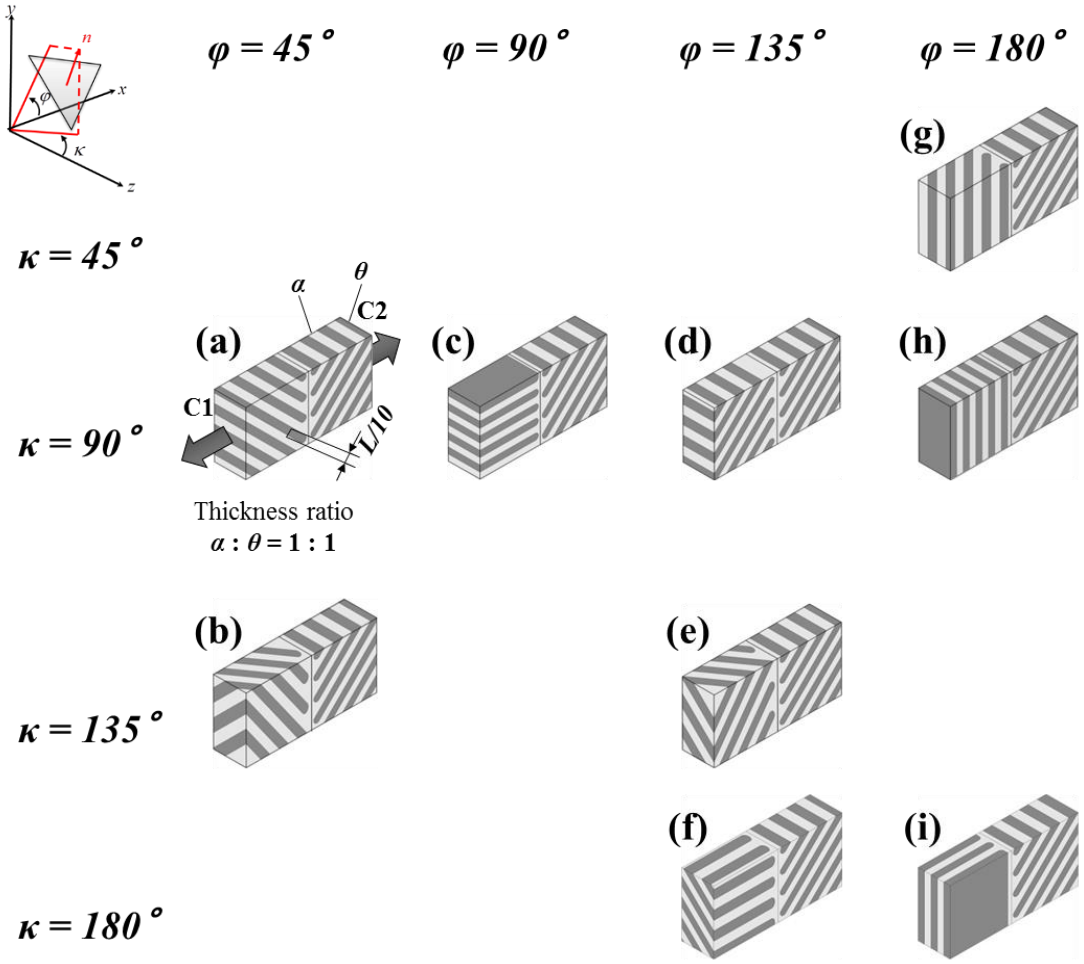

Fig. 32 Diagram of pearlite double-colony models. The dimension of the model is $2L \times L \times L/2$. The thickness of CB, α and θ, are $L/10$. The alignment of θ in C2 is fixed at $\varphi_o = 135°$. The alignment of θ in C1 is inclined at inclination angle φ first, then κ.

inclination at φ, which is an inclination of the orthogonal plane (*xy*-plane) and the second inclination angle, κ which is an inclination of the normal axis of the orthogonal plane (*z*-axis). The models are subjected to nominal strain $\varepsilon_o = 20\%$ for tensile deformation by forced displacement.

6.3.2 Results

Fig. 33 shows the development of equivalent strain ε_{eq} from nominal strain $\varepsilon_o = 1.5\%$ to $\varepsilon_o = 3\%$. Fig. 34, on the other hand, shows the distribution of equivalent plastic strain ε_{eq}^{pl} and plastic tensile strain component ε_{xx}^{pl} at nominal strain $\varepsilon_o = 3\%$. By comparing these results, it is clear that the double-colony models are deforming plastically in the tensile direction. From Fig. 34 it seems that the deformation for the double-colony models initiates near the CB at $\varepsilon_o = 1.5\%$. At $\varepsilon_o = 3\%$ strain then spread inwards into the colonies. Colonies that have θ aligned parallel along the tensile direction, Fig 33(c), Fig. 33(f), and Fig. 33(i). The C1 of these colonies showed almost no strain. When the results of Fig. 33 are compared with the equivalent plastic strain ε_{eq}^{pl} at Fig. 34(c), Fig. 34(f), Fig. 34(i), it can be implied that these models exhibit high concentration of plastic deformation at the CB. However, it can further be digested that the localization of strain at CB is a sum of strain from other components since only the

model in Fig. 34(c) shows the concentration of plastic tensile strain component ε_{xx}^{pl}.

When the θ of both colonies are (more or less) tilted $45°$ from the tensile direction, the plastic strain is widely distributed throughout C1 and C2, as shown by models in Fig. 34(a), Fig. 34(b), Fig. 34(d), Fig. 34(e), and Fig. 34(g). This wholistic deformation prevents any concentration of deformations at the CB. When the alignment of θ in C1 is perpendicular towards the tensile direction, model-(h) in Fig. 33(h) and Fig. 34(h) plastic deform well in both C1 and C2, yet localisation of strain is detected at the CB. Interestingly, this deformation is not influenced by the tensile component.

These results showed two obvious patterns of deformations. First, when the alignment of θ for both colonies are inclined at an angle that is favourable, in this case, $45°$ towards the tensile direction along the longitudinal axis, there are almost no concentration of strain at CB because both colonies, C1 and C2, in the models deform well plastically. Second, when the alignment of θ in one of the colonies is not favourable towards the tensile direction, in this case, the alignment of C1; CB and C2 will endure deformation from various components to compensate for C1. These tendencies agree with the 2-D analyses. It becomes apparent in 3-D analyses, thus to understand the behaviour of deformation occurring in double-colony models, the normal, transversal and shear components will be investigated.

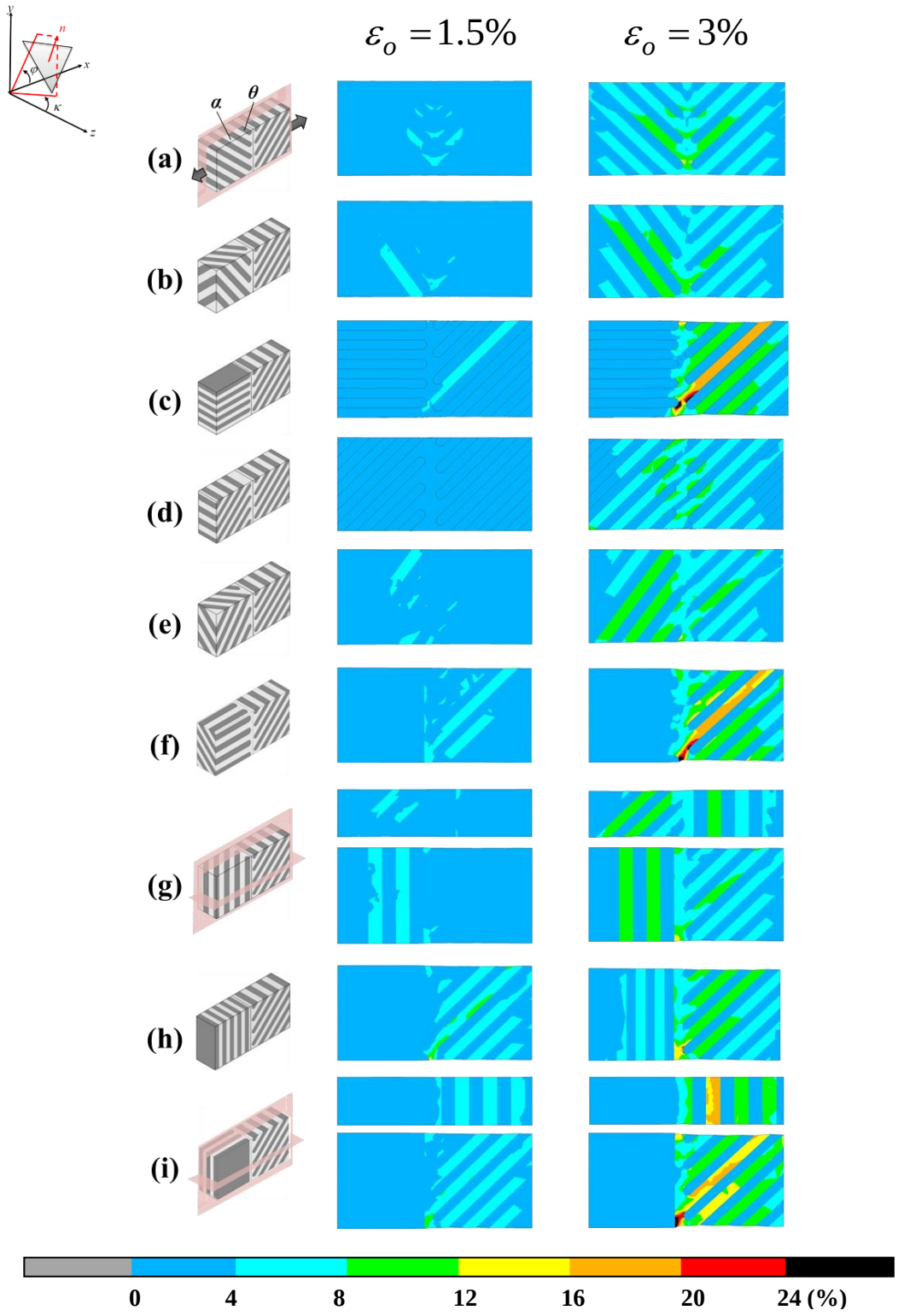

Fig. 34 Development of equivalent strain ε_{eq} in pearlite double-colony models at nominal strain $\varepsilon_o = 1.5\%$ and $\varepsilon_o = 3\%$.

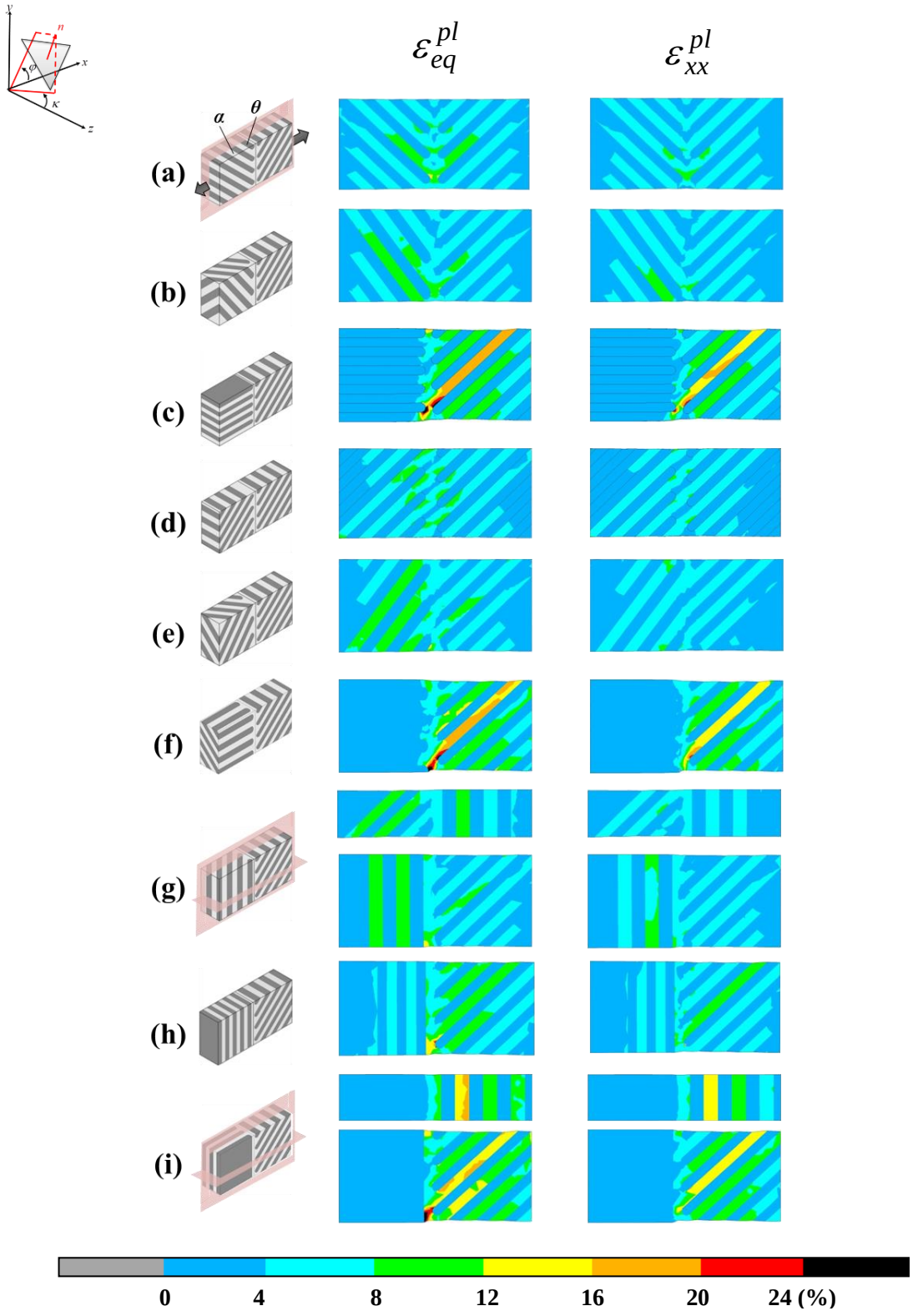

Fig. 354 Distribution of equivalent plastic strain ε_{eq}^{pl} and plastic tensile strain component ε_{xx}^{p} at nominal strain $\varepsilon_o = 3\%$.

Fig. 35 shows the distribution of total normal strain component ε_{yy}^{t} and total transversal strain component ε_{zz}^{t} at nominal strain $\varepsilon_o = 3\%$. Both strain components, normal and transversal, are observed along the CB. The pattern of deformation in C2 is confirmed for the normal component but barely deforms transversally for all models. For the double-colony models in our analyses, when the C1 colonies make 45° inclination transversely as shown in Fig. 35(b), Fig. 35(e) and Fig. 35(g), they exhibit a tendency to deform transversely towards the *z*-axis. Note that the value of total transversal strain component ε_{zz}^{t} is about the same as the value of total normal strain component ε_{yy}^{t}. This can mean that the balanced distribution of strain in both joined colonies prevents/annihilates strain concentration at CB. Fig. 33 showed that strain is initiated around the cementite edge at the CB. C1 colonies that are parallel with the tensile direction, Fig. 35(c), Fig. 35(f), and Fig. 35(i) show almost no deformation, henceforth, C2 colonies have to compensate the deformation. However, C2 only deforms normally. When this happens, strain tends to localized at CB because it is free from θ constrain and can deform in all components. In this analyses, the CB is a perpendicular α lamellar where the edge of θ lamellae in C1 and C2 meet. This makes it the most vulnerable segment of the double-colony models. 2-D analyses for multiple colonies showed that strain tends to initiate where the CB of neighbouring

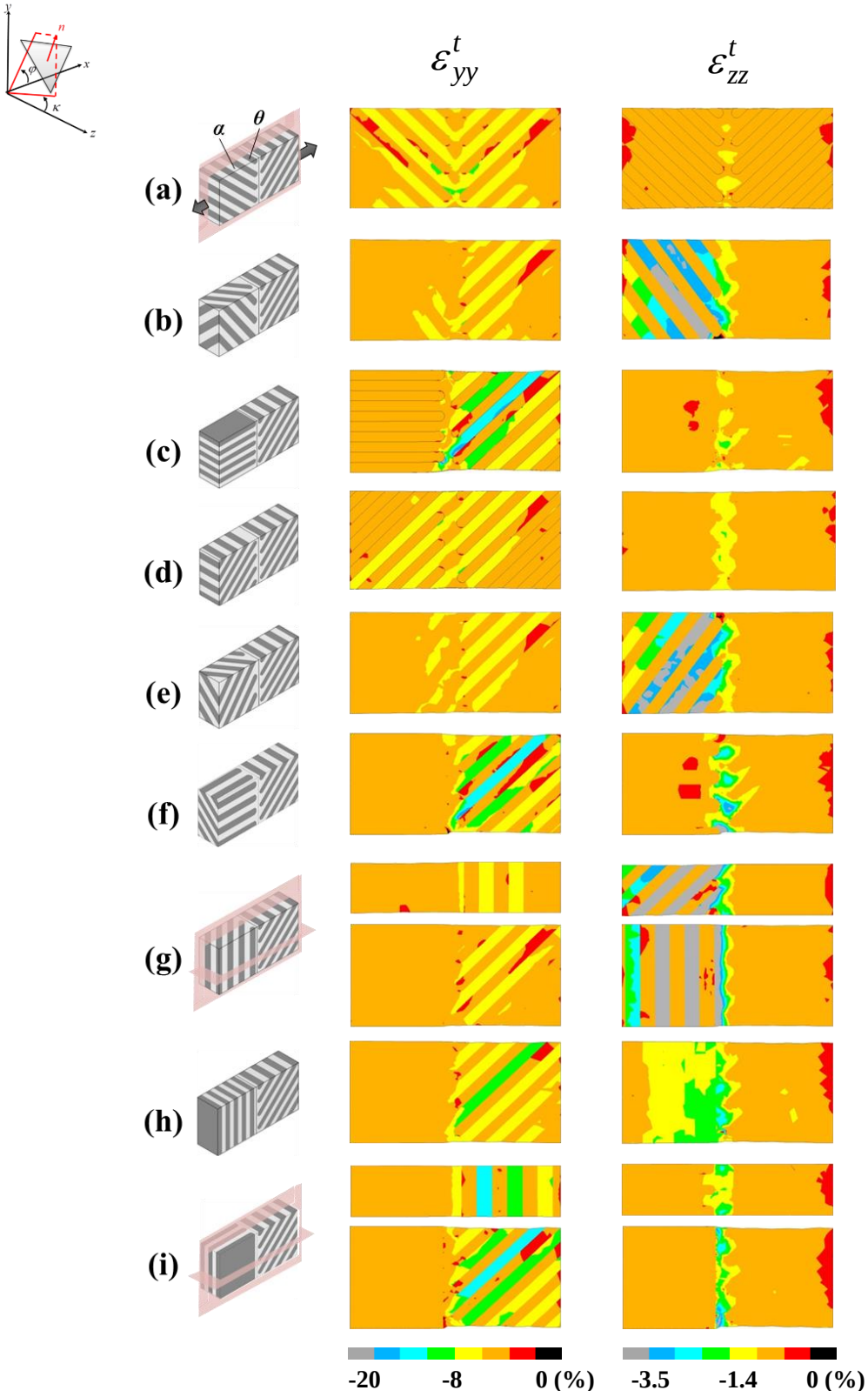

Fig. 365 Distribution of total normal strain component, ε_{yy}^{t} and total transversal strain component, ε_{zz}^{t} at nominal strain $\varepsilon_o = 3\%$.

colonies meet and propagate into the nearest α lamellar before the strain distributes to the next α and eventually the whole colony is submitted to plastic deform. This tendency is also observed experimentally [44,65].

At this point, it may be suggested that the magnitude of joined colonies controls the deformation in CB rather than the direction of the deformation. This idea is in agreement with Fig. 35(a) and Fig. 35(d) where the C1 colonies deform normally but not transversely. These C1 colonies show similar magnitude of total normal strain component ε_{yy}^{t} with C2. These results also show the alignment of θ, which gives the "anisotropy"-like characteristic of the colonies. This means CB has to endure shear deformation. To investigate this possibility, the shear components of double-colonies were looked into.

Fig. 36 shows the distribution of total shear component for ε_{xy}^{t}, ε_{yz}^{t}, and ε_{zx}^{t} at nominal strain $\varepsilon_{o} = 3\%$. C2 tends to shear at the *xy*-plane. This is because the alignment of θ lamellae is inclined at $\varphi = 45°$ without any secondary transversal inclination at the inclination angle, κ. This is obvious when C1 in Fig. 36(a) and Fig. 36(d) are compared with C1 in Fig. 36(b) and Fig. 36(e) which are inclined at $\varphi = 45°$ and $\kappa = 45°$. The later models endured shear at ε_{xy}^{t} and ε_{yz}^{t} components. The concentration of shear strain in all three components at CB for models with secondary

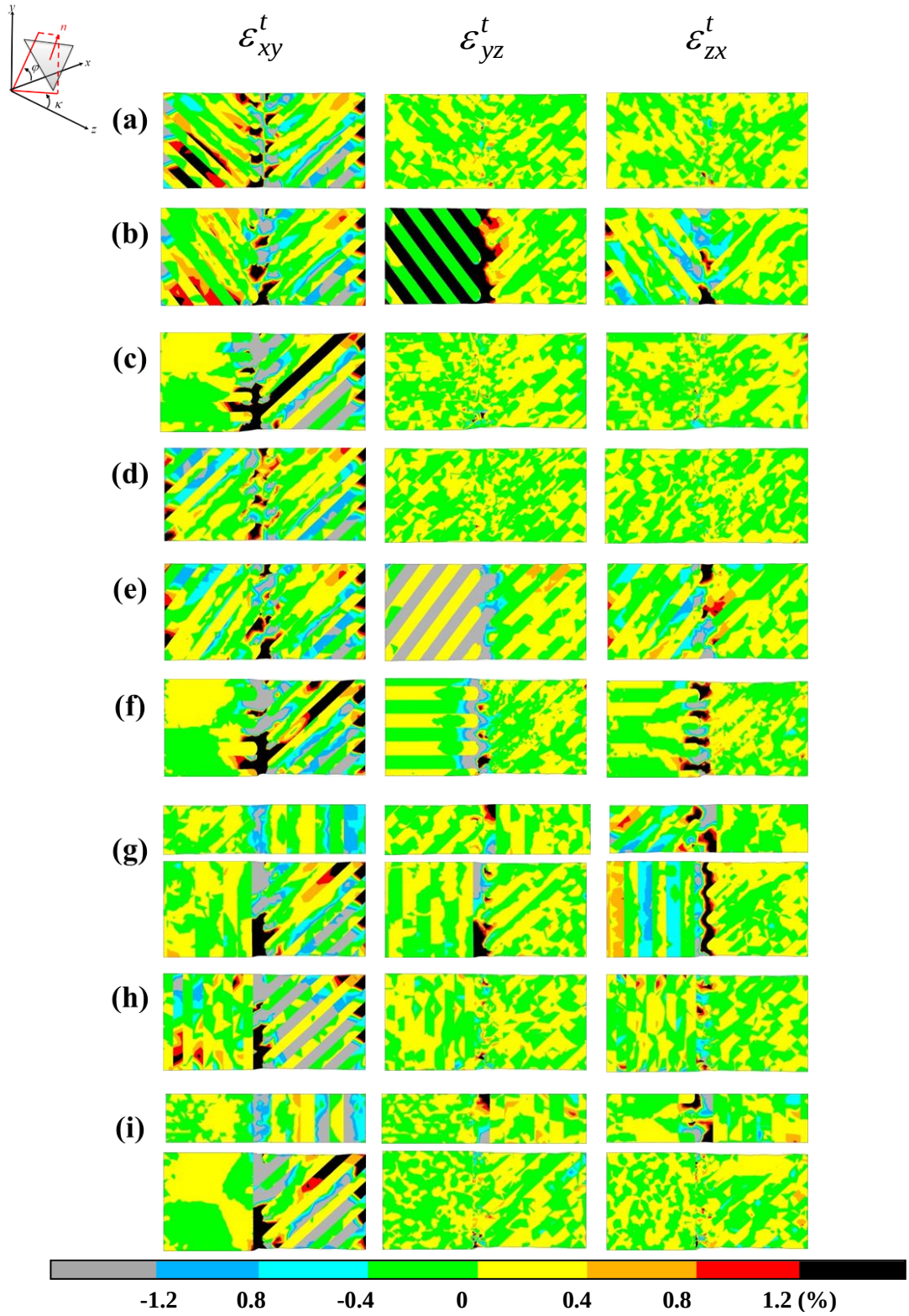

Fig. 6 Distribution of total shear component for ε_{xy}^{t}, ε_{yz}^{t} and ε_{zx}^{t} at nominal strain $\varepsilon_o = 3\%$.

inclination at κ especially in Fig. 36(b), Fig. 36(e), Fig. 36(f) and Fig. 36(g) are prominent. It is an interesting find that when C1 is perpendicular towards the tensile direction, the CB only shears significantly at the total shear component of ε_{xy}^{t} as shown in Fig. 36(h), although it was predicted that the CB should shear at the ε_{yz}^{t} component because this model exhibit deformation along the normal and transverse axes in Fig. 36(h). This study suggests that the alignment of θ lamellar does determine the "anisotropy" characteristic of the colony.

The results also emphasised that CB is the weakest link of the double-colony type model because it endures localised shear deformation before C2 shears when C1 does not deform, as shown in Fig. 36(c), Fig. 36(f) and Fig. 36(i).

Fig. 37 and Fig. 38 show the distribution of total *yz* strain component ε_{yz}^{t} at cross-sections of C1, CB and C2 for model-(b) in Fig. 37(a), model-(e) in Fig. 37(b), model-(f) in Fig. 38(a) and model-(g) in Fig. 38(b) at nominal strain $\varepsilon_o = 3\%$. To study the effect of secondary inclination κ towards the 'anisotropy' characteristics in double-colony models, the deformation in double-colony model-(b), model-(d), model-(f) and model-(g) are amplified five times. Fig. 37 shows the case when both inclination angles φ and κ are inclined at angles that make the θ lamellae 45° towards the tensile direction. With this configuration, the directions of the

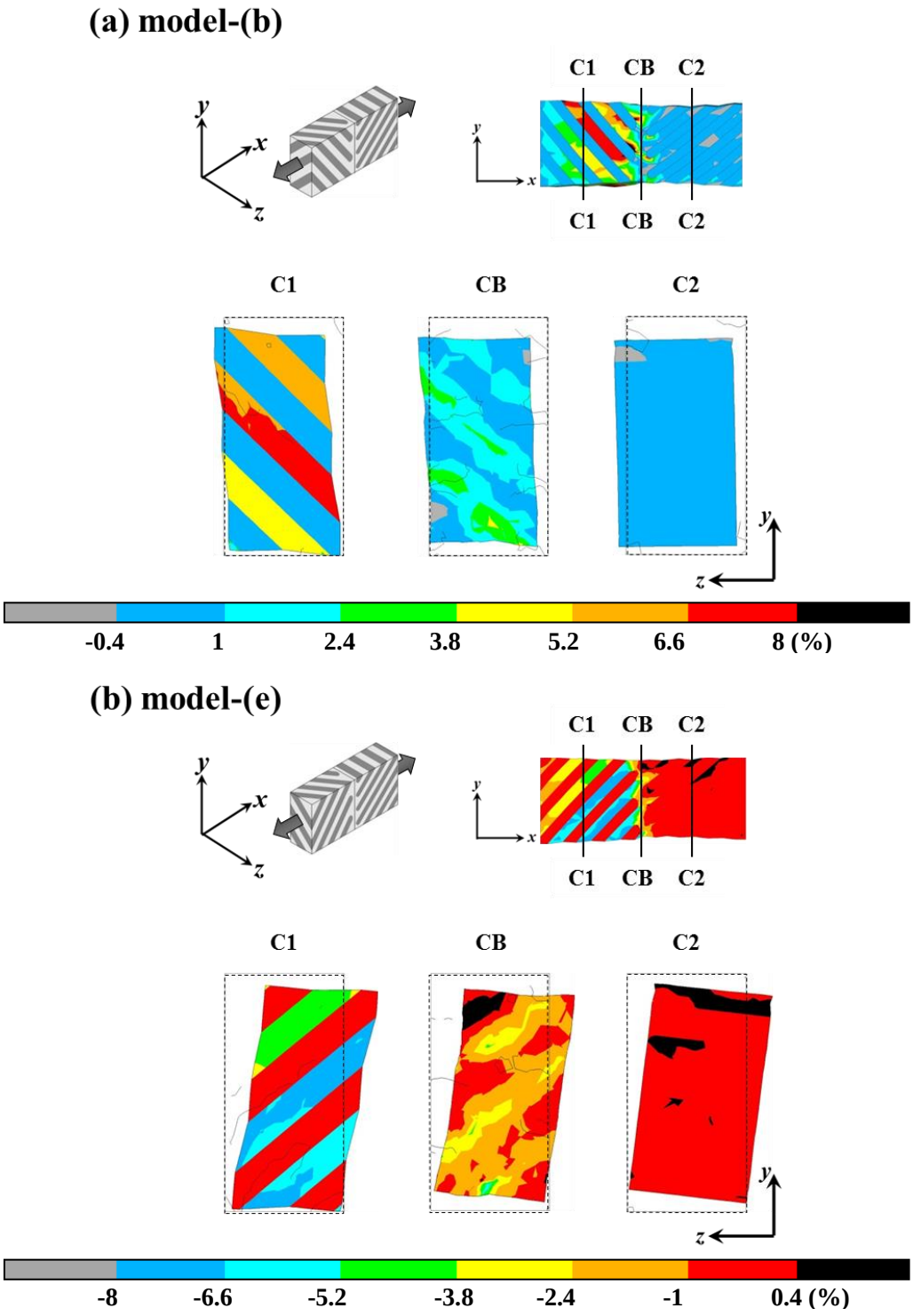

Fig. 377 Distribution of total *yz* strain component ε_{yz}^{t} at cross sections of C1, CB and C2 for model-(b) and model-(e) at nominal strain $\varepsilon_o = 3\%$.

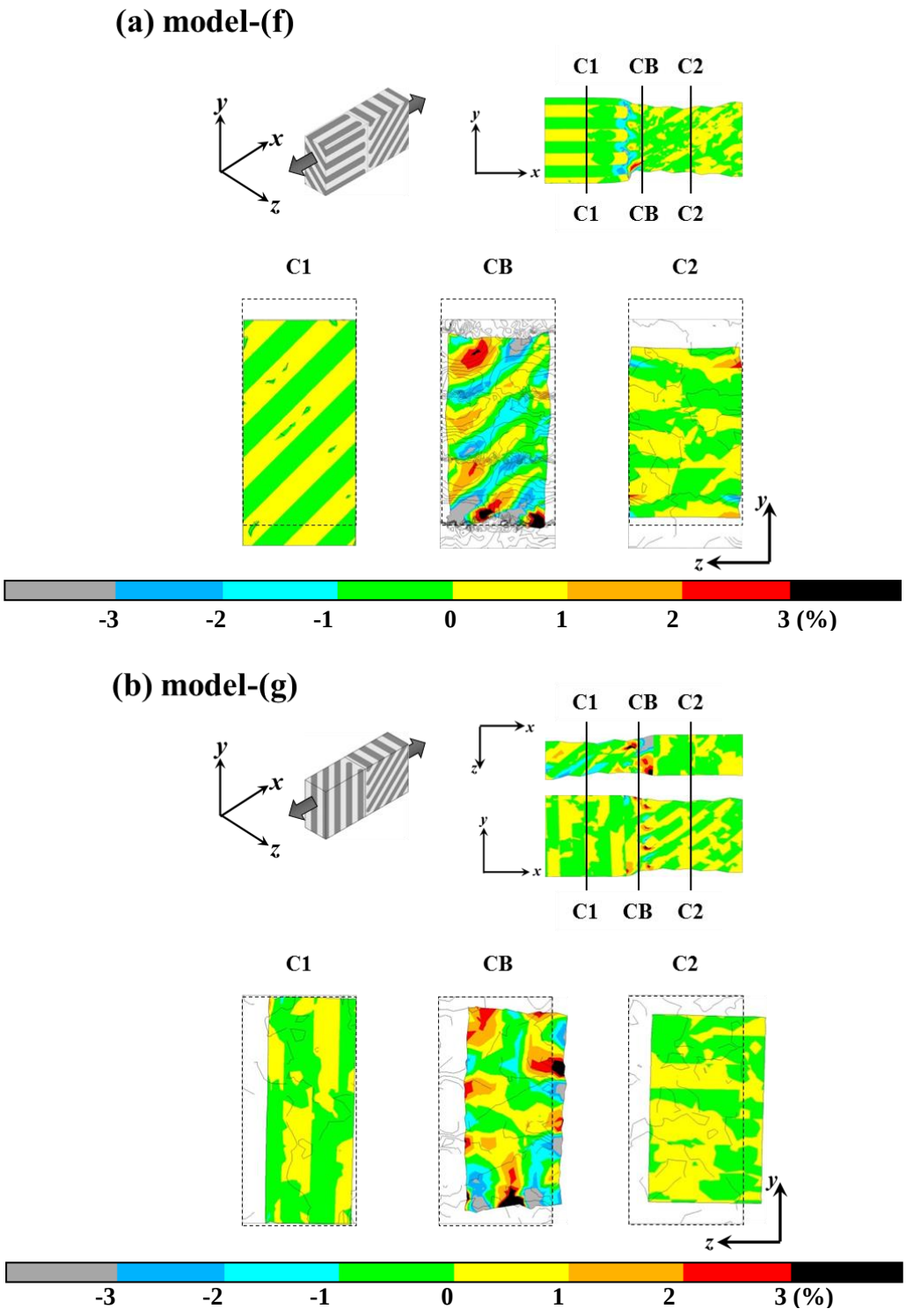

Fig. 388 Distribution of total *yz* strain component ε_{yz}^{t} at cross sections of C1, CB and C2 for model-(f) and model-(g) at nominal strain $\varepsilon_o = 3\%$.

double-colony are polarised into a particular direction and thus create torsion-like deformation at CB. The models endure torsion because C1 and C2 exhibit opposite directional characteristics. This confirms that the alignments of θ in colony are capable of dictating the direction of deformation of the colony thus giving it an "anisotropic" behaviour.

Fig. 38 shows the type of deformation where CB suffers extreme magnitude of deformation when two joined colonies with different deformation behaviours do not deform transversely. On the other hand, Fig. 38(b) suggests the phenomenon of 'deck-of-cards' sliding [22] for C1 in model-(g). This result is interesting because this model exhibits the tendency for θ to realign with the tensile direction.

Fig. 39 shows the distribution of equivalent stress σ_{eq} at nominal strain $\varepsilon_o = 3\%$. To investigate stress partitioning in both θ and α, stress ranges are arranged for each θ and α. They have denoted as σ_{eq}^{θ} and σ_{eq}^{α}, respectively. From the analyses of single-colony models in Chapter 4, it is clear that stress partitioning happens in C1 where the alignment of θ is parallel towards the tensile direction. For double-colony however, the stress value in θ, σ_{eq}^{θ} drops significantly if compared with the stress value of single-colony models. In contrast, stress accommodation-wise, it can be considered a positive change when a colony with a lower yield, C2 is joined

with C1. C2 exhibits adaptation to accommodate higher stress in θ as shown in Fig. 39(c), Fig. 39(f) and Fig. 39(i), unlike the singular version. A slight tendency of stress concentration can be indicated at CB for these types of models, but the value is just around 320MPa.

When both C1 and C2 are both inclined at $45°$ against the longitudinal axis as shown in Fig. 39(a), Fig. 39(b), Fig. 39(d), Fig. 39(e), and Fig. 39(g), the value of stress distribution in α lamellae are more or less balanced in both colonies without any trace of stress concentration in CB at $\varepsilon_o = 3\%$.

It is complicated for double-colony type model-(h), when C1 is perpendicular to the tensile direction. Although the α in C1 did deform plastically and showed a tendency to deform transversely, the equivalent stress σ_{eq}^{α} value in α lamellae is quite small. When C1 is parallel to the tensile direction, α lamellae is constrained by θ so the colony barely shows any deformation. The stress partitioning of the phases is prominent where θ accommodates most of the stress. However, this is not the case for model-(h) when C1 is perpendicular to the tensile direction. Even when α seems to not accommodate stress as shown in Fig. 39(h), if compared with Fig. 39(h) and Fig. 39(h) it is confirmed that α phase in C1 can deform plastically at low stress value.

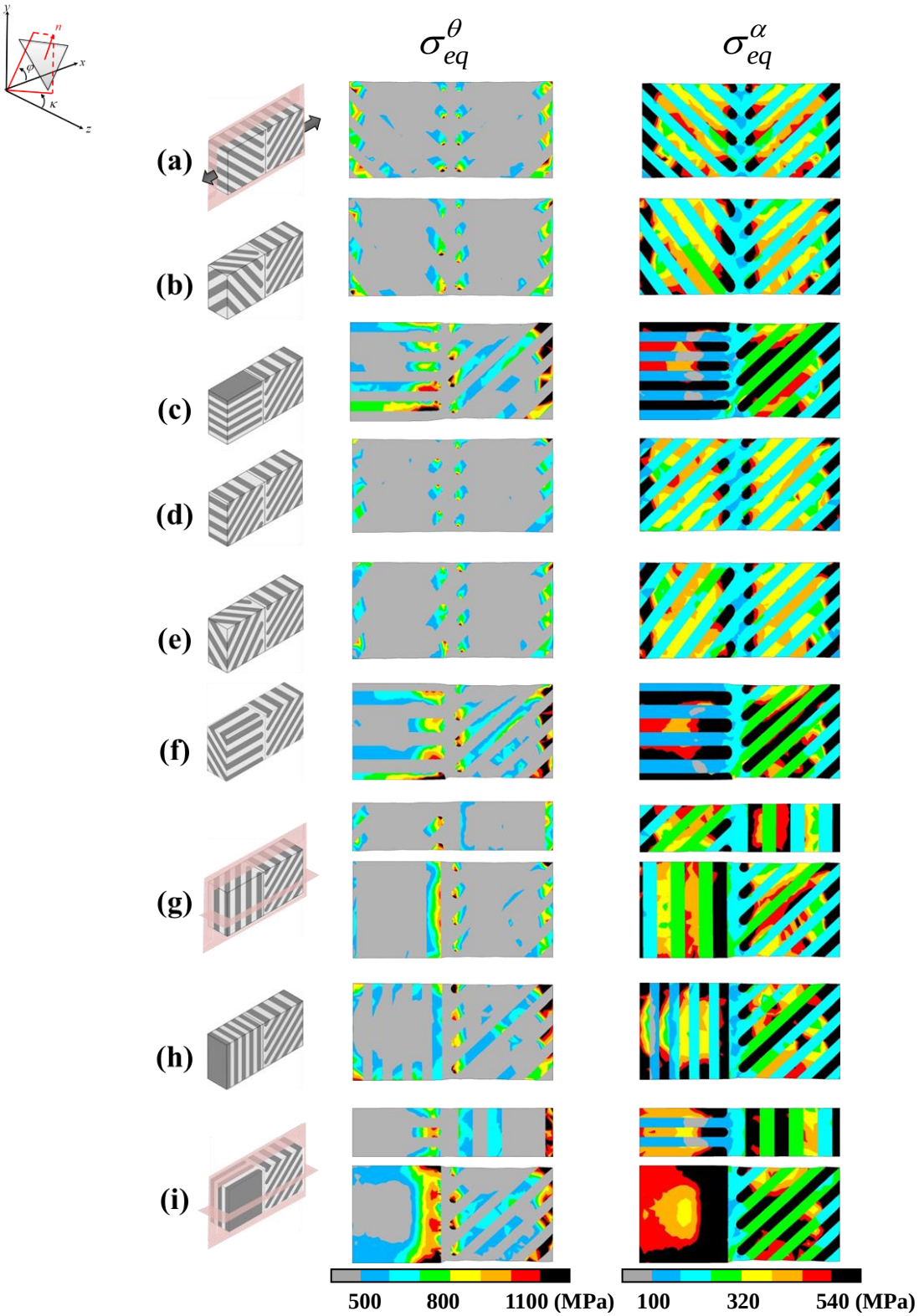

Fig. 39 Distribution of equivalent stress σ_{eq} at nominal strain $\varepsilon_o = 3\%$. Stress ranges are arranged for each θ and α are denoted as σ_{eq}^{θ} and σ_{eq}^{α} respectively.

Chapter 6 Elasto-plastic deformation of double-colony models

To study how the deformation of colonies influence on the overall mechanical responses of the double-colony models, the nominal stress σ_o versus the nominal strain ε_o curves are plotted. Here, the reaction forces of the models are calculated into nominal stress σ_o. Fig. 40 is the stress-strain curve of double-colony models. Since C2 is a constant variable for all the models, it is considered that the flow stress for C2 is more or less constant. Therefore, the difference of stress flow is dictated by C1. When C1 is parallel to the tensile direction, the stress flow is significantly higher than those that are inclined at $45°$ from the tensile direction. Double-colony models with high flow stress show concentration of strain at CB while those with lower responses show an overall deformation in C1 and C2. Therefore, it can be concluded that the difference of mechanical responses, which is expressed by the flow stress of single-colony models, between the colonies will determine the deformation of CB. From this study, the larger the mechanical differences between two adjacent colonies, the prominent the localisation of deformation around the CB.

Although generally for single-colony models, the lower flow stress trades-off with better ductility, it is not necessarily accurate for the double-colony models in this study. In the case of Fig. 40(e), it has been explained by Fig. 37 that the different directions of deformation in colonies caused the double-colony to twist. From Fig. 37(b) it is safe to

say the differences of directions for deformation of adjacent colonies influence the stability of the elasto-plastic deformation for double-colony. As for Fig. 40(i), the configuration of the θ lamellae might be the key to sustaining elasto-plastic deformation although localisation occurs in CB. However, the analyses conducted are not sufficient to elucidate the phenomenon for this particular case. This leads to another direct problem to be solved. We propose a study of how the transversal difference of alignment of (θ) would influence the elasto-plastic deformation of CB and the mechanical response of adjacent colonies.

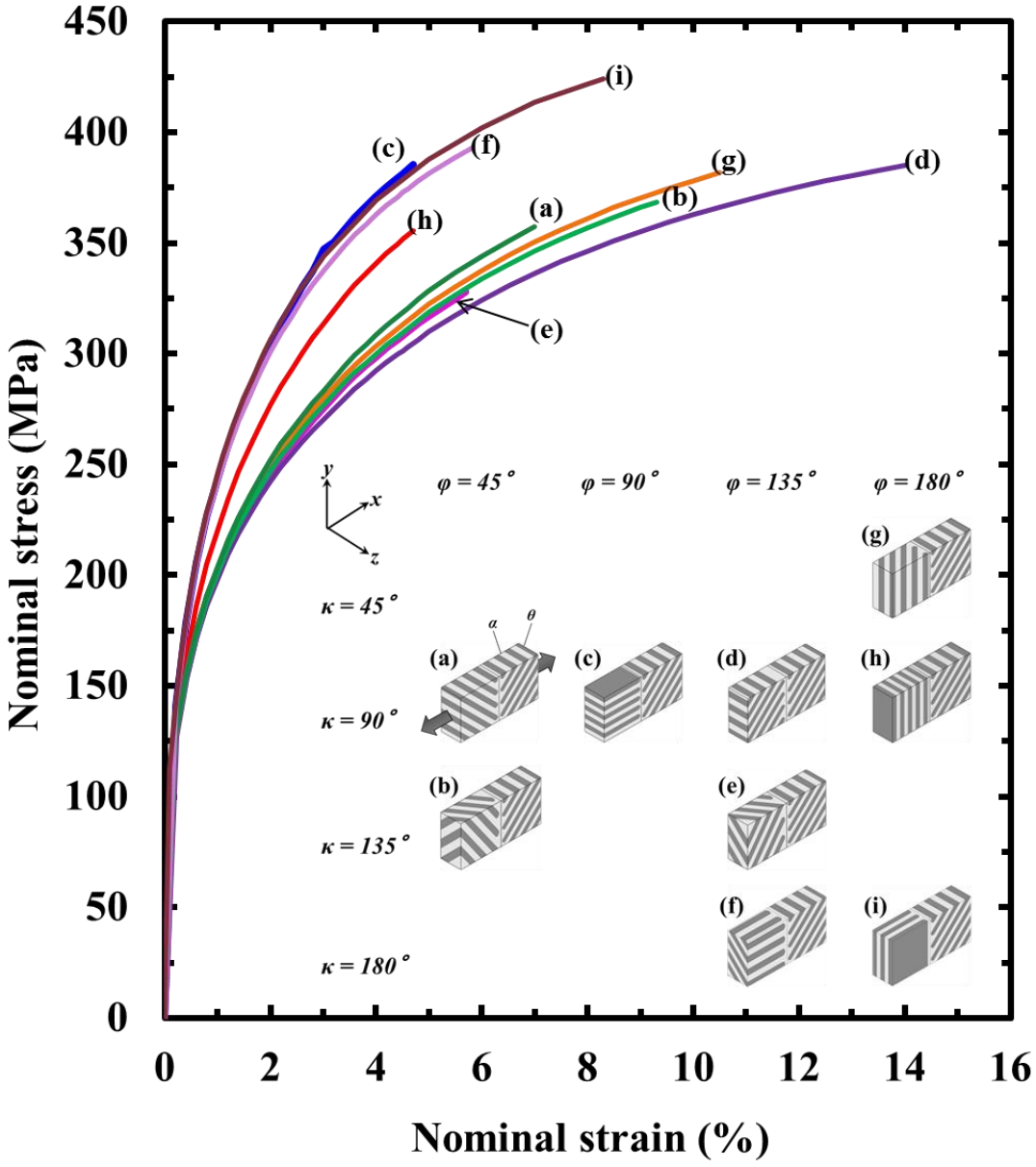

Fig. 40 The nominal stress σ_o vs. nominal strain ε_o curves of double-colony models.

Chapter 7

Discussion

We have studied the elasto-plastic deformation of single-colony, multi-colony, and double-colony models to understand the mechanical responses occurring in the pearlite colony structure.

Fig. 41 shows the distribution of stress components in single-colony model-(a), -(b), -(c), and -(d) in Fig. 41(a), Fig. 41(b), Fig. 41(c) and Fig. 41(d). The stress components are tensile direction stress component σ_{xx}, normal stress component σ_{yy}, transverse stress component σ_{zz}, and *xy*-shear stress component σ_{xy}. The *yz*- and *zx*-stress components are almost zero, so they are ignored. When the lamellar alignment is parallel to the tensile axis, the stress partitioning between the θ and α phases are significant, as shown in Fig. 41(e) and Fig. 41(i). This is due to the stress incompatibility between them. At equal strain condition, the elongation of θ lamellae bears more stress compared with the ductile α lamellae. Although we did not establish any particular crystal orientation for the models, the stress distribution for model-(a)

resembles that of the lamellar structure with Bagaryatsky orientation relationship by Yasuda and Ohashi [59]. This is because Bagaryatsky orientation plastic deformation in α occurs by double-slip compared with Pitsch-Petch orientation, in which plastic deformation occurs by single-slip. Not establishing any particular crystal orientation, the α of single-colony models is considered to have an infinite slip. This gives α the ability to plastically deform in infinite directions. Even so, the model did not shear because θ reaches maximum stress when it is forced to plastically deform together with α. Fig. 41(g) shows the single-colony model in equal stress condition. The stress is almost uniformly distributed in the centre of the model, and stress-partitioning shows up as the parameter closest to the surface of the model. This is because the influence of the Poisson's ratio is enhanced by the compressive nature of θ as shown in Fig. 41(l) and Fig. 41(p). For this model, the shear deformation is almost 0. It is clear that the stress magnitude increases when the lamellar alignment becomes closer to the tensile direction in Fig. 41(f) and Fig. 41(h). Note that, both models are modelled with two inclinations from the *xy*-plane at $\varphi = 45°$. It must be reminded that model-(d) in Fig. 41(d) is further imposed with an extra inclination transversely from the *z*-axis with inclination angle $\kappa = 45°$, as explained in Chapter 3 and Chapter 4. Therefore, due to the rotation, structure-wise, the lamellar alignment of model-(d) is slightly closer to the

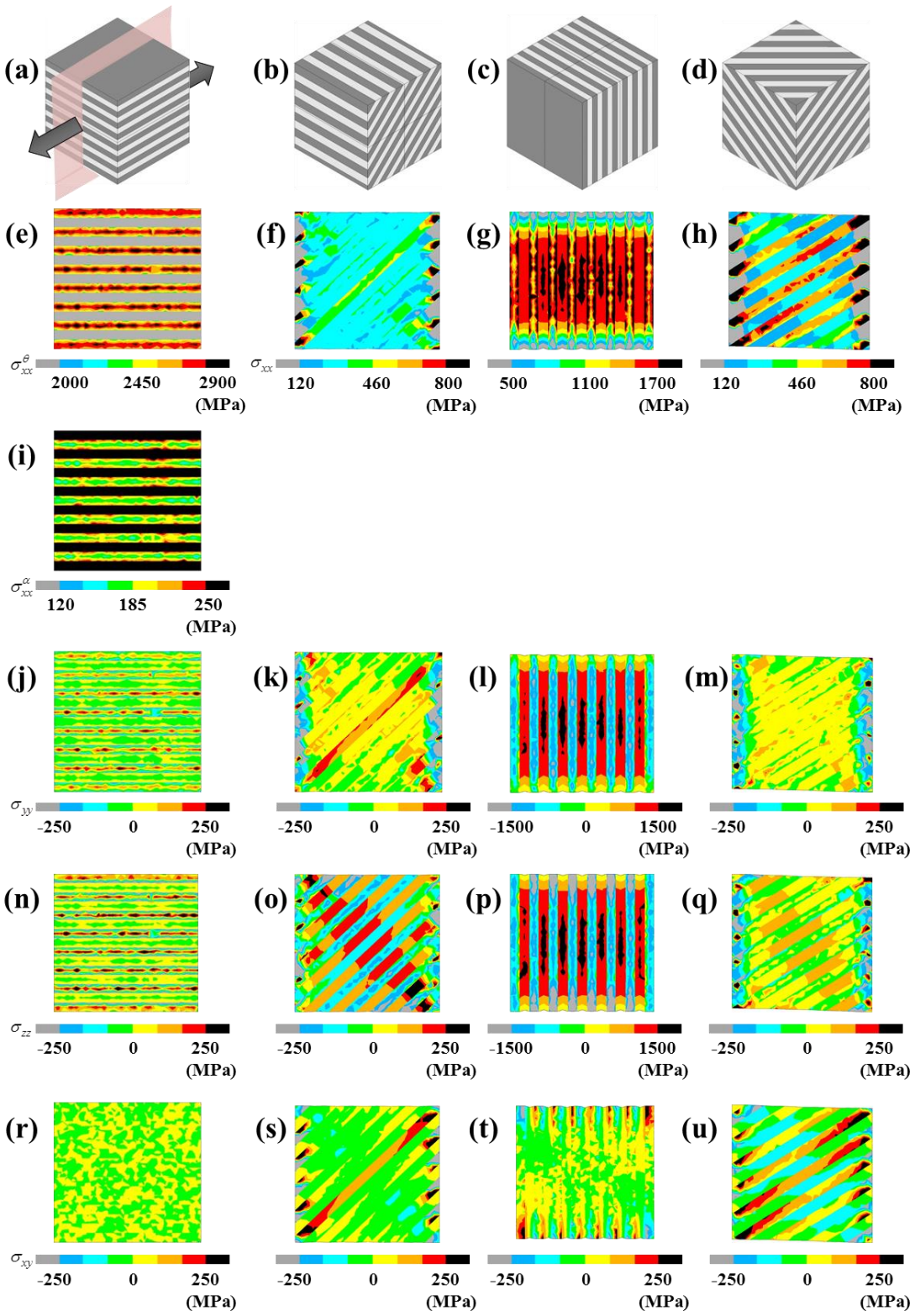

Fig. 41 Distribution of stress components in single-colony models.

tensile direction compared with model-(b) at the *xy*-plane. Plus the middle θ lamellar of model-(b) and some θ lamellar in model-(d) are constrained by boundary conditions on both lateral surfaces. This explains the high stress values, especially the shear stress σ_{xy} as shown in Fig. 41 (s) and Fig.41 (u).

From the study, the stress incompatibility increases as the lamellar alignment become closer to the tensile direction, which influences the stress-partitioning between θ and α. It is interesting that the tensile stress component σ_{xx} for model-(b) and model-(c) exhibit the same tendency to have uniformed stress distribution regardless of their magnitude differences where model-(b) leans towards the α range of stress while model-(c) leans towards the θ range of the stress contour.

Fig. 43 [36] shows the relationship of average equivalent plastic strain with the θ lamellar alignment towards the tensile direction observed experimentally. The figure shows that pearlite colony with alignment around $40°$ have the highest possibility to deform plastically, followed by those that are perpendicular towards the tensile direction. This experimental observation correlates well with our results. When single-colony models of such alignment is combined as double-colony models in Chapter 5, the single-colony models in which alignments are towards the “hard” tendency more or less cease to deform and the deformation accumulates at the ductile colonies and finally

localization occurs around the colony boundary because the deformation cannot progress further into the “hard” region. If we compare the mechanical responses represented by stress vs. strain curve of single-colonies and double-colonies in Fig. 26 and Fig. 40, it can be considered that the mechanical response is the mechanical correspondence between two adjacent colonies. Since the alignment of Colony2 (C2) of the double-colony is constant for all models, the difference that varies the stress and strain responses for the double-colony models are the mechanical responses of Colony1 (C1). The behaviour of plastic deformation in C2 for all double-colony models is more or less the same. The magnitude of the strain, however, is greatly attributed to the influence of the adjacent colony, C1.

First of all, referring to Fig. 42 while considering Fig. 26, colonies that are more or less parallel, at $0° \sim 30°$ towards the tensile direction will exhibit a high value of flow stress, which represents the mechanical responses; whereas if the alignment is around $40°$, the mechanical response displays ferritic strain and stress behaviour. So, for double-colony models, the mechanical responses depend on the lamellar alignments of adjacent colonies. If both colonies are aligned favourably, the mechanical response leans towards the α range of stress contour, and the whole model will plastically deform with no strain concentration at CB. The concentration of strain at the CB

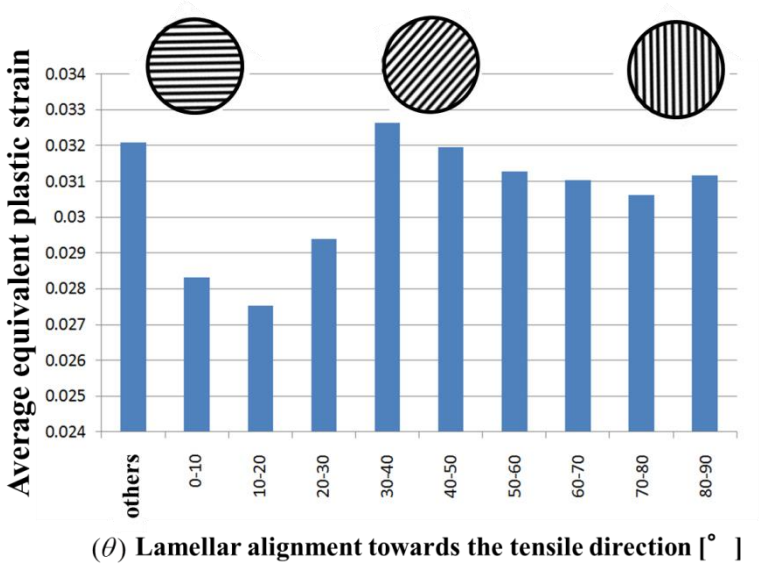

Fig. 42 The relationship between average equivalent plastic strain and θ lamellar alignment towards the tensile direction [36].

followed by localisation of plastic strain in α lamellar becomes easier when the difference of mechanical response between the colonies is large.

Model-(c), model-(e) and model-(h) in Fig. 40 shows models in which the analyses were among the earliest to be stopped. For model-(c), the difference of mechanical response around the colony boundary is too large. This cannot explain why model-(i) could deform plastically although the mechanical-difference is almost the same. Here, by using model-(b) and model-(e), we propose an idea that the transversal difference of lamellar alignment might be a hint to clarify this problem. Model-(b), similar with model-(e), has lamellar alignment that is imposed twice but the former displays better

plastic deformation. On the other hand, it should be reminded that model-(e) underwent severe twisting at the colony boundary compared with model-(b). Note that both model-(c) and model-(i) are parallel towards the tensile axis. Their difference is the transversal alignment. For model-(h), by referring to Fig. 39, there is a define stress partitioning between the θ lamellar and CB.

Bramfitt and Marder [111] found that lamellar alignment of θ influences dislocations faults in α. From the point of view of dislocation movement, Teshima et al. [112] explain that the mobility of dislocations in α are not blocked/restricted by the θ lamellar when the alignment of lamellar is about $45°$ inclined from the tensile axis. Therefore, α can deform more freely while θ remains in the elastic state. θ needs to harbour large stress to plastically deform for the dislocation to move. This is the reason why it is difficult for the single colony with parallel or perpendicular alignment to the tensile axis to plastically deform. Takahashi, Ponge and Raabe [113] suggested that pearlite colonies store a high concentration of geometrically necessary dislocations (GNDs). The constraint of plastic deformation imposed by external source generates GNDs. Although we are not clear about the origin of GND, it is logical that if pearlite colony structure undergoes tensile deformation, strain incompatibility occurring in the randomly aligned lamellar structures might generate GNDs. In their study [113], they

suggested that the differences of yield strength amongst colonies are caused by the difference of GNDs' densities in each colony. This explanation correlates well with the results of this research. Therefore, the combination of 3-D double-colony studies with crystal plasticity is a topic of interest. It is known that dislocation can be treated with heat treatment. Understanding the relationship of colony structure and dislocation will lead to the understanding of controlling pearlite toughness all together since the density of dislocations directly determines the ability to deform and the yield strength.

Chapter 8

Conclusions

We studied the elasto-plastic deformation of colony structure by using 3-D finite element analyses. For this purpose, we investigated the single-colony model to validate the influence of the alignment of cementite lamellar towards the elasto-plastic deformation of a multi-layer structure. From the single-colony structure, we know that when the cementite lamellar alignment is parallel with the tensile direction, the mechanical response is high and the colony deforms uniformly. Under the equal-strain condition, when the lamellar alignment is parallel to the tensile direction, cementite is forced to deform plastically together with the ductile ferrite. This induces stress incompatibility between cementite and ferrite phases, which caused the stress-partitioning. When the cementite alignment is inclined at $45°$, ferrite lamellae were able to deform because of the lack of constraint from cementite. Since cementite mostly remained elastic, the stress level in cementite phase is more or less like that in ferrite. When the cementite alignment is perpendicular to the tensile direction, the

model will be under equal-stress condition. Ferrite lamellae have to compensate the plastic deformation of cementite, which elevated the value of stress. Cementite will eventually yield, and the flow stress will follow that of ferrite, only with larger values.

It was difficult to understand the nature of deformation in multi-colony models, so single-colony models are combined into the double-colony model by joining them at the colony boundary. The colonies are referred as Colony1 (C1) and Colony2 (C2). C2 is a constant variable where the lamellar alignment is fixed at $45°$ to the tensile direction. This means the mechanical response for C2 is constant for all models. The elasto-plastic deformation of double-colony models is determined by the C1, which is the manipulative variable where the alignment of cementite lamellar is ever changing. When C1 is parallel to the tensile direction, the mechanical response is high with localisation at colony boundary (CB). When the lamellar alignments in both C1 and C2 are inclined at $45°$ towards the tensile axis, the double-colony models exhibit a holistic plastic deformation without any localisation around CB. However, the stability of elasto-plastic deformation of double-colony is found to be depending on the direction of deformation for each colony. So although lower flow stress without localisation in CB does promote stable plastic deformation in double-colony models, the stability will be compromised if the deformations of both colonies are not favourable with each other.

These double-colonies twisted at the colony boundary.

To elucidate the elasto-plastic deformation between neighbouring colonies, the study on how the angular differences at the transversal plane of alignment could influence the elasto-plastic deformation around the colony boundary is a point of interest that could lead to further possibilities. We also propose to study double-colony models from the perspective of crystal plasticity because the results shared strong agreements with the observations and proposed ideas concerning the topic.

Chapter 8 Conclusions

Empty page

References

[1] H. C. Sorby, On the application of very high powers to the study of the of the microscopic structure of steel, J Iron Steel Inst, 1 (1886), 140-147

[2] M. Gensamer, E. B. Pearsall and G. V. Smith, The mechanical properties of the isothermal decomposition products of austenite, Trans ASM., 28 (1940), 380-398.

[3] G. V. Smith and R. F. Mehl, Lattice relationship in decomposition of austenite to pearlite, bainite and martensite, Trans. AIME, 150.14 (1942), 211-226.

[4] W. H Brandt, Solution of the diffusion equation applicable to the edgewise growth of pearlite, J. App. Phys., 16.3 (1945), 139-146.

[5] G. W. Rathenau and G. Baas, Grain growth in a texture, studied by means of electron-emission microscopy, Physica, 17.2 (1951), 117-133.

[6] G. W. Rathenau and G. Baas, Electron-Optical Observations of Transformations in Eutectoid Steel, Acta Metall, 2 (1954), 875-883

[7] W. H Brandt, Solution of the diffusion equation applicable to the edgewise growth of pearlite, J. App. Phys., 16.3 (1945), 139-146.

[8] M. Hillert, The formation of pearlite, Procs Decomposition of Austenite by Diffusional Processes (Philadelphia, Pennsylvania, 1960/Oct./19) under the sponsorship of the Ferrous Metallurgy Committee of the Institute of Metals Division, The Metallurgical Society, American Institute of Mining, Metallurgical, and Petroleum Engineers (1962).

[9] F. C. Hull and R. F. Mehl, The structure of pearlite, Trans. ASM, 30 (1942), 381-424.

[10] P. R. Howell, The Pearlite Reaction in Steels Mechanisms and Crystallography : Part 1. From H. C. Sorby to R. F. Mehl, Mater. Charact., 40 (1998), 227-260.

[11] Zubov, V. Ya, Patenting of steel wire, Met. Sci. Heat Treat., 14.9 (1972), 793-800.

[12] B. L. Bramfitt and A. R Marder, Effect of cooling rate and alloying on the transformation of austenite, Metall. Trans., 4 (1973), 2291-2301.

[13] D. S. Zhou and G. J. Shiflet, Interfacial steps and growth mechanism in ferrous pearlite, Metall. Trans. A, 22A (1991), 1349-1365.

[14] D. B. Park, J. W. Lee. Y. S. Lee, K. T. Park and W. J. Nam, Effects of the annealing temperature and time on the microstructural evolution and corresponding mechanical properties of cold-drawn steel wires, Metal. Mater. Int., 14.1 (2008), 59-64.

[15] T. Takahashi, “Advances in high strength bridge wire –from Brookyln to Akashi” (Japanese), Suiyokai, 23 (1999), 26-36.

[16] H. Sutou, Piano-Sen-no-Kyōdo-to-sono-Shūhen (Japanese), B JIM, 9 (1970), 1-13.

References

[17] H. Tashiro, Piano wire of the highest tensile strength steel, Materia Japan, 35 (1996), 1177-1181.
[18] H. Tashiro and T. Tarui, State of the art for high tensile strength cord, SHINNITTETSU GIHO, 88 (2003), 77-80.
[19] K. E. Puttick, The structure, deformation, and fracture of pearlite, J. Iron Steel Inst., 185 (1957), 161-176.
[20] J. D. Embury and R. M Fisher, The structure and properties of drawn pearlite, Acta. Metall., 14 (1966), 147-159.
[21] A. R. Rosenfield, G. T. Hahn and J. D. Embury, Fracture of steels containing pearlite, Metall. Trans., 3 (1972), 2797-2804.
[22] G. Langford, Deformation of pearlite, Metall. Trans. A, 8A (1977), 861-875.
[23] T. Takahashi, M. Nagumo and Y. Asano, Microstructures dominating the ductility of euctoid pearlitic steels, J. JIM, 42 (1978), 708-715.
[24] J. P. Houin, A. Simon, G. Beck, Relationship between structure and mechanical properties of pearlite between 0.2% and 0.8% C, Iron Steel Inst. Jpn., 10 (1981), 726-731.
[25] J. G. Sevillano, Substructure and strengthening of heavily deformed single and two-phase metallic materials, J. Phys. III, 1 (1991), 967-988.
[26] A. M. Elwazri, P. Wanjara and S. Yue, The effect of microstructural characteristics of pearlite on the mechanical properties of hypereutectoid steel, Mater. Sci. Eng. A, 404 (2005), 91-98.
[27] X. Zhang, A. Godfrey, X. Huang, N. Hansen and Q. Liu, Microstructure and strengthening mechanisms in cold-drawn pearlitic steel wire, Acta Mater, 59 (2011), 3422-3430.
[28] T. Shimokawa, T. Ohashi, M. Tanaka and K. Higashida, Investigation of deformation behavior of pearlitic steel by the fusion of material sciences and solid mechanics –A search for a guiding principle for a coexistence of high strength and high ductility, Tetsu-to-Hagane, 98 (2012), 745-750.
[29] J. Toribio, B. González and J. C. Matos, Microstructure and mechanical properties in progressively drawn pearlitic steel, Mater. Trans., 55 (2014), 93-98.
[30] M. Ochiai, S. Nishida, H. Ohba, H. Kawata, Application of hypereutectoid steel for development of high strength steel wire, Tetsu-to-Hagane, 79 (1993), 1101-1107.
[31] Y. J. Li, P. Choi, S. Goto, C. Borchers, D. Raabe and R. Kirchheim, Evolution of strength and microstructure during annealing of heavily cold-drawn 6.3 GPa hypereutectoid pearlitic steel wire, Acta. Mater., 60 (2012), 4005-4016.
[32] C. N. T. Belaiew, The inner structure of the pearlite grain, J. Iron Steel Inst., 1 (1922), 201-227.

References

[33] R. F. Mehl and D. W. Smith, Orientation of ferrite in pearlite, Trans. AIME, 113 (1935), 330-341.

[34] H. Jolivet, Tranformation of austenite on cooling; morphology and genesis of the aggregates formed, J. Iron Steel Inst., 2 (1939), 95-114.

[35] T. Takahashi, M. Nagumo and Y. Asano, Crystallographic features and formation processes of pearlite block, J.JIM, 42 (1978), 716-723

[36] M. Tanaka, Kyushu University, Private communication.

[37] J. Toribio and E. Ovejero, Effect of cumulative cold drawing on the pearlite interlamellar spacing in eutectoid steel, Script. Mater., 39(1998), 323-328.

[38] M. Zelin, Microstructure evolution in pearlitic steels during wire drawing, Acta. Mater., 50 (2002), 4431-4447.

[39] X. Zhang, C. X. Wang, X. M. Liu and Q. N. Shi, Microstructure evolution and mechanical hardening of hypereutectoid pearlitic steel during cold rolling, Acta. Metall. Sin., 20 (2007), 287-292.

[40] X. Zhang, A. Godfrey, N. Hansen. X. Huang, W. Liu and Q. Liu, Evolution of cementite morphology in pearlitic steel wire during wet wire drawing, Mater. Charact., 61 (2010), 65-72.

[41] K. Pankaj, N. P. Gurao, A. Haldar and S. Suwas, Progressive changes in the microstructure and texture in pearlitic steel wire drawing, ISIJ Int., 51(2011), 679-684

[42] M. Umemoto and K. Tsuchiya, Fundamental properties of cementite and their present understanding, Tetsu-to-Hagane, 88 (2002), 117-128.

[43] M. Umemoto, Properties of cementite left unknown, B. ISIJ, 9 (2004), 151-156.

[44] M. Tanaka, Y. Yoshimi, K. Higashida, T. Shimokawa and T. Ohashi, A multiscale approach for the deformation mechanism in pearlite microstructure: Experimental measurements of strain distribution using a novel technique of precision markers, Mater. Sci. Eng. A, 590 (2014), 37-43.

[45] K. Maurer, Deformation of cementation, Philos. Mag., 15.134 (1967), 321-327.

[46] J. G. Sevillano, Room temperature plastic deformation of pearlitic cementite, Mater. Sci. Eng., 21 (1975), 221-225.

[47] M. Ojima, J. Inoue, S. Nambu, P. Xu, K. Akita, H. Suzuki and T. Koseki, Stress partitioning behavior of multilayered steels during tensile deformation measured by in situ neutron diffraction, Script. Mater., 66 (2012), 139-142

[48] J. C. M. Li and Y. T. Chou, The role of dislocations in the flow stress grain size relationships, Metall. Trans., 1 (1970), 1145-1159.

[49] E. O. Hall, The deformation and ageing of mild steel: III discussion of results, Proc. Phys. Soc. Lodd. B 64 (1951), 747.

References

[50] N. J. Petch, The cleavage strength of polycrystals J. Iron Steel Inst., 174 (1953), 25-28.

[51] A. R. Marder and B. L. Bramfitt, The effect of morphology on the strength of pearlite, Metall. Trans. A, 7 (1976), 365-372

[52] K. Kato and T. Ohashi, Multi axial stress field in microstructure of two-phased steels, Proc: JSME 40th Hokkaido Meeting (2011), pp. 3-4.

[53] L. Roslan, Finite Element Analyses of Elasto-plastic deformation in Lamellar Microstructure, Kitami Institute of Technology Master Thesis (2012).

[54] N. Jia, Z. H. Cong, X. Sun, S. Cheng, Z. H. Nie, Y. Ren, P. K. Liaw and Y. D. Wang, An in situ high-energy x-ray diffraction study of micromechanical behavior of multiple phases in advance high-strength steels, Acta. Mater., 57 (2009), 3965-3977.

[55] C. M. Bae, C. S. Lee and W. J. Nam, Effect of carbon content on mechanical properties of fully pearlitic steels, Mater. Sci. Tech., 18 (2002), 1317-1321.

[56] K. Tanaka and S. Matsuoka, The work hardening and fracture of steels containing cementite, Acta Metall., 22 (1974), 153-163.

[57] B. Karlsson and G. Lindén, Plastic deformation of eutectoid steel with different cementite morphologies, Mater. Sci. Eng., 17 (1975), 153-164.

[58] T. W. Butler and D. C. Drucker, Yield strength and microstructural scale: A continuum study of pearlitic versus spheroidized steel, J. App. Mech., 40.3 (1973), 780-784.

[59] Y. Yasuda and T. Ohashi, Crystal plasticity analyses of scale dependent mechanical properties of ferrite/cementite lamellar structure model in pearlite steel wire with Bagaryatsky or Pitsch-Petch orientation relationship, ISIJ Int., 411 (2016)

[60] T. Gladman,, I. D. McIvor and F. B. Pickering. Some aspects of the structure-property relationships in high-C ferrite-pearlite ateels. J. Iron Steel Inst., 210.12 (1972), 916-930.

[61] L. E. Miller., and G. C. Smith, Tensile fractures in carbon steels, J. Iron Steel Inst., 208.11 (1970), 998-1005.

[62] C. Suruga, Numerical analyses of elasto-plastic deformation occurring around the colony boundary of pearlite colony, Kitami Institute of Technology, Bachelor Thesis (2013).

[63] X. Zhang, A. Godfrey, N. Hansen and x. Huang, Hierarchical structures in cold-drawn pearlite steel wire, Acta Mater., 61 (2013), 4898-4909.

[64] M. Dao, B. K. Kad and R. J. Asaro, Deformation and fracture under compressive loading in lamellar TiAl microstructures. *Philos. Mag. A*, 74.3 (1996), 569-591.

[65] N. Murakami and Y. Adachi, Bachelor Thesis (2015), Kagoshima University.

[66] Y. Adachi, S. Morooka, K. Nakajima and Y. Sugimoto, Computer-aided three-dimensional visualization of twisted cementite lamellae in eutectoid steel, Acta Mater., 56 (2008), 5995-6002.

References

[67] D. C. Joy, D. E. Newbury and D. L. Davidson, Electron channeling patterns in the scanning electron microscope, J. Appl. Phys., 53.8 (1982), 81-122.

[68] T. Hideo and M. Ezumi, Scanning electron microscope, U.S. Patent No. 5,872,358, (1999).

[69] F. J. Humphreys, Quantitative metallography by electron backscattered diffraction, J. Microsc., 195.3 (1999), 170-185.

[70] A. Walentek, M. Seefeldt, B. Verlinden, E. Aernoudt and P. Van Houtte, Electron backscatter diffraction on pearlite structures in steel, J. Microsc., 224.3 (2006), 256-263.

[71] A. F. Gourgues-Lorenzon, Application of electron backscatter diffraction to the study of phase transformations, Int. Mater. Rev, 52.2 (2007), 65-128.

[72] A. Walentek, M. Seefeldt, B. Verlinden, E. Aernoudt and P. Van Houtte, Investigation of pearlite structure by means of electron backscatter diffraction and image analysis of SEM micrographs with an application of the Hough transform, Mater. Sci. Eng. A, 483-484 (2008), 716-718.

[73] N. Guo, Q. Liu, Y. C. Xin, B. F. Luan and Z. Zheng, The application of back-scattered electron imaging for characterization of pearlitic steels, Sci. China Tech. Sci., 54.9 (2011), 2368-2372.

[74] N. Guo and Q. Liu, Back-scattered electron imaging combined with EBSD technique for characterization of pearlitic steels, J. Microsc., 246.3 (2012), 221-228.

[75] Y. A. Bagaryartsky, Probable mechnism of martensite decomposition, Dokl Akad Nauk SSSR, 73 (1950), 1161-1164.

[76] N. J. Petch, The orientation relationship between cementite and α-iron, Acta Crystallogr., 6 (1953), 96.

[77] W. Pitsch, Der orientierung zusammenhang zwischen zementit und ferrit in perlit, Acta. Metall., 10 (1962), 79-80.

[78] D. S. Zhou and G. J. Shiflet, Interfacial steps and growth mechanism in ferous pearlites, Metall. Trans. A, 22A (1991), 1349-1365.

[79] D. S. Zhou and G. J. Shiflet, Ferrite : Cementite crystallography in pearlite, Metall. Trans. A, 23A (1992), 1259-1267.

[80] M. X. Zhang and P. M. Kelly, Accurate orientation relationships between ferrite and cementite in pearlite, Scripta. Mater., 37.12 (1997), 2009-2015.

[81] M. A. Mangan and G. J. Shiflet, The Pitsch-Petch orientation relationship in ferrous pearlite at small undercooling, Metall. Mater. Trans. A, 30A (1999), 2767-2781.

[82] M. A. Mangan, P. D. Lauren and G. J. Shiflet, Three-dimensional reconstruction of Widmanstätten plates in Fe-12・3Mn-0・8C, J. Microsc., 188.1 (1997), 36-41

[83] M. V. Kral, M. A. Mangan, G. Spanos and R. O. Rosenberg, Three-dimensional analysis of mircostructures, Mater. Charact., 45 (2000), 17-23.

References

[84] M. De Graef, M. V. Kral and M. Hillert, A modern 3-D view of an “old” pearlite colony, J. O. M., 58.12 (2006), 25-28.

[85] D. Zaefferer, S. I. Wright and D. Raabe, Three-dimensional orientation microscopy in a focused ion beam-scanning electron microscope: A new dimension of microstructure characterization, Metall. Mater. Trans. A, 39A (2008), 374-389.

[86] Y. T. Wang, Y. Adachi, K. Nakajima and Y. Sugimoto, Quantitative three-dimensional characterization of pearlite spheroidization, Acta. Mater., 58 (2010), 4849-4858.

[87] M. K. Miller, Three-dimensional atom probes, J. Microsc., 186.1 (1997), 1-16.

[88] Y. J. Li, P. Choi, C. Borchers, Y. Z. Chen, S. Goto, D. Raabe, R. Kirchheim, Atom probe tomography characterization of heavily cold drawn pearlitic steel wire, Ultramicroscopy, 111 (2011), 628-632.

[89] Y. J. Li, P. Choi, C. Borchers, S. Westerkamp, S. Goto, D. Raabe and R. Kirchheim, Atomic-scale, mechanism of deformation-induced cementite decomposition in pearlite, Acta Mater., 59 (2011), 3965-3977.

[90] Y. J. Li, D. Raabe, M. Herbig, P-P Choi, S. Goto, A. Kostka, H. Yarita, C. Borchers and R. Kircheim, Segregation stabilizes nanocrystalline bulk steel with near theoretical strength, Physc. Rev. Let., 113 (2014), 106104 1-5.

[91] Y. Ling, Uniaxial true stress-strain after necking, AMP J Tech., Vol 5 (1996), pp. 37-48

[92] H. W. Swift, Plastic instability under plane stress, J Mech Phys Solids, Vol. 1 (1952), pp. 1-18.

[93] M. Umemoto, Y. Todaka, T. Takahashi, P. Li, R. Tokumiya and K. Tsuchiya, High temperature deformation behavior of bulk cementite produced by mechanical alloying and spark plasma sintering, Mater. Sci. Eng. A, Vol. 375-377 (2004), pp. 894-898

[94] A. Kanie, Y. Tomota, S. Torii and T. Kamiyama, Elastic stains of cementite in a pearlite steel during tensile deformation measured by neutron diffraction, ISIJ Int, Vol. 44 (2004), pp. 1952-1956

[95] F. Yoshida (1997), Dansei-Rikigaku-No-Kiso, Tokyo, Kyouritsu Shuppan

[96] J. Chakrabarty (1987), Theory of Plasticity, A. Duffy (Ed.), New York, McGraw-Hill Book Company

[97] A. S. Khan and S. Huang (1995), Continuum Theory of Plasticity, New York, John Wiley & Sons.

[98] S. P. Timoshenko and J. N. Goodier (1970), Theory of Elasticity, New York, McGraw-Hill Book Company.

[99] M. Umemoto, (2010, November) Relationship between microstructure and mechanical properties in steels, Work-hardening seminar, Kumamoto

References

[100] R. v. Mises, Mechanik der festen Körper im plastisch-deformablen Zustand, Nachrichten von der Gesellschaft der Wissenschaften zu Göttingen, Mathematisch-Physikalische Klasse (1913), 582-592.

[101] D. R. Bland, The associated flow rule of plasticity, J. Mech. Phys. Solids, 6 (1937), 71-78.

[102] Auckland.ac.nz, Solid mechanics part II: Engineering solid mechanics small strain, <http://homepages.engineering.auckland.ac.nz/~pkel015/SolidMechanicsBooks/index.html>

[103] O. T. Bruhns, The Prandtl-Reuss equations revisited, ZAMM, 94 (2014), 187-202.

[104] A. Mendelson, Plasticity: Theory and application, The Macmillan Company New York and Collier-Macmillan LTD. London, (1964), 34-35.

[105] H. Yahyaoui, H. Sidhom, C. Braham and A. Baczmanski, "Effect of interlamellar spacing on the elastoplastic behavior of C70 pearlitic steel: Experimental results and self-consistent modeling", Mater. Desig., 55 (2014), 888-897.

[106] N. J. Petch, The interpretation of the crystal structure of cementite, J. Iron Steel Inst., 149 (1944), 143-150.

[107] D. P. Clausing, The development of fibrous fracture in a mild steel, Trans ASM, 60 (1967), pp. 504-515.

[108] Y. Yamada, Static strain aging of eutectoid C steel wires, Trans. Iron Steel. Inst. Jpn., 16.8 (1976), 417-426.

[109] T. Tarui, N. Maruyama, J. Takahashi, S. Nishida and H. Tashiro, "Microstructure control and strengthening of high carbon steel wires", (2004), SHINNITTETSU GIHO, 51-56.

[110] K. Shimizu and N. Kawabe, Size dependence of delamination of high-carbon steel wire, Iron Steel Inst. Jpn. Int., 41.2 (2001), 183-191.

[111] B.L. Bramfitt and A. R. Marder, A transmission-electron-microscopy study of the substructure of high-purity pearlite, Metallography, 6 (1973), 483-495.

[112] T. Teshima, M. Kosaka, K. Ushioda, N. Koga and N. Nakada, Local cementite cracking induced by heterogeneous plastic deformation in lamellar pearlite, Mater. Sci. Eng. A, <http://dx.doi.org/10.1016/j.msea.2016.10.018>

[113] T. Takahashi, D. Ponge and D. Raabe, Investigation of orientation gradients in pearlite in hypoeutectoid steel by use of orientation imaging microscopy, Steel Res. Int., 78(2007), 38-44.

Empty page

Accomplishments –Publications and conferences

Publications

1. Tetsuya Ohashi, Lidyana Roslan, Kohsuke Takahashi, Tomotsugu Shimokawa, Masaki Tanaka and Kenji Higashida, A multiscale approach for the deformation mechanism in pearlite microstructure: Numerical evaluation of elasto-plastic deformation in finite lamellar structures, Mater. Sci. Eng. A, 588 (2013), 214-220.

2. Lidyana Roslan, Tetsuya Ohashi, Yohei Yasuda, Kohsuke Takahashi and Chikara Suruga, Finite element analyses of elasto-plastic deformation in pearlite lamellar and colony structures, Key Eng. Mater., 626 (2015), 307-310.

3. Lidyana Roslan, Tetsuya Ohashi, Yohei Yasuda and Chikara Suruga, Elasto-plastic deformation of colony boundaries in pearlite microstructure by finite element analyses, App. Mech. Mater., 786 (2015), 33-36.

4. Lidyana Roslan, Tetsuya Ohashi and Yohei Yasuda, Finite element analyses of elasto-plastic deformation in pearlite colony structures, Proc. 4th International Symposium on Steel Science (ISSS-2014), P14, 131-134.

Conferences

1. 2012/10/6

大橋鉄也，佐藤満弘，リディアナ　ロスラン，高橋宏輔，パーライト相に生じる弾塑性変形の解析‐積層数増加による不安定変形抑制，北海道支部第51回講演会，北見工業大学.

2. 2012/10/6～2012/10/6

大橋鉄也，リディアナ　ロスラン，高橋宏輔，佐藤満弘，微細積層に生じる弾塑性変形の有限要素解析，日本機械学会第25回計算力学講演会 (CMD-2012),神戸ポートアイランド南地区.

3. 2014/9/1～2014/9/5

L. Roslan, T. Ohashi, Y. Yasuda, K. Takahashi and C. Suruga, Finite element analyses of elasto-plastic deformation in pearlite lamellar and colony structures, 12th Asia-Pacific Conference on Engineering Plasticity and Its Application (AEPA-2014), Kaohsiung Taiwan.

4. 2014/9/24～2014/9/26

リディアナ　ロスラン，大橋鉄也，安田洋平，パーライトコロニー界面近傍に生じる弾塑性変位系の有限要素解析，一般社団法人日本鉄鋼協会第168回秋講演大会，名古屋大学東山キャンパス.

5. 2014/9/27

リディアナ　ロスラン，大橋鉄也，佐藤満弘，安田洋平，パーライトコロニー界面近傍に生じる弾塑性変形の三次元有限要素解析，北海道支部第53回講演会，室蘭工業大学.

6. 2014/11/3～2014/11/6

L. Roslan, T. Ohashi, Y. Yasuda, Finite element analyses of elasto-plastic deformation in pearlite colony structures, The 4th International Symposium on Steel Science (ISSS-2014), Kaisai Seminar House Kyoto

7. 2014/11/22～2014/11/24

リディアナ　ロスラン，大橋鉄也，安田洋平，パーライトコロニー構造における弾塑性変形の有限要素解析，日本機械学会第27回計算力学講演会 (CMD-2014)，岩手大学

8. 2015/3/30～2014/3/31

L. Roslan, T. Ohashi, Y. Yasuda and C. Suruga, Elasto-plastic deformation of colony boundaries in pearlite microstructure by finite element analyses, International Conference on Applications and Design in Mechanical Engineering (ICADME-2015), Pulau Pinang Malaysia

Empty page

Appendix

Dissertation defence slide

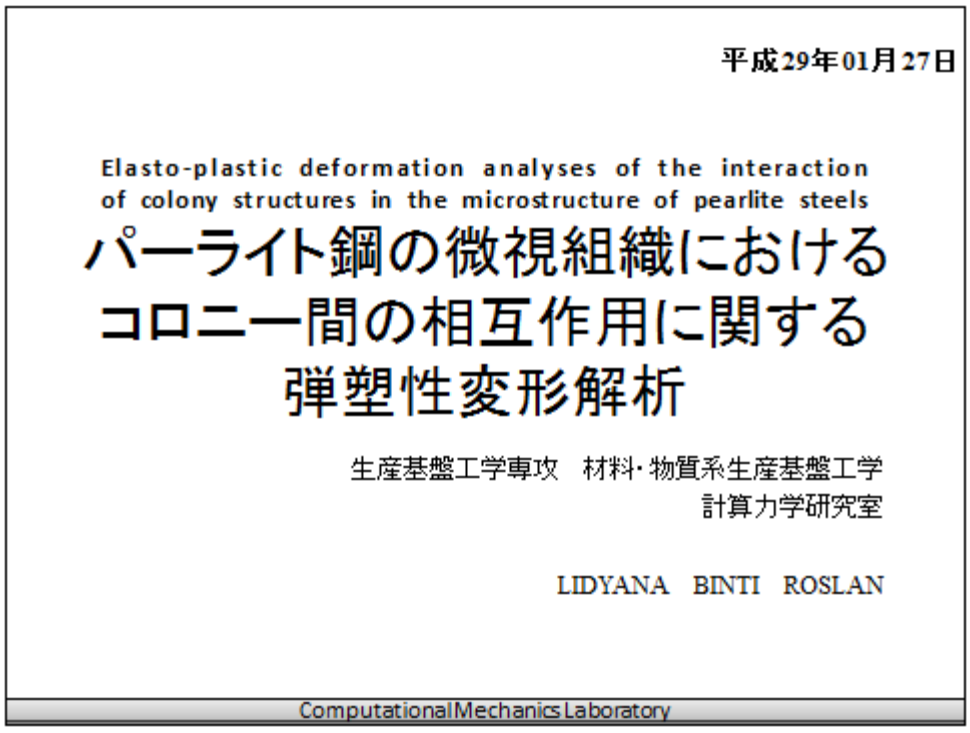

Appendix
Dissertation defence slide

序論

2

- 研究背景
- パーライト鋼の組織
- パーライト鋼の塑性変形
- セメンタイトの塑性変形
- パーライト鋼の延性と強度の特徴
- フェライト層の強化
- フェライト(α)の加工硬化による不安定変形の抑制
- セメンタイト層の配向方向と塑性変形
- 2D的な観察の問題
- 研究動機

Computational Mechanics Laboratory

研究背景

3

- 炭素鋼を実用するため，強度と延性が欠かせない
- パーライト鋼は強度と靭性に優れている
- 建築物の材料等に広く使われている

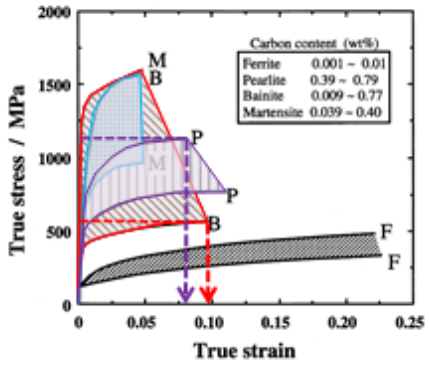

炭素鋼の応力－ひずみ曲線の略図
(M. Umemoto et. al., Metall. Mater. Trans. A (2000))

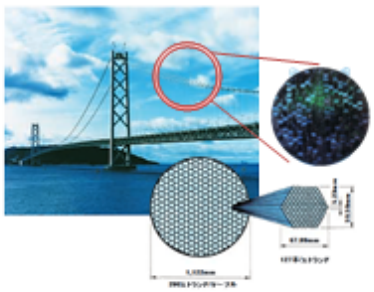

明石海峡大橋のケーブルワイヤ
(T. Tarui, Monthly-NSC (2005))

パーライト鋼の高強度かつ延性特性はその微視組織に由来する

Computational Mechanics Laboratory

Appendix
Dissertation defence slide

パーライト鋼の微視組織

4

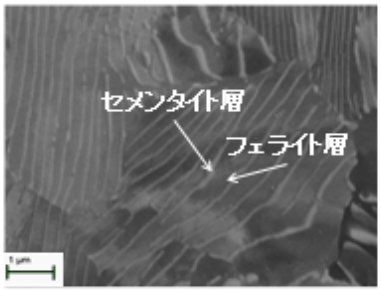

パーライト鋼の微視組織のSEM*画像
(M. Tanaka, Kyushu University, private communication)
*SEM: 走査型電子顕微鏡

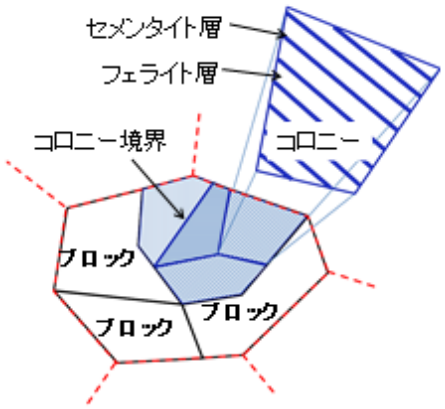

パーライト鋼の微視組織の略図

- セメンタイト： 高強度・脆い
- フェライト： 低強度・延性を持つ
- 交互に積層している

- コロニー： 積層の配向方向が同じ領域
- ブロック： コロニーの結晶方位が同じ領域

Computational Mechanics Laboratory

セメンタイトの塑性変形

5

- 室温：セメンタイトは脆性である
- パーライト鋼の延性特性はセメンタイトの塑性変形に影響を受ける
(G. Langford, Metall. Trans. A (1977))

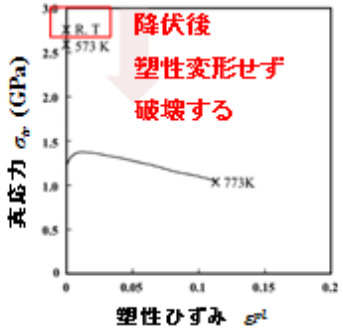

セメンタイトの応力 - ひずみ曲線
(M. Umemoto et. al, Mater. Sci. Eng. A (2004))

単体セメンタイト

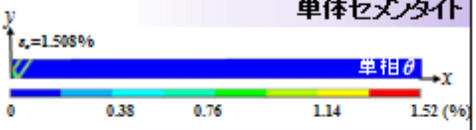

フェライトと積層したセメンタイト

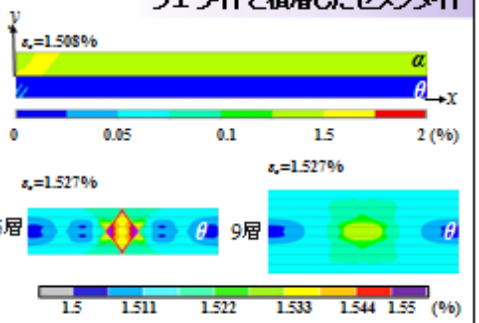

セメンタイト層内の引張方向成分の塑性ひずみの分布 (T. Ohashi et. al, Mater. Sci. Eng. A (2013))

フェライトと積層したセメンタイト ⇨ 局所変形が抑制され、塑性変形が安定化する

Computational Mechanics Laboratory

Appendix
Dissertation defence slide

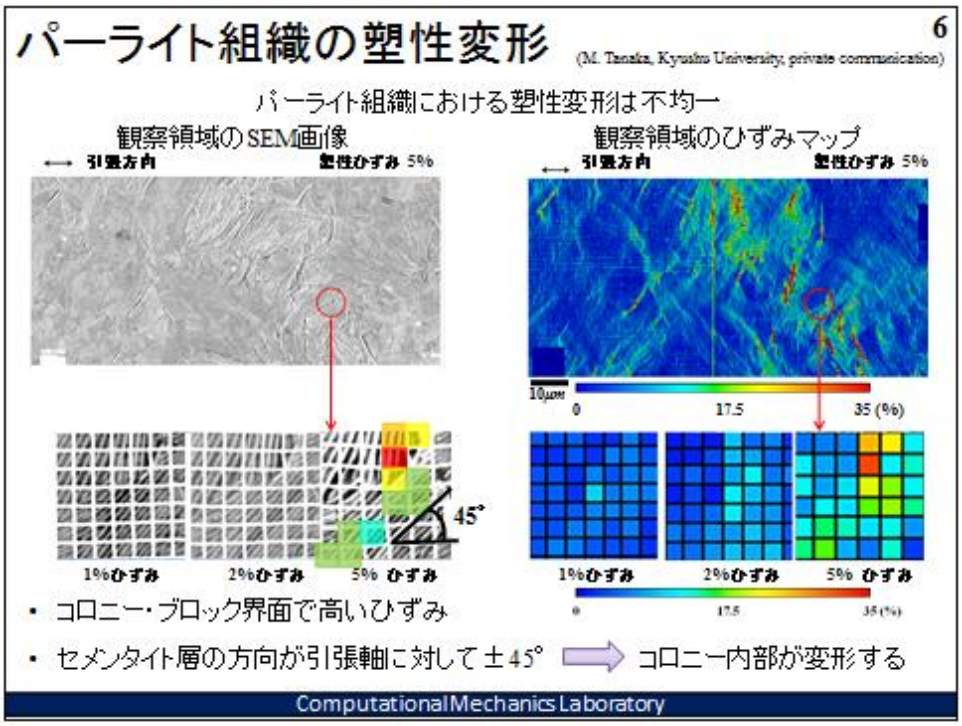

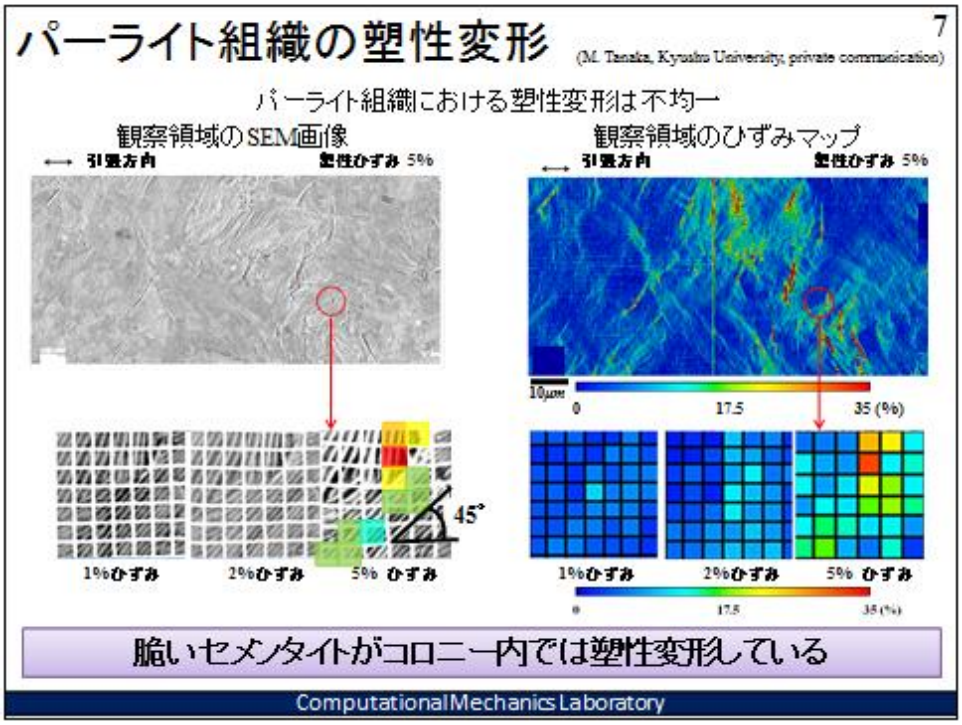

Appendix
Dissertation defence slide

パーライト鋼の延性と強度の特徴

8

ブロック直径が小さくなる　**コロニーサイズが小さくなる**　層間厚さが小さくなる

⇨ 脆性破壊の領域が減少する

⇨ パーライト鋼がより延性になる

⇨ 降伏応力が高くなる

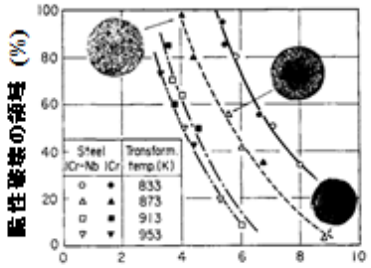

パーライトブロックの直径と脆性領域の関係

(T. Takahashi et. al, JIM (1978))

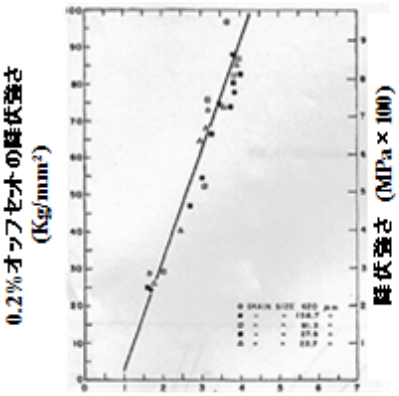

層間厚さと降伏強さの関係

(A. R. Marder & B. L. Bramfit, Metal. Trans. A (1975))

Computational Mechanics Laboratory

フェライト層の強化

9

積層構造の層間厚さが小さくなる

⇨ フェライト層内の転位の密度が高くなる

フェライト層内の転位の密度が高くなる

⇨ フェライトの降伏応力が高くなる

伸線ひずみ $\varepsilon = 0.68$, 転位の密度: $7 \times 10^{14}\ m^{-2}$

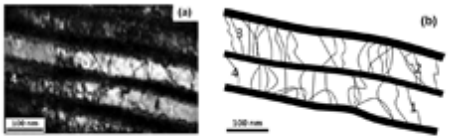

伸線ひずみ $\varepsilon = 2.67$, 転位の密度: $8.8 \times 10^{15}\ m^{-2}$

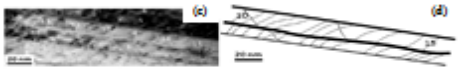

フェライト層内に蓄積している転位のTEM* 画像 (M. X. Zhang et al., Acta Mater. (2011))

*TEM: 透過型電子顕微鏡

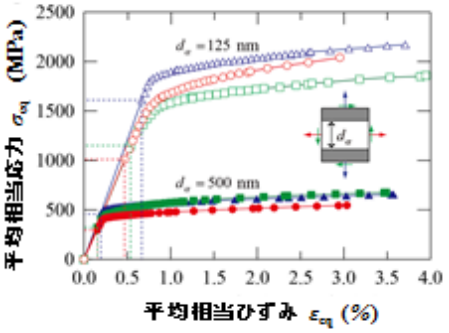

フェライト層の厚さが125*nm*と500*nm*の時の平均相当応力と平均相当ひずみの関係

(Yasuda et al., Key Eng. Mater (2015))

Computational Mechanics Laboratory

Appendix
Dissertation defence slide

フェライト相が強くなるとセメンタイト相の塑性変形へどのような影響を与えるか？ 10

フェライト(α)の加工硬化による不安定変形の抑制

(本論文, 第4.2章)

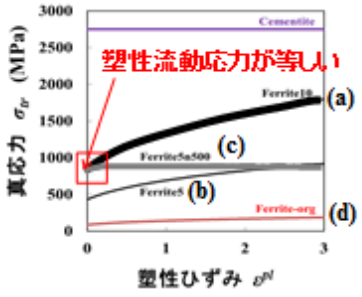

各材料の応力－ひずみ曲線. Cementite[1]とFerrite-org[2]以外，人工的な材料である.

1. M. Umemoto et. al, Mater. Sci. Eng. A (2004)
2. M. Umemoto , Work-hardening seminar Kumamoto (2010)

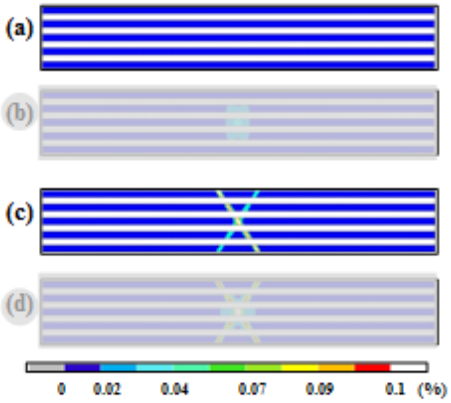

公称ひずみがε_e=1.529%の時の引張軸成分の塑性ひずみε^{pl}の分布

フェライトの加工硬化率が高くなる ⇨ • セメンタイト内の塑性変形が抑制される

ComputationalMechanicsLaboratory

11

フェライト(α)の加工硬化による不安定変形の抑制

(本論文, 第4.2章)

塑性流動が高くなる

⇨ モデルの最大応力が高くなる

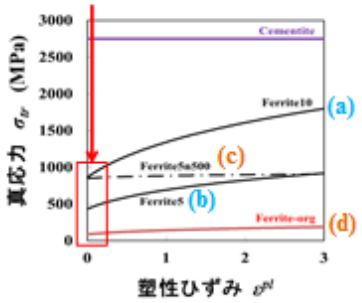

各材料の応力－ひずみ曲線. Cementite[1]とFerrite-org[2]以外，人工的な材料である.

1. M. Umemoto et. al, Mater. Sci. Eng. A (2004)
2. M. Umemoto , Work-hardening seminar Kumamoto (2010)

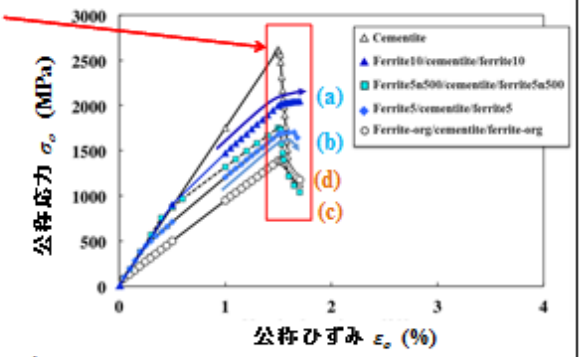

積層構造のモデルの応力－ひずみ曲線

フェライトの加工硬化率が高くなる ⇨ • セメンタイト内の塑性変形が抑制される
• セメンタイト内の塑性変形が安定化する

ComputationalMechanicsLaboratory

Appendix
Dissertation defence slide

セメンタイト層の配向方向と塑性変形

12

- フェライトと積層すること以外，セメンタイト層の配向方向もパーライトコロニーの塑性変形を影響する

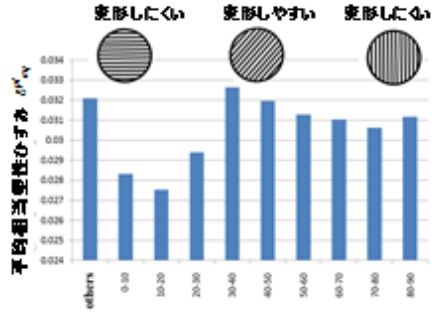

平均相当塑性ひずみ$\bar{\varepsilon}^{pl}_{eq}$とセメンタイト($\theta$)層の配向方向の関係

(M. Tanaka, Kyushu University, private communication)

- セメンタイト層による転位移動が妨害される ⇨ 変形しにくくなる

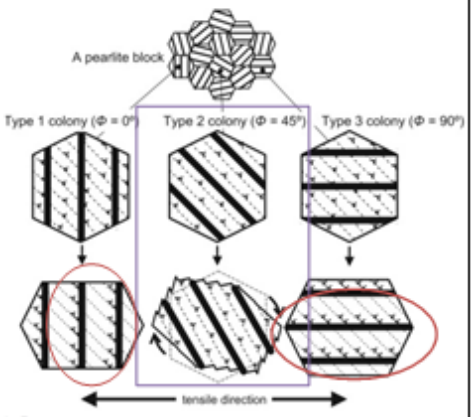

セメンタイト層と転位移動略図

(T. Teshima et. al., Mater. Sci. Eng. A, (2016))

ComputationalMechanics Laboratory

セメンタイト層の配向方向と塑性変形

13

- フェライトと積層すること以外，セメンタイト層の配向方向もパーライトコロニーの塑性変形を影響する

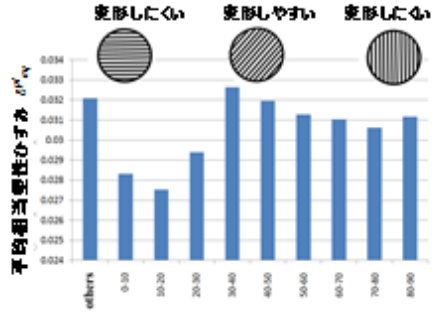

平均相当塑性ひずみ$\bar{\varepsilon}^{pl}_{eq}$とセメンタイト($\theta$)層の配向方向の関係

(M. Tanaka, Kyushu University, private communication)

- セメンタイトの応力が高くなると ⇨ パーライトコロニーが変形しにくい

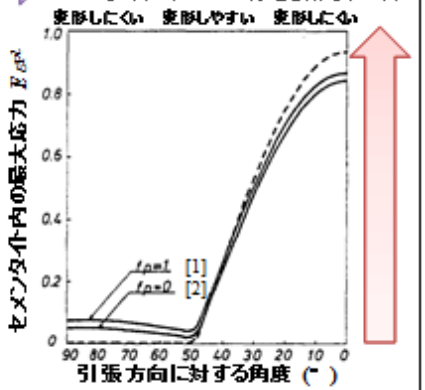

引張方向に対する角度によるセメンタイト内に生ずる最大応力

(K. Tanaka & S. Matsuoka, Acta Metall. (1974))

ComputationalMechanics Laboratory

Appendix
Dissertation defence slide

2-D的な観察の問題

14

コロニー構造のSEMとひずみマップ

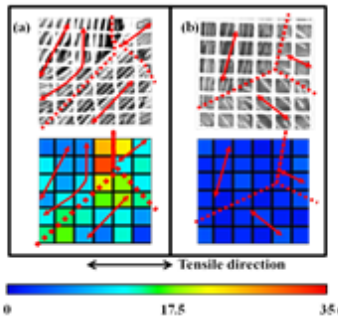

コロニー内・界面近傍に生ずる塑性ひずみの分布 (M. Tanaka, Kyushu University, private communication)

セメンタイト層の3-D的な構造

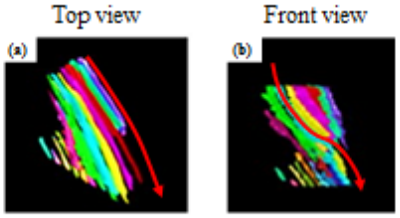

コロニー内のセメンタイト層の配向方向は奥行方向に傾いている・ねじれている
(Y. Adachi et. al, Acta Mater, (2008))

- 配向方向が似ていても，生ずるひずみが異なる場合もある
- 実験：試験片の表面だけしか観察できない
- セメンタイト層の構造が明らかにしなければ，コロニー構造の変形は十分に理解できない

パーライト組織における不均一変形のメカニズムを理解するため:
3-D的な検討が必要

ComputationalMechanics Laboratory

研究動機

15

FIB-SEM*装置により3-D可視化

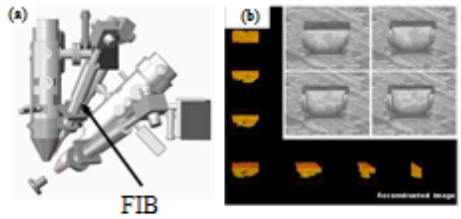

(a) FIB-SEM装置　(b)3D再構成像
(http://www.jeol.co.jp/applications/pdf/sb/fb_a001_00.pdf)
*集束イオン/電子ビーム加工装置

- 一定のステップで複数回加工する
- ステップ毎にSEM像が取得される
- 試料の3-D的な構造情報は正確に再構成できる
- 試料が照射されるため，削れていく
- 同じ資料は加工回しすることができない
- 実験前後の構造情報は得られない

有限要素法 (FEM)

正面から観た積層の配向方向が似ている

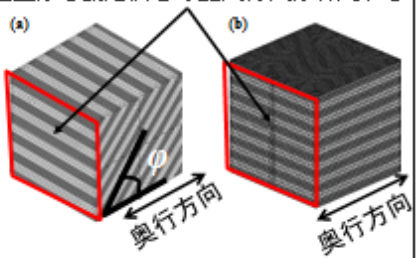

単体コロニーFEMモデル
(a) φ=45°　(b) φ=0°

パーライト組織における変形を検討するため

FEMの2-D・3-D のコロニー構造をモデル化する

コロニー構造の弾塑性変形解析を行う

本日の発表は3-D編のみ紹介する

ComputationalMechanics Laboratory

Appendix
Dissertation defence slide

解析条件

16

- 古典的弾塑性理論
- 材料定義

Computational Mechanics Laboratory

古典的弾塑性理論

17

- 古典的な弾塑性理論に基づいた有限要素を用いたANSYSを使用する

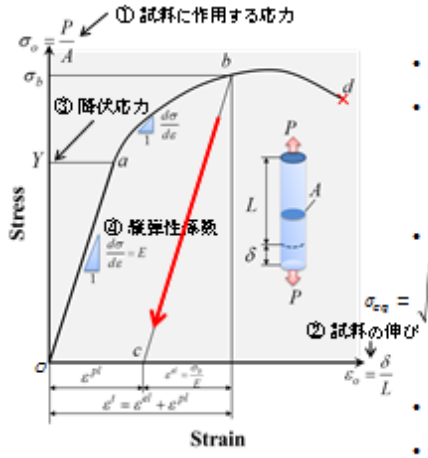

長さL・横断面積Aの金属材料の弾塑性変形の応力－ひずみ曲線

von Mises降伏条件

- 本解析はvon Misesの降伏条件を使用する
- モデルの相当応力，σ_{eq} が降伏応力，Yと等しくなる時，塑性変形が開始

$$\sigma_{eq} - Y = 0$$

- 相当応力，σ_{eq} は単軸・せん断応力成分で表す：

$$\sigma_{eq} = \sqrt{\frac{(\sigma_{xx} - \sigma_{yy})^2 + (\sigma_{yy} - \sigma_{zz})^2 + (\sigma_{zz} - \sigma_{xx})^2 + 6\tau_{xy}^2 + 6\tau_{yz}^2 + 6\tau_{zx}^2}{2}}$$

関連流れ則 (Associated flow-rule)

- 降伏後の応力－ひずみ増分は関連流れ則を従う
- 関連流れ則は降伏条件で提案された降伏関数を材料の塑性ポテンシャルとする

Computational Mechanics Laboratory

Appendix
Dissertation defence slide

本研究の材料定義

18

表 材料物性値

材料	縦弾性係数 E (GPa)	降伏応力 (MPa)	ポアソン比	a (MPa)	b	n
セメンタイト[1]	181	2750	0.3			
フェライト[2,3]	200	86.5	0.3	493	0.002	0.28

セメンタイトの塑性域

- 降伏後，セメンタイト塑性変形せずに破壊するものと仮定する
- 加工硬化： 0はネッキング状態と等しい条件
- 塑性変形が不安定になる条件

フェライトの塑性域

スウィフトの式[3] $\sigma_{tr} = a(b + \varepsilon^{pl})^n$

- 真応力，σ_{tr} は塑性ひずみ，ε^{pl} の指数増分で定義する

σ_{tr} ：真応力　　ε^{pl} ：塑性ひずみ
a, bと n ：実験[2]より得られた定数

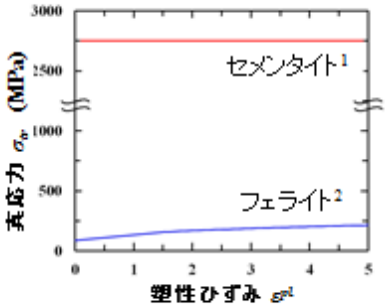

セメンタイトとフェライトの応力 - ひずみ曲線[1,2]

1. M. Umemoto et. al, Mater. Sci. Eng. A (2004)
2. M. Umemoto , Work-hardening seminar Kumamoto (2010
3. H.W. Swift,J. Mech. Phys. Solids (1952)

19

パーライトコロニーの3D弾塑性変形解析

- 単体コロニー編
- 二つコロニー編

Appendix
Dissertation defence slide

パーライトコロニーの3D弾塑性変形解析

20

単体コロニー編

- 3-D単体コロニーのモデリング
- セメンタイト(θ)の配向方向の表し方
- 3-D単体コロニーの解析モデル
- 単体コロニーの塑性流動応力
- 単体コロニーの引張り方向成分のひずみ分布
- 単体コロニーの垂直方向と奥行方向成分のひずみ分布
- 単体コロニーのせん断成分のひずみ分布と異方性

Computational Mechanics Laboratory

3D単体コロニーのモデリング

21

- コロニーの弾塑性変形はセメンタイト層の配向方向に影響を受ける
- セメンタイト層の配置が複雑で観察することがむずかしい

表面から見た配向方向と奥行きの配向方向が分かる3Dのコロニーモデルを作成する

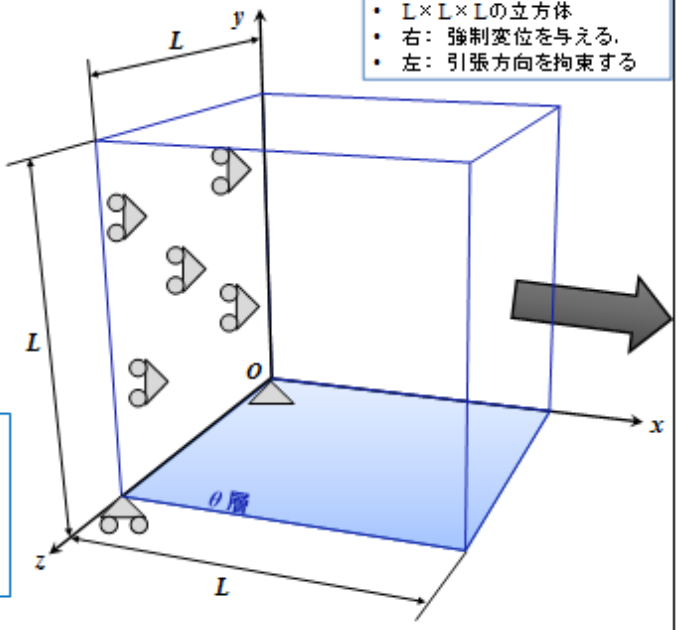

- L×L×Lの立方体
- 右：強制変位を与える，
- 左：引張方向を拘束する

Computational Mechanics Laboratory

Appendix
Dissertation defence slide

セメンタイト層(θ)の配向方向の表し方

22

θ層の配向方向

- 点Pはθ層の中心点
- 点Pの法線ベクトルはn
- θ層の配向方向は法線ベクトルnで表す
- xy面上点Pの正投影は点P_o
- 点P_oをxy面上に角度φを傾ける

実験では，正投影の見方で観察する

点Pを観察する時，xy面上の点P_oとして写る

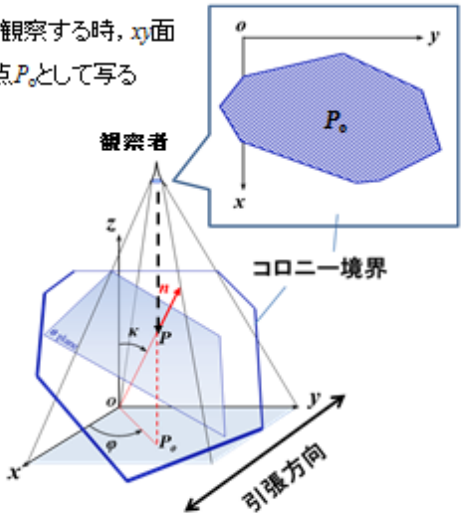

パーライトコロニーの試料を観察する時の略図

ComputationalMechanics Laboratory

セメンタイト(θ)の配向方向の表し方

23

θ層の配向方向

- 点Pはθ層の中心点
- 点Pの法線ベクトルはn
- θ層の配向方向は法線ベクトルnで表す
- xy面上点Pの正投影は点P_o
- 点P_oをxy面上に角度φ傾ける

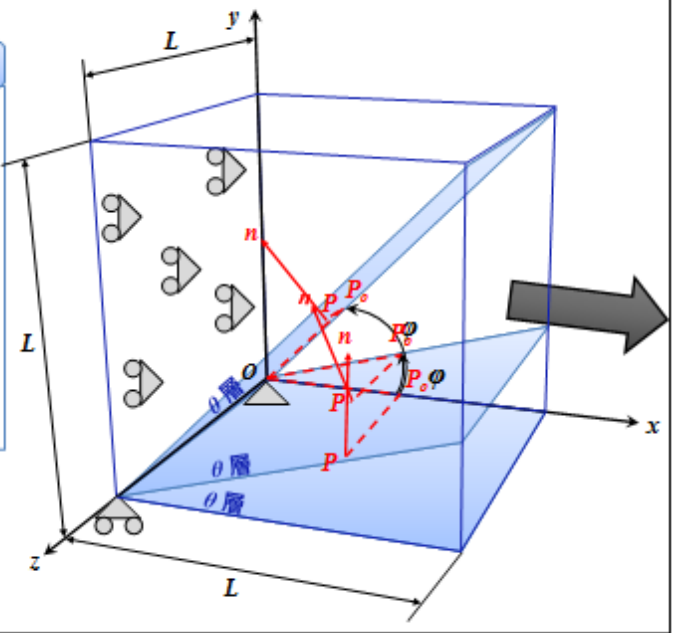

ComputationalMechanics Laboratory

Appendix
Dissertation defence slide

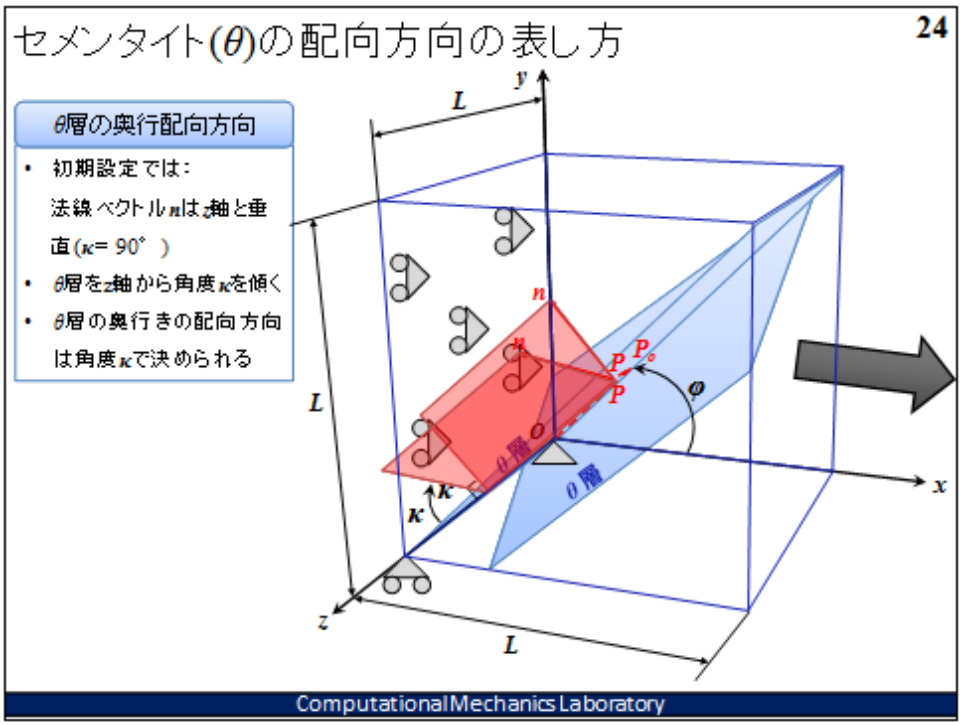

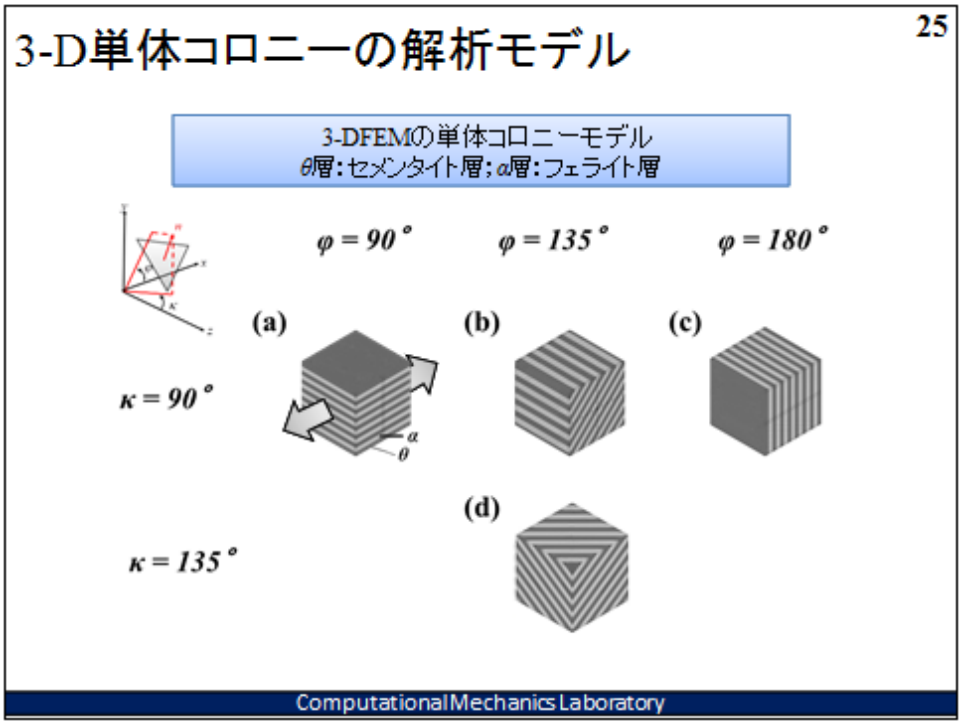

Appendix
Dissertation defence slide

単体コロニーの塑性流動応力

26

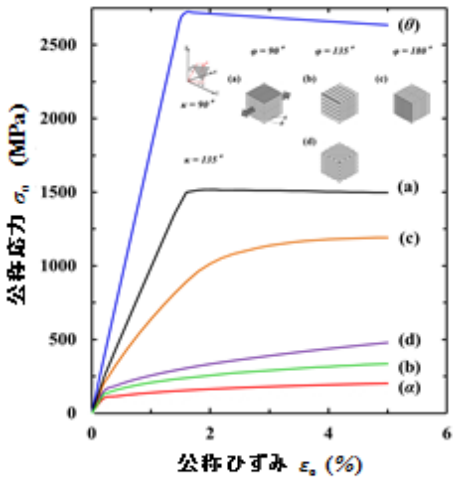

単体コロニーの応力-ひずみ曲線

θ層の配向方向が引張り方向に平行である
- 塑性流動応力が最も高くなる.

θ層の配向方向が引張り方向に45° 傾く
- 塑性流動応力が最も低くなる.

ComputationalMechanics Laboratory

単体コロニーの塑性流動応力

27

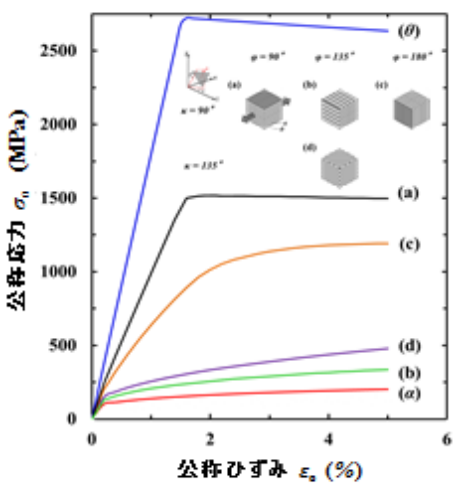

単体コロニーの応力-ひずみ曲線

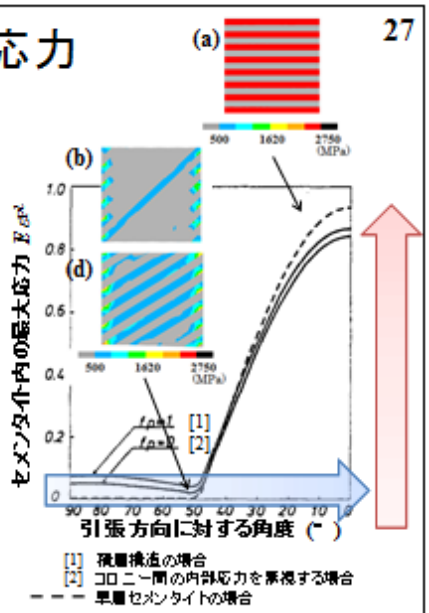

引張方向に対する角度によるセメンタイト内に生ずる最大応力
(K. Tanaka & S. Matsuoka, Acta Metall. (1974))

ComputationalMechanics Laboratory

Appendix
Dissertation defence slide

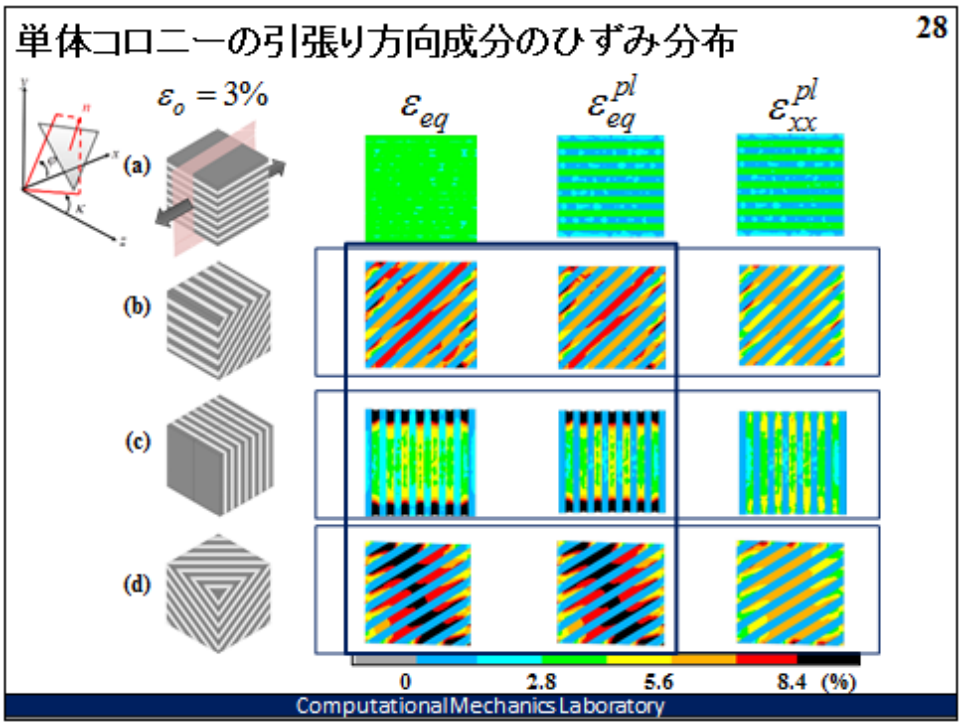

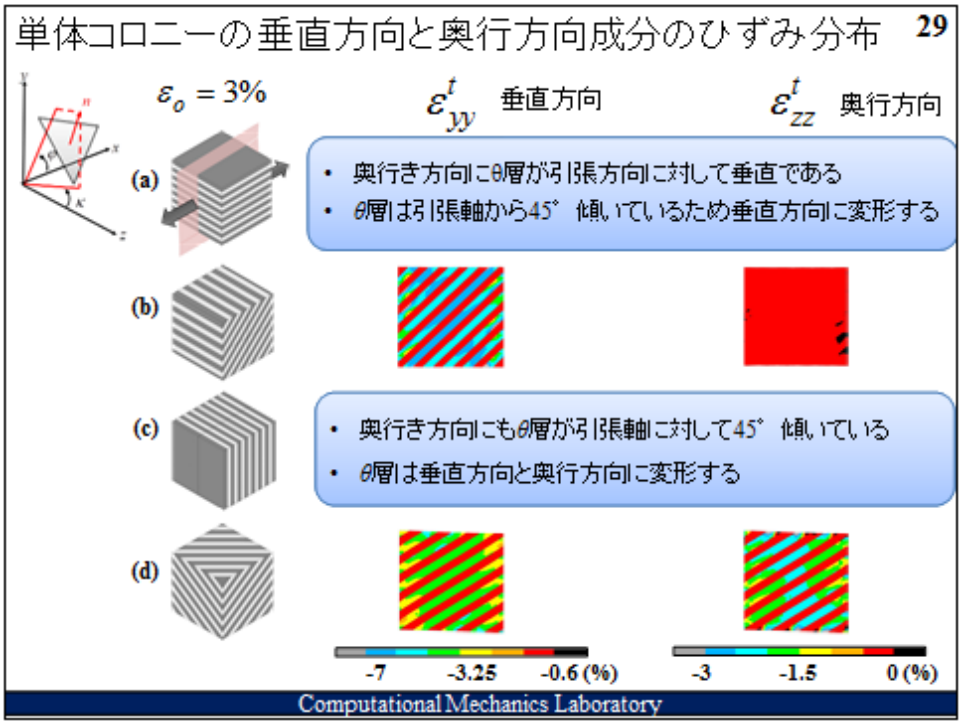

Appendix
Dissertation defence slide

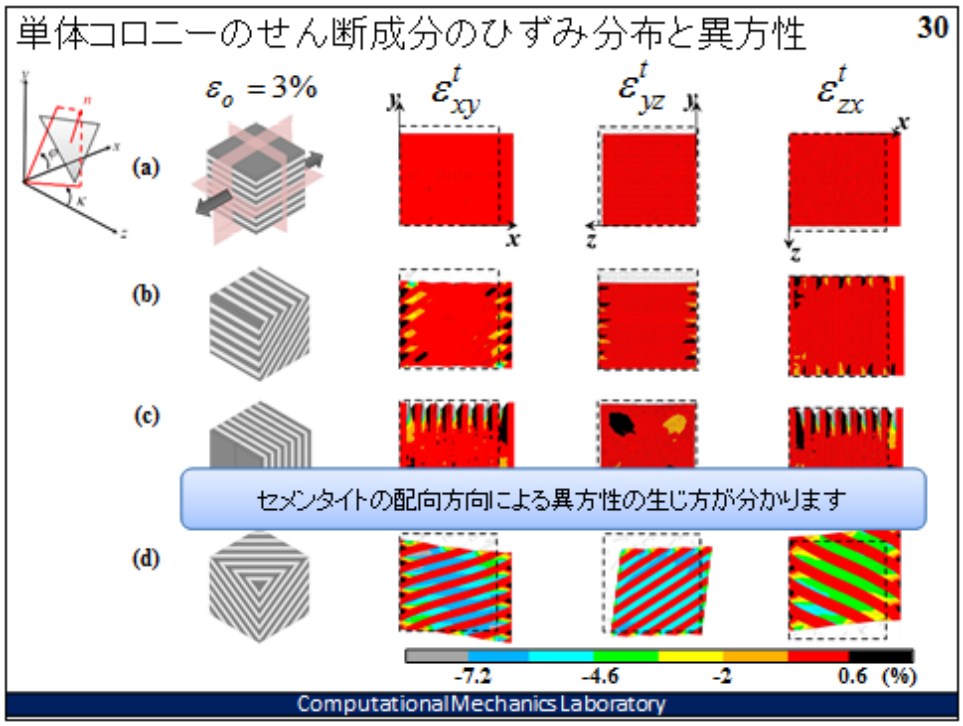

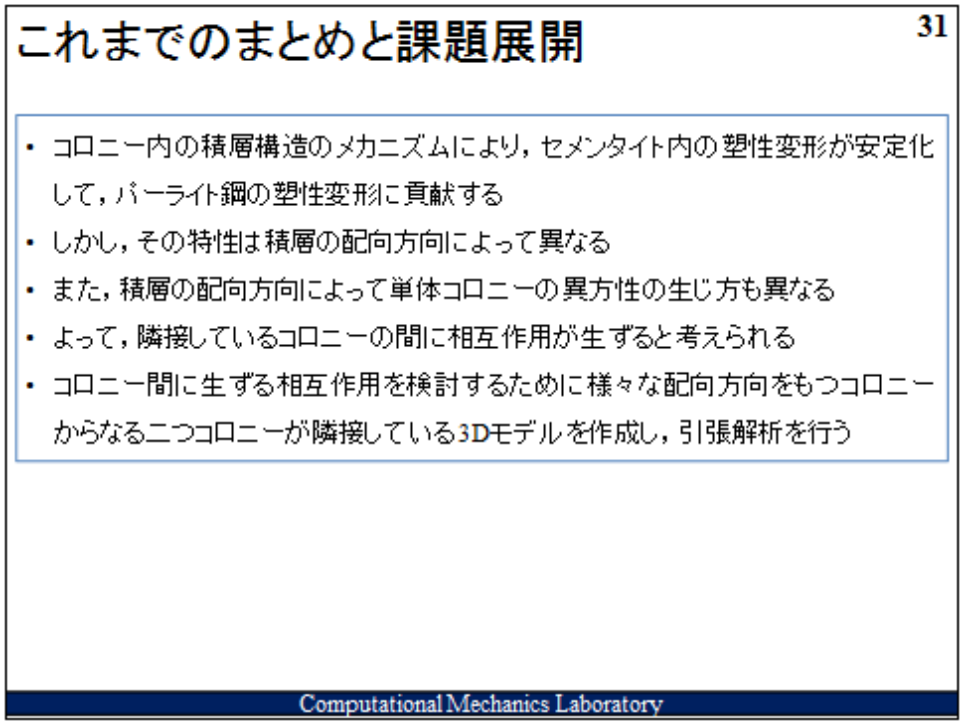

Appendix
Dissertation defence slide

パーライトコロニーの3-D弾塑性変形解析

32

二つコロニー編

- 3-Dの二つコロニーのモデリング
- 3-Dの二つコロニーのモデル
- 二つコロニーの塑性流動応力
- セメンタイト(θ)層の奥行の配向方向による隣接している二つコロニーモデルのひずみ分布
- セメンタイト(θ)層の配向方向による隣接している二つコロニー
- モデルの塑性流動の差
- セメンタイト(θ)層の配向方向による隣接している二つコロニー
- モデルの異方性の生じ方

Computational Mechanics Laboratory

3-Dの二つコロニーのモデリング

33

C1のθ層の配向方向

- xy面上点Pの正投影は点P_o
- 点P_oをxy面上に角度φ傾ける
- θ層の奥行きの配向方向は角度κで決められる

C2のθ層の配向方向

引張軸から45°傾いているように固定する

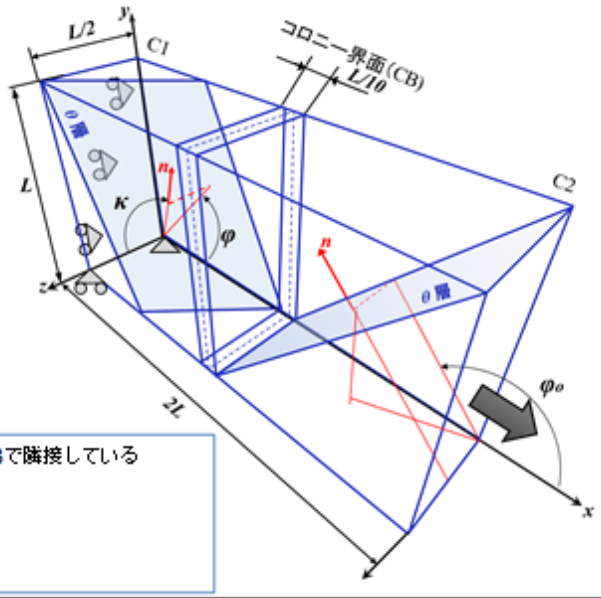

- C1とC2はコロニー界面，CBで隣接している
- 2L×L×L/2の平行六面体
- 右：強制変位を与える，
- 左：引張方向を拘束する

Computational Mechanics Laboratory

Appendix
Dissertation defence slide

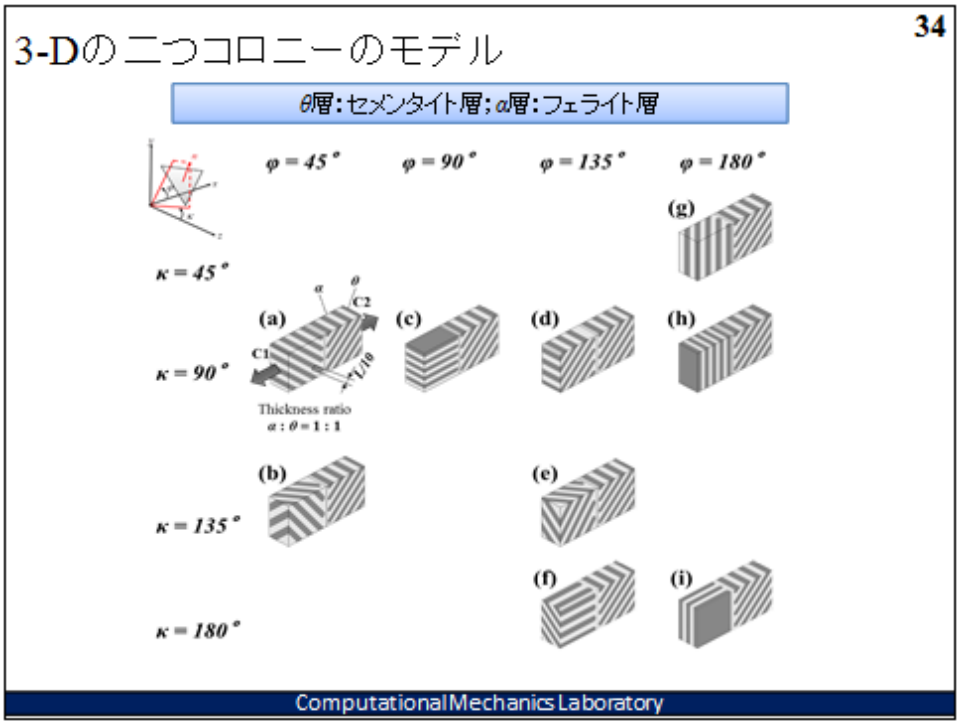

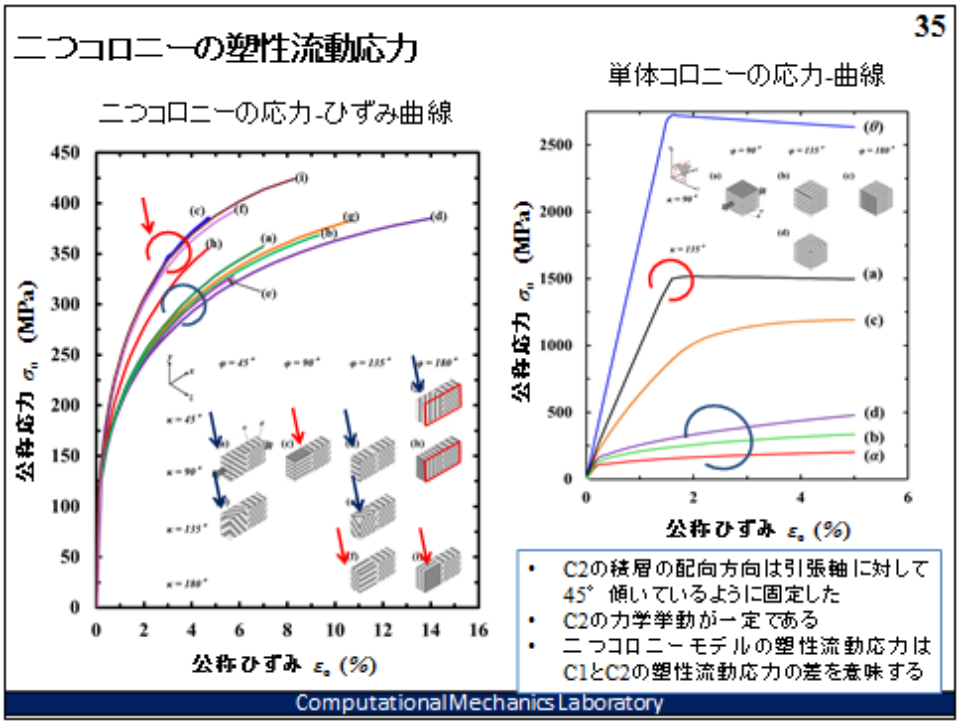

Appendix
Dissertation defence slide

セメンタイト(θ)層の配向方向による隣接している二つコロニーモデルの異方性の生じ方 38

単体コロニーモデル(d)

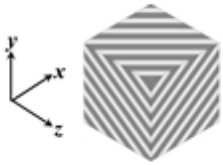

積層の配向方向によって異方性の強い単体コロニーである.

単体コロニーモデル(d)を持つ二つコロニーモデル(b)と(e)

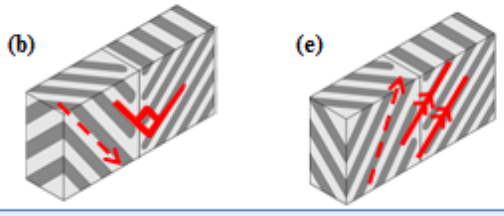

- 単体コロニーモデル(d)を異なる配置で導入する.
- モデル(b)は下向きに配置したため, C1はC2に垂直
- モデル(e)は上向きに配置したため, C1はC2に平行

ComputationalMechanicsLaboratory

セメンタイト(θ)層の配向方向による隣接している二つコロニーモデルの異方性の生じ方 39

公称ひずみがε_0=3%の時のせん断yz成分のひずみε_{yz}分布

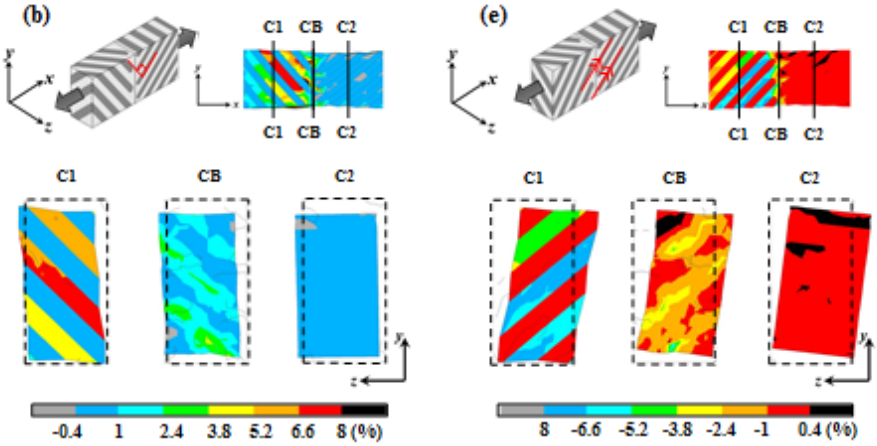

- 隣接しているコロニーの方位が同じ場合, 二つコロニーモデルが奥行き方向に変形する
- 隣接しているコロニーの方位が垂直場合, 二つコロニーモデルの奥行き方向への変形が拘束される

ComputationalMechanicsLaboratory

Appendix
Dissertation defence slide

セメンタイト(θ)層の配向方向による隣接している二つコロニーモデルの異方性の生じ方

40

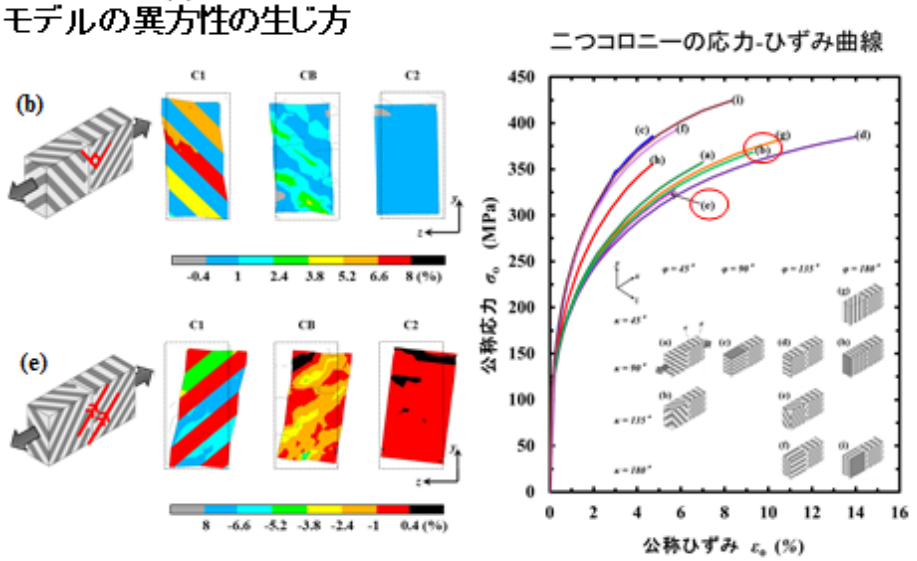

- 力学特性(塑性流動応力・ひずみのマグニチュード等)が同じでも，異方性が強いコロニー構造の方は塑性変形が不安定になることが考えられる

ComputationalMechanicsLaboratory

結言

41

積層構造を持つコロニー構造の弾塑性変形を理解するために，セメンタイトの塑性変形と配向方向による弾塑性変形を検討した．古典的な弾塑性理論に基づいた有限要素法を用いて，2-D・3-Dの弾塑性変形解析を行った．

- フェライトの加工硬化能が高くなるとセメンタイトの塑性変形はより安定化する．
- セメンタイト層の配向が引張り方向に平行であると，コロニーの塑性流動応力が最も高くなる．一方，セメンタイト層の配向が引張り方向に45° 傾くと，塑性流動応力が最も低くなる．
- また，積層の配向方向によって，コロニーの変形の異方性の生じ方が大きく異なる．
- 即ち，積層の配向方向は単体コロニーの変形特性に大きく影響する．
- 隣接しているコロニーの塑性流動応力の差が高いもしくは，変形の異方性の違いによってコロニー界面にひずみ・応力集中が生ずることが確認できた．
- つまり，コロニー構造の集合体であるパーライト鋼の微視組織の弾塑性変形はコロニー間の相互作用にも影響されることが分かった．

謝辞
本研究は科学技術振興事業団，産学共創基礎基盤研究「革新的構造用材料創製を目指したヘテロ構造制御に基づく新指導原理の構築」の委託により行った研究の一部である．記して謝意を表する．

ComputationalMechanicsLaboratory

Appendix
T. Ohashi et al., Mater. Sci. Eng. A, 588 (2013), 214-220

Materials Science & Engineering A 588 (2013) 214–220

Contents lists available at ScienceDirect

Materials Science & Engineering A

journal homepage: www.elsevier.com/locate/msea

A multiscale approach for the deformation mechanism in pearlite microstructure: Numerical evaluation of elasto-plastic deformation in fine lamellar structures

Tetsuya Ohashi [a,*], Lidyana Roslan [a], Kohsuke Takahashi [a], Tomotsugu Shimokawa [b], Masaki Tanaka [c], Kenji Higashida [c]

[a] Kitami Institute of Technology, Koencho 165, Kitami, Hokkaido 0908507, Japan
[b] Kanazawa University, Kanazawa, Japan
[c] Kyusyu University, Fukuoka, Japan

ARTICLE INFO

Article history:
Received 6 August 2013
Accepted 9 September 2013
Available online 17 September 2013

Keywords:
Finite-element method
Steel
Plasticity
Shear bands
Pearlite

ABSTRACT

Elasto-plastic deformations in the microstructures of pearlite are studied by finite-element analyses. Various models for the lamellar structure are made and the material properties of cementite and ferrite are established. Deformation of a bare specimen of cementite is unstable immediately after the yield point, while cementite lamellae show some stability when they are layered with ferrite. When higher values of yield stress and strain hardening are used for ferrite phase, cementite deforms well beyond the elastic range and the distribution of plastic strain is not concentrated. These results show that not only the layered structure but also the improved mechanical property of fine lamellae of ferrite contribute largely to stable deformation in the pearlite microstructure.

1. Introduction

Elasto-plastic deformation in the microstructure of pearlite phase in steels has been a point of interest especially because strength and ductility coexist in pearlitic steels. In the microstructure, fine layers of ferrite and cementite are piled up repeatedly at sub-micrometer intervals. Under an external load, stress states in the ferrite and cementite were found to differ largely [1]; however, the detailed aspects of plastic deformation in each phase remain unknown.

Mechanical properties of single phase specimens of ferrite or cementite with the size of an order of millimeters were investigated experimentally [2,3]. When the experiment was performed at room temperature, the plastic flow stress of pure-ferrite specimens was of the order of a few hundred MPa and the elongation was larger than 20%, while the elastic limit of specimens of single phase cementite was revealed to be approximately 3 GPa and brittle fracture took place immediately after the elastic limit.

Deformation of cementite layers in the microstructure of pearlite has also been studied extensively [4–7] and it was shown that cementite lamellar does deform plastically in pearlite microstructure. Therefore, one very crucial question is why cementite deforms plastically in the microstructure [8]. Understanding the mechanics and mechanism of plastic deformation in the pearlite microstructure will lead to an understanding of the reason for the coexistence of strength and ductility in the steels with pearlite phase.

Inoue et al. [9] studied the stability of elasto-plastic deformation of laminated structures, and they showed that fracture stress and elongation increased with decrease in layer thickness. Recently, Serror and Inoue [10] studied the effect of hardening exponent and other parameters of the ductile component on the stability of a laminated structure. In this paper, we study elasto-plastic deformation in the lamellar structure of pearlite from the viewpoint of computational solid mechanics. Various finite element models for the lamellar structure are constructed and the material properties of each phase are established based on existing experimental data and theoretical possibilities. Unidirectional tensile loading in the direction parallel to the ferrite–cementite interface is considered. This condition mimics the mechanical state in high-strength steel wires used in engineering applications. Stable deformation of cementite layers is discussed from the viewpoints of multi-layering effect with ferrite layers and a possible change of the mechanical properties of ferrite phase, which should arise from the fact that plastic deformation is confined in a sub-micrometer-sized space between the cementite layers.

2. Numerical models for multi-layered structure of pearlite

We employed a classical theory of the elasto-plastic deformation of metals where the onset of plastic deformation is defined by

* Corresponding author. Tel./fax: +81 157 26 9227.
E-mail address: ohashi@newton.mech.kitami-it.ac.jp (T. Ohashi).

0921-5093/$ - see front matter © 2013 Elsevier B.V. All rights reserved.
http://dx.doi.org/10.1016/j.msea.2013.09.032

Appendix
T. Ohashi et al., Mater. Sci. Eng. A, 588 (2013), 214-220

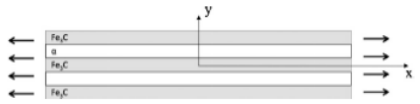

Fig. 1. Schematic illustration of a 5-layered pearlite model. The mid-part of the central layer of cementite is slightly thinned.

the yield condition of von Mises:

$$\sigma_{eq.} - \sigma_Y = 0 \tag{1}$$

where σ_Y and $\sigma_{eq.}$ denote the yield stress of the material and the equivalent stress, respectively. The ferrite phase hardens after the yield point in an isotropic manner, while the cementite phase is assumed to deform plastically without hardening; i.e. the plastic flow stress of cementite is a constant during plastic deformation. We used a commercial software package of ANSYS [11] for finite element analysis, where elasto-plastic deformation is analyzed by the incremental procedure and assuming the associated flow rule. The fact that the cementite phase does not harden during plastic deformation indicates that its plastic deformation can be highly unstable [12]. To follow this situation by numerical analysis, we conducted a number of trial analyses and finally introduced a large number of loading steps where a typical increment of nominal strain during one analysis step is of the order of 10^{-9}. If we introduce larger strain increment, numerical analysis often fails.

Fig. 1 shows a schematic illustration of a five-layered pearlite model. The central layer is always cementite (denoted as Fe_3C) in this study and layers of ferrite (denoted as α) and other cementite are stacked in the y-direction. Volume fractions of the cementite and ferrite layers are close to 0.5; however, the value differs from model to model depending on the number of layers. The mid-part of the central layer of cementite is slightly thinned[1] [13] to mimic possible geometrical non-uniformity in the real structure of pearlite [14,15].

Young's modulus and yield stress of cementite are 181 GPa and 2.75 GPa, respectively [3]. Poisson's ratio of cementite is assumed to be 0.3. When this material is deformed by uniaxial tensile load, the elastic strain at the yield point is about 1.519%. Experimental results of the stress–strain relationship of ferrite were given by Umemoto [2] in the following equation of Swift type [16]:

$$\sigma = a(b+\varepsilon^{(p)})^n \tag{2}$$

where σ and $\varepsilon^{(p)}$ denote stress and plastic strain, respectively, whereas a, b and n are constants. Young's modulus and Poisson's ratio of ferrite are assumed to be 200 GPa and 0.3, respectively.

Strengthening mechanism of ferrite lamellae has been discussed from the viewpoints of the simple rule of mixture for fiber structure, dispersion strengthening, boundary strengthening, solid solution hardening and dislocation forest hardening [17,18]. Among the various mechanisms involved, boundary strengthening has the greatest contribution. It is well known as the Hall–Petch relationship, which states that the mechanical response of metal polycrystals changes as a function of the mean diameter of crystal grains. This means that the mechanical response of materials depends on the representative length scale of the microstructure. This scale effect is especially significant when the length scale is smaller than 1 μm. Typical thickness of the ferrite layer in pearlite is smaller than 100 nm and its plastic flow stress is anticipated to have a strong scale effect, similar to the case in ultrafine-grained polycrystals [19] or micrometer sized specimens [20]. Experimental results [21] showed that yield stress of pearlite increased with decrease in layer thickness of the ferrite, and recent theoretical and numerical approaches [22,23] showed that the critical resolved shear stress for slip deformation as well as the strain hardening ratio increased rapidly when the plastic slip deformation was confined to volumes of smaller length scales. We introduced such types of scale effect of the mechanical response of ferrite layer *a priori* and introduced hypothetical curves of stress–strain relationship using the Swift equation with a modification:

$$\sigma = a(b+\varepsilon^{(p)})^n + c, \tag{3}$$

where a constant c is introduced artificially to give a higher flow stress level in a small length-scale specimen.

Table 1 shows material parameters and numerical constants for the modified Swift Eq. (3) used in this study. Data for the material named ferrite-org are taken from experimental results by Umemoto [2], while data for materials named ferrite5, ferrite10 and ferrite5n are defined by multiples of the parameters a and n for the ones for ferrite-org. Flow stress of the material named ferrite5n500 is 500 MPa higher than that of ferrite5n, while the strain hardening ratios for ferrite5n and ferrite5n500 are the same. Stress–strain curves of cementite and five ferrite materials are shown in Fig. 2. Yield stress and strain hardening rates of ferrite5 and ferrite10 are high compared to the ones for ferrite-org. Yield stresses of ferrite5n and ferrite5n500 are higher than that of ferrite-org, while their strain-hardening rate is lower.

These hypothetical stress–strain relations of ferrite layers in the pearlite lamellar structure are considered to be partially supported by experimental facts [18] that the dislocation density in ferrite layers monotonically increases from the initial value of $7.5\times10^{13}\,m^{-2}$ to a value larger than $1\times10^{16}\,m^{-2}$ after deformation up to a tensile strain of 3.6. This implies that ferrite layers sandwiched by cementite layers have a significant strain-hardening ability. Effects of this ability are examined by introducing ferrite5 or ferrite10. There is still another possibility that the flow stress level of ferrite is high because of the narrow space between the cementite layers, while strain hardening is kept low for some reason. We studied the mechanical response of such structures by introducing ferrite5n or ferrite5n500.

Numerical specimens of single-layer (cementite only) and 3–9-layer models were constructed. Only the mid-layer of cementite was slightly thinned as described above. In Sections of 3.1 and 3.2, the condition of symmetricity is introduced and only one-fourth of the specimen, that is the part $x\geq0$, $y\geq0$, is analyzed to reduce the size of numerical data; however, in Section 3.3, the entire specimen is analyzed to understand the deformation as a whole. It is shown in Section 3.3 that the deformation is approximately symmetric with respect to the x- and y-axes, with some slight non-symmetric behaviors after the onset of shear banding. These

Table 1
Mechanical property of ferrite and cementite. Parameters a, b and n are used for Swift's equation and parameter c is introduced in the modified Swift Eq. (3). Data for ferrite-org and cementite are taken from Umemoto [2] and Umemoto and Tsuchiya [3], while data for ferrite5, ferrite10, ferrite5n and ferrite5n500 are hypothetical ones.

	Young's modulus [GPa]	Poisson's ratio	Yield stress [MPa]	a [MPa]	b	n	c [MPa]
Cementite	181	0.3	2750				
Ferrite-org	200	0.3	86.5	493	0.002	0.28	0
Ferrite5	200	0.3	432.6	2465	0.002	0.28	0
Ferrite10	200	0.3	865.2	4930	0.002	0.28	0
Ferrite5n	200	0.3	348.1	493	0.002	0.056	0
Ferrite5n500	200	0.3	848.1	493	0.002	0.056	500

[1] Shape of the interfaces between the central layer of Fe_3C and α is given by a cosine function $\delta\cos(2\pi x/L)$, where δ and L are 0.5% of the layer thickness and lateral length of the layer, respectively. The thinnest part of the cementite layer is positioned at $x=0$ and the thickness is 98% of the original one.

Appendix
T. Ohashi et al., Mater. Sci. Eng. A, 588 (2013), 214-220

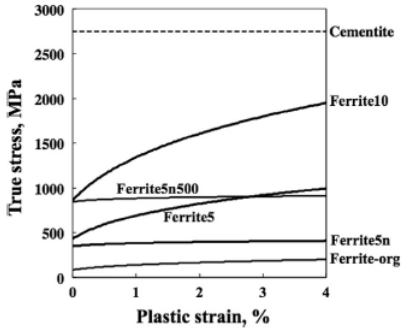

Fig. 2. Stress vs. strain relationship employed in this study for the cementite and five types of ferrite phases.

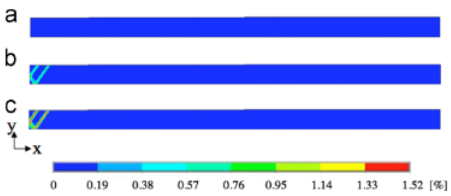

Fig. 3. Distributions of the plastic strain component $\varepsilon_{xx}^{(p)}$ in the bare cementite specimen when the nominal tensile strains are 1.500% (a), 1.504% (b) and 1.508% (c).

non-symmetric behaviors are considered to originate from the unstable nature of the deformation.

Analyses were performed with two-dimensional plane stress assumption with a large deformation framework. Specimens were divided into square or nearly square finite elements whose typical size was about one-eighth of the layer thickness. Quadrilateral 8-node elements were used. A uniform tensile displacement was given to the nodes on the lateral surfaces at $x = \pm L/2$. Approximately uniaxial tensile deformation took place at the initial stage of deformation, and then plastic deformation started in the specimen.

3. Results and discussion

3.1. Deformation of bare cementite specimen and three-layered specimen of ferrite-org/cementite/ferrite-org

Fig. 3(a)–(c) shows the distributions of the normal plastic strain component in the loading direction observed in the single layered specimen when the nominal tensile strains are 1.500%, 1.504% and 1.508%, correspondingly. Plastic deformation does not take place in the specimen when the nominal strain is 1.500%; shortly after this stage, some shear bands are formed at the central part of the specimen. This result shows that plastic deformation in single-layered cementite is nearly unstable and the development of shear bands is extremely rapid.

Fig. 4(a)–(d) shows the close-up views of the development of plastic shear bands at the central part of the three-layered ferrite-org/cementite/ferrite-org model. Plastic deformation in the cementite layer starts when the nominal tensile strain is 1.5068% and develops toward the ferrite layer. It is noted, however, that the value of the plastic strain in the shear bands when the nominal tensile strain is 1.51% (Fig. 4(c)) is smaller than 0.5% and this is

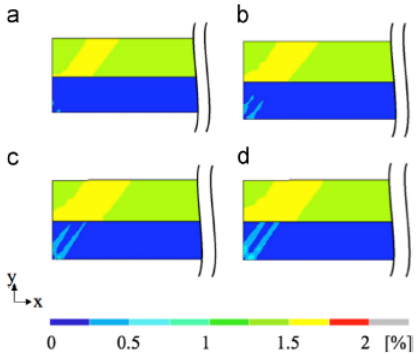

Fig. 4. Development of the plastic strain component $\varepsilon_{xx}^{(p)}$ at the central part of the layered specimen of ferrite-org/cementite/ferrite-org when the nominal tensile strains are (a) 1.5068%, (b) 1.5084%, (c) 1.5100% and (d) 1.5116%.

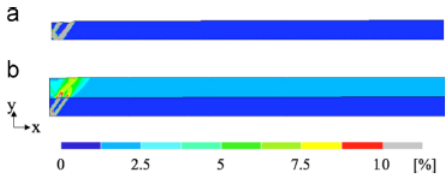

Fig. 5. Distribution of the normal plastic strain component $\varepsilon_{xx}^{(p)}$ in bare cementite specimen (a) and ferrite-org/cementite/ferrite-org layered specimen (b). The nominal tensile strain is 1.7%.

much smaller than that obtained in the single-layered cementite (Fig. 3(c)). That is, ferrite layers effectively suppress the unstable deformation of cementite. Fig. 5(a) and (b) compares the distributions of normal plastic strain component in the tensile direction observed in the bare cementite and the three-layered models when the nominal tensile strain is 1.7%. Plastic strain in the shear band regions in the model of bare cementite (Fig. 5(a)) is larger than that in the shear bands in the three-layered model (Fig. 5(b)) and the localized shear deformation in the three-layered specimen is transferred into the ferrite region. Suppression of localized shear deformation by stacking ferrite and other cementite layers is discussed in Section 3.3.

3.2. Deformation of specimens with layers of cementite and hypothetical ferrite

Fig. 6(a)–(e) shows the distributions of normal plastic strain component in the tensile direction in five different specimens where the cementite layer is sandwiched by ferrite-org, ferrite5n, ferrite5n500, ferrite5 or ferrite10. These specimens are three layered and the nominal tensile strain is 1.55%. Let us compare Fig. 6(a)–(c) and refer to Fig. 2. In the specimen with ferrite5n or with ferrite5n500, shear bands are formed in the cementite layer even though the yield stresses of these ferrite layers are much higher than that of ferrite-org. This suggests that ferrite layers with higher yield stress but lower strain hardening do not contribute to the suppression of shear banding of the cementite layer; instead, the distribution of plastic strain in the ferrite layer is more localized than that in the model with the ferrite-org layer.

Aspects of plastic deformation in the cementite layer drastically change when the strain-hardening ratio and the yield stress of the ferrite layer increase as shown in Fig. 6(d) and (e). Plastic strain

Appendix
T. Ohashi et al., Mater. Sci. Eng. A, 588 (2013), 214-220

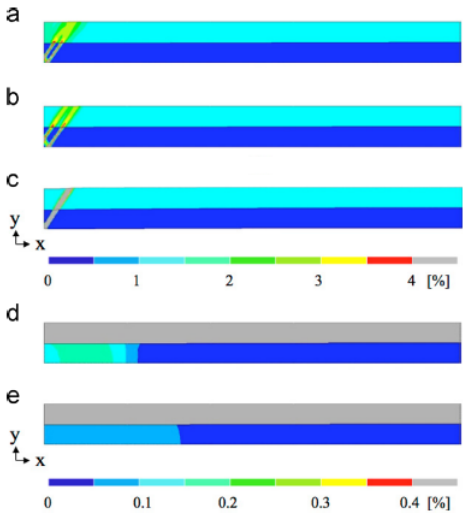

Fig. 6. Distributions of the plastic strain component $\varepsilon_{xx}^{(p)}$ in five different specimens where the cementite layer is layered with (a) ferrite-org, (b) ferrite5n, (c) ferrite5n500, (d) ferrite5 and (e) ferrite10. The nominal tensile strain is 1.55%. Note that different color scales are used for (a), (b), (c) and (d), and (e). (For interpretation of the references to color in this figure legend, the reader is referred to the web version of this article.)

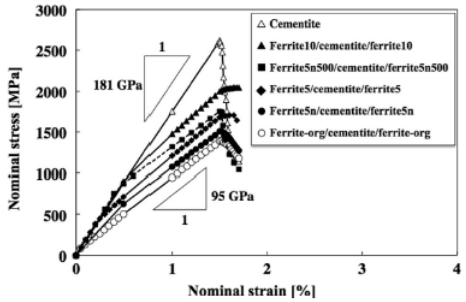

Fig. 7. Load–elongation curves of bare cementite and three-layered specimens.

distributes more or less uniformly in the cementite layer. The maximum value of plastic strain in the cementite layer is smaller than 0.2% and this is about one-twentieth of the value observed in Fig. 6(a)–(c). This means that plastic deformation of the cementite layer is effectively stabilized if the strain-hardening ratio and yield stress of ferrite layers are sufficiently large.

Fig. 7 shows the numerical results of nominal stress vs. nominal strain relations obtained for the bare cementite and five types of three-layered specimens. Bare cementite specimen shows a sudden drop of nominal stress just after the yield point. Before the sudden drop, the gradient of the stress–strain relation is approximately equal to the value of Young's modulus of 181 GPa. This again shows that the bare cementite specimen deformed in a purely elastic manner at first, followed by instable plastic deformation in a very short period of time.

Gradient of the stress–strain relationship of the three-layered ferrite-org/cementite/ferrite-org specimen is close to 95 GPa at first. This value is much smaller than Young's modulus for cementite or ferrite-org, indicating that plastic deformation took place at a very early stage of deformation. When the nominal strain is at about 1.51%, the gradient of the stress–strain relationship becomes negative; however, the stress–strain curve shows some stability compared to the bare cementite specimen.

The deformation curve of the three-layered specimens with ferrite10 shows three stages of deformation. First, the gradient of the deformation curve is slightly larger than 181 GPa, showing that both ferrite and cementite layers are in the elastic state. Plastic deformation starts in the ferrite layers when the nominal strain is at about 0.5%. After this onset of plastic deformation in the ferrite layers, the gradient of the deformation curve becomes smaller. This deformation state lasts until the nominal strain reaches about 1.52%. After this point, the cementite layer starts to deform in an elasto-plastic manner; however, the deformation is approximately uniform by the presence of ferrite layers as shown in Fig. 6(e), and stable deformation continues. The deformation process in the three-layered specimen with ferrite5 is similar to the one with ferrite10, even though the period of stable plastic deformation in the cementite layer does not last long.

In contrast to the case with ferrite10 or ferrite5, three-layered specimens with ferrite5n or ferrite5n500 show sharp drops of nominal stress after their peak. This is due to the concentration of plastic deformation in the cementite layer when the strain-hardening ratio is low in the ferrite layers, as seen in Fig. 6(b) or (c).

Results shown in Figs. 6 and 7 indicate as a whole that the strain hardening of ferrite layers contributes significantly to the stable plastic deformation of cementite layers and this effect is, in turn, assumed to originate from the presence of cementite layers: the mutual constraint of deformation between the soft and hard phases plays a key role in the microstructure. It should also be noted that high strength layers of ferrite with low strain hardening ability is not effective.

3.3. *Stabilization of deformation by multi-layering*

Pearlite colony [24] is basically composed of a number of parallel layers of ferrite and cementite. Deformation behaviors in the layered structures could differ depending on the number of layers. In this section, we construct pearlite models that consist of 3, 5, 7 or 9 layers and analyze their deformation. Also in these models, the central layers are cementite. Thicknesses of the ferrite and cementite layers are the same, except that the central layer of cementite is slightly thinned as described in Section 2, and they are simply piled up alternately. Specimens are subjected to tensile deformation in the horizontal direction by applying uniform tensile displacement on both sides of the specimens. Mechanical properties of ferrite and cementite layers are defined by data for ferrite-org and cementite shown in Table 1.

Fig. 8 shows the development of the equivalent strain in layered structures with 3, 5, 7 or 9 layers, while Fig. 9 shows the distribution of equivalent plastic strain in the 7-layered specimen when the nominal tensile strain is 1.527%. In the three-layered model, shear bands already develop when the nominal tensile strain is 1.5193%, and this result is consistent with that shown in Fig. 3. In the five-layered model, shear bands develop when the nominal tensile strain increases from 1.525% to 1.527%; however, we notice that the plastically deformed region extends to a wider area compared to the one in the three-layered model. The distribution of plastic strain in the ferrite layers spreads widely, too. In the 7- or 9-layered models, the initial plastic deformation in the cementite layer does not show the appearance of the shear band and after such an initial stage, plastic deformation gradually

Appendix
T. Ohashi et al., Mater. Sci. Eng. A, 588 (2013), 214-220

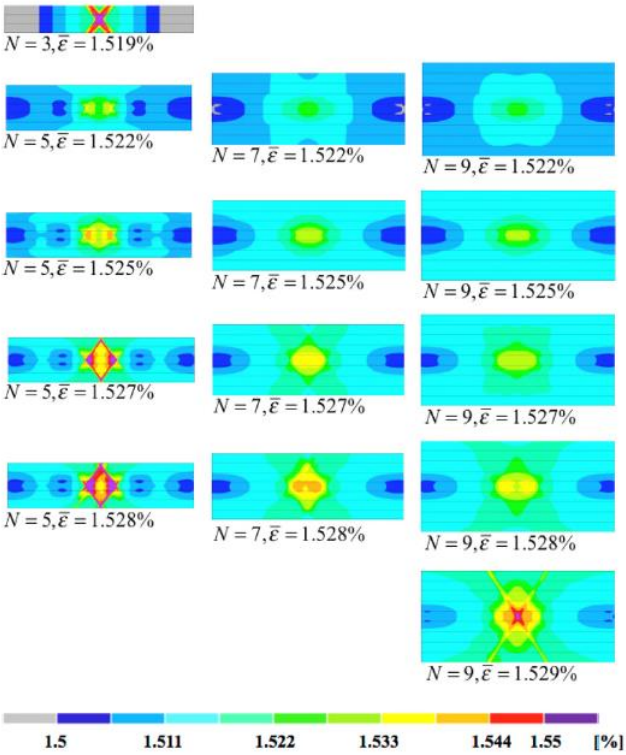

Fig. 8. Distributions of the equivalent strain in the 3-, 5-, 7- and 9-layered specimens. The central layer is cementite and is slightly thinned as described in Section 2. Layers of ferrite-org and cementite are stacked alternately. Number of layers and the nominal tensile strain are denoted as N and $\bar{\varepsilon}$, respectively. (For interpretation of the references to color in this figure legend, the reader is referred to the web version of this article.)

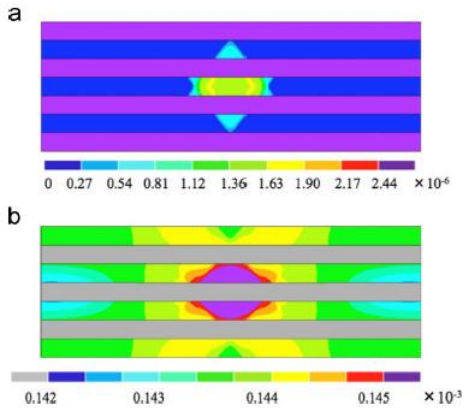

Fig. 9. Distribution of plastic equivalent strain in the 7-layered specimen of ferrite-org and cementite when the nominal tensile strain is 1.527%. (a) and (b) are drawn from the same numerical result but displayed with different color scales to depict the distribution of plastic deformation in cementite and ferrite phases. Plastic deformations in cementite and ferrite layers differ largely and a larger elastic deformation in cementite and a smaller one in ferrite layers compensate for this difference. (For interpretation of the references to color in this figure legend, the reader is referred to the web version of this article.)

localizes. It is also noted that non-uniform deformation takes place not only in the first-nearest layers of the central cementite layer but also in the second- and third-nearest layers and beyond. Equivalent plastic strains in the cementite and ferrite layers differ largely (Fig. 9), while the equivalent strains in both layers are approximately the same (Fig. 8). This difference in plastic deformation in the cementite and ferrite layers is compensated by elastic strain and this accompanies the difference in the stress state in both the layers. From the results shown in Figs. 8 and 9, we understand that the deformation of the central cementite layer shifts to be a stable one because of the presence of adjacent layers of ferrite and cementite.

Distribution of stress in the layered microstructure has been discussed from both experimental [1] and theoretical [25] approaches. Fig. 10 shows the distribution of equivalent stress in the 9-layered specimen. The maximum and the minimum values of the equivalent stress in the cementite layers are 2.75 GPa and about 2.7 GPa, respectively, while the stress in the ferrite layers is about 155 MPa, meaning that the stress partitioning in the cementite and ferrite is significant. During the initial stage of plastic deformation in the cementite layers, stress concentrates around the plastically deformed area. After some plastic deformation in the cementite layer(s), the area with the maximum value of the equivalent stress (=2.75 GPa) expands and the outermost layers of the cementite bear the load more than the central layer.

Appendix
T. Ohashi et al., Mater. Sci. Eng. A, 588 (2013), 214-220

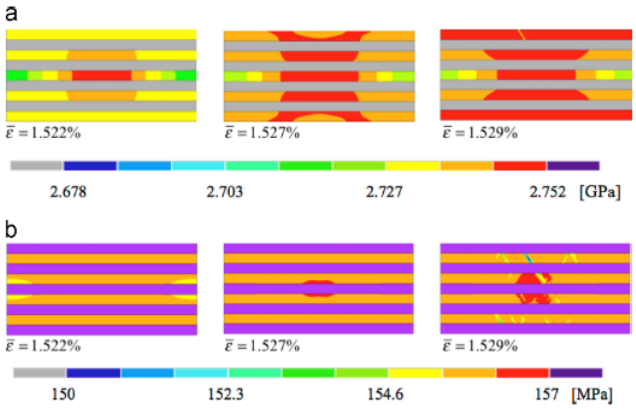

Fig. 10. Development of equivalent stress field in the 9-layered specimen. (a) and (b) are drawn from the same analysis results but displayed with different color scales to depict the stress field in each layer. Range of the equivalent stress in the cementite layers is approximately 2.7–2.75 GPa as shown in (a), while the value in ferrite layers is smaller than 157 MPa as shown in (b). (For interpretation of the references to color in this figure legend, the reader is referred to the web version of this article.)

Stabilization of plastic deformation by multiple layering, as shown in Figs. 8 and 9, appears a minor one compared to the effect by the change of mechanical response of ferrite layers, which we studied in the previous section. However, if the effects of multi-layering of ferrite and cementite and the change of mechanical properties of ferrite layers by the scale effect, or in other words the boundary effect [17,18], are combined, the results could be even more significant. That is, it is considered that the localization of deformation is suppressed not only by a possibly higher yield stress and strain hardening in the ferrite layers, but also by multiple layering of ferrite and cementite.

In a fine lamellar microstructure of heavily drawn pearlite wire, a high concentration of carbon was observed in the ferrite layers [26]. This increase in carbon concentration is assumed to change the yield stress and strain hardening behaviors [18]. Generation of dislocations in the microstructure and their pileup and/or passage at ferrite/pearlite interfaces will also contribute largely to the mechanical response of the two phases [27]. Therefore, the combined effect of geometrical, mechanical and chemical factors is considered to contribute to the strong and, at the same time, ductile behavior of the fine lamellar microstructure of pearlite.

In this study, we assumed that the plastic deformation of cementite was governed by the von Mises condition and the associated flow rule. The plastic flow stress was set to be a constant, whereas the process of plastic deformation due to crystallographic slip [5,8] is another point of interest to be studied.

4. Summary

Fine lamellar structures of pearlite consisting of ferrite and cementite layers were modeled numerically and their elasto-plastic deformation was analyzed by the two-dimensional finite element scheme. Results are summarized as follows:

1. Plastic deformation of the bare cementite specimen was highly unstable under uniaxial tensile load.
2. Plastic deformation of cementite layer(s) was more or less stabilized by the presence of the adjacent layers of ferrite and cementite, whereas a significant effect was observed when the yield stress and strain hardening rates of ferrite were increased.
3. There was a tendency that unstable plastic deformation was suppressed when the number of layers of ferrite and cementite was increased. This effect was assumed to originate from the fact that once plastic deformation started in a small region of cementite, this induced alterations of stress state not only in the adjacent layers of ferrite but also in the cementite and ferrite layers in the far field, meaning that more than one cementite and ferrite layers bore larger external load.

The combined effect of altering the mechanical properties of ferrite layers due to a scale effect and multiple layering could be a next point of discussion. Moreover, a quantitative discussion on the alteration of mechanical response of ferrite layers is needed. Further studies are required on the comparison of data from different approaches on the microscopic mechanical response of ferrite and cementite layers.

Acknowledgment

This research was supported by Japan Science and Technology Agency (JST) under Collaborative Research Based on Industrial Demand "Heterogeneous Structure Control: Towards Innovative Development of Metallic Structural Materials".

References

[1] Y. Tomota, P. Lukáš, D. Neov, S. Harjo, Y.R. Abe, Acta Mater. 51 (2003) 805–817.
[2] M. Umemoto, Tetsu-To-Hagané 81 (1995) 157–166.
[3] M. Umemoto, K. Tsuchiya, Tetsu-To-Hagané 88 (2002) 117–128.
[4] T. Gladman, B. Hommes, F.B. Pickering, J. Iron Steel Inst. 208 (1970) 172.
[5] A. Inoue, T. Ogura, T. Masumoto, Trans. JIM 17 (1976) 663–672.
[6] M. Ojima, J. Inoue, S. Nambu, P. Xu, K. Akita, H. Suzuki, T. Koseki, Scr. Mater. 66 (2012) 139–142.
[7] M. Tanaka, Y. Yoshimi, K. Higashida, T. Shimokawa, T. Ohashi, Mater. Sci. Eng., A (2013, this issue 2013).
[8] J. Gil Sevillano, Mater. Sci. Eng. A 21 (1975) 221–225.
[9] J. Inoue, S. Nambu, Y. Ishimoto, T. Koseki, Scr. Mater. 59 (2008) 1055–1058.
[10] M. Serror, J. Inoue, J. Eng. Mech. 139 (2013) 94–103.
[11] ANSYS Mechanical, Release 13.0, ⟨www.ansys.com⟩, 2010.
[12] J.R. Rice, Theoretical and Applied Mechanics, North-Holland, Amsterdam, 1976.
[13] Z. Marciniak, K. Kuczynski, Int. J. Mech. Sci. 9 (1967) 609–620.
[14] Y. Adachi, S. Morooka, K. Nakajima, Y. Sugimoto, Acta Mater. 56 (2008) 5995–6002.

Appendix
T. Ohashi et al., Mater. Sci. Eng. A, 588 (2013), 214-220

[15] Y.-T. Wang, Y. Adachi, K. Nakajima, Y. Sugimoto, Acta Mater. 58 (2010) 4849–4858.
[16] H.W. Swift, J. Mech. Phys. Solids 1 (1952) 1–18.
[17] J. Embury, R. Fisher, Acta Metall. 14 (1966) 147–159.
[18] X. Zhang, A. Godfrey, X. Huang, N. Hansen, Q. Liu, Acta Mater. 59 (2011) 3422–3430.
[19] N. Tsuji, Y. Ito, Y. Saito, Y. Minamino, Scr. Mater. 47 (2002) 893–899.
[20] M.D. Uchic, D.M. Dimiduk, J.N. Florando, W.D. Nix, Science 305 (2004) 986–989.
[21] A.R. Marder, B.L. Bramfitt, Metall. Trans. A 7 (1976) 365–372.
[22] T. Ohashi, M. Kawamukai, H. Zbib, Int. J. Plast. 23 (2007) 897–914.
[23] T. Ohashi, H.M. Zbib, Mater. Sci. Forum 561–565 (2007) 1827–1832.
[24] T. Takahashi, M. Nagumo, Y. Asano, J. Jpn. Inst. Met. 42 (1978) 708–715.
[25] S. Sadamatsu, K. Higashida, Tetsu-To-Hagané 98 (2012) 328.
[26] T. Tarui, N. Maruyama, J. Takahashi, Nippon Steel Tech. Rep. 91 (2005) 56–61.
[27] T. Shimokawa, T. Oguro, M. Tanaka, K. Higashida, T. Ohashi, Mater. Sci. Eng., A (2013). (submitted for publication).

Appendix
L. Roslan et al., Key Eng. Mater., 626 (2015), 307-310

Key Engineering Materials Vol. 626 (2015) pp 307-310
Online available since 2014/Aug/18 at www.scientific.net

doi:10.4028/www.scientific.net/KEM.626.307

Finite Element Analyses of Elasto-plastic Deformation in Pearlite Lamellar and Colony Structures

LIDYANA Roslan[1, a*], TETSUYA Ohashi[1, b], YOHEI Yasuda[1, c], KOHSUKE Takahashi[1, d] and CHIKARA Suruga[1, e]

[1]Kitami Institute of Technology, Koencho 165, Kitami, Hokkaido 090-8507, Japan

[a]lidyana@newton.mech.kitami-it.ac.jp, [b]ohashi@newton.mech.kitami-it.ac.jp, [c]yasuda@newton.mech.kitami-it.ac.jp, [d]takou@newton.mech.kitami-it.ac.jp, [e]suruga@newton.mech.kitami-it.ac.jp

Keywords: Finite element analysis, Elasto-plastic deformation, Pearlite, Lamellar structure, Colony structure, Cementite, Ferrite.

Abstract. Elasto-plastic tensile deformations in pearlite lamellar and two-colony structures are studied by finite element analyses to investigate the effects of lamellar thickness ratio and difference of lamellae orientation of two colonies in pearlite microstructure. The results obtained from plastic strain distributions in lamellar and colony structures show that plastic deformation in cementite lamellar stabilized when ferrite lamellar is thicker than cementite lamellar thickness and plastic strain concentrates when the difference between cementite lamellar orientation in two colonies are larger than 45°.

Introduction

Elasto-plastic deformation in the microstructure of pearlite has been a point of interest in the field of steel research because it exhibits superior balance of strength and ductility. The microstructure is composed of blocks of the same ferrite crystal orientation colonies. The colonies consist of lamellar structure composed of brittle cementite and ductile ferrite lamellae piled up alternately in the same alignment. Mechanical properties of pearlite are influenced by interlamellar spacing and its ductility depended on the colony boundaries [1]. However the detailed aspects of those properties coexistence are still ambiguous.

In our previous study [2], we found that the brittle cementite lamella could deform into plastic range if yield stress and strain hardening rate of the ferrite phases are sufficiently large, which we considered to take place from the lamellar spacing effect. In the analyses, the models were made to be the same thickness although the characteristics of the microstructural parameters should be significantly influenced by the thickness ratio of ferrite to cementite. Therefore, how the lamellar thickness ratio effects to the pearlite ductile deformation is left for further analysis.

Recently, it is experimentally showed that strain tends to concentrates at block/colony boundaries and where the cementite lamellae alignment are approximately 45° inclined towards the tensile direction [3]. Thus, to increase the ductile property of pearlite, it is important to establish the presence or absence of the degree which plastic deformation tends to concentrates at block/colony boundaries. In this paper, we study how the lamellar thickness of cementite and ferrite affect the stability of cementite deformation and how the difference between cementite lamellae alignment of adjacent colonies affects the deformation of colony boundaries.

Numerical Models for Lamellar and Colony Structure of Pearlite

We employed a classical theory of the elasto-plastic deformation of metals where the onset of plastic deformation is defined by yield condition of von Mises:

$$\sigma_{eq.} - \sigma_Y = 0 \tag{1}$$

Appendix
L. Roslan et al., Key Eng. Mater., 626 (2015), 307-310

where σ_Y and $\sigma_{eq.}$ denote the yield stress of the material and the equivalent stress, respectively. The ferrite phase hardens after the yield point in an isotropic manner, while the cementite phase is assumed to deform plastically without hardening. We used a commercial software package of ANSYS for finite element analysis, where elasto-plastic deformation is analyzed by the incremental procedure and assuming the associated flow rule.

Fig. 1(a) shows the schematic illustration of a five-layered pearlite model. The profile of the entire model is a rectangular plate and the dimension of the model is $L\times7L$.The central lamellar is cementite (θ) and ferrite (α) lamellar and other cementite are stacked alternately in y-direction. The cementite and ferrite lamellar thickness are denoted as d_θ and d_α, respectively. To imitate possible geometrical non-uniformity in the real structure of pearlite [4], the mid-part of the central layer of cementite is slightly thinned. We construct two models with thickness ratio of ferrite to cementite lamellar $d\alpha/d_\theta$=0.375 and 1.5.

Fig. 1(b) shows the schematic illustration of two-colony pearlite model which is consist of two lamellar structures, colony 1 and colony 2. The profile of the entire model is a rectangular plate and the dimension is $L\times2L$. Lamellar orientation in colony 1 is always perpendicular to the tensile direction, while that in colony 2 makes an angle of φ to lamellae orientation in colony 1. The thickness ratio of ferrite to cementite lamellar in the colony model is $d\alpha/d_\theta$=2. We construct three models with φ=30°, 45° and 60°. These models resemble the pearlite specimen in experimental study [3].

The Young's modulus and Poisson's ration of ferrite are 200 GPa and 0.3, respectively. Stress-strain relationship is determined by experimental data [6] which is defined by the swift equation [7] given as follows:

$$\sigma = a\left(b+\varepsilon^{(p)}\right)^n \tag{2}$$

where σ and $\varepsilon_{xx}^{(p)}$ denote as stress and plastic strain, respectively, whereas a, b and n are constants. We assume a=493, b=0.002 and n=0.28. The Young's modulus and yield strength of cementite are 181 GPa and 2.75 GPa [8] respectively. The Poisson's ratio of cementite is assumed to be 0.3. When this material is deformed by uniaxial tensile load, the elastic strain at the yield point is about 1.5193%.

Analyses are performed with two-dimensional plane stress state with a large deformation framework. The quadrilateral 8-node elements are applied so that the models are divided into nearly square finite elements which size was approximately one-eighth of the lamellar thickness. Total number of the elements for a model is approximately 3×10^4. A uniform tensile displacement was given to the nodes on the lateral surfaces at $x=\pm L/2$.

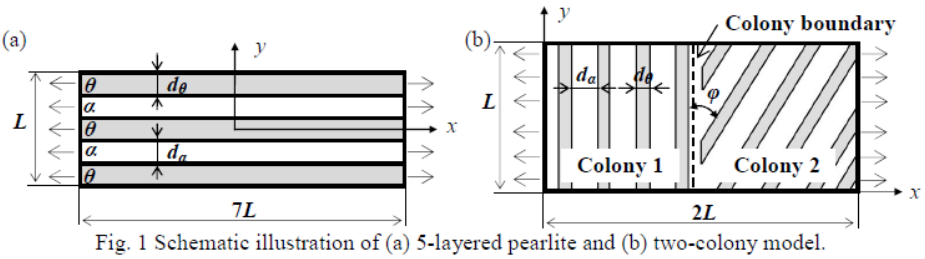

Fig. 1 Schematic illustration of (a) 5-layered pearlite and (b) two-colony model.

Results and Discussion

Deformation of Lamellar Structure. Fig. 2 shows the distributions of the plastic strain component, $\varepsilon_{xx}^{(p)}$ in (a, c) cementite and (b, d) ferrite layer when the nominal tensile strain is 1.527%. The ratios of ferrite lamellar thickness $d\alpha$ to cementite lamella thickness d_θ are (a, b) $d\alpha/d_\theta$=0.375 ($d_\theta>d\alpha$) and (c, d) 1.5 ($d\alpha>d_\theta$), respectively. When the ferrite lamellae are thinner than cementite lamellae, a shear

Appendix
L. Roslan et al., Key Eng. Mater., 626 (2015), 307-310

band is formed through the model. On the other hand, when the ferrite lamellae are thicker than cementite lamellae, the shear band is completely suppressed even though the plastic strain in the ferrite layers becomes higher in narrow region than that in the case $d\alpha/d_\theta$=0.375.

Fig. 3 shows the numerical results of nominal stress vs. nominal strain relations obtained for the lamellar models with the ratios of $d\alpha/d_\theta$=0.375 and $d\alpha/d_\theta$=1.5. The model with the ratio $d\alpha/d_\theta$=0.375 shows higher young's modulus and yield stress than the model with the ratio $d\alpha/d_\theta$=1.5. However, the ratio $d\alpha/d_\theta$=0.375 shows sudden drop of nominal stress just after the yield point, while the drop for the model with the ratio $d\alpha/d_\theta$=1.5 becomes gradual. These results indicate that plastic deformation of cementite lamellae was stabilized by increasing the lamellar thickness of ferrite than that of cementite.

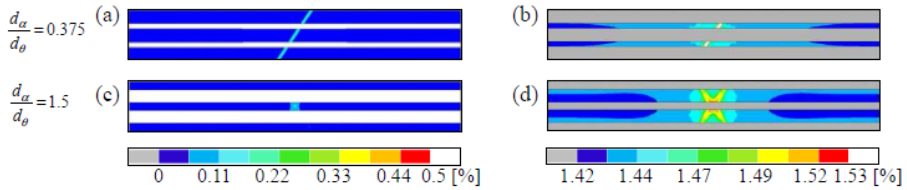

Fig. 2 Distributions of plastic tensile strain component, $\varepsilon_{xx}^{(p)}$ within (a, c) cementite and (b, d) ferrite layer when the nominal tensile strain is 1.527%. The ratios of ferrite lamellar thickness, $d\alpha$ to cementite lamellar thickness, d_θ are (a, b) $d\alpha/d_\theta$=0.375 and (c, d) $d\alpha/d_\theta$=1.5.

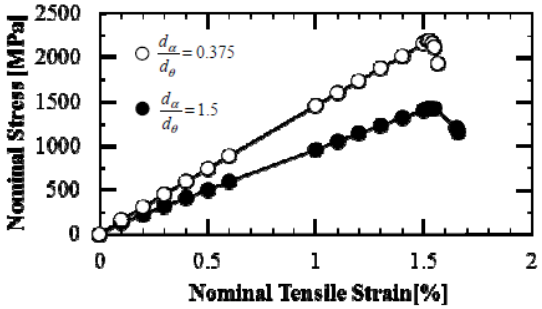

Fig. 3 Load-elongation curves of the lamellar structure models with the ratios $d\alpha/d_\theta$=0.375 and $d\alpha/d_\theta$=1.5.

Deformation of Two-Colony Structure. Fig. 4 shows the distributions of plastic strain component $\varepsilon_{xx}^{(p)}$ in two-colony pearlite model. Differences of the lamellar orientation, φ are (a) 30°, (b) 45° and (c) 60° when the nominal tensile strains are 5, 10, 13 and 18 %. White colored regions indicate that plastic strain is over 80 % and it is found that the high plastic strained band expands in one direction with the increasing of nominal tensile strain. The strain concentration region is different for each model. When the difference of lamellar orientation, φ is smaller than 45°, plastic strain concentrates alongside of cementite lamella as shown in Fig. 4(a). On the other hand, when the difference of lamellar orientation, φ is larger than 45°, plastic strain concentrates around the colony boundary as shown in Fig. 4(c). Therefore, we can confirm the experimental result and prove that the presence of the lamellar orientation degree of which plastic strain tends to concentrates at colony boundaries.

Appendix
L. Roslan et al., Key Eng. Mater., 626 (2015), 307-310

Summary

Fine lamellar and two-colony structures of pearlite consisting of cementite and ferrite layers were modeled and their elasto-plastic deformations were analyzed by the two-dimensional finite element method. Results are summarized as follows;

1. Plastic deformation of cementite lamellae in fine lamellar structure was stabilized by increasing the thickness of ferrite lamellae than that of cementite lamellae.
2. Plastic deformation concentrates around the colony boundary when the difference cementite lamellar alignment between two colonies is larger than 45°.

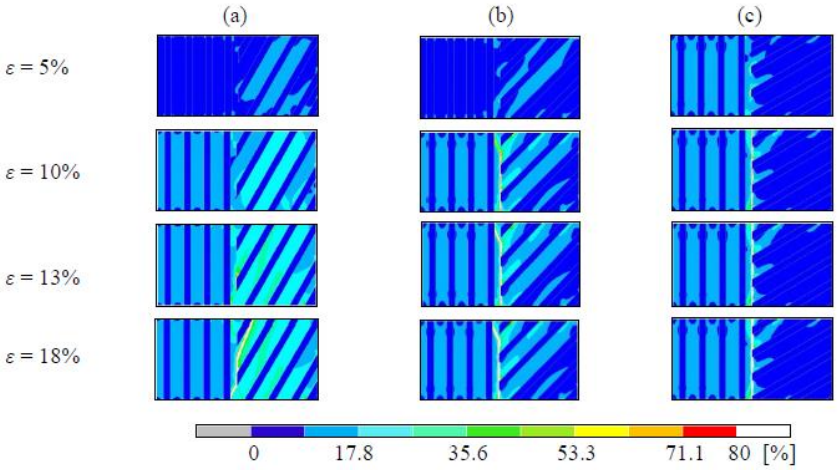

Fig. 4 Distributions of the plastic tensile strain component, $\varepsilon_{xx}^{(p)}$ in pearlite colony. Difference of the lamellar orientation φ is (a) 30°, (b) 45° and (c) 60° respectively when the nominal tensile strains, ε are 5, 10, 13 and 18 %.

References

[1] T. Takahashi, M. Nagumo, Flow stress and work-hardening of Pearlitic Steel, Trans. JIM 11(1970) 113-119.

[2] T. Ohashi, L. Roslan, K. Takahashi, T. Shimokawa, M. Tanaka, K. Higashida, A multiscale approach for the deformation mechanism in pearlite microstructure: Numerical evaluation of elasto-plastic deformation in fine lamellar structures, Mater. Sci. Eng. A 588 (2013) 214-220.

[3] M. Tanaka, Y. Yoshimi, K. Higashida, T. Shimokawa, T. Ohashi, A multiscale approach for the deformation mechanism in pearlite microstructure: Experimental measurements of strain distribution using a novel technique of precision markers, Mater. Sci. Eng. A 590 (2014) 37-43.

[4] Y. Adachi, S. Morooka, K. Nakajima, Y. Sugimoto, Quantitative three-dimensional characterization of pearlite spheroidization, Acta Mater. 58 (2010) 4849-4858.

[5] J. R. Rice, Theoretical and Applied Mechanics, North-Holland, Amsterdam, 1976.

[6] M. Umemoto, Relationships between microstructure and mechanical properties in steels, Tetsu-to-Hagane 81 (1995) 157-166.

[7] H.W. Swift, Plastic instability under plane stress, J. Mech. Phys. Solids 1(1952) 1-18.

[8] M.Umemoto, K.Tsuchiya, Fundemental properties of cementite and their present understanding, Tetsu-to-Hagane 88 (2002) 117-128.

Appendix
L. Roslan et al., Key Eng. Mater., 626 (2015), 307-310

Advances in Engineering Plasticity XII
10.4028/www.scientific.net/KEM.626

Finite Element Analyses of Elasto-Plastic Deformation in Pearlite Lamellar and Colony Structures
10.4028/www.scientific.net/KEM.626.307

DOI References
[4] Y. Adachi, S. Morooka, K. Nakajima, Y. Sugimoto, Quantitative three-dimensional characterization of pearlite spheroidization, Acta Mater. 58 (2010) 4849-4858.
http://dx.doi.org/10.1016/j.actamat.2010.05.023

Appendix
L. Roslan et al., App. Mech. Mater., 786 (2015), 33-36

Applied Mechanics and Materials Vol. 786 (2015) pp 33-36
© (2015) Trans Tech Publications, Switzerland
doi:10.4028/www.scientific.net/AMM.786.33

Submitted: 2014-12-12
Revised: 2015-02-10
Accepted: 2015-02-10

Elasto-plastic deformation of Colony Boundaries in Pearlite Microstructure by Finite Element Analyses

[1, a*]ROSLAN L., [1, b] OHASHI T., [1, c] YASUDA Y. and [1, d] SURUGA C.

[1]Kitami Institute of Technology, Koencho 165, Kitami, Hokkaido 090-8507, Japan

[a]lidyana@newton.mech.kitami-it.ac.jp, [b]ohashi@newton.mech.kitami-it.ac.jp,
[c]yasuda@newton.mech.kitami-it.ac.jp, [d]suruga@newton.mech.kitami-it.ac.jp

Keywords: Finite element analyses, Elasto-plastic deformation, Pearlite, Colony structure, Colony boundary, Cementite, Ferrite.

Abstract. Elasto-plastic tensile deformations in multi-colony structures are studied by finite element analyses to investigate how the deformation in multi-colony structures influence the strain concentration around colony boundary. The results obtained from plastic strain distributions show that plastic strain concentrates around colony boundary when there is a large difference of deformation between adjacent colonies and around the point where boundaries of differently aligned colonies meet.

Introduction

Pearlitic steel is highly demanded in industrial fields because they exhibit excellent combination of strength and ductility. Microstructure of pearlite is a lamellar structure composed of alternatively layered of high-strength yet brittle cementite and ductile ferrite. A region where the alignment of cementite and ferrite lamellae are the same is called colony. Recently, Tanaka et al. [1] indicates that strain tends to concentrate along the colony boundaries and suggested that the alignment of lamellae in adjacent colonies influence this occurrence. The observation also confirmed that cementite in colony structure does deform plastically at room temperature. This is interesting because for pearlite to work harden, cementite needs to be ductile. In addition to this, it is known that the reduction of area percentage of patented pearlite under tensile deformation is inversely proportional to the square root of pearlite colony [2]. However, details of these mechanisms are still unclear. Therefore, we investigate the elasto-plastic deformation of colony structures to help elucidate the mechanism that allows pearlite to show ductility while performing at high-strength.

Our study focuses on the influence of deformation in adjacent colonies towards the concentration of strain around the vicinity of colony boundary. In our previous studies, we constructed two-colony structure models by conjoining two differently aligned lamellar structures. They are composed of cementite and ferrite lamellae. We conducted unidirectional tensile analyses by two- and three-dimensional finite element method. The results showed that, plastic strain tends to concentrates around the colony boundary when the angle difference between cementite lamellae in adjacent colonies is large [3] and when there is a large difference in the mechanical responses between those colonies [4]. In continuation, we investigate the elasto-plastic deformation of colony structures when there are more than two colonies.

Numerical Models for Colony Structure of Pearlite

We employed a classical theory of the elasto-plastic deformation of metals where the onset of plastic deformation is defined by yield condition of von Mises:

$$\sigma_{eq.} - \sigma_Y = 0 \tag{1}$$

where σ_Y and $\sigma_{eq.}$ denote the yield stress of the material and the equivalent stress, respectively. The ferrite phase hardens after the yield point in an isotropic manner, while the cementite phase is

Appendix
L. Roslan et al., App. Mech. Mater., 786 (2015), 33-36

assumed to deform plastically without hardening. We used a commercial software package of ANSYS for finite element analysis, where elasto-plastic deformation is analyzed by the incremental procedure and assuming the associated flow rule.

Fig. 1(a), (b) and (c) show the schematic illustrations of 3 types of multi-colony models. The models are constructed from combinations of differently aligned cementite and ferrite lamellae in a square plate with the dimension of $L \times L$. In our study about lamellar structures, we found that increasing the thickness of ferrite to cementite [3] and the number of the lamellae [5] stabilized the plastic deformation of pearlite lamellar structure by delaying shear banding in cementite phase. On top of that, to imitate possible geometrical non-uniformity in the real structure of pearlite especially around the colony boundary regions [1,2], we considered the thickness of cementite lamellar to be $1/20L$ and the thickness of ferrite to be $1/13L$. Noted that, in model (c), ferrite lamellae thickness ranges from $1/20L$, $1/13L$ and $1/7L$. Whereas, for the colony boundary, in model (a) and (b), cementite lamellae within colonies are separated apart by ferrite layer of 1/20L to 1/13L. Whereas in colony boundaries of model (c) shows a case of when the cementite lamellae are not separated. The models resemble the pearlite specimens.

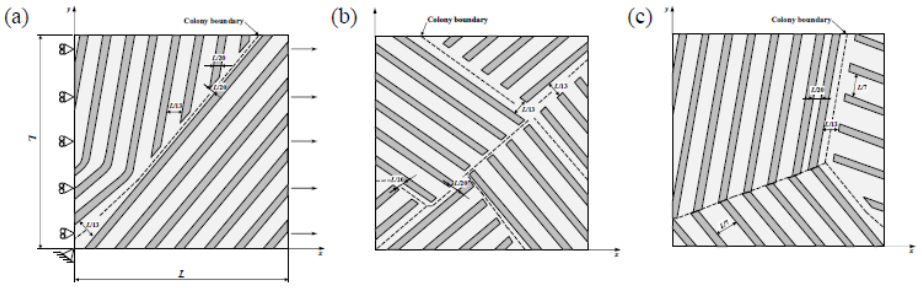

Fig. 1 Schematic illustration of 3 types of multi-colony pearlite models, (a),(b) and (c).

The Young's modulus and Poisson's ration of ferrite are 200 GPa and 0.3, respectively. Stress-strain relationship is determined by experimental data [6] which is defined by the swift equation [7] given as follows:

$$\sigma = a\left(b + \varepsilon^{(p)}\right)^n \tag{2}$$

where σ and $\varepsilon_{xx}^{(p)}$ denote as stress and plastic strain, respectively, whereas a, b and n are constants. We assume $a = 493$, $b = 0.002$ and $n = 0.28$. The Young's modulus and yield strength of cementite are 181 GPa and 2.75 GPa [8] respectively. The Poisson's ratio of cementite is assumed to be 0.3. When this material is deformed by uniaxial tensile load, the elastic strain at the yield point is about 1.5193%.

Analyses are performed with two-dimensional plane stress state with a large deformation framework. The quadrilateral 8-node elements are applied so that the models are divided into nearly square finite elements which size was approximately one-eighth of the lamellar thickness. Total number of the elements for a model is approximately 3×10^4. A uniform tensile displacement was given to the nodes on the lateral surfaces as shown in Fig. 1(a).

Results and Discussion

Fig. 4 shows the distributions of plastic strain component $\varepsilon_{xx}^{(p)}$ in multi-colony pearlite model when the nominal tensile strains are 5, 10, 13 and 15%. White colored regions indicate that the local plastic strain is over 54%. Concentrations of plastic strains are indicated in model (b) and (c) when the

Appendix
L. Roslan et al., App. Mech. Mater., 786 (2015), 33-36

nominal strain is at 5% and in model (a) shows at 10% where the boundaries of differently aligned colony meet. As the tensile deformation progressed, colonies in model (a) both deform plastically and the localization of plastic strain at around the colony boundary is less significant than model (b) and (c). This is because colonies in (a) deformed plastically compared to (b) and (c), where the strain concentrates at the colony boundary between colonies with large difference of deformations. In the case of two colonies [4], when there is a large difference of mechanical responses between the adjacent colonies, plastic strain tends to concentrate at the colony boundary. We have observed that the plastic deformation of colony with large mechanical response is small, while strain distributes well in colony with small mechanical response. It is also worth noticing that model (c), plastic concentration around the colony boundary tend to propagate along the boundary where the colonies are separated by ferrite region compared to boundaries where cementite lamellae in adjacent colonies are next to each other.

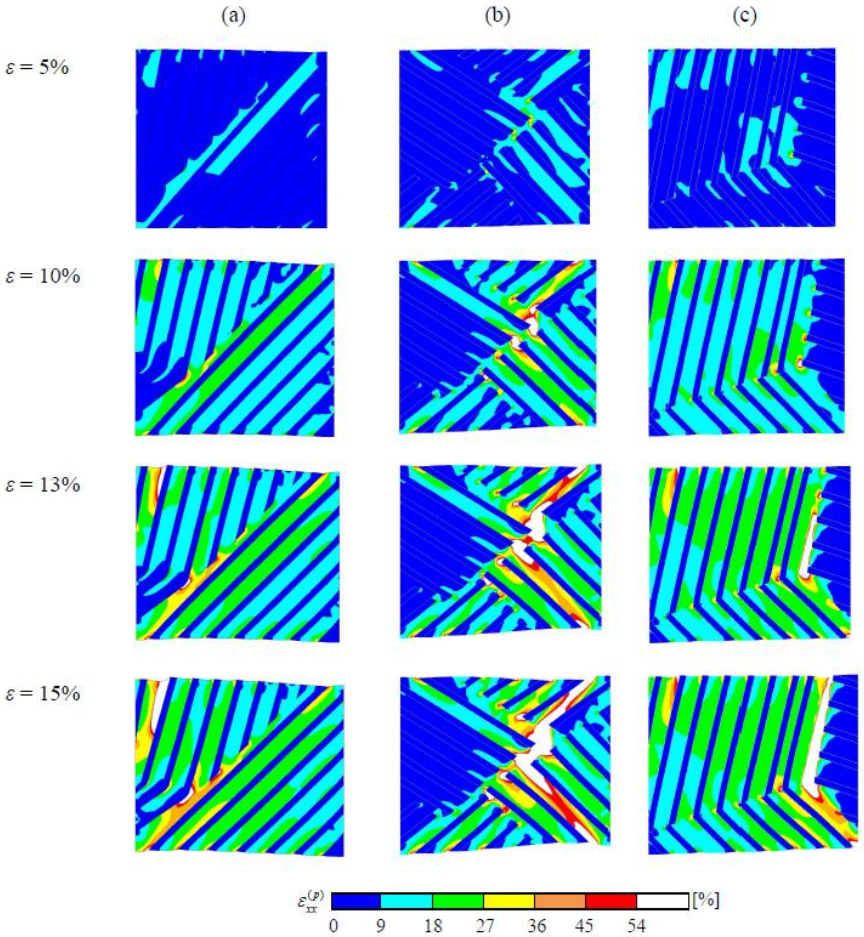

Fig. 2 Distributions of the plastic tensile strain component, $\varepsilon_{xx}^{(p)}$ in pearlite colony of models (a), (b) and (c) respectively. The nominal tensile strains, ε are 5, 10, 13 and 15 %.

Appendix
L. Roslan et al., App. Mech. Mater., 786 (2015), 33-36

The analyses results correlate with our previous studies [3,4] and experimental observation [1] where strain tends to concentrate around colony boundary when there are large difference of deformation in adjacent colonies and concentrated strain will propagate along the colony boundary as the tensile deformation of multi-colony progressed.

Conclusion

Multi-colony structures of pearlite consisting of cementite and ferrite layers were modeled and their elasto-plastic deformations were analyzed by the two-dimensional finite element method. The results show that strain tends to concentrate at colony boundary when the difference of plastic deformations in adjacent colonies is large and concentrated plastic strain tends to propagate into the nearest ferrite.

References

[1] M. Tanaka, Y. Yoshimi, K. Higashida, T. Shimokawa, T. Ohashi, A multiscale approach for the deformation mechanism in pearlite microstructure: Experimental measurements of strain distribution using a novel technique of precision markers, Mater. Sci. Eng. A 590 (2014) 37-43.

[2] T. Takahashi, M. Nagumo,Y. Asano, Microstructures dominating the ductility of eutectoid pearlitic steels, J. Japan Inst. Met. Mater. 48 (1978) 708-715.

[3] L. Roslan, T. Ohashi, Y. Yasuda, K. Takahashi, C. Suruga, Finite element analyses of elasto-plastic deformation in pearlite lamellar and colony structures, Key. Eng. Mat. 629 (2015), 307-310.

[4] L. Roslan, T. Ohashi, Y. Yasuda, Finite element analyses of elasto-plastic deformation in pearlite colony structures, in: K. Higashida, N. Tsuji (Eds.), The 4th International Symposium on Steel Science ISSS-2014 proceedings book, The Iron and Steel Institute of Japan (publishing).

[5] T. Ohashi, L. Roslan, K. Takahashi, T. Shimokawa, M. Tanaka, K. Higashida, A multiscale approach for the deformation mechanism in pearlite microstructure: Numerical evaluation of elasto-plastic deformation in fine lamellar structures, Mater. Sci. Eng. A 588 (2013) 214-220.

[6] M. Umemoto, Relationships between microstructure and mechanical properties in steels, Tetsu-to-Hagane 81 (1995) 157-166.

[7] H.W. Swift, Plastic instability under plane stress, J. Mech. Phys. Solids 1(1952) 1-18.

[8] M.Umemoto, K.Tsuchiya, Fundemental properties of cementite and their present understanding, Tetsu-to-Hagane 88 (2002) 117-128.

Appendix
L. Roslan et al., Proc. ISSS (2014), 131-134

Finite element analyses of elasto-plastic deformation in pearlite colony structures

Lidyana Roslan*, Tetsuya Ohashi, Yohei Yasuda

Department of Mechanical Engineering, Kitami Institute of Technology,
165 Koencho, Kitami, Hokkaido, 090-8507 Japan

Abstract: This paper discusses the influence of cementite lamellae alignments toward the mechanical responses of two-colony structures and how this relationship corresponds to plastic strain concentration around the colony boundary. We investigate the elasto-plastic tensile deformation in two-colony structures of pearlite using finite element method. Two-colony models are two differently aligned multi-layered structure of cementite and ferrite lamellae structures that are next to each other. Deformation of these models are analysed under unidirectional tensile load. From the results, it is shown that mechanical response of a single-colony depends largely on its lamellae direction towards loading axis. When the direction of the lamellae is close to the direction of the external load, the mechanical response of the model is high [1]. On the contrary, if the lamellae direction is inclined 45° towards the loading axis, strain hardening is moderate and the localization of plastic deformation does not take place. In two-colony models, the plastic deformation tends to concentrate around the colony boundary when there is a large difference in mechanical response between those colonies.

1. INTRODUCTION

Pearlite steel is highly demanded in industrial applications because it exhibits superior balance of strength and ductility. The hierarchical microstructure of pearlite contributes to its remarkable properties. The microstructure is consisted of alternately multi-layered high-strength yet brittle cementite phase and ductile ferrite phase. A region where the alignment of cementite lamellae are the same is called a colony. Recently, Tanaka *et al.* [2] showed that plastic strain tends to concentrate around the colony boundaries when cementite lamellae are inclined at a certain angle towards the tensile direction. The experimental observation also suggested that deformation of colony boundaries is influenced by lamellae alignments between adjacent colonies. In their two-dimensional observation, however, there were colony boundaries with similar lamellae alignments but showed different distributions of strain. It is important to investigate these mechanisms of colony deformation in order to understand the mechanical properties of pearlite. In our previous study by two-dimensional analyses, we found that plastic deformation tends to concentrates around the colony boundary when the angle difference between cementite lamellae in adjoined colonies is large [3]. Our next step is to clarify how three-dimensional lamellae alignments between colonies determine the deformation at colony boundaries.

2. NUMERICAL MODELS FOR TWO-COLONY STRUCTURES OF PEARLITE

Finite element models of two-colony structures are constructed and their mechanical properties are established by commercial software, ANSYS. The classical theory of elasto-plastic deformation of metals is employed for the analyses. Here, von Mises yield criterion defines the onset of plastic deformation for the materials and expressed in Eq. (1) as:

$$\sigma_{eq} - Y = 0, \tag{1}$$

where, (σ_{eq}) and (Y) denote the equivalent stress and yield stress of the materials. The elasto-plastic deformation for work-hardening materials is analysed by enforcing stress increment beyond the yield point and the plastic flow follows associated flow rule. This incremental procedure by tensile deformation uses a large deformation framework.

Fig.1 shows schematic diagram of two-colony pearlite model which consist of two differently aligned cementite and ferrite lamellar structures named Colony1 and Colony2. The model is a rectangular parallelepiped with a dimension of ($2L \times L \times 4L$). Thickness of the cementite and ferrite lamellae are the same and (L/10). Cementite lamellae within two colonies are separated (L/10) apart

by a ferrite layer at the mid-section of the model, which we consider to be the colony boundary. In our previous studies, we found multi-layering of brittle cementite lamellae with ductile ferrite lamellae [1] and increase of the lamellar thickness ratio of ferrite to cementite [3] stabilized the plastic deformation of pearlite lamellar structure by delaying shear banding in cementite phase. However, for multi-layered structures in three-dimension, lamellae alignment must be considered in three-dimensional space. Therefore, modelling of two adjoined multi-layered structures with different orientation is not straight forward. In the present analyses, the lamellae thickness of ferrite and cementite are assumed to be the same. Colony1 are rotated along the x-, y- and z-axes. The inclination angles of lamellae in Colony1 are given as (θ_1) at xy-plane, (θ_2) at yz-plane and (θ_3) at zx-plane, respectively. Whereas in Colony2, the alignment is always incline 45° in the tensile direction at the xy-plane, while it is perpendicular to the tensile axis at the zx-plane to induce concentration of plastic strain around the boundary region [2-3]. These models imitate the pearlite specimen seen in experimental study [2]. Tetrahedral 4-node elements are employed in each model. The lamellar thickness (L/10) is approximately the size of 2 pyramidal elements. A uniform tensile displacement was given to the nodes on the lateral surface at yz-plane.

Fig. 2 shows the stress-strain relationship for cementite and ferrite used in this study. Cementite is assumed to deform plastically with a constant plastic flow stress. Ferrite hardens in an isotropic manner after yield point. We assume that the work-hardening of ferrite follows the Swift equation [4] :

$$\sigma = a\left(b + \varepsilon^p\right)^n . \tag{2}$$

In Eq. (2), (σ) and (ε^p) are denoted as true stress and plastic strain respectively, whereas (a), (b) and (n) are constants. Their values are (a = 493), (b = 0.002) and (n = 0.28) after Umemoto [5]. Young's modulus of cementite and ferrite are 181 [6] and 200 GPa [7], while their Poisson's ratio is assumed to be 0.3.

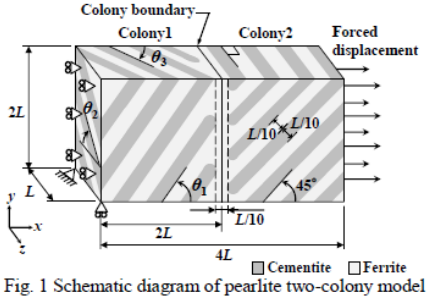

Fig. 1 Schematic diagram of pearlite two-colony model

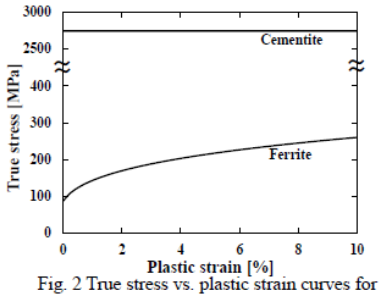

Fig. 2 True stress vs. plastic strain curves for cementite and ferrite.

3. RESULTS AND DISCUSSIONS

3.1. Deformation in the microstructure of two-colony models

Fig. 3 shows the distributions of equivalent plastic strain component (ε^p_{eq}) around the colony boundary in 6 types of two-colony pearlite models when the inclination angles (θ_1), (θ_2) and (θ_3) a of the cementite lamellae alignment in Colony1 are different. The nominal tensile strain (ε_n) of the models is 4%. White coloured regions indicate that plastic strain is larger than 18%. If observed from the xy-plane, lamellae in Colony1 of models (a) and (b), (c) and (d), (e) and (f) are similarly aligned but the distributions of plastic strain around colony boundary are different; especially for (c) and (d) cases, in which the lamellae are aligned differently when observed from other planes. Models (d), (e) and (f) showed broader distribution of plastic strain throughout the colonies because the lamellae alignment in Colony1 is 45° inclined towards the loading axis. On the contrary to this, when the lamellae alignment is parallel to the tensile direction, in the models (a) and (b), deformation in Colony1 is very small. When the deformation in one colony is small, the adjacent colony corresponds with larger deformation and plastic strain concentrates around the colony boundary. The results suggested that deformation of colony boundary depends on the deformability of adjoined colonies which is determined by combination of lamellae alignments.

Appendix
L. Roslan et al., Proc. ISSS (2014), 131-134

3.2. Mechanical response of colony units

To understand the interaction between two-colony structures, we conducted complimentary analyses to study the tensile properties of a single unit colony. A model where a ferrite lamellar is sandwiched between two layers of cementite lamellae is made and two-dimensional elasto-plastic deformation analyses were performed. Fig. 4(a) indicates that colony with lamellae alignment parallel to the loading axis exhibits significantly high value of mechanical response compared to other cases.

3.3. Tensile properties of two-colony structures

Fig. 4(b) shows the total mechanical response of three-dimensional two-colony structures. We put into consideration the results in Fig. 4(a) while comparing Fig. 3 with Fig. 4(b). When the deformation of Colony1 is small as shown in Fig. 3(a) and the mechanical response is largely different from that of Colony2, the difference of mechanical response at colony boundary is large. At the same time, in Colony2, larger value of plastic strain was obtained along the cementite lamellae and concentrate at the colony boundary. Whereas, when both colonies deform as shown in Fig. 3(d), (e) and (f), mechanical response of Colony1 and Colony2 are nearly the same. In this case, plastic strain is distributed throughout the two colonies. Therefore, plastic strain tends to concentrates around colony boundary when there is high difference of mechanical response because the distribution of strain across two colonies is largely different. From the results, we know that the plastic strain concentrate around the colony boundary where the difference of mechanical response between the colonies is significant.

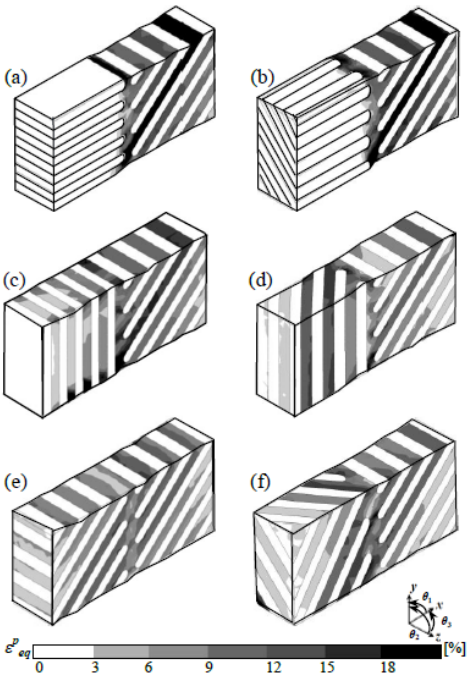

Fig. 3 Distributions of the equivalent plastic strain component (ε^p_{eq}) when the nominal tensile strain (ε_n) is 4%. Orientations of lamellae for Colony1 are as follows: (a) ($\theta_1 = 0°$, $\theta_2 = 0°$), (b) ($\theta_1 = 0°$, $\theta_2 = 45°$, $\theta_3 = 0°$), (c) ($\theta_1 = 90°$, $\theta_2 = 90°$, $\theta_3 = 0°$), (d) ($\theta_1 = 90°$, $\theta_2 = 90°$, $\theta_3 = 45°$), (e) ($\theta_2 = 45°$, $\theta_3 = 0°$) and (f) ($\theta_1 = 45°$, $\theta_2 = 45°$, $\theta_3 = 45°$)

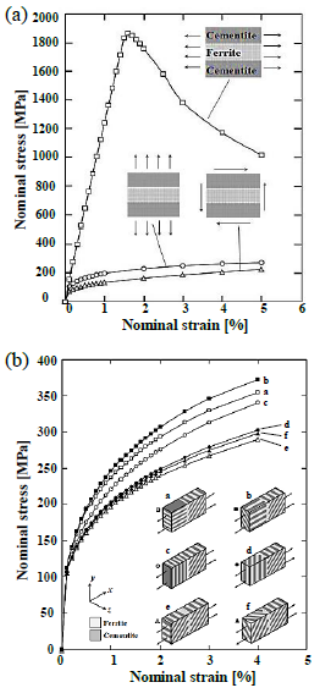

Fig. 4 Nominal stress vs. nominal strain curves for (a) single colony under tensile deformation and shear deformation and (b) three-dimensional two-colony models under tensile deformation.

Appendix
L. Roslan et al., Proc. ISSS (2014), 131-134

4. CONCLUSION

We studied three-dimensional elasto-plastic tensile deformation of two-colony structures of pearlite model using finite element method. The results showed that the mechanical response of colony depended on the alignment of cementite lamellae towards the loading axis. We also showed that plastic strain tended to concentrate around the colony boundary if the difference of mechanical response between two colonies was large. The obtained numerical results explained why two-dimensional observation of pearlite colonies in experiment [2] exhibited different distributions of plastic strain around the colony region even though the alignments of cementite lamellae were similar.

Acknowledgements: This research was supported by Japan Science and Technology Agency (JST) under the Collaborative Research Based on Industrial Demand "Heterogeneous Structure Control: Towards Innovative Development of Metallic Structural Materials".

REFERENCES

[1] T. Ohashi, L. Roslan, K. Takahashi, T. Shimokawa, M. Tanaka and K. Higashida: Mater. Sci. Eng. A, 588(2013), 214–220.
[2] M. Tanaka, Y. Yoshimi, K. Higashida, T. Shimokawa and T. Ohashi: Mater. Sci. Eng. A, 590(2014), 34–43.
[3] L. Roslan, T. Ohashi, Y. Yasuda, K. Takahashi and C. Suruga: Key. Eng. Mat., 626(2015), 307–310.
[4] H.W. Swift: J. Mech. Phys. Solids, 1(1952), 1–18.
[5] M. Umemoto: ISIJ Work-hardening Meeting, Kumamoto Japan (2010).
[6] M. Umemoto: Tetsu-To-Hagane, 88(2002), 117–128.
[7] NAOJ: Chronological Scientific Tables(NAOJ), Maruzen Co., Ltd. Tokyo Japan (2002), 395.

Appendix
L. Roslan et al., Proc. ISSS, 4 (2014), 131-134

The 4th International Symposium on Steel Science ISSS 2014 November 3rd ~ 6th, 2014

P17

Finite element analyses of elasto-plastic deformation in pearlite colony structures

Lidyana Roslan * Tetsuya Ohashi Yohei Yasuda

Kitami Institute of Technology

INTRODUCTION

Pearlite steel exhibits coexistence of strength and ductility. The microstructure is consisted of brittle cementite and ductile ferrite lamellae. The strength of pearlite increases with the inverse of interlamellar thickness[1] because of dislocation accumulation in ferrite[2]. We studied the geometrical strengthening mechanism of pearlite and found that the increase of lamellar thickness ratio of ferrite to cementite[3] and the increase of lamellar numbers[4] delay shear banding of cementite. Recently, observation of colony deformation revealed that strain tends to concentrate at colony boundary[5] . This is important because ductility of pearlite increases with the decrease of block/colony diameter[1] . Therefore, it is crucial to understand the mechanism of deformation at colony boundary.

1). T. Takahashi *et al.*, JIM, 1978, 2). Y. Yasuda *et al.*, Key. Eng. Mat., 2015, 3). L. Roslan *et al.*, Key. Eng. Mat. 2015, 4). T. Ohashi *et al.*, Mater. Sci. Eng. A, 2013, 5). M. Tanaka *et al.*, Mater. Sci. Eng. A, 2014.

Pearlite microstructure

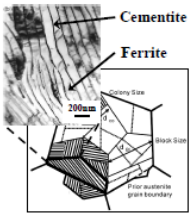

(N. Nakata, Materia, 2011)
(Y. Adachi *et al*, Acta Mater., 2008)

Experimental 2D observation of colony deformation

Distribution of strain at tensile load 2.28kN

(M. Tanaka *et al.*, Mater. Sci. Eng. A, 2014)

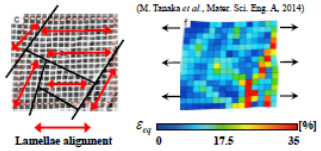

- Strain concentrates at colony boundary when lamellae alignment are inclined are inclined at certain angle to the tensile direction.
- However there are colonies with similar lamellae alignments that shows different strain distributions.

2D elasto-plastic tensile analyses of colony

Distribution of plastic strain component ε_{xx}^{p}

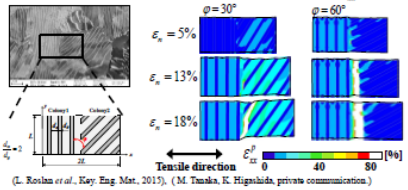

(L. Roslan *et al.*, Key. Eng. Mat., 2015), (M. Tanaka, K. Higashida, private communication.)

- φ is the angle of lamellae alignment difference.
- Strain concentrates along cementite when φ is small.
- Strain concentrates at colony boundary when φ is large.

OBJECTIVE

To study how the lamellae alignments in 3D space influence the colony deformability and strain concentrations at colony boundary.

NUMERICAL MODELS FOR TWO-COLONY STRUCTURES OF PEARLITE

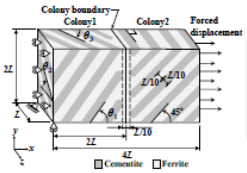

Analysis conditions

- Classical elasto-plastic deformation theory.
- von Mises yield criterion.

$$\sigma_{eq} - Y = 0$$ σ_{eq}: true stress Y: yield stress

- Assumed to follow associated flow rule.

Material properties

Stress-strain curves

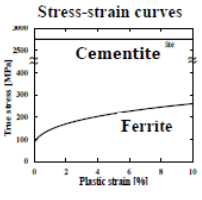

- Cementite is considered to deform plastically without hardening.
- Ferrite plastic flow stress follows Swift equation: $\sigma = a(b + \varepsilon^{p})^{n}$

(H.W. Swift, J. Mech. Phys. Solids, 1952)

σ: true stress ε^{p}: plastic strain a = 493 MPa, b = 0.002 , n = 0.28

(M. Umemoto, ISIJ Work-hardening Meeting, 2010)

RESULTS AND DISCUSSION

Deformation of two-colony structures

Distribution of equivalent plastic strain component ε_{eq}^{p}

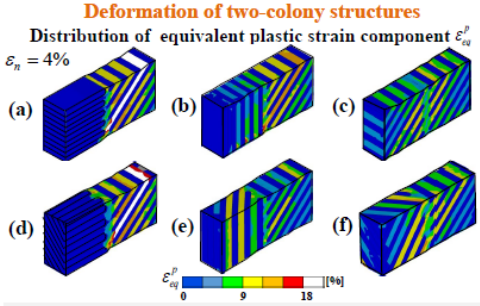

- At xy-plane lamellae have similar alignment but the strain distributions are different.
- When lamellae alignment 45° inclined towards the loading axis, the colony deforms largely compared to when lamellae alignment is parallel to the loading axis.
- Strain concentrates at colony boundary when Colony1 deformation is small.

Mechanical response of colony structures

Load-elongation curves

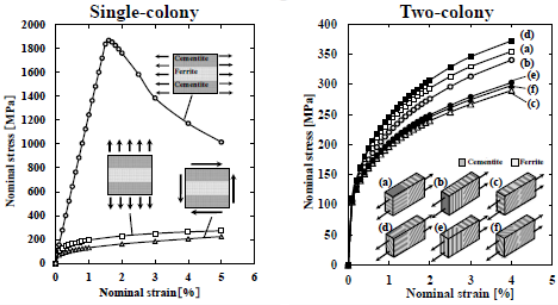

Colony with lamellae alignment that is parallel to the loading axis exhibits high value of mechanical response.

Strain concentrates at colony boundary when the difference of mechanical responses between two colonies is large.

This explained why 2D observation of pearlite colonies by Tanaka *et al.* exhibit different distributions of strain around the colony region even though the alignments of cementite lamellae were similar.

CONCLUSIONS

Mechanical response of colony depends on the alignment of cementite lamellae towards the tensile direction. Plastic strain tends to concentrate around the colony boundary when the difference of mechanical response between two colonies is large.

Acknowledgements: This research was supported by Japan Science and Technology Agency (JST) under the Collaborative Research Based on Industrial Demand "Heterogeneous Structure Control: Towards Innovative Development of Metallic Structural Materials".

パーライト相に生じる弾塑性変形の解析
- 積層数増加による不安定変形抑制 -

Analysis of elasto-plastic deformation in Pearlite structure
-Suppression of shear banding by multiple stacking of Ferrite/Pearlite units-

正　大橋　鉄也[*1]（北見工大）　　正　佐藤　満弘[*2]（北見工大）
○学　リディアナ・ロスラン[*3]（北見工大院）　　学　高橋　宏輔[*4]（北見工大院）
[*1]Tetsuya OHASHI, [*2]Michihiro SATO, [*3]Lidyana ROSLAN, [*4]Kosuke TAKAHASHI
Kitami Institute of Technology, Koencho 165, Kitami Hokkaido

Key Words: *cementite, ferrite, 2 phased pearlite, elasto-plastic, lamellar structure, ferrite thickness effect*

1. 緒言

構造用鉄鋼材料の微視組織には様々なものがある．その中でも極めて高強度であるが脆性なセメンタイトと，低強度だが高延性のフェライトがサブミクロン周期で積層したパーライト組織は強度と延性を兼ね備えた優れた特性を有している．パーライト組織についてはこれまで主として金属工学的な研究がすすめられてきたが，組織構造が複雑であるために，セメンタイト相とフェライト相のそれぞれにどのような変形が生じているのか，また層状構造全体として示している力学特性がなぜ生じているのか，などの力学に関することについてはまだ十分に分かっていない．

本研究室では，これまで有限要素法を用いて，脆いが強い材料のセメンタイトと延性があるが弱い材料のフェライトが積層した 2 相材料の大変形弾塑性解析を行い，2 相材料は単相材料よりも延性がありかつ強い材料に近づくことがわかった．本研究ではセメンタイト単層モデル及びフェライトとセメンタイトを積層したモデルを用い，フェライトとセメンタイトが微細に積層した層状組織に生ずる弾塑性変形を解析する．更に，セメンタイト層とフェライト層の厚さ比が異なることの効果を調べ，パーライト相に生じる不安定変形の抑制について検討する．

2. シミュレーション

2-1 解析モデル

セメンタイト単相材料の解析には Fig.1 に示すようなモデルを用いる．上下表面を余弦関数で与えられる曲線とし，試料中央部に微小なくびれを導入した．くびれの厚さはセメンタイト層厚さの 2%とした．また，このセメンタイト単相材料にフェライト相とセメンタイト相を交互に重ね加えたモデルを作成した．積層数が 5 の有限要素モデルを Fig.2 に示す．本解析では古典弾塑性理論を用いるので，材料寸法は正規化された量である．加えて，フェライト層の厚さを厚くすることによる層状構造の変形への影響を検討する．Fig.3 にセメンタイト層に対してフェライト層が 1.5 倍厚い有限要素解析モデルを示す．

2-2 境界条件

解析モデルの左辺の x 方向変位，左辺下端の点の全自由度を拘束し，右辺に x 方向の強制変位を与えて，せん断帯が発生するまで引張解析を行った．

2-3 材料特性

フェライト材料の真応力と塑性ひずみの関係に関する実験データは，次の Swift の式にまとめられている[(1)(2)]．

$$\sigma = a\left(b+\varepsilon_p\right)^n \qquad (1)$$

ここで室温のフェライトでは a=493MPa，b=0.002，n=0.28 である[(1)(2)]．これを用いて描いた塑性ひずみ－真応力関係を Fig.4 の Ferrite に示す．セメンタイトは，室温において塑性変形せずに破断するため，文献[(2)]から降伏点を求め，数値計算に用いる真応力－塑性ひずみ関係には，Fig.4 のように加工硬化率がほぼ 0 となる等方硬化特性を与えた．セメンタイトは公称ひずみが 1.5193%のときに降伏する．

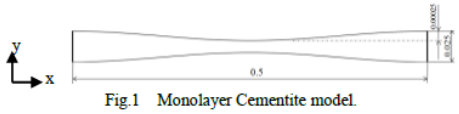

Fig.1　Monolayer Cementite model.

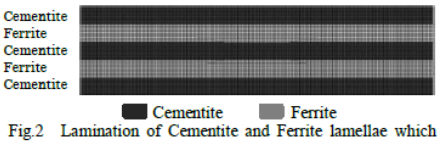

Fig.2　Lamination of Cementite and Ferrite lamellae which are laminated alternatively in the 5 lamellae Pearlite FEM model.

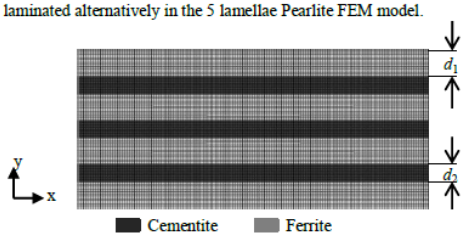

Fig.3　7 lamellae Pearlite FEM model where the thickness of Ferrite layer, d_1 is 1.5 times thicker than that of Cementite layer, d_2.

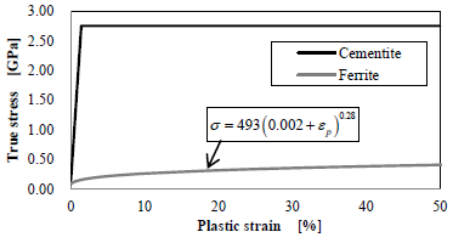

Fig.4　True stress－Plastic strain relation

3. 解析結果と考察

3-1 積層数の増加による変形の安定化

Fig.5 にセメンタイト単相材料，並びにフェライトとセメンタイトが積層した材料の公称ひずみ 1.5193%の時の垂直塑性ひずみ成分の分布を示す．セメンタイト単相材料の(a)の場合，中央部に鋭いせん断帯が生じている．3 層材料の(b)の場合もせん断帯が生じているが，中央部において複数の弱いせん断帯が重なることでひずみが大きくなり，斑模様状にひずみが発生している．5 層材料の(c)の場合，セメンタイト相に塑性ひずみが生じず，まだ安定した変形が続いている．すなわち，積層数を増やしていくとせん断帯の発生が分散・抑制されたことがわかる．

Fig.5 は垂直応力成分 σ_{xx} の分布を示している．セメンタイト単相材料の(a)の場合，せん断帯の形状に応力が集中して生じている．5 層材料(c)は単層及び，3 層材料よりも生じた応力が広い領域に分散された．積層数が増えると応力が分散され，せん断帯を生じさせる力学環境が抑制された．

Fig.6 は公称ひずみが 1.522%の時のパスライン上の塑性ひずみ分布を示している．くびれを入れたセメンタイト相の中央に水平なラインを引き，そのラインをパスラインとする．3 層，5 層材料の場合は塑性ひずみの生じ方が不安定であるが，7 層，9 層，21 層の場合は安定している．積層数が増えると塑性ひずみの局所的な集中が抑制されると考えられる．

3-2 フェライト層の厚さがセメンタイト層の 1.5 倍の場合

フェライト層の厚さが Fig. 3 のようにセメンタイト層の厚さに対して 1.5 倍のモデルについても検討した．Fig.8 は，公称ひずみ 1.522%の時のパスライン上の塑性ひずみ分布を示している．3 層の場合，塑性ひずみが中央部に集中するが，Fig.7 の 3 層の場合より激しくない変動の塑性変形している．また，Fig.7 に比べて，5 層の塑性ひずみが大きく抑制され，7 層とほぼ同じ塑性ひずみ分布をしている．一方 7 層と 9 層の場合は以前より大きい塑性ひずみの値で抑制されている．これから，厚みがあるフェライト相と積層したセメンタイト相が安定して塑性変形ができるようになるとわかる．

すなわち，フェライト層を厚くするとセメンタイト相が安定して塑性変形ができるようになったことに加えて，積層による塑性変形抑制メカニズムが働くために，積層数を増やすとセメンタイト中のより広い領域に安定して塑性変形が生ずることがわかった．よって，フェライト層が厚い場合ではセメンタイト相の塑性ひずみが抑制されるまでにより安定な状態で塑性変形ができるようになることがわかる．

4. 結言

フェライト・セメンタイトが積層した種々のモデル材料の変形過程の詳細を調べるため，セメンタイトを用いた単相材料，フェライトとセメンタイトを用いた複合材料の引張試験解析を行った．その結果，積層数が増えた場合，セメンタイトに生じる応力が分散され，せん断帯の形成が抑制された．そして，フェライト層が厚くまた，積層数が増えると，より安定した塑性変形ができるようになった．二つの条件の組み合わせで強くて延性のある材料に近づくということが確認できた．

参考文献

(1) 梅本　実，単一組織鋼の応力－歪曲線の形状の分類と組織との相関，日本鉄鋼協会加工硬化研究会 資料，2010.
(2) 梅本ら，セメンタイトの基本的特性とその理解の現状，鉄と鋼，2002，p11-2
(3) 加藤　慧士，北見工大 H22 年度卒業論文　2 相鉄鋼材料の微視組織に生じる多軸応力場，2011.3.
(4) 高橋　宏輔，北見工大 H23 年度卒業論文　微細積層構造に生じる力学場の解析，2012.3

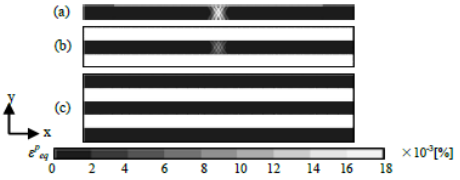

Fig.5 Distribution of plastic strain component ε^p_{xx} when the nominal tensile strain is 1.5193%. a) Monolayer Cementite, b) 3 lamellae Pearlite, c) 5 lamellae Pearlite.

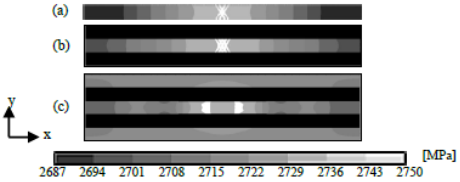

Fig.6 Distribution of tensile stress component σ_{xx} when the nominal tensile strain is 1.5193%. a) Monolayer Cementite, b) 3 lamellae Pearlite, c) 5 lamellae Pearlite.

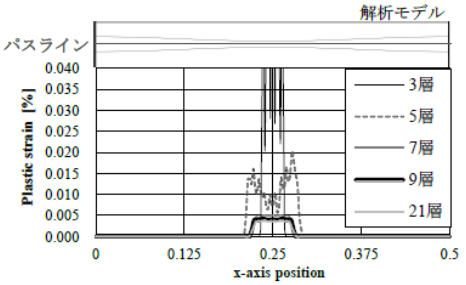

Fig.7 Distribution of plastic strain component ε^p_{xx} along the path-line when the nominal tensile strain is 1.522% for 3-1.

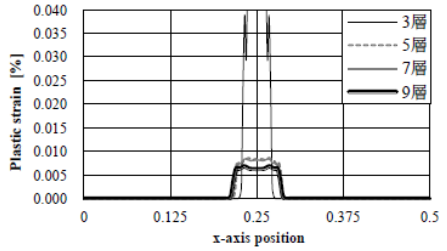

Fig.8 Distribution of plastic strain component ε^p_{xx} along the path-line when the nominal tensile strain is 1.522% when the Ferrite lamellar ratio is 1.5 of the Cementite lamellar.

謝辞

本研究は科学技術振興事業団，産学共創基礎基盤研究「革新的構造用材料創製を目指したヘテロ構造制御に基づく新指導原理の構築」(H22-H24)の委託により行った研究の一部である．記して謝意を表する．

Appendix
北海道支部第 53 回講演会 (2014)

北海道支部　第 53 回講演会・2014 年 7 月 27 日

パーライトコロニー界面近傍に生じる弾塑性変形の三次元有限要素解析

Three-dimensional finite element analyses of elasto-plastic deformation in the vicinity of pearlite colony boundary

学　リディアナロスラン　(北見工大院)　　正　大橋　鉄也（北見工大）　　正　安田　洋平　(北見工大)

Lidyana ROSLAN, Tetsuya OHASHI, Yohei YASUDA
Kitami Institute of Technology, 165 Koencho, Kitami, Hokkaido
Key Words: Pearlite, colony structure, lamellar alignment, elasto-plastic response, finite element analysis

1. 緒言

パーライト鋼は強度と靭性に優れるため，橋梁のケーブルワイヤや鉄道のレールなどの構造材料として従来から広く利用されている．その微視組織は，脆性材料のセメンタイトと延性材料のフェライトが交互に並んだ積層構造をしており，配向方向の等しい積層構造領域（コロニーと呼ぶ）が様々な配向をとって構成されている．積層間隔やコロニーの大きさ[1]はパーライト鋼の力学特性に影響することは実験的に知られているが，詳細なメカニズムについては明確にされていない．

近年，田中らはパーライト鋼の引張試験を行い，積層方向の異なるコロニー界面に生じるひずみの分布に着目した．その結果，配向方向の組み合わせの違いによって，界面に生じるひずみがことなることがわかった[2]．そこで我々は，積層方向の異なる 2 つのコロニーを組み合わせ 2 次元の引張解析をおこなった．解析の結果より，隣接しているコロニーの積層配向の角度差が大きくなると，コロニー界面近傍にひずみが集中することがわかった．しかし，実際の材料では，各層は 3 次元的に配向しており，2 次元的な配向は同じでも 3 次元的な配向は異なる場合があり，その影響は検討できなかった．本研究では，配向方向の異なる 2 つのコロニーが隣接している材料を二次元及び三次元でモデル化し，その力学特性を弾塑性解析によって検討する．

2. 解析方法と解析モデル

本研究は，市販ソフト ANSYS を使用し，パーライトコロニーの力学特性を調べる．特にコロニー界面近傍での力学挙動に着目し，古典弾塑性理論のもと，大変形引張解析を行う．

Fig.1 に解析モデルを示す．　Colony1 と Colony2 の 2 つのコロニーで簡易的にモデル化を行う．それぞれのコロニー内では，層状のセメンタイトとフェライトが交互に積層している．解析モデルを縦 2L，横 4L，奥行き L の直方体とし，それぞれのコロニーを一辺が L の立方体としている．セメンタイト層とフェライト層の厚さは L/10 である．2 つのコロニー内のセメンタイトはコロニー界面で接合せず，L/10 だけ離れている．Colony 2 の内部のセメンタイトやフェライトの配向方向は zx 面に対して 45°，xy 面に対して 90° 傾いている．Colony1 内のセメンタイトやフェライトの配向方向は zx 面に対して θ_1，xy 面に対して θ_2 傾いているものとする．θ_1=0° の時，各層は z 方向に一様となり，θ_2 は定義されない．θ_2=0° の時は，同様に，θ_2 は定義されない．Colony1 の θ_1，θ_2 が変化したときのモデルの力学特性を解析する．モデルの負の x 面を拘束し，正の x 面に引張の強制変位を与えて引張解析を行う．

コロニー内のフェライトとセメンタイトのヤング率をそれぞれ 200GPa，181GPa[5]とし，ポアソン比を 0.3 とする．降伏条件は，以下のミーゼスの式で決定する．

$$\sigma_{eq} - Y = 0 \qquad (1)$$

σ_{eq} は相当応力，Y は降伏応力である．降伏後のフェライトには等方硬化則を仮定する．セメンタイトは温室では脆性破壊するため，降伏後のセメンタイトは加工硬化しないと仮定して解析する．フェライトの塑性域での真応力 σ と塑性ひずみ ε_p の関係は，以下の Swift の式[6]で与える．

$$\sigma = a(b + \varepsilon_p)^n \qquad (2)$$

ここで a は 493MPa，b は 0.002，n は 0.28 である[5]．Fig.2 にフェライトとセメンタイトの真応力 σ と塑性ひずみ ε_p の関係を示す．セメンタイトの降伏応力は 2750MPa である．

3. 結果と考察

Fig.3 は，Colony1 の配向方向を変化させた時の，パーライトコロニーの相当塑性ひずみ分布である．モデルの公称ひずみは 4%である．Fig.3 の(a)~(d)を比較すると，(a)ではコロニー界面近傍で特にひずみが大きいことがわかる．すなわち，Colony2 の配向方向が 45° の場合，Colony1 の積層配向が引張軸に対して平行になるほど，コロニー界面近傍で局所的にひずみが集中すると言える．

Fig.4 にパーライトコロニーモデルの引張軸方向の公称応力と公称ひずみの関係を示す．モデルの拘束面に生じた反力

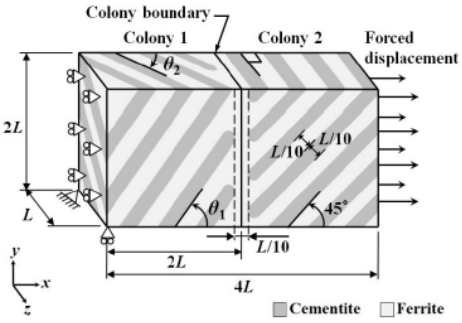

Fig.1 Schematic illustration of two-colony model.

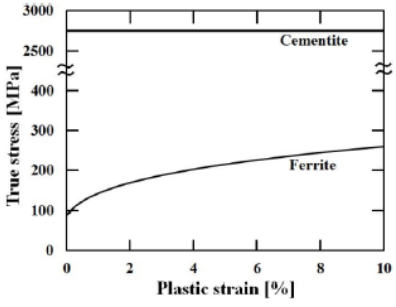

Fig.2　True stress-plastic strain curves.

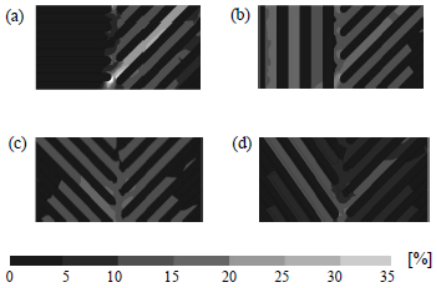

Fig.3 Distributions of the equivalent plastic strain ε^p_{eq} when the nominal strain is 4%. (a) θ_1=0° , (b) θ_1=90°, θ_2=45°, (c) θ_1=45°, θ_2=90° and (d) θ_1=45°, θ_2=45°.

を変形前の拘束面の面積で割ることで，公称応力を求める．また，モデルに与える軸方向の強制変位を軸方向長さで割ることで，公称ひずみを求める．Colony1 の配向角が θ_1=0°の時の公称応力は,他のモデルの公称応力よりも高い．Fig3.の相当塑性ひずみ分布の図と比較すると，コロニーの界面近傍にひずみが大きく集中する場合，パーライトコロニー全体の力学応答は高くなることが分かる．

Fig.5 は，単体のコロニーモデルに引張り及びせん断変形を与えた時の，公称応力と公称ひずみの関係である．モデルを単純化し，積層数と次元を減らしている．二次元平面応力状態で解析している．モデルの積層配向が引張方向に対して平行方向の力学応答は，張り方向に対して垂直方向に配向するモデルとせん断変形を与えたモデルの力学応答よりも高い．すなわち，コロニーの力学特性はコロニーへの負荷方向に依存することがわかる．

Fig.3 の(a)~(d)に示した Colony1 と Colony2 の配向方向の組み合わせと，Fig.5 に示した力学応答を比較し検討すると，Fig.3 の(a)の Colony の組み合わせでは力学応答の差が大きいことがわかる．それに対し，Fig.3 の(b)~(d)の Colony の組み合わせでは，力学応答の差が小さい．Fig.3 の(a)でのみ，コロニー界面にひずみが集中していることから，隣接するコロニー間の力学応答の差が大きくなると，コロニー界面近傍にひずみが集中しやすくなるといえる．

4. 結言

コロニー内のフェライトとセメンタイトの配向方向が，コロニー界面近傍の力学状態と，試料の力学特性に及ぼす影響を調べるため，2 コロニーモデルを用いて引張験解析を行った．その結果，コロニーの力学応答はコロニー内の積層の配向方向に依存しており，隣接しているコロニーの力学応答の差が大きいとコロニー界面への塑性変形の集中がみられる．また，応力ひずみ挙動にも顕著な差異が表れる．

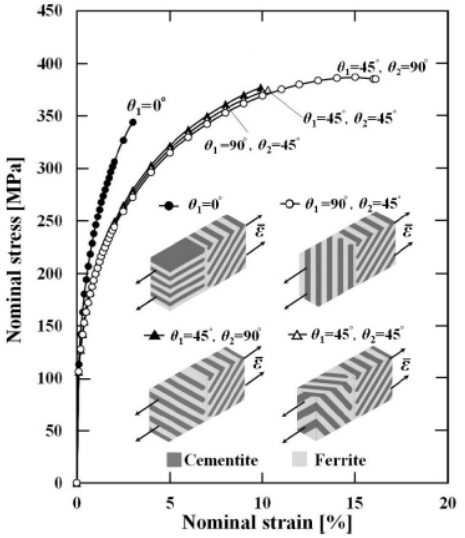

Fig.4 Nominal stress-nominal strain curves of two-colony model. Forced displacement is given by nominal strain $\bar{\varepsilon}$ value. ● denotes θ_1=0°, ○ denotes θ_1=90°, θ_2=45°, ▲ denotes θ_1=45°, θ_2=90° and △ denotes θ_1=45°, θ_2=45°.

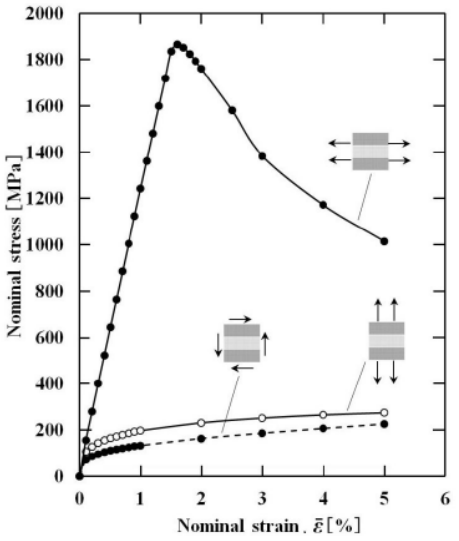

Fig.5 Nominal stress－nominal strain curves of two-dimensional lamellar structure.

参考文献

1) 高橋 稔彦, 南雲 道彦, 浅野 巌之, 日本金属学会誌, Vol.48(1978) , pp.708-715.
2) M. Tanaka, Y. Yoshimi, K. Higashida, T. Shimokawa and T. Ohashi, Mater. Sci. Eng. A, Vol.590(2914), pp.34-43.
3) L. Roslan, T. Ohashi, Y. Yasuda, K. Takahashi and C. Suruga, Key. Eng. Mat., Vol.xx(2014), pp.xxx-xxx
4) T. Ohashi, L. Roslan, K. Takahashi, T. Shimokawa, M. Tanaka and K. Higashida, Mater. Sci. Eng. A, Vol.588(2013), pp.214-220.
5) 梅本 実, 鉄と鋼, vol. 81(1995), pp.157-166.
6) H.W. Swift, J. Mech. Phys. Solids, vol.1(1952), pp.1-18.

謝辞

本研究は、(独) 科学技術振興機構(JST)による産学共創基礎基盤研究「ヘテロ構造制御」の支援を受けて行われたものである．

パーライトコロニー構造における弾塑性変形の有限要素解析

Finite element analyses of elasto-plastic deformation in pearlite colony structures

リディアナ　ロスラン・北見工大院　　大橋　鉄也・北見工大　　安田　洋平・北見工大

Lidyana Roslan, Kitami Institute of Technology　Tetsuya Ohashi, Kitami Institute of Technology　Yohei Yasuda, Kitami Institute of Technology

Keywords: *Pearlite, Colony Structure, Lamellar Alignment, Elasto-plastic Response, Finite Element Analyses*

論文要旨

1. 緒言

パーライト鋼は強度と靭性に優れているため，橋梁のケーブルワイヤーなどの構造材料として広く利用されている．その微視組織は，脆性材料のセメンタイトと延性材料のフェライトが交互に並んだ積層構造している．積層方向が同じ積層構造の領域はコロニーと言い，コロニーの積層は様々な配向をとって構成されている．積層間隔やコロニーの大きさ[1]はパーライト鋼の力学特性に影響することは実験的に知られているが，詳細なメカニズムについては明確にされていない．

近年，田中らはパーライト鋼の引張試験を行い，積層方向の異なるコロニー界面に生じるひずみの分布に着目した[2]．その結果，様々な配向方向の組み合わせによって，界面近傍に生ずるひずみが異なることが分かった．そこで我々は，積層方向の異なる 2 つのコロニーを組み合わせ，二次元の引張解析を行った[3]．その結果，隣接しているコロニーの積層配向の角度差が大きくなると，コロニー界面近傍にひずみが集中することが分かった．しかし，実際の材料では，コロニーは三次元的に配向している．本研究では，配向方向の異なる 2 つのコロニーが隣接している材料を三次元でモデル化し，その力学特性を弾塑性解析によって検討する．

2. パーライトコロニーモデル

Fig.1 に Colony1 と Colony2 の 2 つのコロニーで構成されている解析モデルを示す．解析モデルを縦 2L，横 4L，奥行 L タイトとフェライトが交互に積層している．その厚さは L/10 である．2 つのコロニー内のセメンタイトはコロニー界面では接合せずに L/10 離している．実際の材料では層の厚さなどが不均一である．我々のこれまでの研究より，脆性破壊をするセメンタイト相は，フェライト相と並んで積層する[4]こと及び，そのラメラ間隔の厚さ比[3][4]に影響され，安定した塑性変形ができるようになることを確認した．現段階の三次元的なモデルは複雑な積層方向で構造される．そのため，2 つのコロニーの界面近傍における変形挙動を着目するのに，検討しやすいことを考慮して，セメンタイトとフェライトの厚さを同じにする．モデルの Colony2 の配向方向を固定し，Colony1 の配向方向との違いが力学特性に及ぼす影響を調べる．Colony2 内部のラメラの配向方向は *zx* 面に対して 45°，*xy* 面に対して 90°傾ける．Colony1 内のラメラの配向方向は *x,y,z* 軸に関して回転させる．*xy* 面のラメラ配向と *yz* 面のラメラ配向は *zx* 面に対してそれぞれ θ_1 と θ_2 傾け，*zx* 面のラメラ配向は *xy* 面に対して θ_3 傾いている．

3. 解析

汎用 FEM ソフト ANSYS を使用し，古典弾塑性理論を用いる．Fig.1 のようにモデルの左側面を拘束し，右側面に引張の強制変形を与え，コロニー界面近傍での力学挙動に関する大変形引張解析を行う．

コロニー内のフェライトとセメンタイトのヤング率をそれぞれ 200GPa[5]，181GPa[6]とし，ポアソン比を 0.3 とする．降伏条件には，以下のミーゼスの式を用いる．

$$\sigma_{eq} - Y = 0 \tag{1}$$

ここで，σ_{eq} は相当応力，Y は降伏応力である．降伏後のフェライトには等方硬化則を仮定する．セメンタイトは温室では脆性破壊するため，降伏後のセメンタイトは加工硬化しないと仮定して解析する．フェライトの塑性域での真応力 σ と塑性ひずみ ε_p の関係は，以下の Swift の式[6]で与える．

$$\sigma = a\,(b + \varepsilon_p)^n \tag{2}$$

ここで a は 493MPa，b は 0.002，n は 0.28 とする[7]．Fig.2 にフェライトとセメンタイトの真応力 σ と塑性ひずみ ε_p の関係を示す．セメンタイトの降伏応力は 2750MPa[8]とする．

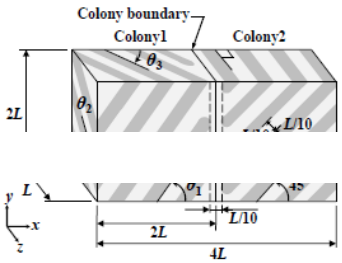

Fig.1 Schematic illustration of pearlite colony model.

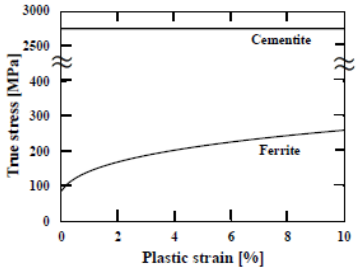

Fig.2　True stress vs. plastic strain curves for cementite and ferrite.

4. 結果と考察

Fig.3 は Colony1 内（左コロニー）ラメラの配向(θ_1, θ_2, θ_3)が異なる 6 のケースについてコロニー界面近傍に生ずる引張軸方向の塑性ひずみ分布を示している．モデルの公称ひずみが 4%である．モデル(a)と(b)，(c)と(d)，(e)と(f)は xy 面に表れる Colony1 のラメラの配向方向がほぼ同じでも，コロニー界面近傍に生ずるひずみの分布が異なる．特に(c)と(d)の場合であり，それは立体的には，ラメラの配向方向が違うためである．ラメラ配向が引張軸方向に対して 45° に傾けたコロニー((d),(e),(f))内には塑性ひずみは広く分布していることが分かった．一方，引張軸方向に平行方向のラメラ配向で構成されたコロニー((a),(b))はほとんど変形しない．この場合，片側のコロニー内の変形が小さくなると，隣接しているコロニーの変形が大きくなり，コロニー界面近傍に生ずるひずみの集中は大きくなることが見られる．よって，界面に生ずるひずみはラメラの配向方向の組み合わせ，すなわち隣接しているコロニーの変形挙動の影響を受けることが分かる．

2 つのコロニーの相互作用を理解するために，先ずは単体コロニーの引張特性を調べる．セメンタイト・フェライト・セメンタイトから成る 3 層の積層構造を構築して，二次元の引張解析を行った．Fig.4(a)に示しているように，引張軸方向に平行方向のコロニーの力学応答が，他のモデルより著しく高いことが分かる．

Fig.4(b) は 2 つコロニーからなる三次元モデルの総合的な力学特性を示している．Fig.4(a)の結果を考慮し，Fig.3 と Fig.4(b) を比較する．片側のコロニーが小さく変形するモデル(Fig.3(a),(b),(c))はコロニー間に生ずる力学応答の差は大きい．一方，Colony1 が全体に変形しているモデル(Fig.3(d),(e),(f))のコロニー間に生ずる力学応答は小さい．力学応答の差が大きくなると，コロニー界面近傍に大きいひずみが集中しやすくなる．つまり，2 つコロニーの力学応答の差が大きい時，隣接しているコロニーの変形量が大きく異なる．モデル(a),(b)の Colony1 のように変形しにくいコロニーがあると，これに隣接するコロニーでは，セメンタイトラメラ沿いにひずみが大きくなり，全体的に変形する．塑性変形が広がり，力学応答の差があるコロニー界面近傍にはひずみが大きく集中すると考えられる．

5. 結言

コロニーの界面近傍の変形挙動に着目した．積層構造している 2 つの領域のモデルを用い，三次元弾塑性解析を行った．その結果，引張軸方向に対するラメラの配向方向は単体コロニーの力学特性に大きな影響を与えることを確かめた．また，コロニー界面近傍のひずみの集中は隣接しているコロニーの力学応答の差に依存することを明らかにした．これらは二次元観察ではおなじように見えるコロニー界面でもひずみの集中の仕方がさまざまである(2)ことの一つの理由であると考えられる．

参考文献

(1) 高橋 稔彦，南雲 道彦，浅野 巌之，日本金属学会誌，Vol.48(1978)，pp.708-715.
(2) M. Tanaka, Y. Yoshimi, K. Higashida, T. Shimokawa and T.Ohashi, Mater. Sci. Eng. A, Vol.590(2014)，pp.34-43.
(3) L. Roslan, T. Ohashi, Y. Yasuda, K. Takahashi and C. Suruga, Key. Eng. Mat, Vol.626(2014), pp.307-310.
(4) T. Ohashi, L. Roslan, K. Takahashi, T. Shimokawa, M. Tanaka and K. Higashida, Mater. Sci. Eng. A, Vol.588(2013), pp.214-220.
(5) 理科年表，国立天文台 編，Vol.75(2002)，pp.395.
(6) 梅本 実，鉄と鋼，Vol. 88(2002)，pp.177-128.
(7) H.W. Swift，J. Mech. Phys. Solids，Vol.1(1952)，pp.1-18.
(8) 梅本 実，日本金属学会 加工硬化研究会 試料，(2010).
(9) M. Umemoto, Y. Todaka, T. Takahashi, P. Li, R. Tokumiya and K. Tsuchiya, Mater. Sci. Eng. A, Vol.375-377(2004)，pp.894-898.

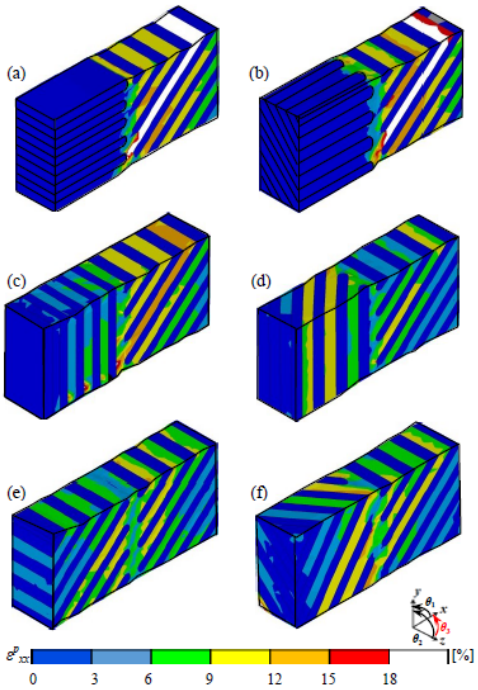

Fig.3 Distributions of the equivalent plastic strain ε^p_{xx} when the nominal strain is 4%. Orientations of lamellae for Colony1 are as follows: (a) θ_1=0° , θ_2=0° (b) θ_1=0°, θ_2=45°, θ_3=0° (c) θ_1=90°, θ_2=90°, θ_3=0° , (d) θ_1=90°, θ_2=90°, θ_3=45°, (e) θ_2=45°, θ_3=0° and (f) θ_1=45°, θ_2=45°, θ_3=45°.

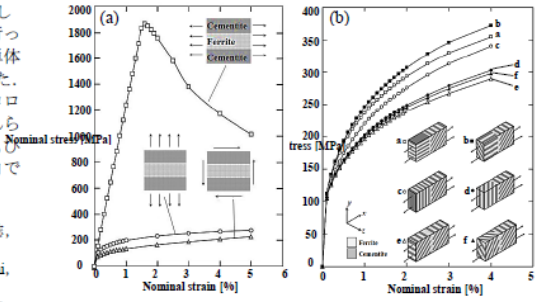

Fig.4 Nominal stress vs. nominal strain curves for (a) single colony under tensile deformation and shear deformation and (b) three-dimensional two-colony models under tensile deformation.

謝辞

本研究は、（独）科学技術振興機構(JST)による産学共創基礎基盤研究「ヘテロ構造制御」の支援を受けて行われたものである．

微細積層構造に生じる弾塑性変形の有限要素解析

Finite element analysis of elasto-plastic deformation in fine lamellar structures

正　大橋　鉄也[*1]（北見工大）　　正　佐藤　満弘[*2]（北見工大）
○学　リディアナ・ロスラン[*3]（北見工大院）　　○学　高橋　宏輔[*4]（北見工大院）
[*1]Tetsuya OHASHI, [*2]Michihiro SATO, [*3]Lidyana ROSLAN, [*4]Kosuke TAKAHASHI
Kitami Institute of Technology, Koencho 165, Kitami Hokkaido

Key Words: *cementite, ferrite, 2 phased pearlite, elasto-plastic, lamellar structure, work-hardening effect, material characteristic*

1. 緒言

鉄鋼材料は多くの目的で使われており，構造物などに使われる場合，延性がありかつ高強度の材料が望まれている．しかし，単一組織材料で高強度かつ高延性の材料は少なく，多くの材料は延性と強度がトレードオフの関係になっている．そのため，材料組織の中で様々な性質を持った部分を組み合わせて複合組織とすることで延性がありかつ強い材料を実現している．そのような複合組織を持った材料を変形させたときに，材料組織の内部で変形がどのような状態になるかという詳細については，まだ明確になっていないことが多い．本研究室では，これまで有限要素法を用いて，脆いが強い材料のセメンタイトと延性があるが弱い材料のフェライトが積層した 2 相材料の大変形弾塑性解析を行い，2 相材料は単相材料よりも延性がありかつ強い材料に近づくことがわかった．本研究ではセメンタイト単層モデル及びフェライトとセメンタイトを積層したモデルを用い，フェライトとセメンタイトが微細に積層した層状組織に生ずる弾塑性変形を解析し，積層数と軟質相(フェライト)の加工硬化能の変化による不安定変形の抑制について検討する．

2. シミュレーション

2-1 解析モデル

セメンタイト単相材料の解析には Fig.1 に示すようなモデルを用いる．上下表面を余弦関数で与えられる曲線とし，試料中央部に微小なくびれを導入した．くびれの厚さはセメンタイト層厚さの 2%とした．また，このセメンタイト単相材料にフェライト相とセメンタイト相を交互に重ね加えたモデルを作成した．積層数が 3 のモデルを Fig.2 に示す．本解析では古典弾塑性理論を用いるので，材料寸法は正規化された量である．

2-2 境界条件

解析モデルの左辺の x 方向変位，左辺下端の点の全自由度を拘束し，右辺に x 方向の強制変位を与えて，せん断帯が発生するまで引張解析を行った．

2-3 材料特性

フェライト材料の真応力と塑性ひずみの関係に関する実験データは，次の Swift の式にまとめられている[(1)(2)]．

$$\sigma = a\left(b+\varepsilon_p\right)^n \qquad (1)$$

ここで a は加工硬化係数，b は定数，n は加工硬化指数であり室温のフェライトでは a=493, b=0.002, n=0.28 である[(1)(2)]．これを用いて描いた塑性ひずみ－真応力関係を Fig.3(a)の Ferrite-original に示す．

Swift 式に用いられる定数に人工的な値を用いて，3 種類の仮想的な材料 Ferrite2a，Ferrite2n および Ferrite1-2n を作成した．用いた定数の値を Table1 に示す．これらの材料の応力と塑性ひずみの関係も Fig.3(a)に示す．セメンタイトは，室温において塑性変形せずに破断するため，文献[(2)]から降伏点を求め，数値計算に用いる真応力－塑性ひずみ関係には，Fig.3(a)のように加工硬化率がほぼ 0 となる等方硬化特性を与えた．セメンタイトは公称ひずみ 1.5193%のときに降伏する．

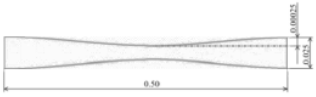

Fig.1　Monolayer Cementite model.

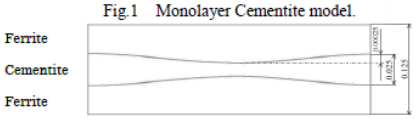

Fig.2　Lamination of Cementite and Ferrite lamellae in Pearlite which are laminated alternatively.

Table1　Values of the constants used in Swift's equation.

Ferrite types	a [MPa]	b	n
Ferrite-original	493	0.002	0.28
Ferrite2a	986	0.002	0.28
Ferrite2n	493	0.002	0.56
Ferrite1-2n	493	0.002	0.14

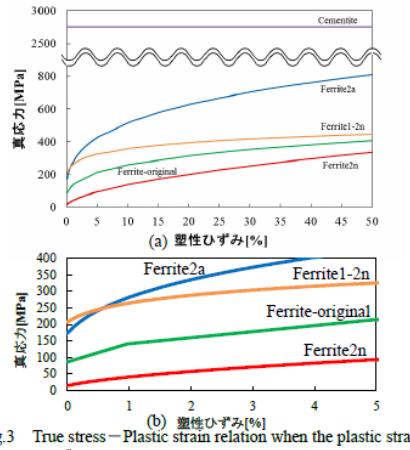

Fig.3　True stress－Plastic strain relation when the plastic strain component ε^p_{xx} range is at a) 0%~50%, and b) 0%~5%.

3. 解析結果と考察

3-1 積層数の増加による変形の安定化

Fig.4 にセメンタイト単相材料，並びに Ferrite-original とセメンタイトが積層した材料の公称ひずみ 1.5193%の時の垂直塑性ひずみ成分 ε^p_{xx} の分布を示す．紫はコンター領域以上である．セメンタイト単相材料の(a)の場合，中央部に鋭いせん断帯が生じている．3 層材料の(b)の場合もせん断帯が生じているが，中央部において複数の弱いせん断帯が重なることでひずみが大きくなり，斑模様状にひずみが発生している．5 層材料の(c)の場合，セメンタイト相に塑性ひずみが生じず，まだ安定した変形が続いている．すなわち，積層数を増やしていくとせん断帯の発生が分散・抑制されたことがわかる．

Fig.5 は垂直応力成分 σ_{xx} の分布を示している．グレーはコンター領域以下であり，紫はコンター領域以上である．セメンタイト単相材料の(a)の場合，せん断帯の形状に応力が集中して生じている．5 層材料(c)は単層及び，3 層材料よりも生じた応力が広い領域に分散された．積層数が増えると応力が分散され，せん断帯を生じさせる力学環境が抑制された．

Fig.6 は公称ひずみが 1.522%の時のパスライン上の塑性ひずみ分布を示している．くびれを入れたセメンタイト相の中央に水平なラインを引き，そのラインをパスラインとする．3 層，5 層材料の場合は塑性ひずみの生じ方が不安定であるが，7 層，9 層，21 層の場合は安定している．積層数が増えると塑性ひずみの局所的な集中が抑制されると考えられる．

3-2 フェライトの材料特性と積層材料の応答

フェライト部分の特性を Ferrite2a，Ferrite2n，Ferrite1-2n に変更し，強制変位を与えた．Fig.7 は，(a)が Ferrite-original の場合，(b)が Ferrite2a の場合，(c)が Ferrite2n の場合，(d)が Ferrite1-2n の場合の公称ひずみ 1.5193%の時のパスライン上の塑性ひずみ分布を示している．(b)の場合，塑性ひずみが中央部に集中して発生している．(a)，(c)，(d)の場合，塑性ひずみが中央部左右に大きく発生しており，(d)，(a)，(c)の順に値が小さい．また，Fig.3(b)に示されているように，(b)の Ferrite2a は他のフェライトよりも加工硬化能が高い．すなわち，加工硬化能が高い場合，塑性ひずみは大きいものの中央に安定して発生し，試料全体としても安定した塑性変形ができるようになったと考えられる．塑性ひずみが 2%の範囲では，(a)，(c)，(d)の加工硬化能はほぼ同じであり，(d)(a)(c)の順に塑性流動応力が低くなる．よって，フェライトの塑性流動応力が高いほど，不安定な塑性ひずみの発生が抑制されることがわかる．

4. 結言

フェライト・セメンタイトが積層した種々のモデル材料の変形過程の詳細を調べるため，セメンタイトを用いた単相材料，フェライトとセメンタイトを用いた複合材料の引張試験解析を行った．その結果，積層数が増えた場合，またフェライトの強度が高くなった場合，セメンタイトに生じる応力が分散され，せん断帯の形成が抑制された．そして，積層数が増え，同時にフェライトの強度が高くなった場合，塑性ひずみが抑制され，安定した塑性変形ができるようになったため，強くて延性のある材料に近づくということが確認できた．

参考文献

(1) 梅本　実，単一組織鋼の応力－歪曲線の形状の分類と組織との相関，日本鉄鋼協会加工硬化研究会 資料，2010.
(2) 梅本ら，セメンタイトの基本的特性とその理解の現状，鉄と鋼，2002，p11-2
(3) 加藤　慧士，北見工大 H22 年度卒業論文　2 相鉄鋼材料の微視組織に生じる多軸応力場，2011.3.
(4) 高橋　宏輔，北見工大 H23 年度卒業論文　微細積層構造に生じる力学場の解析，2012.3.

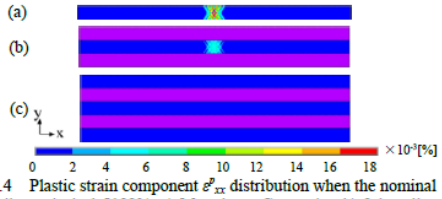

Fig.4　Plastic strain component ε^p_{xx} distribution when the nominal tensile strain is 1.5193%. a) Monolayer Cementite, b) 3 lamellae Pearlite, c) 5 lamellae Pearlite.

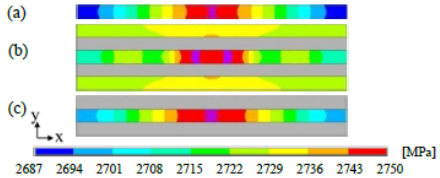

Fig.5　Tensile stress component σ_{xx} distribution when the nominal tensile strain is 1.5193%. a) Monolayer Cementite, b) 3 lamellae Pearlite, c) 5 lamellae Pearlite.

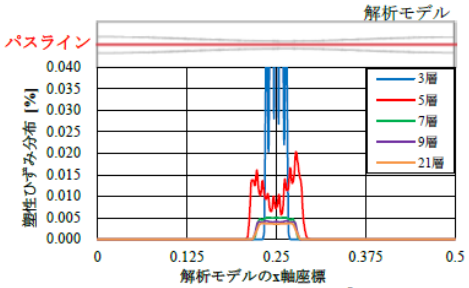

Fig.6　Distribution of plastic strain component ε^p_{xx} along the path-line when the nominal tensile strain is 1.522%.

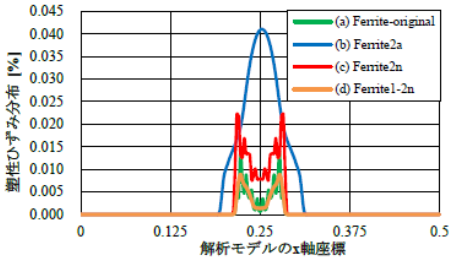

Fig.7　Distribution of plastic strain component ε^p_{xx} along the path-line in 5 lamellae 2-phased Pearlite for each Ferrite types when the nominal tensile strain is 1.5193%.

謝辞

本研究は科学技術振興事業団，産学共創基礎基盤研究「革新的構造用材料創製を目指したヘテロ構造制御に基づく新指導原理の構築」(H22-H24)の委託により行った研究の一部である．記して謝意を表する．

パーライトコロニー界面近傍に生じる弾塑性変形の有限要素解析

Finite element analyses of elasto-plastic deformation in the vicinity of pearlite colony boundary

北見工業大学　○リディアナ　ロスラン，大橋鉄也，安田洋平

1. 緒言

パーライト組織は，高強度であるが脆性的なセメンタイトと，低強度であるが高い延性を持つフェライトがサブミクロン周期で積層した構造である．セメンタイトとフェライトの配向方向が同じ領域をコロニーと言い，パーライトは多数のコロニーで構成されている．田中らは隣接するコロニーの組み合わせによって，コロニー界面に生じるひずみがみが変化することを実験により明らかにした[1]．しかし，その力学応答の詳細は十分に分かっていない．そこで本研究では，2 つのパーライトコロニーからなるモデルを用いて，弾塑性有限要素解析を行う．

2. 解析方法

本解析は市販ソフト ANSYS を使用し，古典弾塑性理論のもと，大変形引張解析を行う．材料の降伏はミーゼスの条件で定義し，降伏後のフェライトは等方的に加工硬化と仮定する．塑性ひずみの増分は Associated flow rule に従うものとする．フェライトの加工硬化特性は梅本らによる実験データ[2]を用いる．また，セメンタイトは加工硬化せずに塑性変形すると仮定する．解析には 2 つのコロニーの領域からなる二次元及び三次元モデルを使用する．

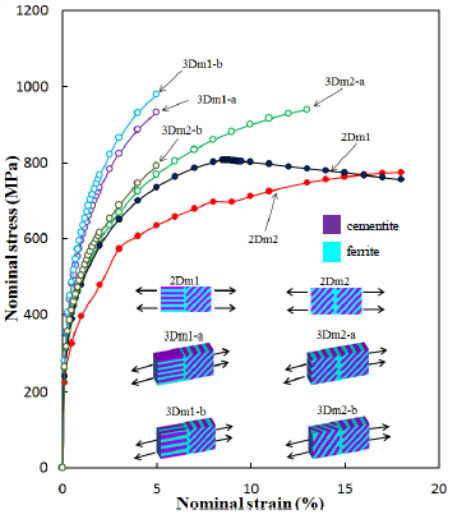

Fig. Calculated stress-strain curves for pearlite colony.

3. 結果

片方のコロニー積層配向が引張方向に対して平行に配向した場合（2Dm1）と片方の積層配向が隣接しているコロニーの配向方向と同じ場合（2Dm2）を比較すると，積層配向に差があるモデルの方は塑性流動応力が高い．しかし，積層配向に差がない場合は，徐々に加工硬化して，安定して塑性変形していることが分かる．三次元モデル（3Dm1-a，3Dm2-a）でも同様の結果が得られる．これらより，コロニーの力学応答特性はコロニー内の積層配向に依存しており，隣接しているコロニーの力学応答特性に大きな差があるとコロニー界面近傍に変形が集中し，試料全体の塑性変形が不安定になりやすいことが考えられる．

参考文献

1) M. Tanaka, Y. Yoshimi, K. Higashida, T. Shimokawa, T. Ohashi, Mater. Sci. Eng. A 590 (2014) 37-43.
2) 梅本　実, 鉄と鋼 81 (1995) 157-166.

謝辞

本研究は科学技術振興事業団，産学共創基礎基盤研究「革新的構造用材料創製を目指したヘテロ構造制御に基づく新指導原理の構築」（H23-H27）の委託により行った研究の一部である．

Lidyana Roslan (*Kitami Institute of Technology, Koencho 165, Kitami, Hokkaido 090-8507*)

Acknowledgement

I have the upmost appreciation for my supervisor and head examiner, Professor Dr. Tetsuya Ohashi. There are no words in me to express gratitude for your patience and diligence on mentoring me. Thank you.

Special appreciations for my vice supervisors and board of examiners, Professor Dr. Jun-ichi Shibano, Professor Dr. Hirotsugu Minami, Associate Professor Dr. Ullah Sharif and Associate Professor Dr. Michihiro Sato. It is my pleasure to defend this thesis to such admirable audiences.

This research was supported by Japan Science and Technology Agency (JST) under the Collaborative Research Based on the Industrial Demand "Heterogeneous Structure Control: Towards Innovative Development of Metallic Structural Materials".

I am honoured to have the chance to learn from Professor Emeritus Dr. Kenji Higashida, formerly from Kyushu University, Associate Professor Dr. Masaki Tanaka from Kyushu University, and Professor Dr. Yoshitaka Adachi from Kagoshima University. Many thanks for the valuable co-operations to aid my studies.

To technical administrator, Mr. Minoru Hasegawa and PhD comrade, Mr. Yelm Okuyama together with all the members of Keisan-riki-gaku-kenkyu-shitsu; thank you for accommodating and assisting the progress of my research. I would like to extend my thanks to Dr. Yohei Yasuda for the advices offered.

I owe this experience to University Sarawak Malaysia (UNIMAS). Thank you Dean of UNIMAS Faculty of Engineering, Associate Professor Dr. Ir Al-Khalid Hj Othman for supporting me through this rough journey and the committee of the Study Leave Unit, especially Ms. Olizer Olivina ak Abdul for putting up with me.

To my family and friends. My mother and fellow Ph.D. colleague, Laila and my father, Roslan. Thank you for believing in me. Dearest grandmother, Ya' and the lots: Beb, Leenna, Bob, and Bebi. Sorry I took too long. My best friends, especially Shota, Liyana and Hannah. Also, Florianna Lendai. Not to forget, Linda Sartika, Dayang Nad, and Nadia Aun. You know I owe you guys this much! To Maru for being awesome. And last, but never least, Tomoki. Thank you.

XOXO

Lidyana Binti Roslan